A Study of the Kinetics of Copper Vapour Lasers

Geoff Hogan

Wolfson College,

Oxford

A thesis submitted for the degree of

Doctor of Philosophy

Trinity Term 1993

at the University of Oxford

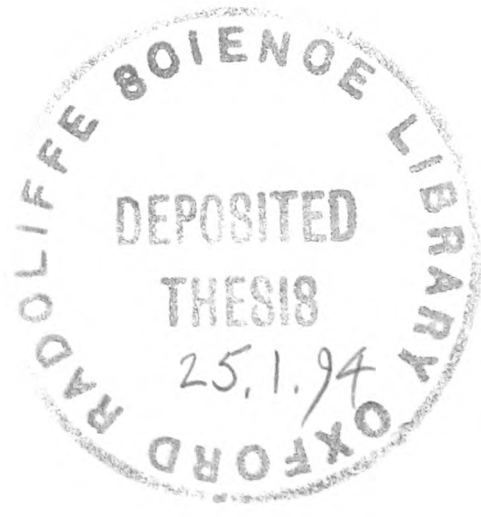

To my Parents, with whose support I started this project

and Jenny, with whom I completed it


Printed on tree-free hemp blend paper

ABSTRACT

A STUDY OF THE KINETICS OF COPPER VAPOUR LASERS

G. P. Hogan

Wolfson College, University of Oxford

Submitted for the degree of Doctor of Philosophy

Trinity Term 1993

A 42 mm bore, 40 W copper vapour laser (CVL) has been set up in a test rig in order to measure the values of many of the parameters of the laser as a function of time in the laser pulse-delay cycle, and of radial position in the plasma tube, while at all times running under standard operating conditions. In this way it has been possible to obtain the world's first truly comprehensive parameter map of the CVL in which all of the measurements have been performed upon the same device, operating under identical conditions and with all times accurately referenced to a datum. It is intended that this set of data is primarily for the benefit of those involved in the computer modelling of the CVL plasma, however initial analysis of the results obtained has been undertaken.

All diagnostic techniques have been carefully selected as offering the highest possible level of accuracy and freedom from assumptions, and each one employed has been described in detail in terms of both theory and practical application. The hook method has been used for the measurement of the population density in the copper ground state, the upper and lower laser levels, one of the copper quartet levels, and one of the neon metastable levels, each with a time resolution of 5 ns, and a radial resolution of 2 mm. The electron density has been measured, also with a radial resolution of 2 mm and with nanosecond time resolution using a two colour interferometric technique employing the measurement of the refractive index of the plasma at 10.6 μm and 670 nm. Measurement has been made of the voltage on the laser electrodes and the current flowing in the laser during the discharge.

Ancillary experiments have been performed to study the CVL discharge which have yielded some unexpected results, and measurements have been performed on a 60 mm bore CVL to determine fully the mechanism of the time delay between the onset of lasing at the plasma tube wall and on axis, and novel observations have been made.

I often say that when you can measure what you are speaking about, and express it in numbers, you know something about it; but when you cannot express it in numbers, your knowledge is of a meagre and unsatisfactory kind; it may be the beginning of knowledge, but you have scarcely, in your thought, advanced to the state of *Science*, whatever the matter may be.

Lord Kelvin (1824-1907)

ACKNOWLEDGEMENTS

I would like to express my gratitude to Professor R A Cowley for the use of the facilities of the Clarendon Laboratory.

I would like to express my sincerest thanks to Professor Colin Webb for his supervision over the period of this project. His enthusiasm and interest has been a constant source of encouragement and inspiration, his availability for comment and discussion has belied the contents of his diary and his good humour has seldom failed.

I would like to thank Dr Tony Andrews for much advice, discussion and the benefit of a seemingly inexhaustible fund of practical experience. Also for much fruitful discussion and advice I would like to thank members of the Laser Group, present and past.

I would like to thank Dr R J Carman for sending me copies of his excellent paper on the modelling of the CVL prior to publication and for permission to refer to his results. I am particularly indebted to him for permission to reproduce one of his diagrams: Figure 7.5 in this thesis.

I would also like to thank the following:

Oxford Lasers Ltd for the use of their facilities and the availability of a 100 W CVL for the experiments described in Chapter 6;

Milan Svoboda from Prague Technical University for his work on some of the novel software used in this project;

George Matthews of the research workshop for forbearance and assistance with the manufacture and modification of innumerable pieces of optical equipment, and even with a few of slightly dubious relevance to the project;

British Nuclear Fuels Plc for financial support of the project and the Science and Engineering Research Council of Great Britain for financial support of the student;

Dandelion and Burdock for the finest tonic in times of stress I have yet come across, and also a steady supply of eggs;

Finally I would like to thank Jenny for her support, patience and a lot of cups of tea.

CONTENTS

GLOSSARY OF ABBREVIATIONS

ASE	Amplified spontaneous emission
AVLIS	Atomic vapour laser isotope separation
BBO	β-Barium borate
CCD	Charge coupled device
CMVL	Cyclic metal vapour laser
CVL	Copper vapour laser
CW	Continuous wave
DC	Direct current
DDG	Digital delay generator
EEDF	Electron energy distribution function
FWHM	Full width at half maximum
GPIB	General purpose interface bus
HR	High reflectance
HyBrID	Hydrogen bromide in discharge
IEEE	Institute of Electrical and Electronics engineers
ICO	Injection controlled oscillator
IR	Infra-red
KDP	Potassium dihydrogen orthophosphate
LLNL	Lawrence Livermore National Laboratory
MOPA	Master oscillator power amplifier
MVL	Metal vapour laser
ND	Neutral density
Nd:YAG	Neodymium doped yttrium aluminium garnet
OL	Oxford Lasers
PC	Personal computer
PDT	Photo dynamic therapy
prf	Pulse repetition frequency
PSU	Power supply unit
QM	Quantum mechanics
rf	Radio frequency
RIMS	Resonance ionisation mass spectrometry

SHG	Second harmonic generation
SLM	Single Longitudinal Mode
US	United States
UV	Ultraviolet
YAG	Yttrium aluminium garnet

LIST OF SYMBOLS

A	Area
A_{ji}	Einstein coefficient for spontaneous emission between levels j and i
a	Electron temperature cooling rate
a, b	Radii
B	Magnetic flux density
C	Specific heat capacity
c	Speed of light in vacuum
$\chi_{(2)}$	Second order non-linear susceptibility
D_a	Ambipolar diffusion coefficient
D_e, D_i	Diffusion coefficient of electron, ion
D_E	Diffusion coefficient for propagation of electric field
D^*	Detectivity
d_{eff}	Effective non-linear coefficient
d^{-1}	Reciprocal dispersion of spectrograph
Δ	Hook separation
Δ_0	Hook separation in the absence of significant line-broadening
Δ	Macroscopic change in parameter
δ	Microscopic change in parameter
δ	Skin depth
∇	The differential operator
E	Electric field strength
e	Elementary charge
e^-	Electron
ε	Wavelength resolving power
ε_0	Permittivity of vacuum
ε_r	Relative permittivity
η	Plane wave impedance
F_s	Product of effective population density and oscillator strength for a particular transition
f_s	Classical constant analogous to oscillator strength
f_{ij}, f_{ji}	Oscillator strength for transition from level i to j, j to i

Δf	Amplifier bandwidth
ϕ	Half angle between two beams in interferometer
g_i, g_j	Degeneracy of levels i and j
γ_s	Classical damping coefficient
I	Intensity
I_0	Initial intensity
I_w^+	Ambipolar ion wall current
i	Imaginary part of complex number; $=\sqrt{-1}$
i, j	designation of two levels, energy $j > i$
J_0	Bessel function of order 0
J	Total angular momentum of atom
K	Hook constant
K_{NL}	Non-linear conversion constant
k	Boltzmann constant
k	wave number
κ	Thermal conductivity
κ_0	Thermal conductivity at 0 K
$\varkappa$	Imaginary part of complex refractive index
L	Orbital angular momentum of atom
l	Length of medium under test
l'	Length of compensating optics
l_c	Coherence length
λ	Wavelength
λ_s	Wavelength of classical resonance of electron
λ_0	Wavelength of transition
λ_1, λ_2	Wavelength values of hook turning points
λ_1, λ_2	Fundamental and second harmonic wavelengths in SHG
λ_D	Debye length
$\Delta\lambda_D$	Doppler broadened line-width
$\Delta\lambda_L$	Lorentzian line-width
m_a, m_e	Mass of atom, electron
m	Interference fringe order
Δm	Interference fringe shift

μ_e, μ_i	Mobility of electron, ion
μ_0	Permeability of vacuum
N	Number density of particles
N_{Cu}, N_{Ne}, N_i	Number density of copper atoms, neon atoms, ions
N_i, N_j	Number density in level i, j
N_i^*	Effective population number density in level i
n_e	Electron number density
n_0	Initial electron density
n	Real refractive index
n'	Real refractive index of compensating optics
n_ω, $n_{2\omega}$	Real refractive index at fundamental frequency, second harmonic
n^o, n^e	Refractive index for ordinary ray, extraordinary ray
$\tilde{n}$	Complex refractive index
ν	Frequency
ν_s	Classical resonance frequency of electron
ν_m	Momentum transfer collision frequency
ω	Angular frequency
ω_p	Plasma frequency (angular)
ω_s	Classical resonance frequency (angular) of electron
P	Power input per unit volume
P_ω, $P_{2\omega}$	Power at fundamental frequency, second harmonic
p	Power coefficient of temperature for thermal conductivity
p_{Cu}	Partial pressure of copper vapour
R	Radius
r	Radial position
r_0	Classical electron radius
ρ	Density
S	Spin angular momentum of atom
(S/N)	Signal to noise ratio
σ	Electrical conductivity
T_g, T_i	Gas temperature, ion temperature
T_e	Electron temperature
T_b, T_t	Temperature characterising bulk, tail of EEDF

T_l	Temperature of cooling water
T_w	Wall temperature
T_0	Operating wall temperature above T_l
T_0	Initial electron temperature
t	Time
$d\tau$	Volume element
τ	Time constant
τ_c	Cooling time constant
τ_i	Lifetime of atom in level i
θ_i	Angle of incidence
θ_m	Phase match angle
V_i	Ionisation potential
V_s	Potential difference across plasma sheath
$\bar{v}$	Mean velocity
W	Power
W_m	Energy stored in magnetic field
Δx	Spatial resolution of 2D detector
y	Vertical position on slit of spectrograph

1. INTRODUCTION: THE CONTEXT OF THE WORK

1.1 THE BACKGROUND TO THE CYCLIC METAL VAPOUR LASERS

1.1.1 PHYSICS

The copper vapour laser (CVL) is a member of the family of cyclic, or self-terminating metal vapour lasers (MVL). These all share the common feature that the upper laser levels are connected to the ground state by a fully allowed resonance transition, which is consequently of very high oscillator strength, whilst the lower laser levels are connected via relatively forbidden transitions and are consequently metastable. The degree to which this is so differs between members of the family and is illustrated for the case of the copper atom by the term diagram of Figure 1.1.

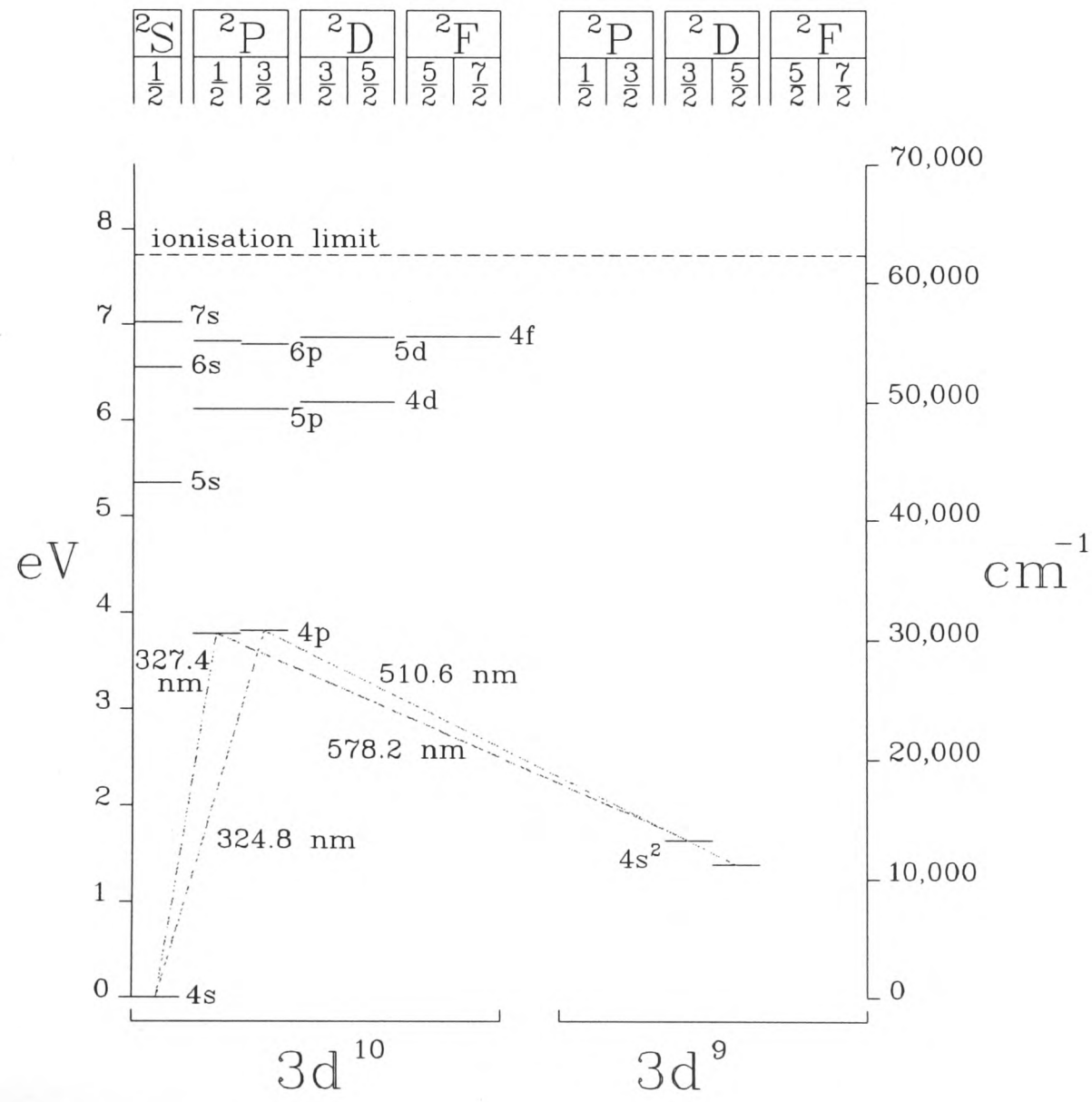

Figure 1.1 Partial term diagram of atomic copper

In the case of copper the lower laser levels are metastable not only because of angular momentum selection rules, but also because, as may be seen from the term diagram, they are of a different electronic configuration. The transition of a copper atom from its $3d^{10}$ 4s ground state to the $3d^{10}$ 4p upper laser levels consists merely in the excitation of the single, outer, 4s electron to 4p, the simplest and most preferred transition. The transition from the copper ground state to the $3d^9$ $4s^2$ lower laser levels, however, involves the promotion of one of the closed, inner shell, 3d electrons out to 4s thus changing the atom core configuration from $3d^{10}$ to $3d^9$. This is consequently not only highly forbidden for optical excitation, but, to be excited in collision, requires that the colliding electron should reach past the outermost electron and excite the core. Such a degree of prohibition does not apply to all members of this class of lasers, however. The lower level need only be relatively optically forbidden to enable population inversion, however it is well implemented in the copper atom and similarly in the gold (in which it is the 6s electron outside the $5d^{10}$ shell which is excited in an exactly analogous manner) which makes excitation in both cases highly selective. In the cases of the lead and manganese lasers, discovered before the CVL, this is not so. In the lead vapour laser the lower laser level is actually of the same configuration as the ground state ($6s^2$ $6p^2$), only the parity change selection rule forbidding the transition between them. In manganese the transitions from ground state to both the upper and lower laser levels involve exciting an outer 4s electron, for the upper level to 4p, for the lower to 3d, forbidden by parity change requirement.

The excitation scheme has two fundamental consequences for the characteristics of these lasers. Firstly they are very efficient. Excitation to the upper laser level is strongly preferred over excitation to the lower level under suitable pumping conditions so the input power can be channelled into the desired excitation process highly efficiently. Excitation in a pulsed electrical discharge provides such conditions so long as the electron temperature is high enough to pump the upper laser levels effectively. As in general both sets of laser levels lie relatively close to the ground state the proportion of the pump energy that can be returned by the laser photon is high, giving a high quantum efficiency. The corollary of this is that if a lower laser level is too low lying its thermal population (especially in those lasers operated at high temperature) must be overcome before population inversion is obtained.

The second consequence of the excitation scheme of these lasers is that they are intrinsically pulsed. For a given laser transition to have a possibility of running in a CW manner it must satisfy the minimum requirement that the lifetime of the lower laser level (τ_i) must be shorter than that of the upper level against spontaneous emission on the laser transition (the reciprocal of the spontaneous emission transition probability A_{ji}). To put that more formally, for laser levels i and j, with degeneracies g_i and g_j:

$$A_{ji}^{-1} > \frac{g_j}{g_i}\tau_i \qquad \textbf{(1.1)}$$

From the property that the lower laser level is metastable, and therefore τ_i is very long, all cyclic MVLs fail to satisfy this condition and are therefore intrinsically pulsed systems.

In 1966 Walter (Walter et al, 1966 b) published a paper in which he outlined a list of criteria for a class of high efficiency, high gain, intrinsically pulsed metal vapour lasers (MVLs) based on the characteristics discussed above. In addition he specified that the metal vapour pressure should be high enough to allow radiation trapping of the resonance line(s), and that the (trapped) lifetime on the laser transition should be long enough to allow inversion to build up over the time course of the discharge pulse. In addition he postulated that it should also be short enough (ie have a large enough A coefficient) to give good gain. Other lasers of this class include gold, manganese, lead and barium, while singly ionised calcium and barium offer analogous operation, though with lower potential efficiency because of the requirement to generate and retain the necessary ion ground state density.

A significant characteristic of these lasers in their longitudinal discharge form has been found to be the necessity of generating an optimal vapour pressure of the metal in question of around 0.3 mbar. This optimal value is found to apply to all lasers of this class and arises from two competing requirements. A relatively large ground state population density of lasant species is required in order to provide plenty of atoms available for excitation and also to ensure efficient radiation trapping of the resonance lines. A large density of lasant atoms, however, has the effect of reducing the electron temperature which is determined by E/N, where E is the accelerating electric field strength, and N in the number density of gas atoms with which the electrons may undergo both elastic and inelastic collisions, thus reducing the mean energy of the distribution.

If the electron temperature is allowed to fall too far the electron collision cross-section for direct excitation from the ground state to the resonance level(s) drops until efficient selective excitation to this level over that to the metastable level(s) becomes unfavourable. Under these conditions, stepwise ionisation via the metastable level(s) becomes significant. As the collisions between the electrons and the buffer gas are predominantly elastic, the sensitivity of laser action efficiency to buffer gas pressure is very much lower than to copper vapour pressure. The reasons for this will be discussed later.

In the simplest implementation of the MVL, in which pieces of the relevant metal form the laser charge, the vapour pressure requirement is satisfied by raising the temperature of the laser tube to a value sufficient to generate this value. Whilst this is not too much of a problem for barium and lead lasers, at around 700°C and 800°C respectively, for an elemental copper laser the appropriate temperature is around 1500°C and engineering difficulties start to arise. Historically this has had two effects. Firstly it has tended to retard research into elemental copper vapour lasers until such time that the appropriate refractory materials, of sufficient purity, and the necessary engineering techniques had been developed to allow systems to be built which offered a reasonable operational life expectancy. Secondly it has initiated a significant amount of work over the years on lasers employing compounds of copper that are more volatile than the element. These may then be dissociated by the discharge pulse thus giving the required vapour pressure of atomic copper but at a much lower temperature. Most research in this direction has been concerned with the copper halides that allow operation at between 500-650°C, but work on more exotic compounds has yielded copper lasers that can operate at temperatures as low as 20°C (Andrews et al, 1977). The development of CVLs employing such copper compounds will be discussed in greater depth in Section 1.1.2 (II), later in this chapter.

1.1.2 HISTORY

1.1.2 (I) Elemental copper vapour lasers

On the morning of Saturday 29th January, 1966 a paper was orally presented to the American Physical Society in which it was reported (Walter el al, 1966 a) that laser action had been observed as a result of a pulsed discharge through a mixture containing helium gas and atomic copper vapour in an externally heated alumina tube. Subsequent

presentations, both oral and written (Walter, 1967; Leonard, 1967) developed the theme and laid the foundations for the development of the copper vapour laser as a pulsed laser system offering a unique combination of high pulse repetition frequency (prf) output on two visible lines, pulse lengths in the range of tens of nanoseconds, and both high average and peak powers. The CVL has now established for itself a position in the laser physicist's armoury as a consequence of this unique combination of properties that is at present unchallenged.

Before Walter's announcement of the copper vapour laser in 1966, however, and his more general discussion of the characteristics of the class of cyclic metal vapour lasers, gain had already been reported in other members of the family.

The scene was set in 1965 when Gould described (Gould, 1965) in a supplement to Applied Optics on "Chemical Lasers" some general principles for the use of electron-atom and atom-atom collisional processes both to populate the upper laser level and to depopulate the lower in some potential laser systems. This allowed the use of energy levels considerably closer to the ground state than was the case when relying on radiative transitions to depopulate the lower laser level, as they could be optically metastable, and consequently the potential for considerably greater (quantum) efficiency. Later that same year gain was reported in first lead vapour (June: Fowles & Silfvast, 1965), and then Manganese vapour (December: Piltch et al, 1965). Then, in January of the following year came Walter's announcement of laser action in atomic copper vapour (Walter et al, 1966 a).

Later in 1966 came the paper referred to above (Walter et al, 1966 b) in which Walter set out the criteria for "Efficient pulsed gas discharge lasers" and in which both a copper vapour laser, giving an average of 20 mW at 660 Hz, and an ionised calcium laser, operating on two analogous lines at 854.2 nm and 866.2 nm, were described with respect to these criteria. Gain was measured on the copper green line and the two Ca^+ lines of >58 dBm^{-1}, limited by saturation in their 80 cm tube, and 42 dBm^{-1} on the copper yellow line. Walter quoted a conversion efficiency value of 0.1% for the copper laser, corresponding to the fraction of the energy stored in the capacitor that was detected as laser output. He also mentioned that of the stored charge, less than a tenth had been discharged into the gas before the end of the laser pulse. He employed separate heater elements, however, to maintain the high operating temperature of his lasers. More recent

systems are self-heated, using the energy deposited in the gas by the discharge, and so the ratio of energy stored in the capacitors to energy extracted as laser photons now represents a more useful overall "wall-plug" efficiency which cannot be directly related to the earlier reported values. Although a number of theoretical values for a maximum achievable efficiency have been calculated over the years they have in general been very far from the figures obtained in most practical systems at present which operate around the 1% overall efficiency mark. A notable exception is the HyBrID laser developed at the University of St Andrews which achieves around 2-3% and which will be discussed further in the next section.

Following his initial work, Walter went on to demonstrate the principle of volumetric scaling by increasing the diameter of the plasma tube from 10 mm to 50 mm, and announcing at the following year's meeting of the American Physical Society an increase in the peak power in the green line from 2 kW to 40 kW (Walter, 1967). This was obtained at a pulse repetition frequency (prf) of 1.25 kHz, and an efficiency (excluding the power input to his heaters) of 1.2%. That a 50 mm diameter volume could be filled with a uniform, stable, longitudinal discharge was not initially expected from observations in pure rare gases, however it later became apparent that it is the pre-pulse electron density left over from the previous discharge pulse that ensures the quality of each subsequent one (Gabay & Smilanski, 1980). Whilst acknowledging that his figures were "neither maximum nor optimum values for this geometry" this announcement indicated one of the major means by which CVL output power may be increased, namely by increasing the active volume of the plasma.

In 1972 came the second significant step in the evolution of the CVL with the publication of a paper (Isaev et al, 1972) by the group at the Lebedev Institute in Russia, describing a system in which the power required to raise and maintain the temperature of the plasma tube came from the electrical discharge itself instead of an external oven. The Russian workers presented results obtained from two lasers of different diameters (8 mm and 15 mm), and obtained an average power output of 6 W (on both lines) from the smaller, and 15 W at 18 kHz, and a peak power of 200 kW, with an *overall* efficiency of 1.0% from the larger. They developed their theme further in a paper describing a laser tube appropriate for the discharge heated operation of pulsed lasers based on a number of metal vapours (Isaev et al, 1972).

Although by the early 1970s significant visible laser power had been demonstrated, this was contained in a poor quality beam, of many times the diffraction limit. The poor beam quality is a natural consequence of a high gain, short pulse system in which the light makes only a few transits of the gain length in a resonator employing plane-plane mirrors. In 1974 this position was changed by the introduction by the Lebedev group (Zemskov et al, 1974) of unstable cavity techniques. This enabled divergence of 80 μrad to be obtained. All the elements were now in place for high power, high efficiency, high quality, visible laser light.

Another very significant advance came about in the application of CVLs in the US AVLIS (atomic vapour laser isotope separation) programme with the realisation that a well designed CVL unit would operate even more effectively as an amplifier than as an oscillator and that units could be stacked in series to give much higher powers than could be obtained from a single system. This is the master oscillator, power amplifier (MOPA) configuration (Anderson et al, 1975). This arrangement has the additional advantage that power may be extracted in a high quality beam if a low divergence seeding beam is provided by the oscillator with optimal timing with respect to the amplifier cycle. This is the basis for the injection controlled oscillator configuration (ICO) in which two CVLs operate with coupled unstable resonator cavities, the output being of very high quality for further amplification, if necessary, through a string of amplifiers (Naylor et al, 1986; Warner, 1986). Average powers of hundreds of watts, and then kilowatts, of high quality (ie focusable) visible light were possible, and were soon realised.

Over the years a number of seemingly minor modifications in the design of CVLs have proved to be responsible for significant improvements in performance. These have included modified thermal insulation arrangements to give an improved longitudinal temperature profile for the plasma tube, closer to the ideal top hat type function, and modifications to the laser discharge circuits using saturable inductors, initially as a "magnetic assist", and later as "magnetic pulse compression" (Petr et al, 1983; Nehmadi et al, 1989), although this latter tends to be detrimental to timing jitter. Most importantly however the reliability, simplicity and the ease of maintenance required is now sufficiently good that the performance available from commercial CVLs is accessible to end users who are not specifically laser trained. This, probably more than anything else, has had the biggest impact on CVL acceptability.

1.1.2 (II) Copper vapour lasers using compounds of copper

Parallel to the development of the elemental CVLs with their inherent engineering difficulties associated with the high temperatures required, a number of groups were looking at different methods of producing the necessary density of copper atoms without having to maintain the entire bore of the laser at 1500°C. In 1968 Asmus and Moncur (Asmus & Moncur, 1968) used exploding copper wires to create the copper plasma and in 1972 Russel (Russel et al, 1972) accelerated a heated mixture of copper vapour, argon and helium through a nozzle at supersonic speeds. While offering little to the development of practical CVLs these techniques did demonstrate that by employing a high speed flowing active medium, a longer output laser pulse can be generated, utilising a greater portion of the pump discharge pulse.

A considerably more promising avenue towards building CVLs with lower operating temperatures has been that of using chemical means by exploiting more volatile copper compounds. By far the greatest amount of work in this direction has been concerned with the copper halides. CuI (with maximum output at around 600°C) was tried successfully in 1973 (Liu et al, 1973), and, later that same year, superradiance was observed from CuCl (Chen et al, 1973), with a peak slightly below 400°C. Two years later CuBr was also added to the list with operation at around 450°C (Akirtava et al, 1975; Shukhtin et al, 1975 b) and it is on this latter compound that most copper halide work has been performed over the last few years.

A modification to this approach has been made by the St Andrews University group and uses an elemental copper charge together with a buffer gas mixture consisting of neon together with around 6% HBr, such that the CuBr is generated *in situ* (Livingstone, 1992). This has been dubbed the HyBrID (Hydrogen Bromide In Discharge) laser. It has been shown to be both highly efficient with a maximum efficiency of 3.1% having been reported in the literature to date (Jones et al, 1993) at an output power of 112 W and scalable to high powers with 149 W at an efficiency of 2.4%, and with over 170 W maximum power presently available. These lasers are capable of running in a stable, self-heated mode over a wide range of prfs, offering a very short start up time from cold and operation insensitive to wall temperature over a range of at least 500-800°C (Jones et al, 1992).

The residual product of the Cu + HBr reaction, the hydrogen, has also been shown to offer improvements in both power and efficiency in copper halide lasers (Astadjov et al, 1985; 1988), and other work suggests that this beneficial effect may extend to elemental CVLs (Huang et al, 1986; Hayashi et al, 1992; Withford et al, 1993). Many other additives have been applied to elemental and copper halide lasers in an attempt to increase power, efficiency or both. Vetter & Nerheim (Vetter & Nerheim, 1977) added HCl to a CuCl laser, and Livingstone & Maitland (Livingstone & Maitland, 1989) used halogen (bromine and chlorine) gas in a low temperature laser with walls incorporating lengths of copper tubing in a predecessor to the HyBrID laser.

Two US patents were filed by Karras (Karras, 1973; 1974) for a flowing gas laser incorporating caesium which has resonance levels very close in energy to the copper metastable levels, supposedly offering a mechanism for rapid depopulation of the copper metastable levels to allow very high pulse rate operation. The caesium idea was simultaneously being considered elsewhere (Krause & Bielski, 1974) and has been revived again recently (Saito & Hotuki, 1992), however this last report is at present only available in the original Japanese.

Unfortunately, in common with a number of this class of performance enhancing additives, the addition of caesium suffers from the disadvantage that, in order to depopulate the copper metastable levels sufficiently rapidly to have an effect on the time scale of the laser pulse the caesium population density would have to be so high that it would have a major effect on the copper kinetics as its ionisation energy is around half that of copper and the discharge would be dominated by caesium. As far as depopulating the metastable levels during the inter-pulse period is concerned, as Karras suggests, the rate of electron collisional depopulation is already considerably faster than that required to keep up with the rate of change of thermal population allowed by the cooling of the plasma. It is thus the rate of decrease in the gas temperature (which buffers the electron temperature) that determines the pre-pulse lower laser level population, and it is consequently this that must be accelerated if significantly faster depopulation of the copper metastable levels is to be accomplished. In addition to this a number of studies have suggested (eg Bokhan; 1984, Lewis, 1985) that the thermally determined rate of electron/copper ion recombination also contributes to the limitation of the range of high prf operation in a conventional design CVL. This theory will be discussed further in

connection with the results of Chapter 8 of this thesis. In the gold vapour laser however the frequency range of operation on the (312.2 nm) ultraviolet line is considerably narrower than that of the (627.8 nm) red line, reflecting its much greater thermal population owing to the lower energy of the $^2D_{5/2}$ level, its lower laser level. In the very specific, non-equilibrium case of Karras' flowing gas laser, in which the copper vapour is cooled by expansion through nozzles, the problem of thermal population may be relieved, but in this case metastables (and electrons and ions) can be removed from the active volume by means of the flow.

Both the original CuI and CuBr lasers used a double pulse discharge regime, in which the first pulse was intended to dissociate the copper molecule and the second to pump the laser transition. In a slightly earlier publication, however, Shukhtin (Shukhtin et al, 1975 a) had shown, using the hook method, that the duration of existence of free copper atoms after the dissociation discharge pulse was relatively long, with high populations for at least 1 ms. In this paper he investigated copper iodide and chloride as well as the bromide he was shortly to present and found the temporal profile of the behaviour of the three halides very similar, peaking at around 150 μs. This observation then offered the possibility of repetitively pulsed, and burst mode systems in which, after an initial period during which equilibrium dissociation was established, it could then be maintained. The maximum laser pulse energy available from the continuously pulsed system, however, is not so great as from a burst mode one, which is in turn not so great as that from a double pulse system as, in the latter case, the maximum available energy may be discharged into the second pulse without fear of depositing excess energy into the gas and thus raising the temperature above optimum, and also the pre-pulse copper metastable population is negligible. In burst mode gas heating may be minimised, but an equilibrium metastable population will soon be established, and with it a pre-pulse electron density which will assist with each subsequent discharge, though at a cost to electron temperature. In Chen's CuCl work (Chen et al, 1973) a single pulse, at a 10 Hz repetition rate, was used to perform both functions of dissociation and excitation. Considerable problems with discharge stability were however experienced with the longitudinal discharge. Chen finally resorted to a transverse discharge between pin type electrodes.

The idea of surrendering the longitudinal geometry, with its problems of discharge stability, for a transverse format has attracted a number of workers. Piper (Piper, 1975), employed it on a copper iodide laser, and ten years later Kim and Im (Kim & Im, 1985) undertook to address the considerable high temperature engineering difficulties involved in bringing the technology to an elemental copper system. In 1990 they succeeded in operating a transverse discharge CVL at 5 kHz in steady-state mode (Kim & Sung, 1990). In general, however, this avenue has been abandoned, particularly for elemental CVLs, owing to the problems of maintaining metal electrodes at high temperatures for extended periods. The principal problem is that of the stability of the metal crystallites in the electrodes which denature to powder as a result of decrepitation along grain boundaries after prolonged periods at high temperatures. In addition there are the problems of conductive heat loss down the low inductance, low resistance (electrical and therefore also thermal) feed-throughs to the electrodes, thus demanding increased input power, and differential expansion of electrode materials.

In addition to the halides other copper compounds have been tested for suitability as sources of copper vapour at temperatures lower than those required for elemental copper including copper acetylacetonate in which lasing has been observed at temperatures as low as 20°C (Andrews et al, 1977).

An additional advantage of lower temperature operation is that the reduced outgassing of impurities from the plasma tube and insulation makes long term sealed off operation more feasible, although the first report of a sealed CVL was of an elemental one (Bokhan et al, 1975). Transverse discharge techniques also become somewhat more realistic at lower temperatures.

1.2 APPLICATIONS OF THE COPPER VAPOUR LASER

The unique properties of the copper vapour laser that lend it to specific applications are its ability to provide relatively short (a few tens of ns) pulses of visible laser light at high repetition rates, with pulse energies of the order of a few millijoules, (and consequently peak powers of the order of a hundred kW or more) and high mean power. In addition CVLs may be arranged in chains of amplifier units with a single master oscillator to increase the pulse energy many times. As a result of this unique combination of features there are a number of applications for which the CVL is the laser

of choice, and these may conveniently be divided into those in which it is used to pump a dye laser to provide high prf tunable laser light, and those in which the CVL output is used directly.

1.2.1 AVLIS

Into the first category of CVL pumped dye laser techniques falls AVLIS (atomic vapour laser isotope separation). Different isotopes of any atom exhibit electronic energy levels shifted relative to each other as a result of both the different mass and charge distribution of the nucleus. As a result, absorption lines of different isotopes display a slight isotope shift with the result that narrow-band light, carefully tuned, can excite one isotope selectively, in a number of steps, to ionisation. The ions thus generated may then be collected on a charged plate to allow highly selective isotope separation to be accomplished. Perhaps the most industrially important application of this technique is in the enrichment of uranium for the nuclear power industry. In order to obtain maximum throughput a high prf dye laser pump source is required with sufficient power to saturate each step in the ionisation with a repetition rate capable of matching to sonic flow rates of gas, and for this the CVL in an amplifier chain configuration is ideally suited.

1.2.2 RIMS

A similar application to AVLIS is that of RIMS (resonance ionisation mass spectrometry) in which a number of pulsed dye lasers are so tuned as to ionise a single species selectively, in a number of steps. The ions so formed are introduced into a time of flight mass spectrometer thus providing an extremely high degree of selectivity (around 1 in 10^{12}) in the analysis of samples. Again the high available prf allows the whole available sample to be used, thus ensuring efficient operation.

1.2.3 PDT

A third application in which the CVL offers a suitable pump source for a dye laser is in the medical field of photodynamic therapy (PDT) in the treatment of cancer. A therapeutic agent is administered in an inactive form and then allowed to permeate the body for a few days until it has been cleared out of most healthy tissue, whilst being selectively concentrated in tumour cells. The drug may then be optically activated to its

operative form by irradiation with light of an appropriate wavelength to be transmitted through tissue, thereupon destroying the carcinoma cells in which it resides. In this way many of the unpleasant side effects of chemotherapy may be avoided, or minimised, by limiting the distribution of the drug in its cytotoxic form to those cells which it is desirable to kill. The activating laser radiation may be delivered down one, or a number of optical fibres to allow access to non superficial tumours, and to ensure even destruction of extended structures. In this application it is the ability of the CVL to generate high repetition rate pulses, with high peak powers in comparison with cw pump systems, which enables dye lasers of simple monolithic design to be employed. Such dye lasers have very much less stringent requirements on optical stability and alignment as they will inevitably be driven well over threshold by each pump pulse, giving a high gain system. This means that the whole system can be much more robust, a very desirable quality in a device for use in an hospital rather than laboratory environment. The CVLs available for this kind of work can be air cooled, compact and relatively mobile, requiring no more services than a single phase, 13 A wall plug, a direct consequence of its high efficiency. The 627.8 nm line of the gold vapour laser can also be used in this application.

In all of the foregoing applications the CVL is used to pump a dye laser. However there are several important applications in which the laser output is used directly.

1.2.4 MATERIALS PROCESSING

Work is currently being undertaken on the use of the CVL in materials processing. Once again the high repetition rate, high peak power and relatively short wavelength offers a number of advantages for the high quality micro cutting and drilling of thin metal foils with minimal build up of collateral debris. The mechanism involved in the processing of metals using the CVL is one of direct ablation of metal by the laser pulse, rather than that of oxygen assisted combustion, or heat absorption followed by removal of the molten metal, as are employed in more conventional CO_2 or Nd:YAG systems. Consequently the depth of metal around the cut edge shows a region affected by heat generally considerably less than 1 μm deep. Using higher power systems work

is currently under way on the high quality drilling of much thicker samples of metals such as copper several millimetres thick. Recent results from studies of cutting 1 mm thick copper sheet has demonstrated the extremely high quality character of the cut which, together with the very small quantities of material removed, make it ideal for applications in which both resultant pieces of material must be utilised and possibly fitted together again later.

1.2.5 ULTRA-HIGH SPEED PHOTOGRAPHY

The short pulse length, high prf character of the CVL makes it highly suitable for photographic applications as an ultra-fast, high repetition rate stroboscope. This allows the capture on film of turbulence in fluid flow, ballistics, turbines, spray droplets and fine (eg 10 μm thick) threads in textile spinning processes, with the advantages of high intensity, compared with conventional flash sources, much shorter pulse lengths, and good collimation (Walder, 1990). Even operating at 20 kHz or more the duty cycle of the light pulse is low enough to keep absorption, and thus subject heating, to a minimum. In addition, a number of optical manipulations may be performed such as fibre optic delivery, back lighting using a retro-reflective screen to allow Schlieren photography of shock waves and the use of a green filter in front of the camera to allow photography in the presence of other light to improve contrast. The flexible response of the CVL to a range of prfs, combined with its ability to accept an external trigger pulse allows it to be synchronised easily with a high speed, multi-frame camera.

1.2.6 ADAPTIVE OPTICS

The problem with Earth-based astronomical telescopes is that between them and the objects that they are attempting to observe there is a highly turbulent atmosphere which can cause distortion of the observed wave-front. This may be observed when viewing a point light source such as a star with the naked eye as the familiar twinkling, caused by interference of light having followed slightly different paths through the atmosphere. When a telescope is used to view the object the light from it is brought no longer to a point focus, but an extended image, and the effect of the turbulence is to cause blurring of the image. This has the effect of placing a maximum value on the resolution obtainable from Earth-based telescopes (in the form of a maximum telescope

diameter beyond which no further improvement in resolution may be obtained) dependent upon the nature, and thickness of the atmosphere above the telescope.

If the optics of the telescope, however, have the ability to deform minutely in order to restore the original quality of the observed wave-front on a time scale fast enough to counteract the effects of the turbulent atmosphere, the resolution can be considerably improved. In order to accomplish this it is necessary to have a reference wave-front, the effects of the atmosphere upon which it is possible to measure. The star of interest itself may be used. By sampling a small proportion of the incoming light, after the telescope, and measuring the distortion of the wave-front, the phase conjugate of the observed distortion can be applied to an optical corrector component, such as a deformable mirror, to compensate for it. If the corrector is included in the train of optics before the beam sampler then this latter component will be able to monitor the efficiency of the corrector in ensuring that the observed wave-front is at all times planar. The drawback of this scheme is that in general the object of interest is of very low intensity and to deprive the final image of even a small proportion of the available light, in the beam sampler, is undesirable. An alternative strategy is to make use of a neighbouring star, however there is not often a suitable one available of sufficient proximity not to introduce errors owing to angular anisoplanatism.

It is possible to generate an artificial guide star using the Rayleigh back-scattered light from a high intensity pulsed laser, whose beam may then be positioned as close as desirable in angle to the object of interest. To accomplish this the laser source must provide high energy pulses in order for sufficient energy to be scattered in the backward direction to be detected, short pulse length such that, once defined in height by gating, the Rayleigh guide star is of short, well defined length. To be able to make corrections to the optics on the millisecond time scale required the pulse repetition rate must be of the order of multi-kilohertz. Once again this combination of requirements is met admirably, and uniquely, by the CVL.

Recent research in this field has been concerned with the use of a CVL pumped dye laser, tuned to a sodium resonance line, to generate fluorescence from sodium naturally present in the ionosphere. This has the advantages of much higher intensity than Rayleigh back-scatter, and a guide star located above the majority of the atmosphere, rather than within it, and with a better defined height.

1.2.7 OTHER APPLICATIONS

The green copper line lies in a region of the spectrum that suffers minimum absorption by sea water and is consequently suitable for underwater range-finding and the depth measurement of coastal waters (Feldman et al, 1982). The yellow copper line is also useful, finding applications in dermatology in the treatment of "port-wine stains".

1.3 SUMMARY OF CVL DIAGNOSTIC RESEARCH

The types of research performed so far to advance our understanding of the operation of the copper vapour laser, and to a certain extent on other members of the family of cyclic metal vapour lasers, may conveniently be divided into three categories. Firstly (historically) is the empirical approach whereby modifications are made to the system in its more usual form of the day, and the effects are observed and reported. The results of this process of advancement I have already discussed (Section 1.1.2), so here I will concentrate on the more diagnostic avenues of research. Secondly there are the non- or minimally-perturbing measurements of a parameter of the laser either directly, or by using some form of probe. Such measurements are often made in conjunction with making changes in the operating parameters of the laser, and the interpretation of the observations. Finally has come the theoretical work of attempting to generate a mathematical model of some part, or all of the kinetics involved in the operating laser. As such models become more accurate and reliable they allow us an insight not only into the laser as it presently operates, but also the probable results, either beneficial or deleterious, of making specific changes to the system.

1.3.1 MEASUREMENTS

In order to build up an understanding of the mechanisms determining the operation of the CVL system it is desirable to know the kinetics involved both directly in laser action, and indirectly in setting up the thermodynamic and kinetic environment for it. There are however a number of problems with making the measurements required to build up the understanding of the kinetics that would be desirable. Although off line experiments to determine such parameters as copper transition oscillator strengths (Corliss, 1970; Bielski, 1975), electron collision cross-sections (Trajmar et al, 1977) and the copper vapour pressure curve (Dushman, 1949) may usefully be performed on passive

vapour cells, the majority of measurements must be made on the plasma of an operating CVL. This means attempting to interrogate an environment experiencing plasma tube wall temperatures of the order of 1700 K, in the case of the elemental CVL, and axial gas temperatures 1000 K or more greater, in the presence of discharge current pulses peaking at many hundreds of amps, with breakdown voltages typically of 10-20 kV, and with an intra-cavity laser flux density of hundreds of MWm^{-2}. In addition this environment is changing with time, is not at thermodynamic equilibrium for at least part of its cycle, and displays considerable radial and a certain amount of longitudinal heterogeneity. In order to obtain useful information in the face of these difficulties there are two levels of approach.

Firstly a significant amount of information may be obtained simply by passive techniques, measuring only those parameters that may be directly observed external to the laser. The voltage pulse may be measured both at the thyratron and on the laser head using high voltage oscilloscope probes. The discharge current through the laser may be monitored with a 'Pearson' type current coil, or a low inductance shunt, and the power input to the plasma may be calculated using the time averaged current and charging voltage, or the energy in the storage capacitors. The laser pulse may be studied in terms of its two components at 510.6 nm and 578.2 nm: their temporal and spectral profiles, intensity and relative timing with respect to each other and, for instance, the voltage pulse. These may all be done as a function of radial position. The average power output of the laser may be measured, and its efficiency in terms of watts of laser light out per kilowatt of power employed, or millijoules per pulse output for each joule of input energy, and the specific energy, and average or peak power in terms of μJcm^{-3} or $(k)Wcm^{-3}$ may be derived. Likewise the change in divergence of the laser light over the duration of the output pulse may be observed, telling us of the number of round trips, of the particular optical cavity employed, it has performed. The results of these measurements may then be compared as, ideally, one operating parameter is changed: the buffer gas pressure, the copper density, the pulse repetition frequency (prf), the charging voltage, the input power or the storage capacitance.

All these measurements may be made without invading the laser plasma in any way, however in order fully to understand the processes involved in the operation of the laser, and hence how optimal use may be made of them, we need to know how the

populations in the different atomic and ionic levels of the copper, the buffer gas, and, if applicable any relevant additives or impurities, evolve with time through the discharge pulse and over the course of the interpulse period, and how they are distributed radially. In addition we need to know the electron density, the electron and gas temperatures, the optical power density within the cavity, the radial electric field, the mean time between collisions for each of the species, as well as the nature of those collisions, all as a function of time and position again, and much more. In order to build up a practical, working model, however, not all of these parameters need be either measured or known, though the more data that can be accumulated the more confident of any theory or model that fits them it is possible to be.

In obtaining these measurements not only must the nature of the CVL plasma be contended with, but also it must not be perturbed in any more than a negligible way. As a result most measurements to date have used one of a range of optical diagnostic techniques by which an optical signal, either originating within the test laser, or introduced as a probe beam, is interrogated in terms of its amplitude, line-shape or phase to yield information concerning its source, its path or both.

The most elementary of these optical techniques is the simple observation of the amplitude and duration of the copper laser pulse as described above, and measurements of this kind have naturally been performed on even the very earliest systems, if for no other reason than to optimise the operating conditions empirically. From the beginning the output power, or pulse energy, was related to that put into the system in order to calculate the efficiency, and this, in addition to the maximum power or pulse energy, gave a more sensitive guide to how well it was optimised.

1.3.1 (I) Hook measurements

Soon after the introduction of the CVL direct measurement of population densities began to be desirable. This first arose as an attempt to evaluate the dissociation of copper halide molecules into free copper atoms and the relevant halogen, to compare different halides. In this work Shukhtin (Shukhtin et al, 1975 a) used the hook method to measure the population density of ground state copper atoms, and from the results he obtained he went on to build the first of a dynasty of copper bromide lasers (Shukhtin et al, 1975 b). The technique he employed, originally proposed in 1912 (Rozhdestvenskii,

1912), fulfils many of the criteria for a "good" diagnostic procedure. The probe introduced into the laser is a beam of light of low enough spectral intensity to perturb the investigated population by a negligible amount. This is as a result of the fact that the probe beam is at least quasi broad-band. It has the added advantage of being accurate as a result of making use of the spectral region in the far wings of an absorption line, and consequently highly insensitive to line broadening mechanisms. The method will be discussed in detail in Chapter 3, here it is merely considered in terms of its access to valuable data without impact on any parameter of interest.

As the population densities found in the copper atomic levels of interest are generally high enough to be accessible by the hook method, it has stood out over the years as the method of choice for population density measurements. It has been employed in a number of very high quality studies, including measurements of upper and lower laser levels and the copper ground state. In the early days of the technique it was applied to the measurement of ratios of oscillator strengths in spectral doublets, eg Prokofiev (Prokofiev, 1924; 1927) looking at potassium, then to both the measurement of oscillator strength in known population and measurement of populations in excited levels by combination with emission techniques (Ladenburg, 1933). These measurements however were made, of necessity, under steady state conditions, usually using a carbon arc light source.

With the introduction of electronic flash tubes the potential was available for time resolution, but this was typically of the order of 1 μs or more because of the requirement for sufficient intensity to expose a photographic emulsion. In Shukhtin's measurements, for instance he claims time resolution of 3 μs. Once dye lasers were applied to the technique, however, time resolution of the order of a few nanoseconds was immediately available, (Miyazaki et al, 1975; Miyazaki & Fukuda, 1977), increasing the power of the hook method in the study of time dependent phenomena enormously. Whereas before this, in his classic review of the hook method (or hakenmethode) Marlow had been prompted to write "Although the hakenmethode is one of the most accurate methods of f-value measurement, it is infrequently mentioned or employed as an experimental tool in the English literature." (Marlow, 1967), it soon became far more popular, proving the mainstay of population density research in CVLs. From 1980 Smilanski's group in Israel has used the hook method in a number of studies into the CVL (Smilanski & Levin,

1980; Tenenbaum et al, 1981) with the Lawrence Livermore National Laboratory (LLNL) being involved soon after in collaborative projects (Smilanski et al, 1981) and on their own (Warner & Seeley, 1983; Molander, 1989) and some excellent studies by Brown, initially at the University of New England, Armidale, and then Macquarie University (Brown, 1988; Brown et al, 1989; 1990). In parallel with these studies there have been a number of appraisals of the hook method, and suggested improvements (Bachor & Kock, 1980; Sandeman, 1979).

1.3.1 (II) Other techniques

Although the hook method has been the primary active diagnostic technique employed in studies on the kinetics of the CVL, it has been by no means the only one. As will be discussed in Chapter 3 a major limitation of the hook method is its lack of sensitivity, and consequently if small population densities must be measured absorption techniques must be employed. This has particularly applied to the copper metastable population, particularly in the late afterglow, for which it is often convenient to use the output of a second CVL as a probe beam source (Lewis, 1985; Izawa et el, 1989).

In addition to these studies measuring atomic population densities there have been a number of projects to measure other plasma parameters including electron temperature, electron density and gas temperature. The first of these was attempted in 1975 by measuring the incoherent microwave radiation emanating from a copper chloride laser tube to measure the electron temperature as a function of laser tube temperature (Sovero et al, 1975). Many studies have been undertaken to measure the electron density in CVLs. The first was in 1977 (Batenin et el, 1977) and employed a 10.6 μm wavelength laser probe source to measure it during the interpulse period, however owing to a time resolution of ~ 1 μs the electron density during the discharge current pulse was calculated using measured current and voltage profiles. Since then most attempts to obtain electron density values in the CVL have attempted to measure the Stark broadening component in observed lines of hydrogen impurity (Lewis, 1985), sometimes attempting, by the use of multiple lines from the Balmer series, simultaneously to evaluate the Doppler broadening and thus evaluate the gas temperature (Blau et al, 1992; 1993). One drawback of this approach is the extreme low intensity of the Balmer spectrum obtained from the hydrogen impurity in the laser, greatly exacerbated if any attempt at radial resolution

is made. In addition, the calculations to arrive at an electron density figure involve the deconvolution of theoretical Stark and Doppler broadening profiles (both typically about 5-40 GHz) from a complex lineshape, with fine structure on the same scale.

1.3.2 THEORETICAL MODELLING

1.3.2 (I) Early models

As early as 1967, the year after the first announcement of laser action in copper vapour, the first paper was published presenting a mathematical model of the kinetics of the copper vapour laser (Leonard, 1967). In it Leonard also addressed the reasons for wanting to generate a theoretical model, specifically of the CVL, and described it as being "not only to perform parametric studies of the laser's performance on a computer, but also to guide future experimental studies in the most promising directions". Although much high quality experimental work has been performed on the CVL, as discussed in Section 1.3.1 above, this has not negated the need for computer modelling, for the reasons given by Leonard, and on the contrary, with a steadily increasing body of detailed data against which to confirm or refute predictions of a given model, more confidence may be placed in any model that appears to simulate successfully the observed kinetics. If the only parameters to be fitted by a model are pulse length and energy, merely obtaining a reasonable match for these quantities is somewhat less convincing than when predicted temporal and radial behaviour of a number of atomic levels in both the copper and the buffer gas, as well as electron density and gas temperature profile may also be compared.

1.3.2 (II) More sophisticated models

There are a number of factors in the operation of the CVL that render its modelling far from trivial, even assuming that all the required cross-sections are known accurately. Indeed the measurement of cross-sections is in itself the subject of much research. For a start, almost all elemental copper, and many copper halide lasers, are run as high prf, repetitively pulsed devices. For this reason each laser discharge-delay cycle may not be considered in isolation as the thermodynamic environment prior to each discharge pulse is determined by the state of dynamic equilibrium set up and maintained by the current pulses and relaxation periods prior to it. As many of the parameters input

to the model, such as prf, charging voltage and capacitance values, contribute to determining this pre-pulse environment in addition to their immediate effect upon an individual discharge cycle, a model that considers only a single pulse, in isolation with the assumption of initial conditions, cannot be as good as one which by many iterative cycles sets up its own pre-pulse equilibrium conditions.

Further complications arise from the fact that, within the plasma tube, radial homogeneity may not be assumed. For small diameter tubes this may be confined to considering a radial gas temperature profile, electron temperature profile and consequent population density distributions, however once a diameter of around 40 mm is reached additional temporal effects must also be considered as the plasma skin depth effect, owing to the transmission of a high speed current pulse through the conducting medium, begins to be significant.

Longitudinal homogeneity may also not be assumed since, over the length of the discharge between the two electrodes, the gas temperature changes by a very large factor from several hundred Kelvin to about 2,500 K, or more, on axis. For this reason, while the kinetics over the "active length" of the plasma tube may be dominated by the copper vapour, in the region close to the electrodes (where the gas and plasma tube wall temperatures are far lower and the copper vapour pressure is negligible) all inelastic electron collisions must be with the neon. Clearly, in the end region the neon must provide *all the* electrons needed to maintain continuity of current.

Finally, in the situation where the electron density is not high enough to ensure sufficiently rapid Coulomb relaxation between electrons, and where many inelastic electron-atom collision processes tend to deplete the high energy tail of the electron energy distribution function (EEDF), it may no longer be satisfactorily considered as a simple Maxwellian (Vriens, 1973) characterised by a single electron temperature, but rather as a distribution with two, or more (Vriens, 1974), components.

1.3.2 (III) Kushner models

It has been the models in which the considerations discussed above have been satisfactorily included that have marked significant advances in reliability. In 1981 Kushner first published his "self-consistent" model in which many discharge cycles were run through iteratively until a consistent solution was obtained (Kushner, 1981).

Although in the original publication of this work its predictions were compared with experimental observation only in respect of laser output power, discharge current and optimum prf at given tube temperature, when presented later that year at the International Conference on Lasers '81, under the acronym CuKIN (Warner & Kushner, 1981) its predicted results for population in the green laser levels were compared with those obtained using the hook method with extremely good agreement. In 1983 the radial effects discussed above were also included into what was now a very powerful model, now christened CuRAD, and published in a classic paper by Kushner and Warner (Kushner & Warner, 1983).

1.3.2 (IV) Carman models

In 1993 a model incorporating Vriens' methods of describing the EEDF in terms of a bi-Maxwellian (Vriens, 1973), with a bulk component, up to the first excitation energy of neon, characterised by temperature T_b, and a high energy tail above that, characterised by temperature T_t ($T_b > T_t$), and where the vast majority of the electrons fall into the bulk group, has been presented by Carman (Carman et al, 1993). The predictions of this model have been compared with the results of a high quality hook method survey of a number of excited state densities in the copper and neon (Brown, 1985; Brown et al, 1989; 1990) and have shown extremely good agreement. In addition this model has considered the kinetics in the cool end regions of the plasma tube explicitly. The hook measurements had been made on an 18 mm diameter laser, and it is to this that the model has been applied and consequently, although thermodynamic radial effects have been considered in detail in both the experimental and theoretical work, the skin depth effect had not.

Work is currently under way to extend the application of this model to larger bore devices by incorporating the refinements of Kushner and Warner (Kushner & Warner, 1983).

As work continues on mathematical computer models, and computer processing power steadily becomes greater and cheaper, it can be expected that the contributory processes will be better understood and better incorporated in an iterative process of advancement of understanding of CVL kinetics. Through this, it is hoped, will come an

improved ability both to interpret the empirical observations of improvements made, and to predict potential new lines of investigation by which the copper vapour laser may realise its full potential.

1.4 GENERAL REMIT OF THE PRESENT STUDY

In spite of the large number of experimental studies that have been performed on the CVL, a few of which have been referenced in Section 1.3.1, all those appearing in the literature to date have suffered from the same flaw. Although many of the parameters have been measured somewhere in the world at some time, no one has yet published a full set of measurements of all the accessible plasma parameters. Such a set should ideally be made on a single laser, under identical operating conditions, in a non-perturbative way, such that they may all be related together with confidence as offering a comprehensive parameter map of that system. Individual and groups of measurements have been made on a wide variety of CVLs, with a wide range of diameters and lengths, operating frequencies, capacitance values, charging voltages, discharge speeds, power input, and different wall temperatures and copper densities. With measurements made on such a heterogeneous assortment of devices their results may not be directly compared. Only when a detailed parameter map of a single system is available can the mathematical models really be tested, their worth evaluated and, once satisfactory agreement obtained, predictions trusted.

It was the acquisition of such a coherent body of data that formed the basis for the present study. Population density measurements were to be made of the copper ground state, the upper and lower laser levels and preferably one or more additional copper levels and a neon metastable level. The electron density also should be measured. All measurements should be made on the same laser system, operating under identical, standard, lasing conditions; should be time resolved, with sufficient detail, radially resolved and represent "best practice" in terms of relative and absolute accuracy, and thus should be as free from assumptions as possible. In addition a full set of the "passive" measurements of discharge current and voltage, along with all the operating parameters of the laser should be recorded to accompany them.

If possible an experimental facility should be established that, in addition to providing the results required for this study of measurements made on a laser under

standard operating conditions, should allow the convenient repetition of such measurements on the same system under conditions of non-standard operation, electrical, mechanical, or other modification, or on an alternative system such that comparison might be made.

1.5 THE LASER UNDER INVESTIGATION

The laser chosen for this study was originally an Oxford Lasers (OL) model CU-25: a 25 W, water cooled device with a plasma tube of 42 mm bore and a concentric 200 mm diameter earth return path incorporating the water cooling tubing. As the original plasma tube had experienced many hours of operation, and was cracked, it was decided fairly early in the project to replace the entire laser tube with one of slightly more modern design offering 40 W average output power from a plasma tube of the same dimensions by the maintenance of an improved longitudinal thermal profile. Despite the fact that neither the laser head, nor the discharge electronics represented the present "state of the art", this was felt to be unimportant provided that all the measurements could be made on it under a standard set of operating conditions.

Once the upgrade had been completed and the desired "running in" period undergone a process of optimising the system, within the confines of the "standard" operating parameters for the laser, was undertaken to ensure that it was running to its best ability.

In addition to the new tube a few minor modifications were made to allow the necessary measurements to be made conveniently. Firstly, two new rear cavity mirrors were coated (in-house) on fused silica substrates to allow the investigative probe beams to be coupled into the CVL cavity. For measurements at wavelengths well away from the copper laser lines the special dielectric coating had a nominally high reflectance at the copper laser wavelengths, but high transmission elsewhere, allowing good transmission at, for example, the copper resonance line wavelengths. Unfortunately although this coating did exhibit $<0.5\%$ transmission at both laser wavelengths on the spectrophotometer, once the laser was running at full output power sufficient had been absorbed to cause generalised heating of the mirror with the result that around 4 W of laser light, predominantly yellow, leaked through. It is not thought, however, that this will have had a significant effect on the ground state density results.

For those measurements to be made at the laser wavelengths, or close to them, it would not have been possible to have manufactured a mirror to have provided optimal optical feedback for the laser cavity, whilst allowing a significant fraction of the probe beam to have been coupled in. For this reason a mirror was made up using a standard high reflectance (HR) coating, but in which a slot of around 2 mm width had been left uncoated across the diameter of the substrate. To ensure that the "shadow" of this uncoated portion did not coincide with the region to be interrogated by the probe beam when this mirror was used the entire cavity of the CVL was tilted at an angle of around 0.3° to the horizontal, corresponding to a drop of 3 mm in 550 mm, being that required for the "shadow" to clear the probe beam satisfactorily by the time they entered the plasma. In this way even measurements made at the copper laser wavelengths were made on actively lasing plasma.

In order to make the electron density measurements in which a two colour probe beam was used (see Section 4.3 for details), employing both 670 nm and 10.6 μm radiation, a completely new set of windows and mirror substrates was required for the CVL that would not only transmit both probe wavelengths adequately, but could also transmit well the copper laser wavelengths and the black body radiation from the CVL plasma tube. Absorption of either could cause both potential problems with beam steering and, more significantly, the risk of thermal damage. BaF_2 was chosen as the most suitable material for both the plasma tube windows and the cavity mirrors and so, for the electron density measurements, three uncoated disks were used for the windows and output coupler.

A fourth disk was coated in-house with a cryolite and ZnS coating which was intended to be HR at the copper laser wavelengths and fairly high transmission at the red and 10.6 μm. Unfortunately the coating turned out to be highly absorbing at 10.6 μm by which time there was insufficient time to have another made up and consequently the electron density measurements had to be made under non-cavity conditions. Whilst this was obviously not ideal it is considered that the intra-cavity radiation field during the CVL laser pulse is likely to have negligible effect on the production, distribution or loss of electrons. In general, the presence or absence of an optical cavity will have negligible effect on the majority of parameters of the laser, the laser levels excepted, but all measurements (with the exception of the electron density as discussed above) were made

in the presence of a cavity for the sake of consistency. It did have the ancillary benefit that general performance of the laser could be monitored over the course of the project in terms of laser output power, which ensured that the system was always operated under the same conditions.

Apart from the modifications to the laser cavity necessitated by the measurements to be made, it was also necessary to be able to monitor both the voltage on the laser head and the current flowing through the laser tube. In order to accomplish the former holes were made in the high voltage end flange of the CVL, and in both the earth return top plate and the outer case of the laser head above so that the 4 mm plug of a Tektronics high voltage probe could be inserted into the flange.

To monitor the current flowing through the laser three protocols were tested. The first two made use of a modified earth return top plate which included a 2" wide section onto which a Pearson model 110A current monitor could be slipped, and into which, also, was incorporated a low inductance, 20.1 mΩ resistance section with a BNC socket wired across it. The third probe consisted of a Pearson model 2878 current monitor positioned around one of the eight identical 6 mm bolts holding the laser earth end flange onto the (water cooled) concentric earth return path. Owing to electrical noise problems (and the desirability of being able to assess accurately the proportion of the current being monitored) the probe on the earth end stud was finally selected and a bulkhead BNC adapter was built into the laser head case through which connection could be made to the probe.

An additional set of modifications to the laser head was required in an attempt to minimise the rf electrical noise radiated by the discharge pulse and induced and capacitatively coupled current pulses in the case of the laser head and the steel-topped optical table upon which all the experimental apparatus was mounted. Aluminium foil was wrapped around the umbilical connecting the laser head to the CVL power supply unit (PSU), in which its thyratron tank was situated, and earthed at both ends, and electrical insulation of the laser tube mountings from the case combined with low impedance separate earthing of the optical tables brought the problem under control.

Finally it was noticed from initial experiments consisting of a series of measurements of the copper ground state population density, over a period of about an hour, that a small but observable drift in population occurred. This correlated with, and

was attributed to, a very small drift in head voltage over time probably as a result of slight variations in the laboratory power supply as heavy power users turned equipment on and off. In an effort to minimise the effect of this the test laser PSU was connected to a voltage stabiliser. In addition to this the entire experiment was automated, as discussed in Chapter 3 and Appendix 1, which had the effect of reducing the time taken for the measurement of a complete sequence of time points from $\sim$50 minutes to $\sim$5 minutes. Following these precautions drift was no longer a problem.

By this combination of fairly minor modifications to a standard commercial CVL we converted it into a test rig in which access could be gained to all the parameters of interest.

Parameters of the test laser	
Plasma tube diameter	42 mm
Plasma tube length	1500 mm
Buffer gas	Neon
Buffer gas pressure	25 mbar
Pulse repetition frequency	6,500 Hz
Charging voltage on storage capacitors	16 kV
Power input (based on stored energy)	5.8 kW
Average laser power output	40 W
Plasma tube wall temperature	1700 K
Storage capacitance	7 nF
Peaking capacitance	2 nF

Table 1.1

1.6 OUTLINE OF THE REMAINDER OF THESIS

In Chapter 2 the measurements to be made will be discussed in more detail. Not only will the question of which populations and parameters should be studied be addressed, but also some of the information potentially available from such measurements. A number of phenomena that will be encountered in attempting both to

make, and to interpret such measurements will be discussed. The issues of both the temporal and spatial resolution required of the measurements will be discussed, and the phenomena of ambipolar diffusion and the skin effect will be addressed. Finally the origin of the radial gas temperature profile within the plasma tube will be considered and an attempt made to calculate the axial gas temperature on the basis of power dissipated in the plasma and the thermal conductivity of the neon buffer gas.

In Chapters 3 and 4 the experimental details of the measurements of atomic level population density and electron density by the hook method and infra-red refractive index measurement respectively will be described in terms of both theory and practical details. The advantages of the techniques used over alternative methods will be discussed as will their limitations and accuracy.

In Chapter 5 a study into the nature and temporal behaviour of the discharge current pulse within the CVL will be presented. The deductions drawn from the results obtained will be discussed, and their significance and implications considered.

The results of a study into the origins of the observed radial dependence of the timing of the onset of gain in the CVL, undertaken on a 100 W laser with 60 mm diameter plasma tube, will be presented in Chapter 6. The relative importance of discharge related effects, such as the skin effect and the radial pre-pulse electron density profile, will be compared with laser kinetic effects. The difference observed between the two copper laser lines will be discussed.

In Chapter 7 the results obtained from the hook method measurements of population densities in a number of atomic levels in the copper and the neon buffer gas on the axis of the plasma tube will be presented. The results will be discussed, and inferences drawn from them. The shapes of the plots of population density against time will be analysed, and the possible significance of the timing of observed features considered. Finally a speculative plot of electron temperature during the discharge pulse and early afterglow will be presented, based on deductions made from the population density measurements.

The measured electron density as a function of time, first on axis, and then as a function of radial position in the plasma tube will be presented in Chapter 8, and the significance of the results discussed. The significance of the pre-pulse electron density

will be discussed, and related to the change in electron density during the discharge. The observed rates of decay of electron density will be examined and the form interpreted.

In Chapter 9 the timing and shapes of the 510.6 nm and 578.2 nm laser pulses as a function of radial position will be considered and related to the results of the study of Chapter 6. The radial variation of peak pulse height will also be considered. The results of measurements of atomic population densities, made at a number of radial positions in the plasma tube will be presented. The full time and radially resolved population density results will be examined and related to the timing and radial profile of the gas temperature, electron density, electron temperature and the timing of both laser pulses.

In Chapter 10 the conclusions drawn from the study, the success of the project, and the potential for future work will be examined.

2 MEASUREMENTS AND CONSIDERATIONS

2.1 GENERAL REMARKS

As was suggested in the previous chapter, the number of results desirable for a full understanding of the kinetics of the laser under a given set of operating conditions, and the number that are truly necessary for reasonable confidence that a particular hypothesis fits the facts in all significant respects are very different.

As discussed in Chapter 1 the measurements to be made can be divided into two broad fields: those that involve the monitoring of the "external" parameters of the laser: the nature and timing of the output laser pulse, the voltage and current characteristics of the discharge pulse and, looking a little deeper, the plasma tube temperature; and those that involve the direct measurement of the plasma parameters: atomic population densities in the copper and buffer gas, electron density and, ideally, either directly or indirectly, electron energy distribution function (or, more readily, a representative electron temperature) and gas temperature.

2.2 TEMPORAL RESOLUTION REQUIRED

2.2.1 DURING DISCHARGE PULSE

Owing to the nature of the CVL as a pulsed laser all measurements must be made with sufficiently high time resolution to follow the time-dependent behaviour of the population, or parameter, under investigation. The absolute value of this time resolution depends upon both the parameter or population being measured and also the position in the laser cycle and need not, therefore, be constant for a given measurement. At one extreme, early on in the laser cycle, during the discharge current pulse, direct collisional excitation of the copper ground state rapidly populates a number of atomic (and ionic) levels, most notably the upper laser levels. Almost immediately this must compete with stimulated radiative depopulation to the lower laser levels, a process associated with the travelling wave of laser radiation. If the measurement technique is to follow the variation in the upper laser level population over this period faithfully it should have time resolution of at least half the period of the fastest phenomenon likely to give rise to structure in the parameter under investigation. In the present case this corresponds to the

round trip time of the wave of laser radiation within the optical cavity. For the cavity around the test laser which is 2288 mm long this corresponds to a value of 7.6 ns. As was hinted above this need not be maintained over the full time course of the laser cycle provided that the time constants for the processes determining the value of the parameter being studied at other points in the cycle are known to be longer.

2.2.2 EARLY AFTERGLOW PERIOD

In the absence of the laser radiation field giving rise to stimulated emission from the upper laser levels the time constant of the discharge current pulse is considered. In the test laser it displays a rise time of 100 ns, a ringing period of around 270 ns and a total duration of around 1.5 μs. Following the cessation of the current pulse it is dependent upon predominantly three body, electron-mediated recombination to reduce the ionic population and feed the high lying atomic levels (Lewis, 1985), collisional and radiative processes to bring the excited atomic level populations back to thermodynamic equilibrium with the ground state at the electron temperature, collisional energy loss mechanisms to bring down the electron temperature, and, possibly the provision of high energy recombination electrons to tend to buoy up the electron temperature (so called recombination heating of the plasma (Petrash, 1990)).

2.2.3 LATE AFTERGLOW PERIOD

As the measurements extend further into the interpulse period it is likely that, in general, the time resolution demanded will be decreased, however the feeding of the population in the copper metastable lower laser levels, initially by laser action, later by spontaneous radiative (and collisional) processes, must also be considered, and likewise the effects of recombined population as it cascades through the term diagram.

In considering the time resolution required to observe other parameters, such as neon population densities and the electron density, similar considerations must be addressed, though without the effects of stimulated emission.

2.3 SPATIAL RESOLUTION REQUIRED

In determining the spatial resolution required it is necessary to be able to obtain a sufficient number of radial data points to be able to assess the radial profile of the parameter in question at a given time point. This may be a relatively complex function with the combined effects of the plasma tube wall providing a sink for heat, as well as a site for additional recombination and depopulation. The deposition of energy is into the bulk of the gas by the discharge, however it may only be lost at the wall, consequently giving rise to radial heat flow and thus a radial temperature profile. The skin effect, as a result of a high effective frequency current pulse gives rise to non-simultaneous, and consequently non-homogeneous excitation across the diameter of the plasma tube. The higher diffusion coefficient of electrons with respect to the ions causes charge separation until the retarding effect of the generated field on the mobility of the electrons causes them to be retarded while the diffusion of the ions is enhanced until both species diffuse at the same rate, characterised by the ambipolar diffusion coefficient. These effects are likely to give rise to powerful secondary phenomena such as radial particle density profiles and electron density and temperature profiles, giving the potential for significant excitation and de-excitation rate differences. When combined these effects are likely to generate radial profiles of some parameters that could be fairly complex, in addition to values that in some cases fall very rapidly to zero at the plasma tube wall. These effects will be discussed in greater detail elsewhere.

In view of the foregoing considerations it would be desirable to specify spatial resolution on the scale of the finest radial structure likely to be encountered, namely the plasma sheath, of thickness of the order of a few Debye lengths (λ_D) where:

$$\lambda_D^2 = \frac{2 k T_e \epsilon_0}{n_e e^2} \qquad \textbf{(2.1)}$$

where T_e and n_e are the electron temperature and density respectively. During the afterglow $\lambda_D \approx 1$ μm in the test laser (for an average electron temperature of 2000 K and average electron density of 20 $\times 10^{12}$ cm^{-3}).

2.3.1 PRACTICAL LIMITATIONS ON SPATIAL RESOLUTION

In order to cause minimal perturbation of the operation of the CVL, however, the diagnostic techniques to be used involve the introduction of an optical probe beam into the plasma from one end, so that only line integrals of the values of the parameters are being measured. For this reason it is not feasible to demand radial resolution to measure extreme superficial structure, where the greatest rate of change will be observed, that is better than the physical linearity of the plasma tube wall along a line of sight. Owing to inaccuracies in manufacture, distortion owing to thermal effects, principally tube sag from slight softening of the alumina, and the condensation of copper around the walls of the plasma tube in the cooler end regions close to the electrodes the practical limit to spatial resolution is set at about 1 mm.

2.4 NUMBER DENSITY OF GROUND STATE COPPER ATOMS

2.4.1 EQUILIBRIUM CONDITIONS

From measurements of the ground state population density alone a great deal of information can be gained. The local values of the pre-pulse copper ground state population density can give us information concerning the thermal environment within the plasma tube in terms of both gas and electron temperatures. This is in addition to its place in building up the full parameter map of the laser plasma.

There are a number of processes contributory to loss of copper from the plasma: the slow flow of the buffer gas, to prevent the build up of impurities, carries with it around 1 part in 200, around 10^{16}, copper atoms per second, this being slightly counteracted by the counter flow of copper ions during the voltage pulse as a result of cataphoresis, contributing an average flow rate of around 10^{15} Cu^{+} ions per second. There is the loss of copper owing to diffusion from the ends of the high copper density, hot plasma region into the cooler end stubs close to the electrodes where it will rapidly condense out, this process giving rise to a loss of population (from both ends) of the order of 10^{16} copper atoms per second. In addition to this longitudinal diffusion of copper from the plasma there is a small, and almost certainly negligible where the plasma tube is not cracked, radial diffusion of copper through the alumina plasma tube wall and into the alumina paper thermal insulation around it, before condensing out in a chromatographic layer within the insulation.

In order to replenish copper atoms lost by all of the above mechanisms it is required that there exists a sufficient surface area of clean liquid copper distributed along the length of the hot region of the plasma tube to act as a reservoir. In addition to having a sufficient number of copper blobs it is important that the surface of each blob is sufficiently free from contamination, for instance molybdenum or tungsten sputtered from the electrodes.

Assuming the liquid copper charge within the plasma tube is capable of providing the replacement for this loss of copper from the plasma then the partial pressure of copper throughout the hot region of the tube should be constant and equal to the vapour pressure of copper at the temperature of the copper blobs. This subject will be discussed in greater depth in the following section. The temperature of the copper blobs will, in turn, be equal to that of the plasma tube wall. For this to be true in a non steady-state device like a CVL requires that the tube wall has sufficiently large heat capacity for its temperature to be constant with time, and the distribution of thermal insulation around it to be sufficiently well planned for the temperature to be constant along the length occupied by the copper charge; the "hot" region. While the first criterion is readily realised, the second is less so and will be determined by the quality of the design of the laser tube. The insulation in the test laser has been designed so as to optimise longitudinal thermal homogeneity.

2.4.2 RADIAL DISTRIBUTION OF COPPER

It would appear then that if it is possible to measure the total copper radial number density profile, then from the value at the wall can be determined the wall temperature from the copper saturated vapour pressure curve, and thence the radial temperature profile across the plasma tube.

Provided that the mean free path for copper-copper collisions is much smaller than the tube diameter, it is expected that the partial pressure of neutral copper vapour should be constant across the plasma tube diameter. The electrical discharge deposits energy into the volume of the gas, in a non-isotropic manner, however, while cooling occurs from the walls. This gives rise to a temperature profile in the neon-copper gas mixture, highest on the axis, which is reflected in the local values of particle densities. Without knowing the temperature at a given radial position, the local particle density cannot be

calculated from the wall value of vapour pressure. Conversely, however, if the vapour pressure is known an approximate temperature profile can be calculated from the local particle density. There are, however, a number of caveats to this approach.

For the majority of the CVL inter-pulse period the populations in the excited states of the copper atom remain in equilibrium with the ground state at the electron temperature (eg Lewis, 1985; Kushner & Warner, 1983; Carman et al, 1993) which falls slowly, buffered by the gas temperature, from around 10 μs after the end of the discharge pulse. Owing to the lifetimes against electron collisional de-excitation encountered in the copper excited levels at the electron densities encountered (including the metastable lower laser levels), and the relatively slow rate of change of temperature this equilibrium is easily maintained. The rates of third body (predominantly electron: see Lewis, 1985; Carman et al, 1993) mediated electron-ion recombination, on the other hand, is relatively slow and there can be, consequently, a residual electron/ion density the potential effect of which must be considered. That this is so is illustrated by the beneficial effects the pre-pulse electron density has on the stability, and distribution of the discharge observed in large diameter high repetition rate CVLs.

Ambipolar diffusion, briefly mentioned above, gives rise to enhanced radial diffusion of ions because of the need to preserve overall charge neutrality in the plasma. In addition, in order to do this against a far greater rate of electron collisions with the tube walls because of their higher mobilities, a region of net negative space charge immediately adjacent to the wall develops, the plasma sheath, of a few Debye lengths thickness, from which further slow electrons are repelled but ions are attracted. The second effect is that the electron exclusion zone of the plasma sheath decreases thermal contact between the electron population and the wall by allowing only those electrons with sufficient kinetic energy to cross the sheath potential. This can be calculated (Von Engel, 1965):

$$V_s = \frac{k T_e}{2e} \ln\left(\frac{T_e m_a}{T_g m_e}\right) \qquad \textbf{(2.2)}$$

which gives a value of, during the afterglow, about -0.9 V for $T_e = T_g \approx 1700$ K (the wall temperature). It has been suggested that, owing to their considerably greater

mobility and the enormous mass differential between the electrons and the copper and neon atoms and ions, the electron-electron kinetic energy coupling, and thus thermal conductivity, is far greater then the coupling between the electrons and the heavy gas particles. For a given heat flow, therefore, the radial electron temperature profile will be considerably flatter than that of the gas, and it thus approaches the gas temperature at a uniform value approximating to the average gas temperature (Kushner & Warner, 1983) or a value around the peak gas temperature (Carman et al, 1993). The radial measurements of copper lower laser level populations as a function of time in the afterglow made by Lewis (Lewis, 1985) suggest that, although the radial population density profiles may be flat, or even concave over the first few microseconds of the afterglow (as observed by Carman), if these levels are in Boltzmann equilibrium with the ground state at the local electron temperature, thereafter they revert to mimicking the gas temperature profile, an observation also reported by Izawa (Izawa et al, 1989).

The effect of this is that even if the copper partial pressure is radially constant, giving rise to a number density gradient with no radial diffusion, ambipolar diffusion of ions will still occur. The ambipolar diffusion coefficient D_a is given by (eg Howatson, 1965):

$$D_a = \frac{D_e \mu_i + D_i \mu_e}{\mu_i + \mu_e} \tag{2.3}$$

in which D_e and D_i, and μ_e and μ_i are the diffusion coefficients, and mobilities of the electrons and ions respectively. From the Einstein relation:

$$D_e = \frac{kT_e}{e}\mu_e \tag{2.4}$$

and likewise for the ions. As the electron mobility is very much larger than the ion mobility, D_a may be written:

$$D_a \approx D_i\left(\frac{T_e}{T_i} + 1\right) \tag{2.5}$$

Since the diffusion coefficient for the ion is very similar to that of the neutral atom this means that the ambipolar diffusion coefficient is greater than the neutral atom diffusion coefficient by a factor $(T_e/T_i + 1)$ and consequently ambipolar diffusion outwards will dominate over the conventional density diffusion of copper inwards.

The radial flow of ions as a result of ambipolar diffusion gives rise to the ambipolar diffusion current. The rate of flow of ions per unit length can be calculated assuming that the radial distribution of electron density has the form of a cylindrical Bessel function J_0 (based on the Schottky theory of the positive column - see eg Webb, 1976):

$$I_w^+ = 7.85\, D_a n_e(0) \qquad \textbf{(2.6)}$$

in which I_w^+ is the ambipolar copper ion particle wall current (multiplied by e this would yield the charge current) at the plasma tube wall, and $n_e(0)$ is the electron density on the axis of the plasma tube. For a plasma tube of 42 mm diameter this gives an arrival rate of ions at the plasma tube wall of 4.0×10^{19} $m^{-2}s^{-1}$. This can be compared with the arrival rate of neutral copper atoms of $1/4\, N_{Cu}\, \bar{v}$ which can be calculated as 3.6×10^{21} $m^{-2}s^{-1}$.

If equilibrium exists between the molten copper blobs at the wall temperature and the partial pressure of copper vapour adjacent to them then, under non plasma conditions, the rate of evaporation should equal the rate of arrival of vapour atoms. The rate of evaporation in $kgm^{-2}s^{-1}$ is designated W by Dushman (Dushman, 1949) and for copper at 1705 K he gives $W = 1.13 \times 10^{-2}$ $kgm^{-2}s^{-1}$ at which temperature he gives the vapour pressure as 0.1 torr (= 13.3 Nm^{-2} or a number density of 566×10^{12} cm^{-3}). This value of W corresponds to a rate of copper atom evaporation of 1.07×10^{23} $m^{-2}s^{-1}$ from the liquid copper blobs. Where the vapour is in the form of a plasma and there is an appreciable number density of ions, the neutral copper will attempt to establish an independent equilibrium radial number density profile as a result of the radial gas temperature profile. In this situation, however, the rate of return of neutral copper atoms to the wall will be augmented by the arrival of ions borne by the ambipolar diffusion current (in addition to the random processes), which, on arrival, recombine as a result of the presence of the third body in the form of the wall, thus adding to the total arrival rate of neutral copper. The effect of this would be to generate a vapour pressure of neutral copper at the wall that is depressed relative to that predicted by the wall temperature; the saturated vapour pressure at the wall temperature is not achieved. From the calculations presented above, however, the ambipolar current is likely to represent only about 1% of the total arrival of copper at the wall.

Because of the effect of ambipolar diffusion, in order to calculate an accurate gas temperature profile it would be preferable to employ the distribution of an atom with a negligible ion density, such as the neon buffer gas. Unfortunately, however, there are no suitable strong absorption lines terminating at the neon ground state, owing to its closed shell structure, amenable to access by the hook method or even by absorption measurement.

From the above discussion it may be seen that if a significant proportion of the species under investigation is ionised, and thus the ambipolar diffusion current is relatively large, care must be exerted if it is intended that results are to be calibrated against published vapour pressure curves, using a measured value of plasma tube wall temperature. If the ion density represents a relatively small proportion of the copper population, however, the perturbation owing to ambipolar diffusion may be sufficiently small that recombined ions represent an insignificant proportion of the total copper density arriving at the wall. Comparison with calculated vapour pressure may be made and thus allow a useful check of the hook method measurement provided that the plasma tube wall temperature is approximately uniform along the length of the active region, and is known accurately. In a standard CVL it is likely to be this last factor that has the greatest influence on the accuracy of calculated population density values where transition oscillator strengths are known to a reasonable degree of accuracy.

It must be remembered, however, that the arguments used to calculate radial temperature profile by using the radial distribution of copper ground state density, even allowing for the contribution of the ambipolar wall current, are essentially equilibrium arguments. In the case of the CVL plasma however, even immediately prior to the discharge pulse, the copper ion density is far from the Saha equilibrium value at the local electron temperature T_e, given by:

$$\log_{10}\frac{n_e N_i}{N_{Cu}} = -5040\frac{V_i}{T_e} + \frac{3}{2}\log_{10}T_e + 15.4 \qquad (2.7)$$

where V_i is the ionisation potential of copper in electron volts and n_e, N_i, and N_{Cu} are the number densities of the electrons, ions and neutral copper atoms respectively. This is because of the slow rate of recombination (see Chapter 8) compared to the interpulse period. For an accurate gas temperature radial profile to be calculated in this way

requires that the rate of recombination at all radial positions be very much slower than the rate of partial pressure re-equilibration. In Chapter 7 it will be shown that the time constant for the recovery rate of the copper ground state population density (as a consequence of recombination and the falling electron temperature and hence falling equilibrium excited state populations, and thermal redistribution of population density) is around 70 μs on axis, and in Chapter 9 it will be seen that the figure is very similar at other radial positions. It will also be seen in Chapter 8 that the rate of decrease in electron density is fastest on axis over the majority of the interpulse period which suggests that this causes insignificant departure from a radially constant partial pressure of copper.

2.4.3 TEMPORAL VARIATION OF COPPER DENSITY

Having considered the measurement of the pre-pulse ground state population density as a function of radial position it is now appropriate to address the information to be gained from the temporal profile of the ground state population density at a given radial position. This may conveniently be divided into two regimes.

Firstly the period during the discharge current pulse may be considered. This is the time during which population is excited out of the copper ground state to higher lying levels in the atom and ion by electron collisions. In this way the proportion of the ground state pumped to other levels may be directly observed. In addition, if the absolute timing of our population density measurements is known then the time course of this depopulation of the ground state may be directly related to that of the current pulse through the laser tube, and, more significantly, that of the laser output pulse (confirming the collateral importance of making these measurements, including the latter radially resolved). In this way the proportion of the discharge energy that goes into pumping the ground state after the laser output pulse has ceased may be observed directly. Naturally the time course of the depopulation of the ground state does not necessarily reflect efficiency of transferring that population to the upper laser levels, however population pumped after the end of the laser pulse cannot contribute usefully to laser action.

As discussed above it is expected that the ground state density radial profile should reflect the buffer gas radial temperature profile, at least to some extent. However, what

is less obvious is how the absolute, or relative, population pumped from the ground state will vary with radial position. It will depend upon electron density profile and, possibly to a lesser extent owing to flattening out of the rate coefficient curves of the predominant inelastic collision processes above about 2.5 eV (see Figure 7.5, Chapter 7), the electron temperature. This latter is in turn determined both by the electric field strength and the collisional energy loss processes available to the electrons, and therefore the electron mobility (proportional to mean free path). In addition, once the skin effect begins to be significant, there begins to be a radial dependence of the electric field strength E with a propagation delay time for the axial field to rise. Again how this depends upon discharge, or other operating parameters of the laser may be monitored, and compared with overall efficiency, and total power output from the laser.

The second phase of the time course of the ground state density is that of recovery following the end of the discharge current pulse. There are two general processes contributing to this recovery. Once thermal equilibrium is re-established following the discharge pulse the atomic level population densities will be populated according to a Boltzmann distribution at the electron temperature. In addition to this, though, the total atomic population is slowly being augmented by recombination of the copper ion population, principally by electron stabilised three body recombination, at a rate proportional to $T_e^{-5.8}$ at high electron temperature ($T_e > 3100$ K), and T_e^{-5} for values in the proximity of the gas temperature ($T_e < 3100$ K; Carman et al, 1993). Immediately following recombination, however, the atom is left in a high energy, high angular momentum state, close to the ionisation limit, from which it returns to a lower lying level by a series of radiative or superelastic transitions. The extent to which recombination will have a significant effect upon the population in a given level will depend upon the relative rates of recombination into that state and upwards and downwards transition rates from it. In the case of the ground state, therefore, the direct effect of recombination is smeared out and it need only be considered as its effect upon the total available copper population. The total observed ground state repopulation rate is therefore the resultant of the recombination rate and the decay of the electron temperature, provided the latter is slow enough for collisional relaxation of the copper metastable level populations to remain in equilibrium. Although both the rate of recombination and distribution over states are T_e dependent it would be unwise to attempt to make any direct observations

from the time course of the ground state population density recovery rate as it is determined by a second order differential equation the coefficients of which are not accurately known, it being much more accurate to derive T_e from the population in a low lying state such as the metastable.

All the observations discussed above may be made directly from the time and spatially resolved ground state measurements without recourse to a sophisticated computer model, however it is in combination with those made on other levels that their role in confirming the accuracy of such models, and in the comparison with lasers operating under slightly different conditions, that the potentially greatest strength of these measurements lies.

2.5 POPULATIONS IN UPPER LASER LEVELS OF COPPER

The rate coefficients for direct collisional excitation from the copper ground state to the $3d^{10}\ 4p\ ^2P_{1/2,3/2}$ upper laser levels have been computed by a number of groups, including Scheibner and Hazi (Scheibner et al, 1987; Scheibner & Hazi, 1993). In order to make any kind of evaluation of the observed time profiles of these populations, however, a large number of excitation processes to and from each, in addition to that of stimulated emission in the presence of the laser radiation field, must all be considered, thus rendering any meaningful analysis of these measurements in isolation almost impossible. In combination with measurements of populations in other levels, however, and the appropriate rate coefficients incorporated into a computer model representing all the significant processes it should be possible to calculate the electron temperature required to generate the observed rates. It should of course be remembered, as discussed in Section 1.3.2 (IV), that the real electron energy distribution function is unlikely to be a true, single Maxwellian, owing to the depletion of the high energy tail of the distribution by inelastic collisions, and the insufficient electron density for Coulomb interactions to restore the distribution. Such effects may be incorporated into the model explicitly (Carman et al, 1993) to take into consideration the departure of the energy distribution from a true Maxwellian form. This would be to reverse the more usual role of the computer model in which the profiles of the population densities are predicted according to an electron energy distribution predicted, in turn, by the circuit and plasma parameters of the laser.

One very important reason for obtaining the population measurements for the upper laser levels is that the value obtained from a hook method population density measurement, in common with most optical techniques, is not simply the population of a single level, but rather "effective population density", N_i^*:

$$N_i^* = N_i\left(1 - \frac{g_i N_j}{g_j N_i}\right) \tag{2.8}$$

where N_i and N_j represent the population densities in the lower and upper levels respectively of the transition being used in the measurement, and g_i and g_j represent their statistical weightings. This will be discussed in greater detail in Chapter 3, however it is evident that such a measurement will only yield a value for N_i explicitly when it is very much larger than N_j. When thermodynamic equilibrium exists at temperatures not far removed from room temperatures, the energy spacing between the upper and lower levels will ensure that this provision holds for visible transitions. However under non-equilibrium conditions this will not necessarily hold, especially in the case of laser levels between which population inversion must exist at least transiently, and so, to calculate N_i from N_i^*, N_j must first be obtained. As the only convenient transitions with which to measure the copper lower laser level populations are the laser transitions themselves it is vital that if the lower laser level population densities must be measured, then the upper level population densities must also be known.

It has long been observed that the temporal profile of the CVL laser pulse from a plane-plane cavity displays a characteristic shape consisting of a series of humps of decreasing amplitude separated by the optical round trip time of the cavity. This is explained in terms of a wave of laser radiation propagating down the laser tube, temporarily depleting the population in the upper laser level and decreasing gain. If this is true then it should be possible to observe this effect in the population of the upper laser level, provided that the temporal resolution of the measurement system is sufficiently good.

2.6 POPULATIONS IN LOWER LASER LEVELS OF COPPER

Over the history of the development of the CVL it is possibly about the behaviour of the populations in the metastable lower laser levels that most research has centred.

This is not surprising in a cyclic laser system as the gain, and hence output power, efficiency, maximum and optimum prf depend at least partially upon this population, and the rates at which it is increased and depleted. While the population of the copper metastable levels by the lasing process is now thought to be only one of many processes bringing about the cessation of lasing there is no doubt that there is a considerable amount of information to be gained from the accurate measurement of the populations in these levels.

In particular, at the electron temperatures encountered in the CVL the thermal Boltzmann population in the lower laser levels is large enough to be potentially measurable throughout the laser cycle, if not by the hook method then by an absorption technique. The potential for overlapping the ranges of these two techniques by measuring the absorption in the wing of the absorption profile at a wavelength selected for the ability to have residual transmission even at maximum population density means that the sensitivity and dynamic range of the absorption technique could be calibrated with the absolute accuracy of the hook method. In this way it should be possible to follow the population density in the lower laser levels throughout the laser cycle and thus obtain a value of the electron temperature for all times at which a quasi-equilibrium between them and the ground state is maintained.

2.7 POPULATIONS IN OTHER ATOMIC LEVELS

In addition to the copper ground state and the four laser levels it would be desirable to measure the population densities in a number of other atomic levels in both the copper lasant and the neon buffer gas. Whilst there are a number of atomic levels above the upper laser levels, into and through which excited copper may be expected to pass during and following the discharge pulse, it is clearly not practicable to measure the population densities in them all. Possibly the most interesting, however, is the family of ($3d^9$ $4s(^3D)$ 4p) quartet levels of the same core configuration as the lower laser levels. These levels represent the next group above the upper laser levels, though, like the lower laser levels they are very weakly connected with the ground state. They are, however, well connected to the lower laser levels, and collisional excitation from the upper laser levels also has a reasonable cross-section.

The $^4F_{9/2}$ level was chosen as representative of this group as it has the highest degeneracy and a reasonably strong transition with which to access it. Although the group of quartet levels lie relatively close in energy and might be expected to be populated according to their degeneracies, the cross-sections for collisional coupling between the levels are not known and some work suggests that this might not be the case (Smilanski, 1979; Carman et al, 1993).

As well as excited levels in the copper it would be of interest to make measurements of the population density in one or more levels in the neon buffer gas. As the neon ground state is a closed shell configuration the first excited states lie far too high above it for there to be any visible or near-visible transitions to allow direct measurement of the ground state density using an optical technique. It was decided therefore to measure the population density in a representative of the group of four $2p^5$ 3s levels, between which close collisional coupling is known to exist both by heavy body excitation collisional transfer (Parks and Javan, 1965) and electron collisional transfer (Phelps, 1959). Owing to the high neon ground state population density all transitions from these levels to the ground state are highly trapped, making these levels metastable. For this reason they can be used to monitor the passage of excited population from the ground state to higher lying levels and ionisation, and the subsequent recombination.

2.8 ELECTRON DENSITY

It is through the medium of the electrons that energy is imparted from the discharge circuit into the copper/neon gas mixture, with, among other processes, the transfer of population from the copper ground state to the upper laser levels that gives rise to laser action. The pre-pulse electron density determines the nature of the discharge, especially during the vital early stages when direct excitation to the upper laser levels can very much exceed that to the lower levels, giving rise to gain. The radial profile of the electron density, together with that of the electron temperature determines the radial homogeneity of excitation (and de-excitation) to and from excited levels at different radial positions, and hence, in part, that of laser operation itself.

For many reasons therefore the temporal and spatial variation of electron density is a vital parameter to know if understanding of the behaviour of the CVL is desired.

2.9 LASER PULSE TIMING: THE SKIN EFFECT

When a high frequency, or rapidly changing current is present in a conductor it is constrained to flow predominantly close to the surface by the effect of the electric field generated by the rapidly changing magnetic flux density, the skin effect. An equation describing this may be derived from Maxwell's equations:

$$\nabla^2 E = \mu_0 \frac{\partial}{\partial t}(\sigma E) \tag{2.9}$$

in which displacement current has been neglected in comparison with the conduction current. This gives rise to a skin depth δ from the surface of the conductor, the distance by which the electric field has fallen to 1/e of its value at the surface. The skin depth for a conductor of conductivity σ for a signal of frequency ω is given by:

$$\delta = \left(\frac{2}{\omega \mu_0 \sigma} \right)^{1/2} \tag{2.10}$$

With its high pre-pulse electron density the CVL plasma represents such a conductor and, although its conductivity, given by:

$$\sigma = \frac{e^2 n_e}{m_e \nu_m} \tag{2.11}$$

(where ν_m is the electron-heavy particle momentum transfer collision frequency, and n_e is electron density) is about five orders of magnitude lower than that of metallic copper, a skin depth of about 3 cm can be calculated. For the laser under investigation, of 21 mm radius therefore, a significant radial variation of current flow may be expected. In their CVL modelling paper of 1983 (Kushner & Warner, 1983) Kushner and Warner point out that Equation 2.9 has the form of a diffusion equation, with diffusion coefficient $D_E = 1/\mu_0\sigma$, and calculate a time constant for the electric field on axis of a plasma of radius R cm to reach 1/e of that at the surface, τ, as:

$$\tau \approx \frac{0.15R^2}{D_E} = 0.15R^2\mu_0\sigma \tag{2.12}$$

They use expression (2.9) explicitly in their model as σ varies radially and temporally with both electron density and temperature, and the effective ω also changes with time. An approximate value of τ for the laser under study may be calculated, however, using an average value of n_e of 2×10^{12} cm^{-3} (obtained from the measurements reported in Chapter 8, and a value of ν_m of 3.8×10^9 s^{-1} (as used by Kushner and Warner, 1983).

The effect of this on the CVL discharge is that the current flows in the superficial layers of the plasma a short time before it propagates through to the axis, and consequently excitation near the plasma tube wall commences slightly before that at the axis. For a 42 mm diameter plasma tube both this delay and its effect are relatively minor, however, owing to the R^2 dependence, rapidly become significant as plasma tube diameter is increased. A thorough understanding of this, and other, radial effects is therefore essential to both accurate computer modelling, and proposed volumetric scaling projects and is addressed in Chapter 6. In addition to the temporal consequences of the skin effect, a significant propagation delay can lead to the plasma close to the axis experiencing the discharge at a later point in its profile, with consequential shorter duration, and less efficient pumping. This therefore represents a detrimental effect of high pre-pulse electron density as a lower value would give a lower pre-pulse conductivity allowing the electric field to build up across the whole diameter of the plasma tube before significant skin effect set in.

The observed phenomenon of the onset of gain near the plasma tube wall earlier in the discharge pulse than at the tube axis has been attributed to the skin effect. An alternative explanation involves the pre-pulse populations in the two copper metastable lower laser levels. In much of the literature (eg Kushner & Warner, 1983; Carman et al, 1993) any influence upon the radial dependence of laser pulse timing of the pre-pulse metastable populations is dismissed owing to the fact that the radial profile of the electron temperature was predicted to be flat owing to the far greater electron-electron collisional coupling than electron-atom/ion coupling, and the high thermal conductivity of the electrons. Assuming that the population density in the two metastable levels is at equilibrium with the copper ground state at the local electron temperature this would give rise to a radial metastable population density profile that is lowest on axis (as is the ground state radial profile), or at best relatively flat, thus causing a laser pulse timing effect in either the opposite sense to that observed, or making no contribution at all.

Direct measurement of the population density in the two copper lower laser levels, however, (Lewis, 1985; Izawa et al, 1989) show that late in the afterglow the radial profiles are actually convex, with maxima on axis. The potential therefore exists for a contribution to the observed radial dependence of the onset of gain as a result of the additional time required to overcome the enhanced pre-pulse lower laser level populations on axis.

In addition to these two phenomena, the results of experiments will be described in Chapter 5 which suggest very strongly that the timing and shape of the discharge current pulse, and also the laser output pulse, are determined to a high degree by the pre-pulse electron density. This parameter is also radially dependent, with a maximum on axis, which, again from the results of Chapter 5, could lead to later excitation and lasing on axis.

In Chapter 6 the experiments performed on a 60 mm diameter CVL to attempt to separate the relative importance of these possible contributory factors are described.

2.10 RADIAL GAS TEMPERATURE PROFILE

The fundamental equation describing the conduction of heat in a medium of thermal conductivity κ , density ρ, and specific heat capacity C, with power input P per unit volume, uniformly distributed is (Carslaw & Jaeger, 1959):

$$\nabla.(\kappa \nabla T_g) + \rho C \frac{\partial T_g}{\partial t} = -P \qquad \textbf{(2.13)}$$

Taking an expression for the variation of thermal conductivity with temperature:

$$\kappa = \kappa_0 T_g^p \qquad \textbf{(2.14)}$$

Equation 2.13 can be solved to give gas temperature T_g as a function of radius for cylindrical geometry, bounded by a wall of temperature T_w at radius $r = R$:

$$T_g(r) = \left[T_w^{p+1} + \frac{P(p+1)}{4\kappa}(R^2 - r^2) \right]^{1/(p+1)} \qquad \textbf{(2.15)}$$

Fitting of Equation 2.14 to published experimental data yields values for neon of

$p = 0.64$ and $\kappa_0 = 1.32 \times 10^{-3}$ $Wm^{-1}K^{-1.64}$ (Lewis, 1985). In the case of the study laser the radius $R = 21$ mm, $T_w = 1700$ K, and the power input (calculated from energy stored in the storage capacitors) is 5800 W into a volume of 2.08×10^{-3} m^3, giving a value for $P = 2.79 \times 10^6$ Wm^{-3} (or 2.79 Wcm^{-3}). These values allow an axial gas temperature of 3270 K to be calculated.

This figure should be regarded as a maximum value as it assumes that all of the power stored in the storage capacitors is deposited uniformly in the plasma. This is known not to be the case for a number of reasons. Significant power is dissipated in the thyratron, with figures of around 30% (eg Nehmadi et al, 1989; Carman et al, 1993) being reported. In Section 3.3.6 the effect of the longitudinal temperature profile along the plasma tube and the gas column is discussed in terms of the distribution of copper vapour. The result is that there exist end regions of the plasma tube where the temperature falls from the value maintained along the majority of its length to the lower value of the water cooled electrodes. These cooler end regions therefore permit the condensation of copper onto the plasma tube walls, and so have a partial pressure of copper vapour that falls rapidly from the value in the "hot" region to negligible levels. In these "cool" end regions the discharge must be carried by the neon in the absence of copper vapour, with the result that, in order to maintain the average electron density to ensure continuity of current, the electron temperature must be much higher to ionise neon which has an ionisation potential of 21.6 eV, nearly three times that of copper. For this reason, the power per unit volume deposited into the end regions must be significantly higher than the average, with that into the bulk correspondingly lower. Carman (Carman et al, 1993) calculates that power deposited into the end regions per unit volume is "2-3 times higher" than in the central region. Taking this ratio to be 2.5, and using the lengths for the "cool" and "hot" regions, of 2×0.1 m and 1.3 m respectively, discussed in Section 3.3.6 reduces the value of power per unit volume input to the central region by 28%.

In an attempt to allow for the effects described above it would appear to be reasonable to reduce the value of P by 50% to 1.4×10^6 Wm^{-3}. If this figure is used and a revised axial gas temperature over the central region of the plasma tube is calculated, then a figure of 2570 K is obtained.

In Chapter 9 an axial gas temperature of 2680 K, over the central "hot" region, is calculated from the pre-pulse radial distribution of copper ground state density. The theoretical value therefore, calculated as above and making due allowance for power dissipated in the thyratron and in the end regions of the plasma tube, is in good agreement with the value calculated from the radial copper distribution.

3 THE HOOK METHOD

The hook method is an optical diagnostic technique employing a probe beam for the measurement of the product of the line integral of the effective population density in a given atomic level, over its line of sight, and the oscillator strength of the optical transition employed in the measurement. A little of the history of the hook method has been presented in Chapter 1, in this chapter the technique will be presented in terms of its suitability for the measurements required in the present study. The theory will be discussed and the equipment employed in its present implementation outlined, together with the specific characteristics required from individual items.

3.1 THEORY

The hook method is an interferometric technique employing an interferometer crossed with a spectrograph to obtain spectrally resolved phase information from a probe beam concerning its path through the region of interest. The technique measures the spectral dependence of the refractive index of the region of interest, in the case of the present study the plasma of the CVL, in the neighbourhood of a transition line. Strictly, the parameter required is n, the real component of the complex refractive index $\tilde{n} = n(1-i\varkappa)$. The real part of $\tilde{n}$ determines the phase of a wave as it propagates through a medium, and the imaginary component determines the amplitude, and thus corresponds to the absorptivity. From this it may be noted that such interferometric techniques as the hook method are, in fact, related to absorption measurements via $\tilde{n}$.

3.1.1 THE REFRACTIVE INDEX

A general expression for the complex refractive index $\tilde{n}$ obtained from classical electromagnetic theory is:

$$\tilde{n} - 1 = \frac{e^2}{\varepsilon_0 m_e} \sum_s \frac{F_s}{\omega_s^2 - \omega^2 - F_s e^2/3m\varepsilon_0 + i\gamma_s \omega} \qquad (3.1)$$

in which ω_s and γ_s are the angular frequency and the classical damping coefficient respectively of electron oscillation resonances in the classical atom (eg Korff & Breit,

1932). The behaviour of the real and imaginary parts of $\tilde{n}$ in the neighbourhood of a typical absorption line is illustrated in Figure 3.1.

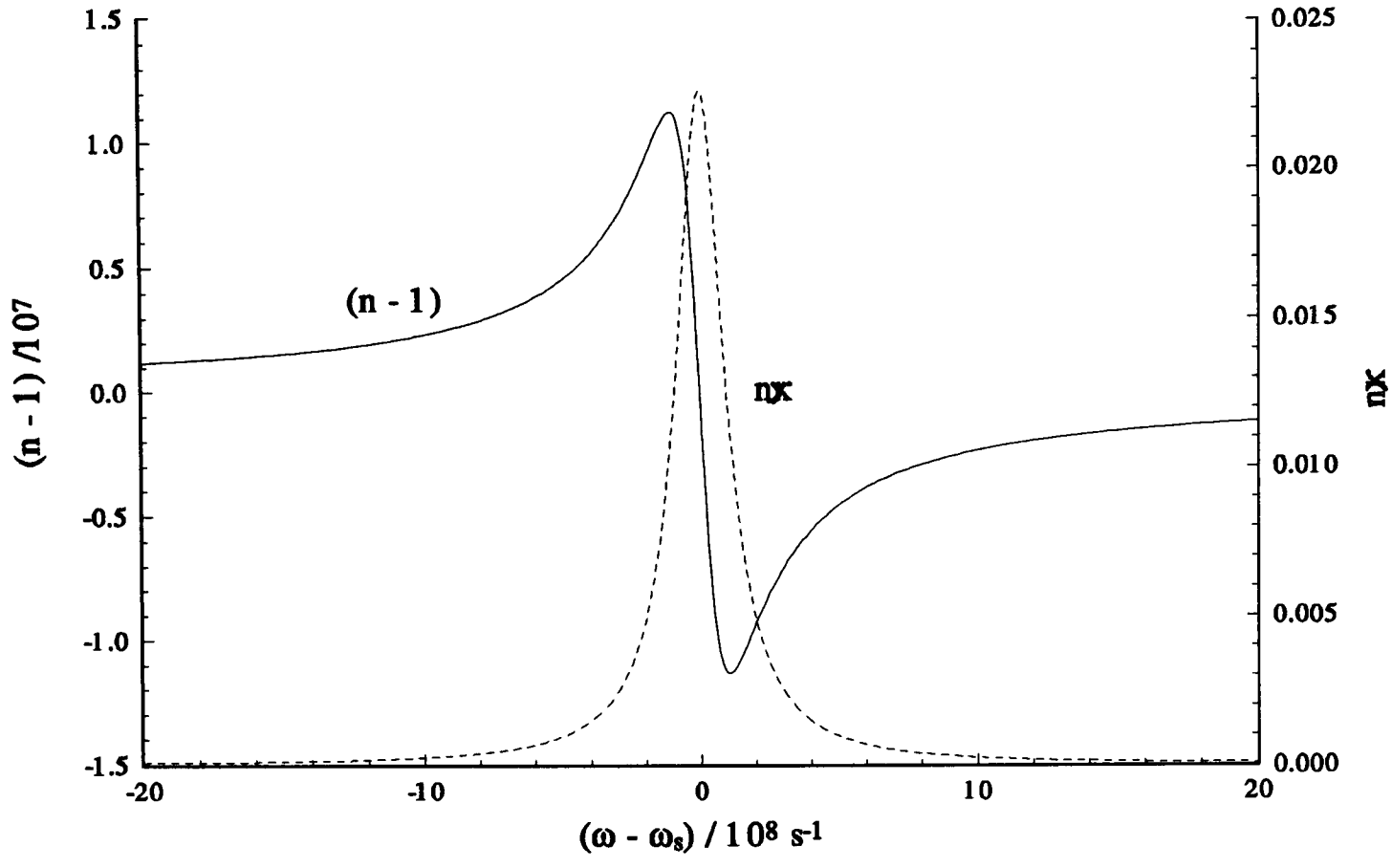

Figure 3.1 Real and imaginary refractive index close to an absorption line

3.1.2 OSCILLATOR STRENGTH

Prior to the introduction of quantum mechanics Ladenburg (Ladenburg, 1921) proposed that for a medium with N atoms per unit volume the parameter F_s could be represented:

$$F_s = Nf_s \tag{3.2}$$

In this formula f_s is a dimensionless constant of the atom relating to the transition from state i to state j, which (for an isolated atom) occurs at angular frequency ω_s. The value of f_s was proportional to the Einstein absorption probability for the transition, and thus also to the Einstein A coefficient for spontaneous emission. With the introduction of quantum mechanics the definition of F_s underwent a slight modification to:

$$F_s = N_i f_{ij} + N_j f_{ji} \tag{3.3}$$

Since by definition the emission oscillator strength f_{ji} is related to the absorption oscillator strength f_{ij} by:

$$f_{ji} = -\frac{g_i}{g_j} f_{ij} \tag{3.4}$$

then:

$$F_s = N_i f_{ij}\left(1 - \frac{g_i N_j}{g_j N_i}\right) = N_i^* f_{ij} \tag{3.5}$$

in which N_i^* is the "effective population density" frequently encountered in calculation of emission and absorption rates, and mentioned in Chapter 2.

From these expressions it is possible to derive one for the refractive index of a gas in the neighbourhood of an absorption line, and into which it is possible to introduce a number of simplifications. If the spectral region outside the absorption line, only, is to be considered, ie for which $\left(\omega_s^2 - \frac{F_s e^2}{3m\varepsilon_o}\right) - \omega^2 \gg \gamma_s\omega$, the $i\gamma_s\omega$ in Equation 3.1 may be neglected and the refractive index of the gas is entirely real. In addition, in a gas at relatively low pressure the particle density N is low enough that the $F_s e^2/3m\varepsilon_0$ term may also be neglected. Finally, if a gas is in thermal equilibrium at temperatures for which kT is small compared to $\hbar\omega_s$, as often will be the case, the population density N_j will be very much smaller than N_i and F_s becomes Ladenburg's value: $F_s = Nf_{ij}$. Under non-equilibrium conditions this condition may well be violated and the full expression must be used, this being patently the situation in a laser plasma in which inversion occurs. Employing these simplifications the real refractive index may be expressed by the Sellmeier dispersion formula:

$$n - 1 = \frac{r_0}{4\pi}\sum_s \frac{F_s \lambda_s^3}{\lambda - \lambda_s} \tag{3.6}$$

in which r_0 is the classical electron radius:

$$r_0 = \frac{e^2}{4\pi\varepsilon_0 m_e c^2} \tag{3.7}$$

Typically absorption lines will lie sufficiently far apart that the effect of one on the refractive index in the neighbourhood of another is sufficiently small that only one term in the summation of Equation 3.6 need be considered. The situation where this is not the case will be discussed further, it is evident then that n and $N_i^* f_{ij}$ for a given transition are directly related and thus if n can be measured a value for $N_i^* f_{ij}$ can be obtained. However, in order to exploit Equation 3.6 directly to measure $N_i^* f_{ij}$ would require measurements of both refractive index n, and wavelength λ of extremely high precision and accuracy as the variation of n with λ in proximity to an absorption line is rapid. A far more prudent strategy is to exploit the well established theoretical relationship between n and λ and measure n as a function of λ. By taking this approach we relinquish the requirement of making an absolute measurement of n as it is only with relative values that we are concerned.

3.1.3 INTERFEROMETRY

The general strategy for the measurement of differences in refractive index in a medium is the use of an interferometer by which to observe the phase shift between a probe beam, having passed through the medium, and a reference beam. If this approach is to be adopted a means of spectral dispersion is also required.

The discussion above illustrates how the theoretical basis of the contemporary implementation of the hook method has been arrived at. How this has been implemented in the case of the present project is illustrated in Figure 3.2. The description of individual components, and the specifications required of them, will be undertaken in Section 3.3, however the diagram serves to illustrate the optical layout employed.
The basic design is of a Mach-Zehnder interferometer crossed with a stigmatic spectrograph. The probe beam source consists of a pulsed dye laser, modified to give quasi broad-band output, and the detector is a CCD camera with a 4 mm $\times$ 4 mm detector area.

3.1.4 THE FRINGE EQUATION

The refractive index of the plasma within the CVL may be assigned a value n, extending over length l. In the reference arm of the interferometer the compensation plates may be represented by values of n' and l' where l' is the thickness in addition to

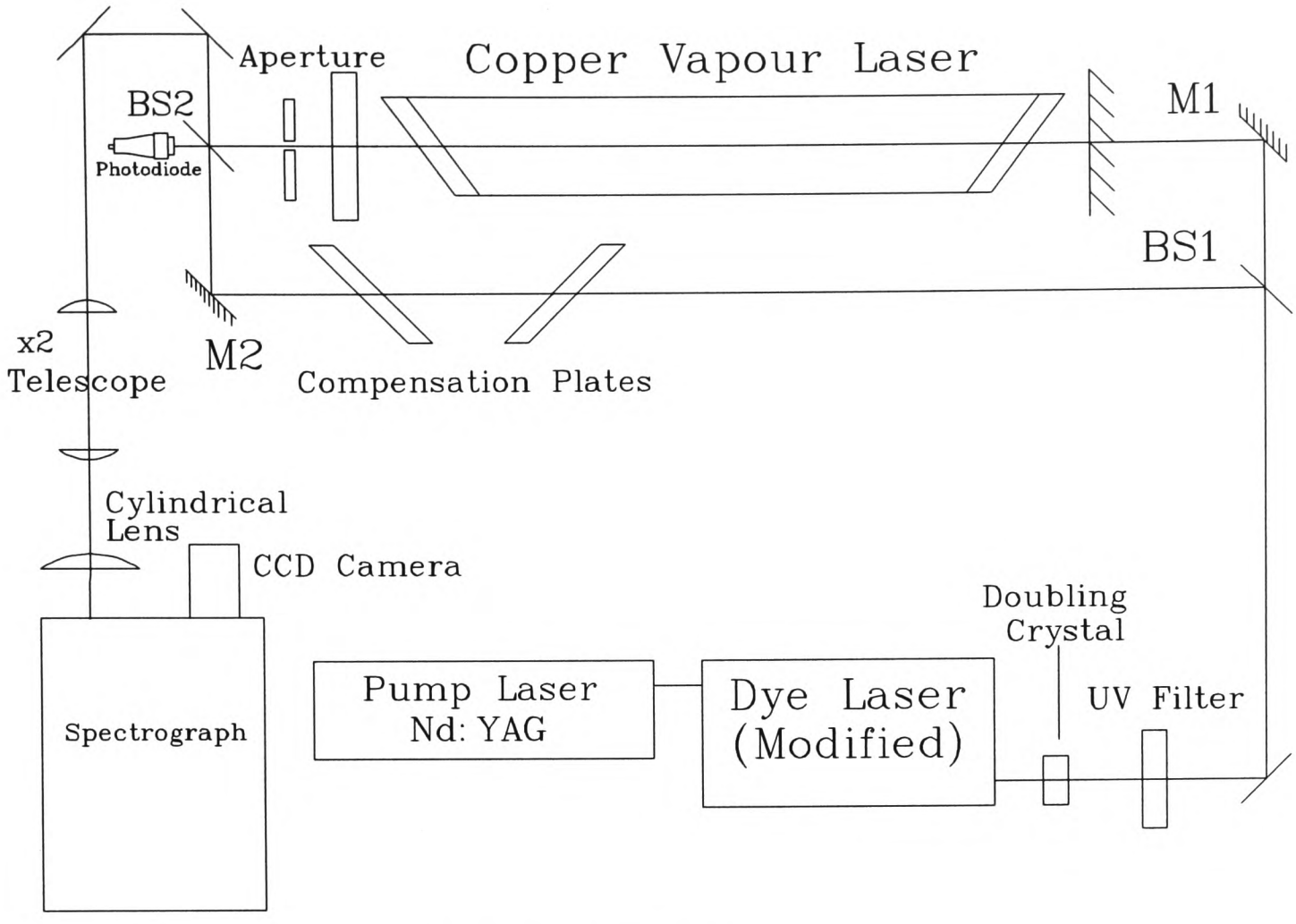

Figure 3.2 Optical layout for hook measurements

any equivalent components in the other arm of the interferometer, such as windows etc. If slight vertical tilts are introduced to the optical components of the interferometer such that the probe and reference beams meet at the entrance slit of the interferometer with a half angle ϕ, then interference fringes will be formed with successive maxima in the vertical y direction up the slit given, for wavelength λ, by:

$$(n-1)l - (n'-1)l' + \phi y = m\lambda \tag{3.8}$$

where m is an integer - the order number of successive fringes. Whether such fringes are actually visible at the slit will depend upon the bandwidth of the probe beam, the fringe order m (determined by the optical path difference between the two arms of the interferometer), and the presence of any absorption lines in the wavelength interval illuminated by the probe beam. Once the pattern has been dispersed by the interferometer, however, and the slit imaged upon the detector, $n(\lambda)$ is displayed on the detector in the form of Equation 3.8. If no absorption lines are present over the imaged wavelength interval then the displayed fringe pattern will consist of a series of parallel (over the bandwidth observed) bands that for zero optical path difference between the two

beams ($m=0 \pm\Delta m$) will be horizontal. By the introduction of a compensation plate into one of the arms of the interferometer, an optical path difference can be introduced so that the fringes will be tilted away from the horizontal. If an absorption line falls within the observed bandwidth, large excursions in $n(\lambda)$ about line centre, as described by the Sellmeier formula, will cause fringes of the form of Figure 3.1 to be displayed on the detector.

3.1.5 THE HOOK CONSTANT

In order to calculate F_s a compensation plate is introduced into the reference arm of the interferometer which has the effect of tilting the fringes as described above. If the tilt is arranged to be in the correct direction the rapid change in gradient in the wings of the absorption line can be converted into the distinctive hooks illustrated in Figure 3.3.

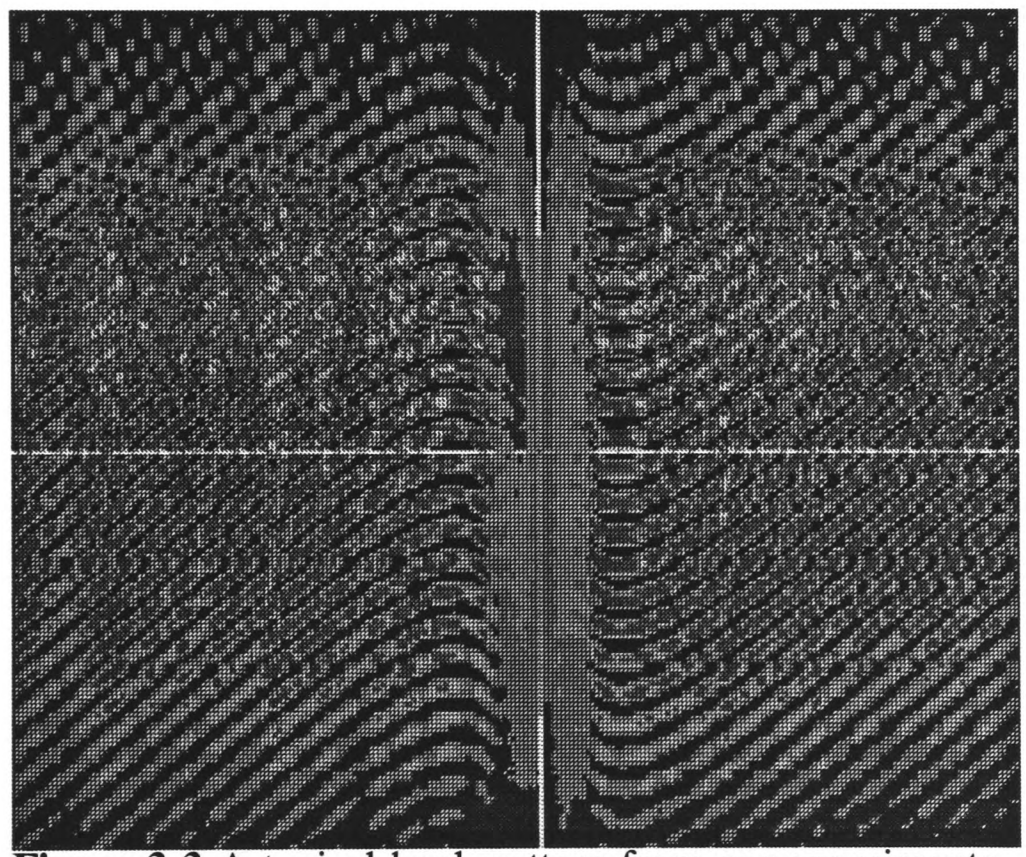

Figure 3.3 A typical hook pattern from our experiments

As Equation 3.8 represents the fringe equation it may readily be differentiated to obtain an expression in terms of $dn/d\lambda$ for the turning points of the hooks, at which $dy/d\lambda = 0$:

$$l\frac{dn}{d\lambda} = m + l'\frac{dn'}{d\lambda} = -K \qquad \textbf{(3.9)}$$

In Equation 3.9 the new constant K is introduced, termed the hook constant or interferometer constant. From the Sellmeier formula $dn/d\lambda$ may then be obtained in

terms of F_s, λ, λ_0 (where λ_0 is the wavelength of the transition and is equivalent to the classical parameter λ_s) and constants:

$$\frac{dn}{d\lambda} = \frac{-F_s r_0 \lambda_0^3}{4\pi} \frac{1}{(\lambda - \lambda_0)^2} \tag{3.10}$$

Since the dispersion $dn'/d\lambda$ of the reference arm is sensibly constant over the small wavelength interval of interest, from Equations 3.9 and 3.10 two values of $(\lambda-\lambda_0)$ may be obtained ($\lambda_2>\lambda_0$ and $\lambda_1<\lambda_0$) that satisfy these equations simultaneously for constant K and consequently represent the positions of the hooks. If we now write the separation of the two turning points, the "hook spacing", $\Delta = (\lambda_2-\lambda_0)-(\lambda_1-\lambda_0)$, we are in a position to write F_s in terms of Δ, K and constants:

$$F_s = \frac{\pi}{l r_0} \frac{K}{\lambda_s^3} \Delta^2 \tag{3.11}$$

Provided f_{ij} and l are known, then the only requirement to the calculation of N_i^* from a measured Δ is that of obtaining the value of K.

To determine K the fringe equation (Equation 3.8) is rearranged to give ϕy in terms of the other constituents and if two fringes, of order m and $m + \Delta m$ at wavelengths λ and $\lambda + \Delta\lambda$, but at the same vertical height up the fringe pattern (ie ϕy is the same in each case) are considered then the fringe equations may also be equated and, by rearrangement it may be shown that:

$$K = -m - l' \frac{dn'}{d\lambda} = \frac{\Delta m}{\Delta\lambda}\lambda - \frac{dn}{d\lambda} l + \Delta m \tag{3.12}$$

From this it may be seen that in order to evaluate K all that is required is to evacuate the test cell (without disturbing the interferometer in any other way - to remove the $dn/d\lambda$ term) and count the number of fringes crossing an horizontal straight line, over a known wavelength interval. In practice the $l.dn/d\lambda$ term will always be very much smaller than $\lambda.\Delta m/\Delta\lambda$ and may therefore be neglected, thus removing the necessity of evacuating the test cell. It merely remains, therefore, to measure K in a region of the spectrum close to λ_s, but unperturbed by the effects of absorption lines. In practice the Δm term will also frequently be negligible in comparison to the $\lambda.\Delta m/\Delta\lambda$ term and may also be neglected.

3.1.6 RESOLUTION

In general ε, the wavelength resolution obtainable from the hook method, is determined by the reciprocal dispersion of the spectrograph (d^{-1}) and the resolution on the detector (Δx) according to: $\varepsilon = \Delta x d^{-1}$ (Bachor & Kock, 1980). The parameter Δx depends on the resolving power of the detector itself, such as grain size for a photographic emulsion or pixel size for a discrete element type detector such as a CCD camera or vidicon, and the entrance slit width of the spectrograph which is imaged upon the detector. In order to optimise the resolution of the system for a given value of Δx the slit width should be made as small as possible compatible with obtaining sufficient transmitted light intensity, down to the resolution value of the detector itself at which point further reduction brings no further improvement and Δx = slit width = pixel size.

A number of techniques have been suggested to improve the small hook separation limit and accuracy obtainable for a given value of ε. These have included the "hook vernier" method of Sandeman (Sandeman, 1979) and the "phase method" (Kozlov & Plekhotin, 1974; Frich et al, 1977). In their review of these techniques in terms of the minimum hook separation resolvable Bachor and Kock have suggested that the vernier method will always offer an improvement in the ratio of 9:25. However they state that, for high resolution systems (eg $\varepsilon \approx 4$ pm), the phase methods offer only slight improvement, but that with a lower resolution setup improvement, up to around that of the vernier method, is possible. While these alternative methods can extend the dynamic range of the hook method, decreasing the minimum measurable population by a factor of about three, for large hook spacings they offer no improvement in accuracy despite the more involved analysis procedures.

For the present study, owing to the large number of hook patterns to be measured and the consequent requirement for semi-automated analysis (see below Section 3.3.7 and Appendix A1) the standard hook method has been employed in all but one very specific case where the added sensitivity of the hook vernier method was required.

3.2 CHARACTERISTICS OF THE HOOK METHOD

3.2.1 ADVANTAGES

As an optical diagnostic technique the hook method has the ability to interrogate a region to be studied with a probe beam of low spectral intensity, thus obtaining

information in a non-perturbing manner. By employing a probe beam of relatively small diameter (eg a laser beam) two dimensional resolution is available. The third dimension will always be represented by the line integral of $N_i^* f_{ij}$ along the line of sight of the beam. By employing a pulsed probe beam, and a sufficiently sensitive detector, it is possible to obtain a hook pattern from a single pulse, thus offering temporal resolution corresponding to the duration of the probe pulse. Provided the pulse retains sufficient energy to give reasonable exposure of the detector, the length of this pulse may be reduced to give the time resolution required, compatible with the stability and physical constraints of the system. Figures of a few nanoseconds are very readily accessible with commercial laser systems.

The foregoing qualities apply to many optical diagnostic techniques, however the hook method has the additional advantage that in general (see Appendix A2) no accurate knowledge of, or assumptions about, the line-width or broadening mechanisms of the absorption line in question are required, provided only that the hook separations are more than about 10 times the homogeneous line-width. This means that for the vast majority of its dynamic range the hook method offers a technique that is free from assumptions and can thus provide highly accurate measurements. Dynamic range, too, is very great owing to the Δ^2 dependence. The dynamic range is therefore only limited with a given optical configuration by the ratio of the smallest observable hook separation to the largest, a function of the resolution ε of the system, and the physical extent of the detector. In addition the calibration constant K may be changed and remeasured between successive measurements to extend the maximum range still further.

3.2.2 LIMITATIONS

The most severe shortcoming of the hook method, and the one that most seriously limits the number of circumstances under which it may be used, is lack of sensitivity. Even using the hook vernier method and a high resolution system a minimum $F_s l$ value of between 10^{15} and 10^{16} m^{-2} is all that can be obtained. In common with all optical diagnostic techniques employing a tuned probe beam, in order to obtain an accurate absolute value for the population density we also require to know both the oscillator strength of the transition to be employed and the length over which the population is distributed. In addition, if, as in the case of the present measurements, the gas or plasma

is not longitudinally constrained to a well defined region, the population density is not constant over the whole absorption path then this too must be considered in subsequent calculations. In comparing measurements made using the same line, however, both f_{ij} and l will generally be the same and the relative values may be compared with considerable confidence. The temporal profile of an atomic level population density may therefore be more accurate than the absolute value of an individual measurement. Measurements made on different levels, however, though utilising lines with different values of f_{ij} still represent the same l and consequently in comparing such measurements uncertainty in the two f values only will determine relative accuracy.

There are a number of situations in which significant problems will be experienced in attempting to use the hook technique. The first occurs when the population in the upper level of the transition of interest is significant in comparison with the population to be measured. The second occurs when there is a second transition lying close to that to be employed in the measurement. The third situation when care must be exercised is when the transition of interest is broadened to a significant fraction of the hook separation. Discussion of these problems, under what conditions they might be significant, and what measures can be taken to make measurements in their presence is discussed fully in Appendix A2.

3.2.3 ACCURACY

In order to assess the accuracy of measurements made using the hook method there are a number of procedures that can be employed. If, from some level, there are two upward transitions that can be accessed by the hook method then comparison of measurements of the same population using both lines allows detection of relative discrepancy in the two f values as any inaccuracy in l will act the same in both measurements. This is not, unfortunately, rigorous as errors in f value measurements are unlikely to be represented by a random scatter about a mean, especially in the case of related lines from the same lower level. Systematic errors too will not be highlighted by comparative measurements of this kind.

Of possibly greater value in the assessment of absolute accuracy is the comparison of measured values with known figures where these are applicable and available. There are, unfortunately seldom situations where this may be performed with confidence,

especially in the case of an operating CVL. Measurement of total population density in a test cell with an accurately known vapour pressure allows assessment of f_{ij}, and gives confidence in the method, however it gives no assistance in the assessment of l in the CVL, and merely duplicates one of a number of techniques for the measurement of f_{ij}. This measurement may also be performed, however, in the CVL as, in close proximity to the plasma tube wall, the copper number density will be determined by the vapour pressure of copper at the tube wall temperature and if this latter value can be measured then the expected total copper density can be calculated. A critical discussion of the significance of ground state population density measurements with respect to representing total copper population has been presented in Section 2.4.1.

Measurement of the plasma wall temperature may be accomplished using a calibrated and characterised optical pyrometer and a convenient way of extinguishing the CVL. In the present study the requirement for accurate relative timing between a probe laser pulse and the CVL pulse meant that external pulse sources and delay generators were employed to take control of all laser timing (see Section 3.3.4). Provision was therefore available to gate off the trigger pulses to the CVL PSU using a remote, external trigger switch. The optical pyrometer was set up on a hinged mount by which it could be reproducibly moved from a position out of the CVL beam into one of alignment with the bore of the plasma tube, at a slight angle to it, and focused on a point on the plasma tube wall at approximately the mid-point of the length. Having set the alignment and locked the focus on the hot tube the pyrometer was then moved out of the line of the laser beam while the CVL reached full operating temperature. This having been done the pyrometer was set to continuous measuring mode, with the trigger locked, the CVL "kill" switch activated and the pyrometer rapidly lowered into position. In this way a continuous series of measurements could be made, without further touching the system, initially at 5 second intervals, starting 5 seconds after deactivating the CVL, extending to 10 second intervals after the first minute. Having repeated this a number of times a cooling curve for the plasma tube could thus be plotted and extrapolation back to operating temperature undertaken with reasonable confidence.

Further details of these measurements and the cooling curve thus obtained, are presented in Section 9.2.3 (I).

3.3 EXPERIMENTAL IMPLEMENTATION

The specific instrumental requirements of the hook method as applied to this study will now be discussed by considering the different units illustrated in the schematic of the layout illustrated in Figure 3.2, following the probe beam path around the system.

3.3.1 THE PROBE BEAM SOURCE

3.3.1 (I) Requirements

In discussing the theory of the hook method above, a number of essential, or desirable, qualities of the probe beam source were highlighted. Firstly it must be sufficiently broad-band to allow the maximum expected hook separation to be illuminated with sufficient intensity to ensure adequate exposure of the detector to be employed, but without risking either totally losing structure at the centre of the field or even risking damaging the detector. It can therefore be either genuinely broad-band over all the wavelengths to be used, such as for instance an electronic flash tube, or tunable and quasi broad-band. Ideally it should offer approximately uniform intensity illumination over a band-width of at least two or three nanometres evenly spaced on either side of the line of interest. In addition to illuminating the hooks it must be possible for the necessary measurements to allow the calculation of the hook constant K to be made in a region of the spectrum sufficiently far from any absorption lines to be unperturbed.

If time resolution is required then the pulse length must be short enough to provide the necessary resolution, however it must also be of sufficient intensity to allow exposure of the detector in a single pulse. It must be possible to define the path of the probe beam around the optical layout such that such spatial resolution as might be necessary may be obtained whilst still maintaining sufficient intensity. Again, if time resolution is required it must be possible to synchronise the timing of the probe pulse with any point in the CVL cycle with jitter commensurate with the time resolution required. Finally the source must have sufficient lateral coherence to allow clear fringes to be generated at the optimum value of K and at all wavelengths of interest (including away from the absorption line to allow determination of K).

3.3.1 (II) The dye laser

The combination of requirements discussed above is most readily met by a dye laser pumped by a Q-switched, pulsed, high energy laser. For the present study a Nd:YAG solid-state laser was chosen as the pump source as, although the fundamental output is at 1064 nm and is thus unsuitable for pumping any of the dyes to be used in this study, it is of sufficiently high pulse energy to allow efficient frequency doubling and tripling by second and third harmonic generation using non-linear crystals. Subsequent Brewster angle prism harmonic separation allows almost lossless selection of the desired harmonic. The second and third harmonics, at 532 nm and 355 nm respectively, offer very suitable pump wavelengths for a wide range of readily available laser dyes offering outputs from just into the near ultraviolet ($\sim$375 nm) to the near infra-red[1].

The pulse length and maximum pulse energy of the two stage, Q-switched, flashlamp pumped Nd:YAG laser chosen for the present application is around 7 ns with 800 mJ at the fundamental, at 10 Hz prf, 350 mJ at 532 nm, and 150 mJ at 355 nm. As the laser employed a two stage oscillator-amplifier configuration it was possible to adjust the output power down from these maximum values by allowing the oscillator stage to operate at maximum efficiency but adjust the discharge voltage on the amplifier flash tubes until optimum intensity was observed on the detector. Owing to the Brewster angle harmonic separator the polarisation of the laser output was horizontal for the fundamental and third harmonic, and vertical for the second harmonic.

The dye laser selected for the study was also of the two stage oscillator-amplifier design, though with a single circulator pumping the dye solution through first the oscillator stage and then the amplifier.

3.3.1 (III) Quasi broad-band operation

In common with more or less all standard commercial dye laser systems our device, as purchased, gave narrow-band output specified by the manufacturers as

---

[1]Fourth harmonic generation was also possible, though requiring a separate harmonic separation assembly employing a Pellin-Broca prism, offering direct generation of tunable near UV from a few modern dyes, though only down to wavelengths of around 325 nm. The range of dyes available in this region of the spectrum is limited, however there has been little testing with a Nd:YAG 266 nm pump source, and their efficiency is frequently low.

0.075 cm^{-1} (0.02 Å) FWHM at 570 nm. This bandwidth was obviously far too narrow to allow implementation of the hook method and consequently some degree of modification was required. The oscillator cavity tuning mechanism of the dye laser consisted of a grazing incidence 2400 lmm^{-1} diffraction grating, around which a high reflectance mirror could be driven by a high precision stepper motor to provide the wavelength-selective feedback. An achromatic, low loss prism beam expander between the oscillator dye cell and the diffraction grating allowed the angle of incidence required to fill the grating to be reduced from about 89° for direct incidence to about 85° thus improving efficiency. The diffraction grating was mounted, pre-aligned, on a rigid base that was clipped, spring loaded, into accurate configuration onto three pre-settable mounting points such that it could be removed and replaced into alignment without further adjustment. To modify the system for quasi broad-band operation it was necessary to remove the grating block and make an exact replica of the base onto which could be mounted a fused silica prism. Having experimented with both 60° and 45° fused silica prisms satisfactory performance was found from the dispersion afforded by the 60° prism, which was mounted in the minimum deviation orientation with $\theta_i \approx 49°$. This gave an output band-width of 2.8 nm FWHM.

Pumped by the Nd:YAG laser we were thus able to generate tunable, quasi broad-band laser pulses of 5 ns duration and, for 532 nm pumping, up to 100 mJ energy.

3.3.2 BROAD-BAND FREQUENCY DOUBLING

To make hook measurements of the copper ground state population density it was necessary to make use of one or both of the resonance lines at 324.8 nm and 327.4 nm respectively. Although these are just in the range accessible by some of the modern short wavelength dyes, rather than attempt fourth harmonic generation of the Nd:YAG output in order to pump these relatively inefficient dyes it was decided to frequency double the dye laser output by second harmonic generation (SHG) in a non-linear crystal. This approach would have a number of advantages, but one significant disadvantage. Although at first sight it would appear sensible to undertake the non-linear processes as early as possible in the system thus making use of the higher energy of the pump pulse, it is upon the intensity of the input pulse that the efficiency of a non-linear process will depend, rather than the total energy and thus the smaller diameter of the dye laser beam

compared with the Nd:YAG beam (1 mm: 5 mm) means that the ratio of the areas would far outweigh the conversion efficiency of the dye laser (typically 20-30%). The cost of large non-linear crystals is considerably greater than for smaller ones which, combined with the cost of large aperture, high energy, harmonic separation would render the cost of this strategy very high. In addition, operation of dyes at these wavelengths is very much at the limit of those at present available, conversion efficiency is low and the dyes are of poor stability. The significant disadvantage of SHG of the dye laser output is that it must be accomplished whilst retaining sufficient bandwidth to allow the hook measurements to remain possible.

3.3.2 (I) Theory of SHG

The restriction to broad-band SHG is the requirement that if power is to be converted from the fundamental to the second harmonic in a medium it is necessary that the polarisation wave at the second harmonic, created by the fundamental, and with a phase velocity and wavelength determined by the refractive index of the medium at the fundamental frequency, remain in phase with the electromagnetic wave at the harmonic, with phase velocity and wavelength determined by the refractive index at the doubled frequency. For this to be possible it is required that these two values of refractive index are equal, which does not generally occur. The result of this is that whilst the conversion from fundamental to second harmonic polarisation wave increases with path-length through the medium, there is an increasing phase lag between the electromagnetic and polarisation waves which results in power being gradually coupled back into the fundamental. Conversion efficiency therefore initially increases with distance into the medium up to a maximum value at a distance determined by the difference in wave number, Δk, for the two waves, whereupon it decreases symmetrically back to zero. As the passage through the medium continues this periodic increase then decrease also continues, for which a coherence length l_c is defined as half the period, for that fundamental frequency (with wavelength λ_1), for that medium, in that orientation (Koechner, 1988):

$$l_c = \frac{\pi}{\Delta k} = \frac{\lambda_1}{4(n_{2\omega} - n_{\omega})} \qquad (3.13)$$

in which n_ω and$n_{2\omega}$ are the refractive index of the medium at the fundamental and second

harmonic frequencies respectively. The value of the nonlinear conversion constant K_{NL} for a given frequency, ω_1, is given by:

$$K_{NL} = 2\eta^3 \omega_1^2 d_{eff}^2 \tag{3.14}$$

where $\eta = \left(\frac{\mu_0}{\varepsilon_0 \varepsilon_r}\right)^{1/2}$ is the plane wave impedance and d_{eff} is the effective non-linear coefficient of the medium. For the low efficiency approximation we can obtain an expression for the conversion efficiency in terms of l_c:

$$\frac{P_{2\omega}}{P_\omega} = l_c^2 K_{NL} \frac{4}{\pi^2} \frac{P_\omega}{A} \sin^2\left(\frac{\pi l}{2 l_c}\right) \tag{3.15}$$

in which P_ω and $P_{2\omega}$ are the power at the fundamental and second harmonic respectively for a beam of area A and a distance l travelled through the non-linear medium. If $n_{2\omega}$ could be made equal to n_ω then $l_c = \infty$ and Equation 3.15 reduces to:

$$\frac{P_{2\omega}}{P_\omega} = l^2 K_{NL} \frac{P_\omega}{A} \tag{3.16}$$

and conversion efficiency is proportional to l^2, intensity and K_{NL}.

In order for the $\chi_{(2)}$ non-linear susceptibility term responsible for SHG to be non-zero the non-linear medium must possess a degree of asymmetry. As a result of this it will have an optic axis and therefore be birefringent. The two orthogonal polarisations of randomly polarised light will thus experience different refractive indices. The value of that of the extraordinary ray n^e, with E-field not orthogonal to the optic axis, being dependent upon the angle of propagation with respect to the optic axis, while that of the ordinary ray n^o being independent of orientation. For a negative uniaxial material, such as the non-linear crystals KDP and BBO, n^e - n^o is negative, and this can be exploited by adjusting the angle of propagation until, at the phase match angle θ_m, $n^e_{2\omega}(\theta_m) = n^o_\omega$. This condition is known as type I phase matching and allows efficient SHG along the full length of the non-linear medium for an input beam linearly polarised perpendicular to the optic axis. An alternative condition allowing efficient SHG of a beam polarised either randomly, or linearly at 45° to the optic axis is that: $n^e_{2\omega}(\theta_m) = \frac{1}{2}(n^e_\omega(\theta_m) + n^o_\omega)$, or type II phase matching. For a given orientation of input beam phase matching occurs for a unique input frequency.

3.3.2 (II) The effect of bandwidth in SHG

If a range of frequencies is present in the input beam, as is the case in our quasi broad-band probe beam, SHG efficiency for a given length of medium will fall off on either side of that for which phase matching has been arranged. This will have the effect of generating an intensity profile on the second harmonic output from an input of uniform intensity. The bandwidth over which the doubling efficiency falls to one half that at the phase matched wavelength is called the spectral acceptance, $\Delta\lambda$, and is proportional to wavelength λ_1, and inversely proportional to length l of medium. For type I phase matching:

$$\Delta\lambda = \frac{0.44\,\lambda_1}{l}\left(\frac{\partial n_\omega^o}{\partial\lambda_1} - \frac{1}{2}\frac{\partial n_{2\omega}^e(\theta)}{\partial\lambda_2}\right) \qquad (3.17)$$

As the efficiency of SHG is also proportional to input intensity, if a broad-band input beam already shows an intensity profile, the profile at the second harmonic can show a very rapid spectral dependence.

3.3.2 (III) Detector dynamic range

The extent to which the hook method is susceptible to an intensity profile across the bandwidth of the probe beam depends upon the dynamic range of the detector. If this is limited, as will be the case with a digital detector such as a CCD for which only 256 intensity levels are available for an 8 bit device, then sufficient uniformity must be maintained across the fringe pattern to allow the accurate measurement of the positions of the most widely spaced hooks. What is therefore required of the non-linear medium is both a high spectral acceptance and large non-linear coefficients so that a short length of material can be employed. In choosing the length of the SHG crystal to be employed the $1/l$ dependence of spectral acceptance, and thus spectral uniformity, must be set against the l^2 dependence of efficiency, and will depend upon the dynamic range and sensitivity of the detector.

3.3.2 (IV) BBO

The material chosen was β-Barium Borate (BBO) which is a modern non-linear crystal exhibiting the properties required of relatively high spectral acceptance of

0.67 nm.cm at 650 nm for SHG with type I phase matching, and high non-linear coefficient of d_{eff} six times that of KDP for SHG at 1064 nm with type I phase matching. KDP is a well established non-linear material providing benchmarks with which parameters of more recent materials are compared. In addition to the favourable non-linear parameters BBO also displays a number of other beneficial properties including low hygroscopic susceptibility and extremely high damage threshold. A 5 mm cube of BBO was purchased to allow broad-band SHG of the beam from the dye laser.

3.3.3 OPTICS

In selecting optics the most significant consideration must be given to the potentially very high peak intensity of the probe beam owing to the requirements for both short pulse length, to give the desired time resolution, sufficient energy per pulse to expose the detector in a single pulse after dispersion by the spectrograph and small beam diameter to allow good spatial resolution. For this reason all mirrors involved in the beam steering of the probe beam and in the interferometer consisted of uncoated 90° fused silica prisms.

Two sets of beam-splitters were obtained for the hook method measurements, all coated for 50% transmission at 45°. One set were coated for the visible wavelengths 400 - 700 nm, the other for the UV wavelengths 250 - 400 nm, all hard laser coatings. In specifying and using these components it is necessary to consider the polarisation of the beam incident upon them as they will only offer 50% transmission at 45° for one polarisation. The visible beam-splitters required to be optimised for the p-polarisation, while those for the UV (following SHG) should be optimised for the s-polarisation.

As an aid to accurate alignment of the probe beam with the CVL plasma tube a pair of iris apertures were included at both ends of the CVL. They also allowed definition of the radial resolution of the probe beam in the presence of divergence (specified as 0.5 mrad for the dye laser).

In order to discard a large proportion of the power of the CVL, after alignment a large beam dump consisting of a drilled, anodised heat-sink was placed between the CVL and the iris. The alignment of the interferometer, once accomplished, was sufficiently stable that reasonable hooks could usually be obtained without adjustment once the CVL had returned to temperature having been turned off overnight.

The arrangement of the interferometer will be seen from Figure 3.2 to be such as to allow the probe beam to be reflected at the final beam-splitter BS 2, rather than transmitted following the suggestion of Prowse (Prowse, 1967) to eliminate astigmatism as a result of refraction at BS 2. This would only arise in the case of a non parallel probe beam, however it represents general good practice.

A 2× magnification telescope was incorporated prior to the entrance slit of the spectrograph to match the height of the 2 mm diameter probe beam to that of the 4 mm square sensitive area of the CCD detector. The final optical component before the spectrograph was an f = 40 mm fused silica cylindrical lens to allow the probe beam to fill the 102 mm square mirror of the 1 m focal length Czerny-Turner spectrograph to maximise image brightness and spectral resolution.

3.3.4 TIMING

3.3.4 (I) The Timing reference

A key feature of the present study is that all measurements were to be accurately and reproducibly referenced to a single time origin, uniquely defined. It was therefore decided to reference all timing measurements to the base of the leading edge of the CVL laser pulse (both colours) from the plasma tube centre, which was thus arbitrarily defined as time t = 0 ns. The reason for this was twofold. Firstly, using a photodiode as described later in this section, timing could be checked unambiguously at the beginning of a set of measurements. Secondly the rate of rise of the laser pulse was considerably faster than that of either the voltage or current pulses, thus allowing more precise calibration.

3.3.4 (II) Generating trigger pulses

To achieve accurate timing between the probe beam pulse and the CVL pulse two digital delay/pulse generators were obtained. As can be seen from Figure 3.4 the first was employed as a master oscillator to generate the 6.5 kHz trigger pulses for both the CVL PSU and, following a programmed delay D1, the second digital delay generator (DDG). Once triggered, the DDG will not accept further trigger pulses until it has completed its programmed timing cycle. Following the trigger pulse the DDG provided three output pulses. The first pulse emerged after a programmed, fixed delay D2 and

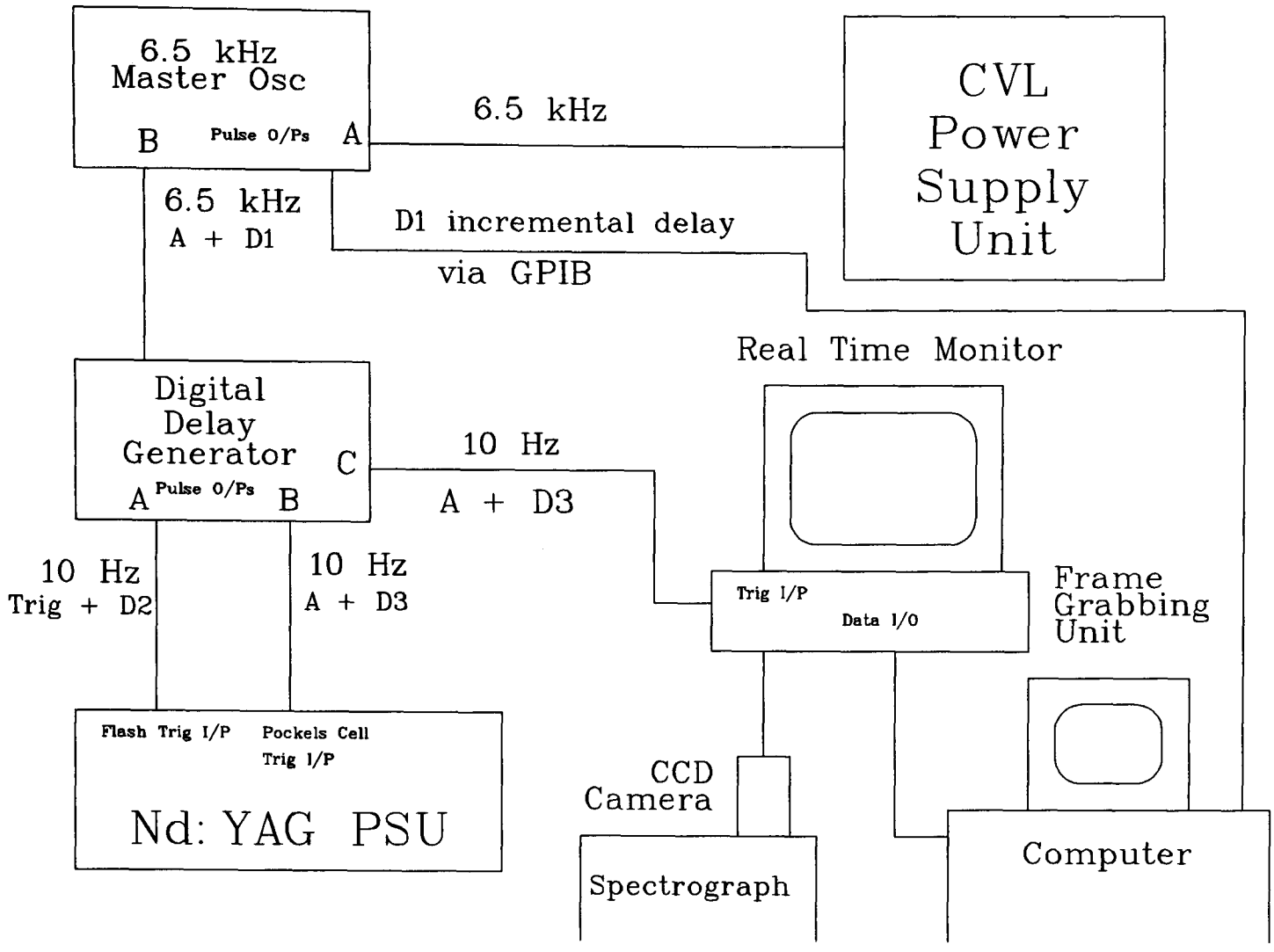

Figure 3.4 Schematic of timing electronics for hook measurements

triggered the flash tubes of the Nd:YAG laser. The reason for this delay was merely to allow delay D1 to be set at zero for the first measurement timing point. To minimise timing jitter of the probe laser pulse a second trigger pulse was provided after a fixed delay, corresponding to the optimal build-up time (180 μs) of the Nd:YAG, after the first, to trigger the Pockels cell Q-switch. Simultaneously with this second pulse a third was generated to trigger the frame grabbing detection system. A final delay was included into the DDG programme to ensure that for any fixed delay D1 the pairs of trigger pulses to the pump laser maintained a repetition rate of 10 Hz for which the optics and electronics of the Nd:YAG had been optimised. In this way, by adjusting delay D1 the probe pulse could be synchronised accurately and indefinitely with any point in the CVL timing cycle, with the CVL running at a totally unperturbed 6.5 kHz at all times, and the Nd:YAG laser at an exact 10 Hz except when called upon to increment its delay by a few nano- or microseconds.

3.3.4 (III) Computer control

Both delay generators incorporated a GPIB (general purpose interface bus) card allowing each to have dialogue with a master controller card in a remote personal computer (PC) according to the IEEE 488.2 protocol. Although this was not employed in these experiments for the second DDG, it allowed the incremental delay D1 in the master oscillator to be set by the PC as part of a computer programme in overall control of the hook measurements. The CCD detector was part of a complete image grabbing system, designed to be interfaced with a computer such that each image, comprising 256 × 256 pixels from the CCD, was transferred into a frame buffer at each trigger pulse, from which it could be transferred into the memory of the computer. Once in the computer memory it could be manipulated, have measurements made and be saved to hard disk in the form of a 256 × 256 array for subsequent analysis. Although the system was purchased with its own operating environment for the computer this was far too slow and cumbersome for our application and so the software utilities responsible for the individual functions, such as transferring an image from the frame buffer to memory, and saving it to disk, were obtained from the manufacturers in the form of source code units, written for compilation under Borland Turbo Pascal v6.0.

Using the Turbo Pascal language interface for communication via the GPIB link, again obtained from the manufacturers of the controller card, it was possible to write a computer programme that was able to set delay D1, grab the next hook pattern, assign to it a logical filename and save it to disk. It could continue to grab and save subsequent hook patterns until the desired number of duplicates had been obtained (generally two), and then increment D1 to repeat the hook measurements for the next time point. Once the interferometer had been aligned, and the CVL had fully reached stable operation this programme would take total control of the acquisition of the hook patterns until the full set of time points had been acquired. A schematic of the operation of the programme is illustrated in Figure 3.5. The modular, nested loop structure of the programme can be seen which gives a high degree of flexibility. In particular it allowed the use of different delay increments for measurements at different points in the CVL pulse-delay cycle. This means that during the early stages of the current discharge through the CVL, when populations are changing rapidly, measurements could be made at 10 ns intervals,

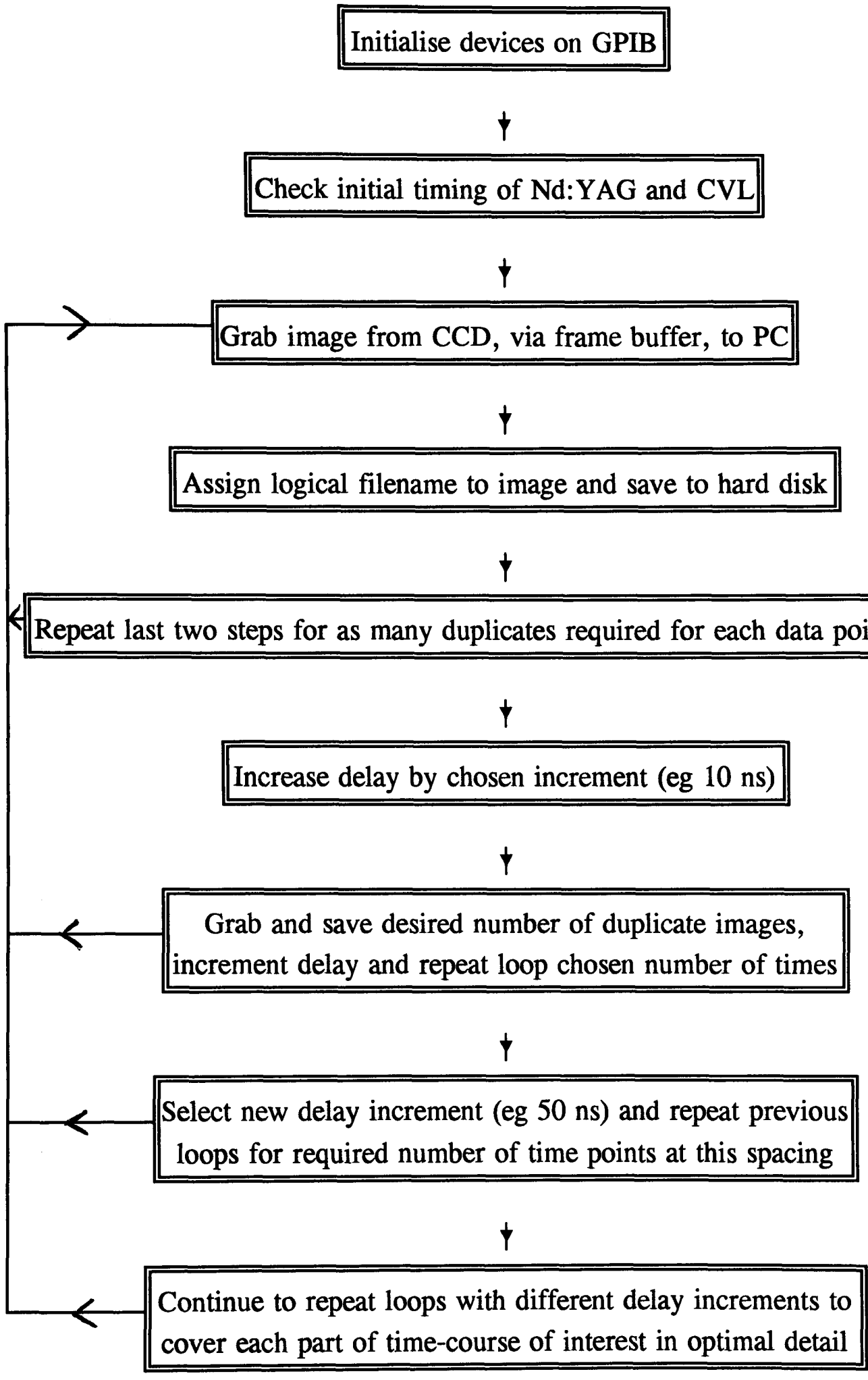

Figure 3.5 Schematic of programme to make hook measurements

whereas in the late stages of the afterglow period it was sufficient to make measurements at intervals of 10 μs.

Using the programme described above, 184 hook patterns (representing 92 time points including a final replica of the first time point) could be acquired in only 5 minutes. This short time ensured that the operation of the CVL remained entirely free of any drift over the time course of the experiments, as verified by the fact that the final measured value of ground state population density (the only level with significant pre-pulse population) should be, and in practice always was, equal to the first, within experimental error.

To make measurements at other radial positions it was merely necessary to move the entire CVL head on its translation stage, transverse to the probe beam path by a preset amount and run the hook acquisition programme again.

3.3.4 (IV) Calibrating the hook constant

Having made measurements at all the radial positions it was necessary to obtain fringe patterns from which the hook constant K could be obtained. To ensure complete freedom from any perturbation as a result of the absorption line, fringe patterns were obtained at a spectrograph offset of 20 Å on each side of the line (ie corresponding to an indicated 60 Å when using the spectrograph in third order), at each radial position, for all excited energy levels. These should all yield the same value of K, and in this way possible sources of error could be eliminated. Because of the proximity of the two resonance lines (324.8 nm and 327.4 nm), and the permanent population in the ground state, it would not have been wise to attempt to measure K between the lines and consequently the calibration was only made on the short wavelength side of the 324.8 nm line, and the long wavelength side of the 327.4 nm line, 30 Å away from line centre. Observation of other measurements justified this and showed no sign of systematic variation as a result of either the radial position or wavelength of the observation. The observed maximum scatter in the measured value of K was $\leq \pm 1\%$, and was in general closer to $\pm 0.5\%$.

3.3.4 (V) Measuring timing jitter

To set up the timing delays, and to measure relative timing jitter between the probe beam pulse and the CVL pulse the vacuum photodiode shown in Figure 3.2 was placed at the unused port of beam-splitter BS 2. By careful selection of filters it was possible to observe both the probe pulse and the CVL pulse simultaneously on the oscilloscope attached to this photodiode. In this way it was possible to set up timing delays empirically, which, owing to their simultaneous observation, were entirely free of instrumental artefacts, such as lead lengths etc. The photodiode itself had a rise time of < 100 ps. In addition to this the timing jitter between the two pulses could be directly observed, and the specifications of the individual components confirmed. The overall timing jitter has been measured as ± 3 ns, corresponding to ± 2 ns from the CVL, ± 1 ns from the probe beam (representing the sum of the Nd:YAG and dye laser), with ± 100 ps specified by the manufacturers for the timing electronics.

3.3.5 CHOICE OF TRANSITIONS AND DYES

The levels for which population densities were to be measured, and the reasons for their choice have been discussed in Chapter 2. In recapitulation the levels were: the copper ground state, the upper laser levels, the lower laser levels, a copper level not belonging to the main sequence (a quartet level) and one of the neon metastable levels. The requirements for the choice of lines to be employed for these measurements via the hook method were as follows:

They should be lines of high oscillator strength, terminating, at the lower end, on the level to be measured.

The upper level should either maintain at all times a population considerably lower than that of the lower level (ie transient population should not accumulate as a result of direct collisional excitation or differential feed and depopulation rates), or the population should be directly measurable itself.

Finally it is desirable that there should not be another line in close proximity.

If the same population could be measured by two different lines this should be done, allowing a secondary check on the system, and the oscillator strength values.

Over the years there have been many studies providing measurements of the oscillator strengths of various lines in the spectrum of neutral copper. These measurements have been made using a variety of techniques, and in some cases the discrepancies in the values obtained have been fairly considerable. In an excellent paper in 1975 (Bielski, 1975) Bielski presented a critical review of all the available measurements and discussed the merits of the various techniques, equipment and calculations employed. In the light of this, together with some calculations of his own, he arrived at a table of what he considered to be the best available values. He also offered figures for what he considered to be the accuracy of the values.

Table 3.1 lists the levels to be measured, the lines used, the oscillator strengths with estimated accuracies (obtained from Bielski, in the case of the copper lines, and the American National Bureau of Standards data (Weise et al, 1966) for the Neon line) and the dyes used in each case. Included in the table is one line which was close to another and of which account had to be taken, and one line used to measure the population density in the $2s^2\ 2p^5\ 3s\ ^3P_0$ metastable level in the neon buffer gas. Figure 3.6 is a full copper term diagram showing all energy levels below 70,000 cm^{-1}, and including the transitions used.

Lower level	Upper level	λ /nm	f_{ij} ±err%	Dye
$3d^{10}\ 4s\ ^2S_{1/2}$	$3d^{10}\ 4p\ ^2P_{3/2}$	324.75	0.433 ±5%	DODCI doubled
$3d^{10}\ 4s\ ^2S_{1/2}$	$3d^{10}\ 4p\ ^2P_{1/2}$	347.40	0.218 ±5%	DODCI doubled
$3d^9\ 4s^2\ ^2D_{3/2}$	$3d^{10}\ 4p\ ^2P_{1/2}$	578.21	0.0048 ±10%	Rhodamine 6G
$3d^9\ 4s^2\ ^2D_{5/2}$	$3d^{10}\ 4p\ ^2P_{3/2}$	510.55	0.0051 ±10%	Coumarin 485
$3d^{10}\ 4p\ ^2P_{1/2}$	$3d^{10}\ 4d\ ^2D_{3/2}$	515.32	0.820 ±10%	Coumarin 503
$3d^{10}\ 4p\ ^2P_{3/2}$	$3d^{10}\ 4d\ ^2D_{5/2}$	521.82	0.747 ±10%	Coumarin 485
$3d^{10}\ 4p\ ^2P_{3/2}$	$3d^{10}\ 4d\ ^2D_{3/2}$	522.01	0.089 ±10%	----
$3d^{10}\ 4p\ ^2P_{3/2}$	$3d^{10}\ 5s\ ^2S_{1/2}$	809.26	0.225 ±10%	LDS 821
$3d^9\ 4s\ 4p\ ^4F_{9/2}$	$3d^9\ 4s\ 5s\ ^4D_{7/2}$	465.11	0.109 ±20%	LD 466
$2p^5\ 3s\ ^3P_0$ (Ne)	$2p^5\ 3p\ ^1D_1$ (Ne)	626.65	0.394 ±10%	Rhodamine 640

Table 3.1 Energy levels studied, transitions and dyes used

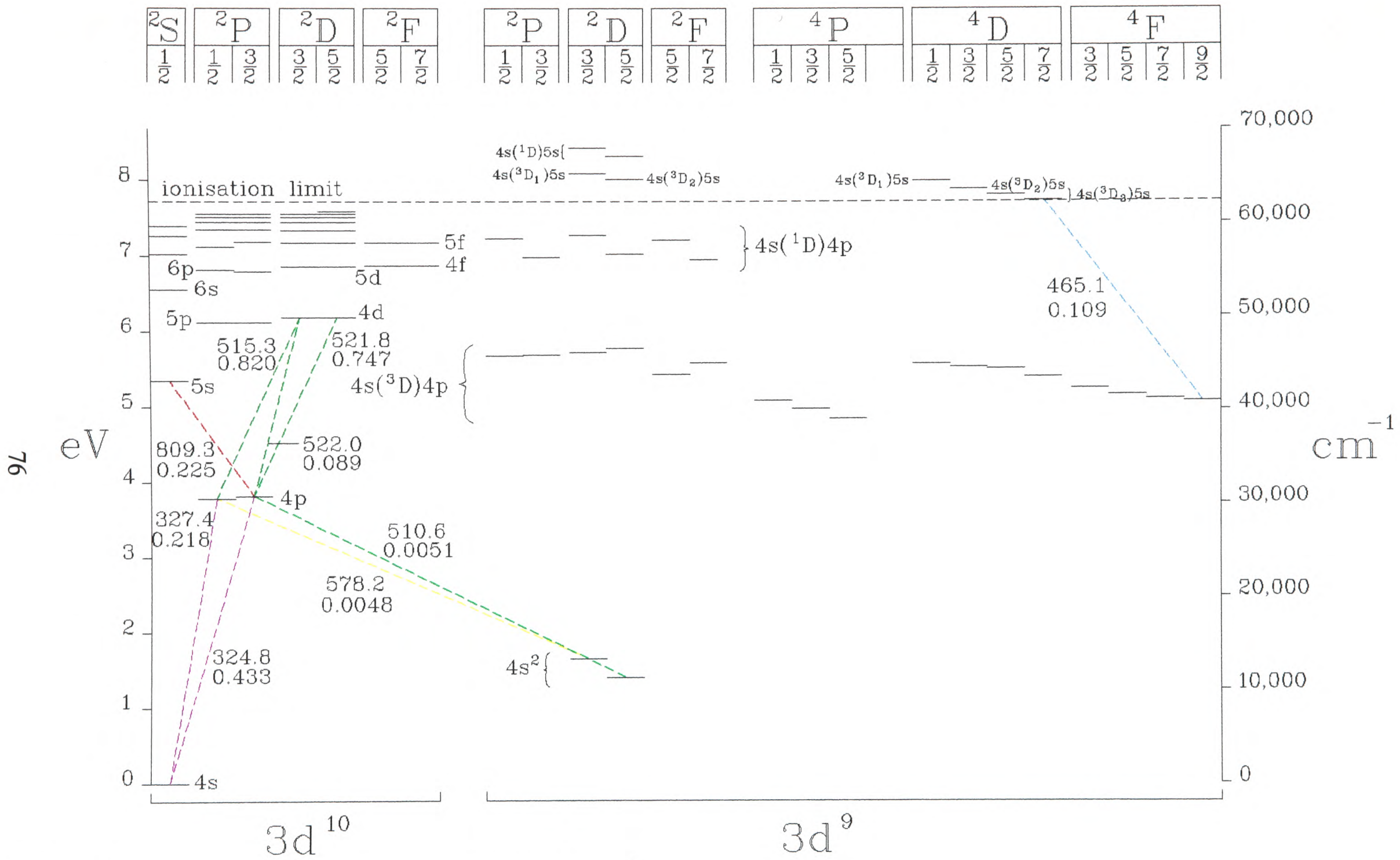

Figure 3.6 Copper term diagram; all levels below 70,000 cm^{-1}

3.3.6 ESTIMATION OF POPULATION LENGTHS TO BE USED

In order to convert the measured hook separation into a population density it is necessary to be able to define the value of the parameter l, the effective length over which the population is estimated to extend. In the case of the copper population measurements it is known that there is no accurately defined length over which it extends at uniform density, and outside which there is negligible density as the density can be expected to fall from its maximum value, which is assumed to extend over the majority of the length of the plasma tube (the "hot" region), to a negligible value at the discharge electrodes which are in direct contact with the water cooled end flanges of the laser head. Between the end of the "hot" region and the electrodes is the "cool" region, a length over which the plasma tube wall temperature falls rapidly and partial pressure of copper vapour falls to zero.

In calculating the population densities in the copper levels the value of 1.3 m will be used. This was obtained from observation of the cold plasma tube and measurement of the copper condensation regions at each end. These measured 120 mm at the cathode end, and 110 mm at the anode end of the 1.5 m plasma tube. These condensation zones, however, correspond to the full length over which the wall temperature is lower than that of any copper blobs within diffusion distance. The copper vapour pressure is therefore too high for the wall temperature and thus condensation occurs. This condensation region therefore consists of a longitudinal temperature gradient up to the full working temperature of the laser. Copper vapour is carried from the "hot" region by diffusion as a result of the partial pressure gradient, resulting in an excessive vapour pressure for the wall temperature and thus condensation. The condensation region may therefore contain a significant number density of copper, though falling rapidly towards the electrodes. The length of 1.3 m was chosen as, between the ends of the 1.27 m of full temperature and the electrodes, a temperature gradient of the order of 75 Kcm^{-1} exists, giving rise to a reduction in copper vapour pressure to about 25% in 1.5 cm. The accuracy of this figure for effective length may be regarded as no better than $\pm 2\%$.

In calculating the population densities in the neon excited levels it might be assumed that as neon is to be found throughout the whole length of the plasma tube that the full length of the distance between the discharge electrodes should be used. This is not found to be correct and further discussion on this topic will be made in Section 7.5.1.

3.3.7 AUTOMATION

In Section 3.3.4(iii), a programme was described which allowed the computer to take control of the running of the experiment, setting the timing for a series of sequential delays to allow a full set of hook patterns to be obtained, and saving each to disk with a unique, logical filename. By implementing this programme the set of measurements at a given radial position could be obtained in around 5 minutes. Repeating this procedure at the 7 radial positions, spaced at 3.5 mm intervals along a radius, could be comfortably managed, together with the calibration fringe patterns to obtain K, in about 45 minutes. Acquisition of the hook measurements was thus very efficient. Owing to the intrinsically bulky nature of the individual measurements in terms of disk storage space, however, we knew we would also have to address the problem of the sheer volume of raw data being produced by the study.

In its raw form each measurement data point consisted of a 256 × 256 pixel image, stored by the computer as a digital array, occupying 64 kB of storage space. Two duplicate data points were acquired for each time point, 92 time points at each radial position, and 7 radial positions for each transition. Consequently in a 45 minute experiment 1,288 hook patterns and 80.5 MB of data were acquired. In addition it was desirable to address the problem of accurately and efficiently analysing the very large number of hook patterns being generated. A programme was therefore written to assist in overcoming both these problems. This programme is described in detail in the paper reproduced in Appendix A1, together with an overview of all the measures taken to automate the hook method for this study.

A brief description of the hook processing programme however is that it reduces each image from a 256 × 256 array to 2 series of 256 data points using a Fourier transform technique, each pair representing the relative phase of each column in the original image. In each of these files the full informational content of the original hook pattern was retained. For archival purposes a commercial file compression algorithm was incorporated into the end of the programme and the original 80.5 MB of hook patterns had been reduced to 7 compressed files of 1 MB each. A final programme was written that allowed the simple, accurate analysis of these phase information files to convert them into hook spacing values for each one.

Modifications of these last two programmes were written to facilitate the calculation of the hook constant K from the calibration fringe patterns.

Using this suite of programmes the acquisition and analysis of the hook patterns could be accomplished in a highly efficient way.

4 REFRACTIVE INDEX MEASUREMENT OF ELECTRON DENSITY

There are a number of ways of measuring the electron density in a plasma. The technique most frequently applied to measurements in the CVL is that of measuring the line-width of one or more emission lines from the Balmer series of hydrogen and attempting to deconvolute the theoretical Stark broadening lineshape component from all the other contributions to the spectral profile. As was briefly discussed in Chapter 1, and will be more fully detailed below, there are a number of shortcomings with this method and so it was decided to attempt to measure the contribution of the electron density to the refractive index of the plasma in the infra-red (IR).

4.1 THEORY

The plasma of the CVL may be regarded as a combination of two different fluids: the heavy particles (gas atoms and ions) and the free electrons. In the previous chapters the refractive index of the plasma was discussed in terms of the contribution from the electrons bound to the atoms and ions, and this allowed the measurement of the population densities of some of these particles. In this chapter effects due to the free electrons will be considered which allow their number density to be measured.

4.1.1 THE REFRACTIVE INDEX CONTRIBUTION FROM THE ELECTRONS

In Chapter 3 the bound electrons were addressed at the classical level by considering them as particles bound to the atom by a lossy, elastic restoring force, and thus as capable of exhibiting damped harmonic motion with a characteristic, resonant frequency. Similarly free electrons, if displaced from their equilibrium positions, can be thought to generate a space charge, also giving rise to a restoring force. In this way a characteristic resonant frequency arising from the free electrons, the plasma frequency ω_p, can be calculated. Where the electron temperature is very much less than the mass energy of the electrons, and the dimensions of the plasma are very much larger than the mean free path of the electrons, ω_p is dependent only upon free electron density n_e and collision frequency for momentum transfer ν_m (Heald and Wharton, 1965):

$$\omega_p = \left(\frac{n_e e^2}{\varepsilon_0 m_e} - \frac{\nu_m^2}{4} \right)^{1/2} \approx \left(\frac{n_e e^2}{\varepsilon_0 m_e} \right)^{1/2} \quad (4.1)$$

as in a low pressure plasma $\nu_m \ll \omega_p$.

From this can be calculated a complex refractive index for the electrons only:

$$\tilde{n}^2 = 1 - \frac{\omega_p^2 (\omega + i \nu_m)}{\omega(\omega^2 + \nu_m^2)} \approx 1 - \frac{\omega_p^2}{\omega^2} \quad (4.2)$$

For the case in which ν_m is small, and at frequencies well above ω_p (such as optical frequencies), then $\tilde{n}$ is fully real, ie absorption is negligible. In the CVL plasma the conditions above hold well for radiation of wavelength $\ll 1$ cm and the simplified forms of Equations 4.1 and 4.2 may be used.

The total refractive index at any wavelength is therefore the sum of the contributions from the heavy particles and the electrons. In the visible region of the spectrum the electron contribution is very small owing to its ω^{-2} dependence, however at longer wavelengths, such as the mid infra-red and longer, the electrons dominate the refractive index. By measuring the refractive index of the plasma at such a wavelength the ratio ω^2_p/ω^2 can be obtained, and thus ω_p and thence n_e calculated. This therefore is the basis for our electron density measurement.

4.1.2 INTERFEROMETRY

The Mach-Zehnder interferometer was set up once again with the CVL in one arm, as in Figure 4.1. With the beam steering optics aligned to give a uniform intensity at the detectors (rather than linear interference fringes as in the hook method) any change in the refractive index of the plasma can be observed as a change of intensity on the detector. Thus any change in n_e gives rise to a variation in intensity which depends upon n_e according to:

$$I = \frac{I_0}{2} \left(1 + \cos \left(\frac{2\pi l (n-1)}{\lambda_0} \right) \right) \quad (4.3)$$

where I_0 is the intensity of the probe beam as it enters the interferometer and n is the real part of $\tilde{n}$, defined by Equations 4.2 and 4.1 in terms of n_e.

Using fast detectors connected to a fast oscilloscope and a CW probe beam, changes in refractive index, or n_e, could then be observed directly and measured.

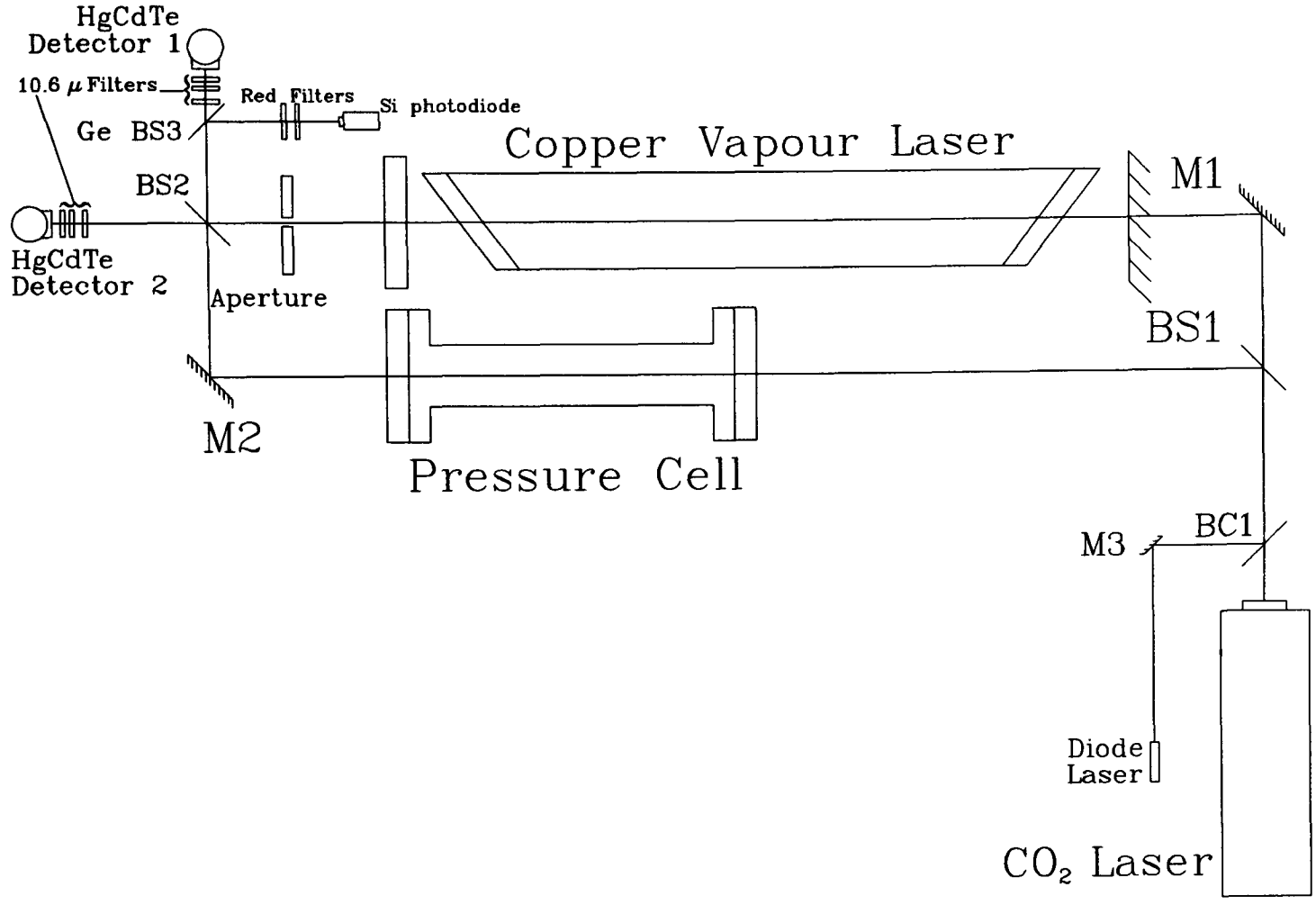

Figure 4.1 Optical layout for electron density measurement

A technique similar to this was first applied to the CVL in 1977 (Batenin et al, 1977) by a group in Moscow. The Russian workers however could only attempt to follow the change in electron density during the afterglow period using this technique since the fast response detectors of 10.6 μm radiation were not then available. They attempted to calculate the electron density during the current pulse from measured current and voltage profiles.

4.2 CHARACTERISTICS OF THE REFRACTIVE INDEX MEASUREMENT OF ELECTRON DENSITY

4.2.1 ADVANTAGES

In common with the hook technique, the measurement of the electron density in a plasma by measuring the refractive index in the mid infra-red has the advantage over most other techniques that very few assumptions are required. In addition to this the only limitation to the time resolution available is that of the detection system required. In Chapter 1 reference was made to the principal alternative technique of measuring the Stark broadening component of a suitable emission line, such as one of the Balmer group

of lines from the spectrum of hydrogen impurity. In order to use this technique to obtain a measurement that is not time or radially resolved requires considerable complex calculation to deconvolute the multiple components of the measured line-width, and many assumptions to assess their relative magnitudes. These components include Doppler broadening as well as fine structure, and are frequently of comparable magnitude and they can seldom be known with the precision desirable. The acquisition of multiple lines on each of which the different line-broadening components have a different relative effect helps to determine their relative magnitudes, but a high level of accuracy is still not possible owing to the very small effects to be measured.

If, as in the present situation, time resolution is required then the experiment becomes more complicated still. Owing to the low density of hydrogen in the CVL plasma, and consequently very low intensity of the spontaneous emission signal, it is not at present possible to use fast photodiodes as the detectors, or any kind of narrow width time gating technique. It is therefore necessary to use sensitive photomultiplier tubes and use boxcar averaging techniques which reduces the time resolution possible and can potentially introduce artefacts.

If spatial resolution is required also, the method of collecting spontaneous emission from a defined cylinder within the plasma devised by Webb (Webb, 1968) and employed in the experiments of Chapter 6 of this thesis and described there, must be used. This further reduces the intensity of the signal to be acquired, making the potential for reasonable time resolution considerably worse.

4.2.2 LIMITATIONS

Again in common with the hook method, the penalty for the freedom from assumptions is that of relatively low sensitivity. In addition to this is the fact that this technique does not measure absolute electron density but only changes. If absolute values are required then it becomes necessary to measure the initial value by measuring the change as it falls to zero. If this is not practical then another method must be found to obtain the initial value.

The limitation to the sensitivity is the accuracy with which a fraction of a fringe shift may be measured in the output of the infra-red detectors. This will depend upon a number of experimental factors including the stability of the optical bench and its

freedom from vibration, air movement within the interferometer and the signal to noise ratio *(S/N)* available from the IR detectors and pre-amplifiers. This may be calculated from the detectivity D^* specified for the detector, the power W incident upon the detector of area A, connected to an amplifier of bandwidth Δf by the expression:

$$D^* = \frac{(S/N)\,(A\Delta f)^{1/2}}{W} \qquad \textbf{(4.4)}$$

In addition the presence of electromagnetic noise (eg radiated by the CVL discharge) and the ability of the experimenter to eliminate it from the detector signal can have a significant effect.

From Equation 4.1 the fringe shift Δm produced by a change in electron density Δn_e over a length l, at a wavelength λ_0 in air can be calculated:

$$\Delta m \approx -\frac{l\ \omega_p \Delta\omega_p \lambda_0}{4\pi^2 c^2} \qquad \textbf{(4.5)}$$

For the case of the CVL to be used for this study, for which l = 1.5 m this can be rewritten:

$$\Delta m = -6.72 \times 10^{-10}\ \lambda_0 \Delta n_e \qquad \textbf{(4.6)}$$

for n_e in cm^{-3}.

Depending upon the factors discussed above, the minimum measurable electron density change can be calculated from Equation 4.5 according to the minimum resolvable fringe shift and could be expected to lie between about 0.25 and 0.01 fringes without excessive precautions, and is estimated to be about 0.05 fringes in the system employed for the experiments described here.

Within the constraints of the fringe shift resolution it can be seen from Equation 4.5 that, for a given electron density, the fringe shift can be increased by increasing the path length l over which it is measured, or the wavelength λ_0 of the probe beam (provided that its frequency remains greater than the plasma frequency). If the length of the test cell is fixed it may be possible to increase l by multi-passing the probe beam through it by means of mirrors. The use of wavelengths significantly longer than 10.6 μ is seldom practical for reasons to be discussed below.

4.2.3 ACCURACY

The accuracy with which a given measurement may be made, (including that of the initial, baseline electron density) depends upon the accuracy with which the length l is known (and, if not fixed, that of λ_0), and the accuracy with which the fringe shift, both as a result of the change in plasma frequency, and that corresponding to the maximum change in intensity, may be measured. If the measured fringe shift from the change in electron density is greater than one half fringe then it is possible to include the maximum amplitude change, yielding a "self calibrating" interference signal from the detector.

The accuracy with which fringe shifts may be measured is determined by the same factors as discussed in Section 4.2.2 above that control ultimate sensitivity. When measurements of electron density are made that are well above the limit of sensitivity, and many fringe shifts are generated, then the absolute accuracy with which an individual fringe shift may be measured becomes of relatively lower importance.

If a high degree of accuracy is required then there are additional precautions that must be taken. The first concerns the accurate assessment of the full amplitude of the fringe shift. If the change in refractive index owing to the change in electron density is sufficient to generate a phase change greater than π radians then it is possible to ensure that the full amplitude change may be observed within the interferogram, thus providing a self-calibrating measurement. If however the fringe shift is smaller than this then it is necessary to obtain an independent calibration of the maximum extent of amplitude change. It is essential that this is undertaken under identical conditions to the original measurement. In the case of the radially resolved measurements described in the present study, for instance, it would be necessary to obtain an independent fringe amplitude calibration at each radial position. The reason for this is that if the optical transmission of any part of the system was not entirely constant at all positions, such as would be the case if there were any spots of condensed copper on the windows of the laser head, this would affect the maximum fringe amplitude available, and thus the calibration required.

This effect can be observed in a temporal as well as a spatial dimension. Clouds of dust disturbed within the plasma tube, or in the reference arm of the interferometer will also cause variation in the calibration of the measurement. Fortunately the time scale of the CVL pulse cycle is sufficiently fast that such variation within a measurement is unlikely to be significant, but between measurements, and between a measurement and

its calibration scan, variation can occur. It was in an attempt to minimise such artefacts that the two HgCdTe detectors were purchased, as discussed in Section 4.3.1 (IV) below.

If measurements are made always commencing from the point of minimum intensity (maximum destructive interference), as they were in the present study, then the amplitude of this signal can also give a sensitive indicator of differential scattering or absorption effects in one arm of the interferometer.

It must be remembered that the data processing required to convert the observed amplitude of interference signal into a measurement of electron density is that of a cosine function (Equation 4.3). This is significant in two respects. Firstly it is very sensitive to accurate calibration of the maximum fringe amplitude, as described above, and secondly the effect of inaccuracy (and likewise noise on the signal) is disproportionately magnified at some phases of the signal, relative to others. Consequently at phases around 0, π, 2π radians, etc, noise (and likewise the effect of an inaccurately positioned point) will appear disproportionately large in comparison with that around $\pi/2$, $3\pi/2$ radians, etc. This is most likely to be encountered when the starting or finishing point of the phase shift occurs within one of these "sensitive" regions.

The final contribution to the overall accuracy of a technique of this kind is that of the accurate assessment of the starting and finishing points of the phase shift, and as described immediately above, this is at its most critical when these points occur close to an extremum of the cosine function. For this reason it might appear that to arrange for all measurements to start at a phase of π radians (minimum fringe amplitude) would be unwise, despite its convenience, and the ability to monitor amplitude effects. It does, however, have the advantages that its position may be assessed unambiguously, relatively easily (as opposed to that of, say, the amplitude mid point), and also it offers the best chance, in cases of phase shifts of between π and 2π radians, of obtaining a trace incorporating the full amplitude of fringe shift. For this reason if multiple cycles of fringe shift are to be observed, then it is likely to be more appropriate to commence from a phase of $\pi/2$ radians.

As a result of the considerations discussed above, and in the light of a problem with the detectors discussed in Section 4.3.2 (IV), it is estimated that the absolute accuracy of measurements generating a fringe shift between π and 2π radians is $\pm 10\%$ or better, and that of those of less than π radians is about $\pm 25\%$ or better. These figures

represent the signal at the core of the noise as a noise signal will be observed, superimposed upon the true signal, as a result of the noise figure of the pre-amplifier which will then be manipulated with the signal during the data handling.

4.3 EXPERIMENTAL IMPLEMENTATION

4.3.1 THE EQUIPMENT AND EXPERIMENTAL LAYOUT

The optical components for the measurement of electron density were mounted on the optical bench as in Figure 4.1 above.

4.3.1 (I) The choice of probe beam source

Previous studies had suggested that electron densities of the order of 10^{13}-10^{14}cm^{-3} should be expected. The commonest, most easily available and convenient laser source in the mid infra-red is the CO_2 laser which offers output on a number of lines in the spectral region around 10.6 μm, either CW or pulsed. Since CO_2 lasers are frequently used in industry as well as in research laboratories, standard optics for 10.6 μm are readily available and a number of optical materials offer good transmission at this wavelength as well as in the visible.

For λ_0 = 10.6 μm Equation 4.6 above gives a fringe shift of 0.07, or a 14% change in amplitude for 100% fringe visibility, for $n_e = 10^{13}$ cm^{-3}. Although a larger fringe shift would have been desirable this is a perfectly measurable figure and, because of the linear dependence of Δm on λ_0, it would have required a considerably longer wavelength to have increased the fringe shift significantly. The unavailability of fast detectors and suitable optical materials, and the cost of the optics and beam source required to operate at longer wavelengths rendered this unreasonable. The primary probe beam source selected therefore was a 4 W CW waveguide CO_2 laser, incorporating closed loop, thermostatically controlled water cooling which, together with the mechanically stable ceramic laser head, ensured operation on a single longitudinal mode (SLM), without any hopping between modes.

4.3.1 (II) The two wavelength experiment

As the experiment concerns the fringe shift at 10.6 μm over the course of the CVL discharge cycle it was necessary to determine what proportion of the change in

refractive index was due to a change in electron density, and how much came about as a result of changes in the atom and ion densities. To separate these contributions it was therefore necessary to perform the experiment at 10.6 μm, and also at a much shorter, visible wavelength. A convenient source for the visible radiation was a small, 2 mW laser diode, giving CW output at 670 nm. Both the CO_2 and diode lasers were mounted on a single plate together with a small right angled prism to act as a mirror (M3 in Figure 4.1), and a ZnSe beam combiner (BC1) coated to reflect all the red beam whilst transmitting all the IR one. Adjustments were provided to ensure that both beams could be aligned to be accurately collinear, and parallel to the optical bench on which the unit was mounted. In addition to providing the second, visible wavelength for the measurement, once the two beams had been aligned the visible beam greatly assisted in the alignment of the beam path through the Mach-Zehnder interferometer.

4.3.1 (III) Optical materials

As the experiment was to be performed at two very different wavelengths it was necessary that all the optics were appropriate for both wavelengths. While this obviously precluded Ge for the interferometer beam-splitters ZnSe could conveniently be used. Standard mirrors for use with 10.6 μm laser radiation were also appropriate for use in the visible.

In order to allow the transmission of both wavelengths through the CVL it was necessary to replace both the CVL windows and the cavity mirrors as discussed in Section 1.5. For the reasons outlined there the material chosen for this purpose was BaF_2, and uncoated BaF_2 disks were used for both windows and output coupler. However, again for the reason given before, no rear cavity mirror was used for these measurements.

4.3.1 (IV) Detectors used

Three detectors were used in all: for the IR radiation two liquid nitrogen cooled, HgCdTe photovoltaic devices (supplied by Laser Monitoring Systems Ltd) with matched pre-amplifiers (which also provided the bias current) and a single Si photodiode (Elliot Scientific model DET2-SI) to allow the detection of the visible wavelengths. In addition to the red laser diode radiation the Si photodiode could be used to detect a little of the

green ASE from the CVL to give an accurate timing marker to which to relate the IR measurements (provided that the effect of optical and electrical path lengths had been taken into account). Each HgCdTe detector had a 100 μm square active area and was specified by the manufacturers as having a bandwidth of 100 MHz. The bandwidth of the pre-amplifiers was specified as DC to 75 MHz. The Si photodiode was specified as having a rise-time of $\sim$300 ps into a 50 Ω load.

The reason for using two HgCdTe detectors was that by mounting them at the two outputs of the final beam-splitter BS2 it would be possible to ensure that any observed change of intensity at Detector 1 came about as a result of interference effects rather than absorption, scattering or deflection of either beam. This is because, in the absence of such effects, the two interference signals should have a phase shift between them of π radians and consequently their sum should give a signal of constant amplitude provided that both detectors and their pre-amplifiers are matched. It was later found however, by observing both the probe and reference beams independently, that no amplitude effects occurred and thus the signal from a single detector could be used.

In order to minimise detection of the background IR black body emission from the CVL plasma tube, which peaks at 1.7 μm, 10.6 μm transmission band-pass filters were mounted in front of the two detectors. As the level of black body background would not be expected to change over the discharge pulse cycle it would merely add a constant offset to both signals to be removed later, as described below. The background does however have the undesirable effect of decreasing the available dynamic range of the detectors and making it harder to assess the contrast of the fringes obtained. Neutral density (ND) filters suitable for use in the infra-red were also mounted in front of the detectors to optimise the available signal for the dynamic range of the detectors, and to ensure equal amplitude signals from each. In the case of Detector 2 they were also required to compensate for a 45° Ge disk mounted in front of Detector 1 that reflected the visible light out of the IR beam, and towards the Si photodiode. Between these last two components was also mounted a number of filters to remove any residual IR, and remove (or reduce, depending upon the measurement to be made) the ASE signal from the CVL.

4.3.1 (V) The compensation cell

The final component was the compensation pressure cell which was included in the reference arm of the interferometer. This consisted of a brass tube with window mountings normal to the tube axis to take the same size BaF_2 flats as the CVL, and a fitting connected to a gas line. The gas line was connected to a three way tap, independently and rigidly mounted, by which the cell could either be sealed off, connected to a regulated helium supply at about 2 bar, or opened to the atmosphere. Using this cell it was possible to introduce an additional phase shift to the interference signal without introducing any walk-off effects, or coupling any vibration to the system, and lock it at any chosen point.

The compensation cell therefore performed two valuable functions. It allowed the amplitude of a full 2π phase shift to be observed on both detectors, thus calibrating phase shifts of less than this amount, and it allowed the starting point of the fringe shifts to be set to any arbitrary value to facilitate subsequent analysis. It was chosen that the starting point be that of minimum fringe amplitude, ie full destructive interference for the reasons given above.

4.3.1 (VI) Other experimental details

The detectors were all connected to a 500 MSs^{-1} digital oscilloscope (Tektronics model 2440). In the same way as the digital delay generators described in Chapter 3, the oscilloscope incorporated a GPIB card allowing it to be connected to a master controller card in the host computer allowing dialogue between the two devices. Via this connection, digitised oscilloscope traces could be transferred to the computer for manipulation and analysis. The oscilloscope sweep was triggered by a synchronisation pulse from the master oscillator providing the trigger pulses for the CVL, so that absolute time correspondence was assured at all times. The ASE signal from the CVL, detected by the Si photodiode, allowed all traces to be referred accurately to the same absolute time origin as the hook method measurements.

A remote, hand held, momentary action, trigger switch (with appropriate switch bounce supression) was connected to the inhibit socket of the master oscillator, and also to the oscilloscope. In this way the CVL discharge could be gated off for a few hundred

milliseconds, and the oscilloscope triggered simultaneously in order to obtain the value of the initial, pre-pulse electron density.

As in the earlier measurements, iris apertures were used to help align and define the probe beams. The final spatial resolution, however, was determined by the size of the detector sensitive areas: 100 μm $\times$ 100 μm square for the HgCdTe IR detectors, and 1 mm^2 circular for the Si visible one.

4.3.2 THE EXPERIMENTAL PROTOCOL

4.3.2 (I) Alignment

The interferometer was first aligned with the red beam, and its alignment was then confirmed for the IR using 10.6 μm beam detector plates in a range of sensitivities to match the rapidly diverging (though diffraction limited) beam. Despite the slow time response of the more sensitive grades of detector plate it was easy to observe visually stripe interference fringes when the interferometer optics were misaligned.

4.3.2 (II) Measurement of the refractive index of neon at 10.6 μm

To check the correct functioning of the equipment, and also obtain the value of the refractive index of the neon buffer gas at 10.6 μm, preliminary measurements to determine the refractive index at both wavelengths were carried out. For each wavelength this involved connecting the output of the appropriate detector to a chart recorder so that the exact number of interference fringes could be counted while neon was bled into the (cold) CVL between two measured pressures. The results obtained for n - 1 were compared with the values calculated from the empirical expression of Cuthbertson (Cuthbertson & Cuthbertson, 1931), obtained from measurements at 12 wavelengths between 289.4 nm and 546.2 nm. The results of the present work were in perfect agreement with Cuthbertson's value at 670 nm, and very good agreement (better than 0.2%) at 10.6 μm. As the values of refractive index at the two wavelengths differed by only 0.5% the fringe shift observed, as a result of any change in the buffer gas, at the two wavelengths can be taken to be in inverse proportion to the wavelengths. Any effect observed at 670 nm would thus be 15.8 times smaller when observed at 10.6 μm.

4.3.2 (III) The acquisition of the raw data

For each radial position it was necessary to acquire 4 oscilloscope traces at each wavelength during the CVL pulse delay cycle, and 4 at each wavelength to measure the initial (pre-pulse) electron density. In order to provide good time resolution for the fast rising electron density during the current pulse, as well as enabling observation of its behaviour over the full interpulse period, 2 traces were acquired with different timebases on the oscilloscope. Immediately following this a second pair of traces were obtained under identical conditions except without the probe beam. In this way traces could be obtained containing all systematic, spurious optical and electrical signals, including residual background black body radiation, rf radiation as a result of the discharge, and any offset in operating point of either detector as a result of an imperfectly balanced power supply. Typical interference signal and background traces from the HgCdTe detectors, taken on the fast time base of 200 ns/div, may be seen in Figure 4.2.

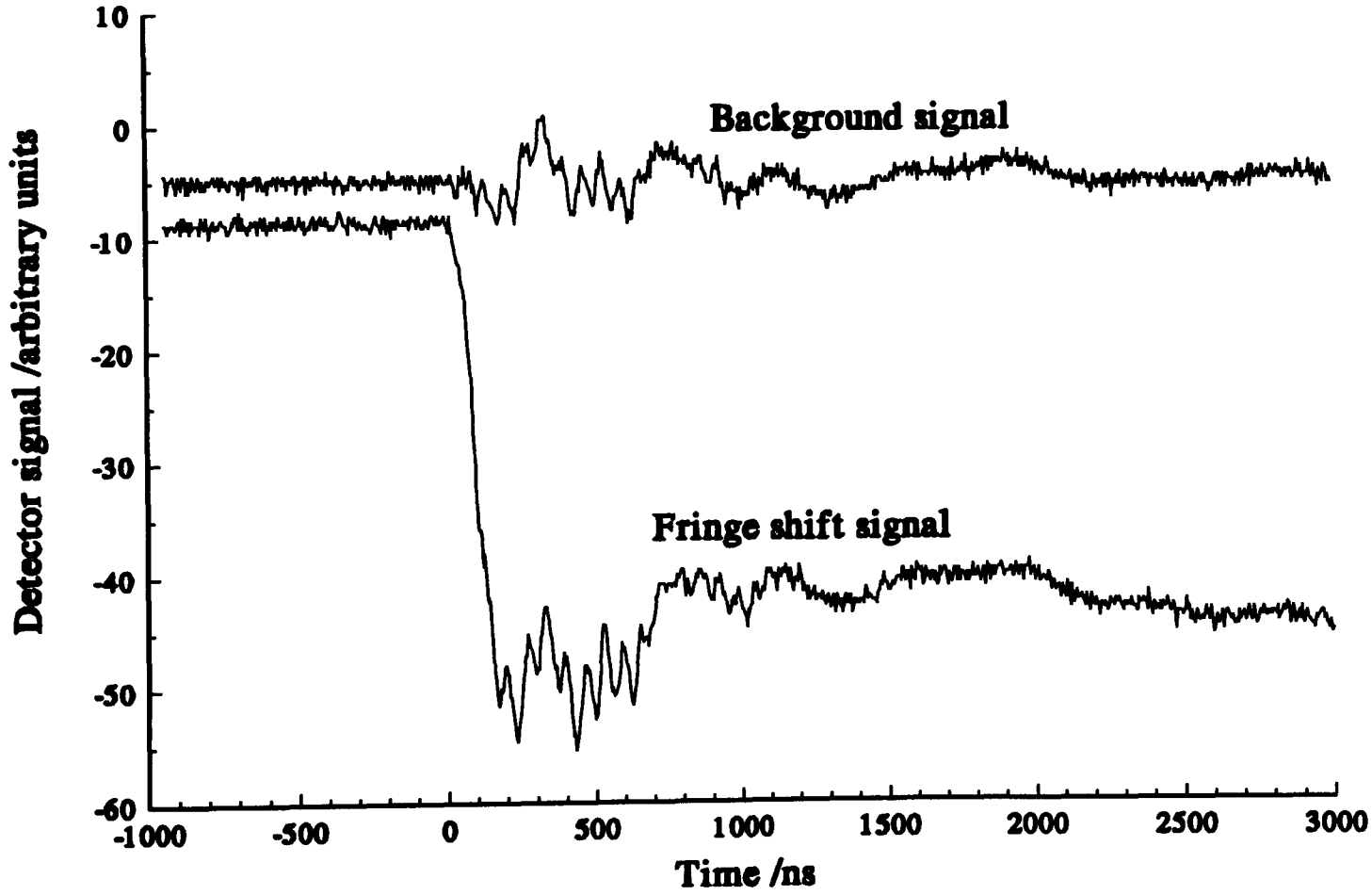

Figure 4.2 Typical traces obtained from the HgCdTe detectors.

The signal corrected for the background may be seen in Figure 4.3.

4.3.2 (IV) Initial handling of the raw data

Each of these traces was then transferred to the computer via the GPIB link and stored on hard disk. Following this the appropriate manipulations of subtracting the background trace from the signal one, and the conversion of the detector signal first into

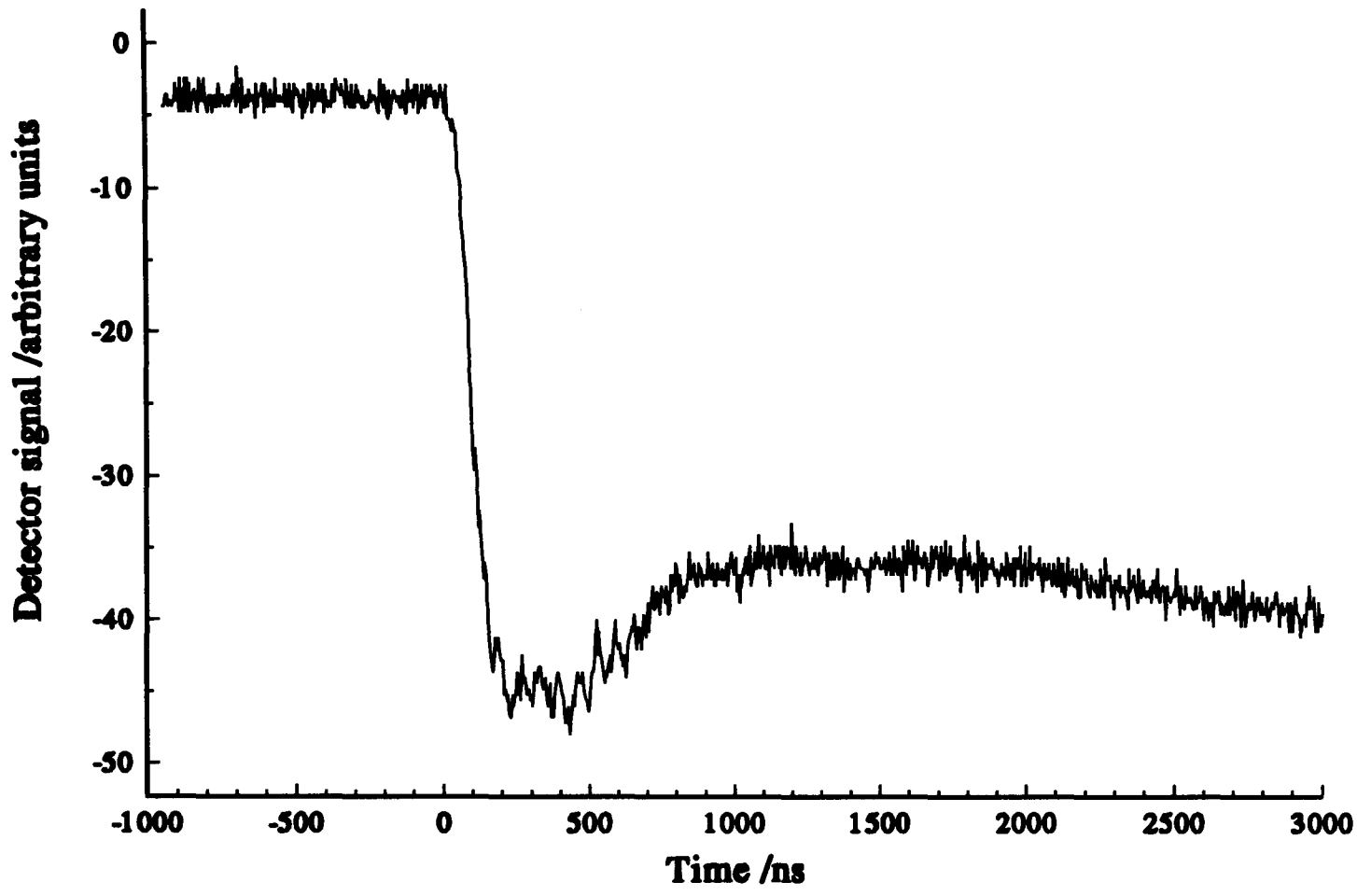

Figure 4.3 Fringe shift trace corrected for background signals

a phase shift (requiring normalisation of the signal to the maximum amplitude fringe shift, measured by varying the pressure in the compensation cell, if the trace itself did not itself contain this information), and thence to a change in electron density.

It was in calibrating this maximum fringe shift signal amplitude that a curious anomaly emerged that was to cause problems with the subsequent data analysis. Despite the fact that the HgCdTe detectors were being used well within the bandwidth specified by the manufacturers (100 MHz) and similarly the matched pre-amplifiers (75 MHz) the maximum observed amplitude of signal for a fringe shift was 17% lower for the high frequency rising electron density signal (corresponding to a frequency of about 600 kHz) than for the slow falling electron density signal (about 4 kHz), and fringe shift generated using the compensation pressure cell. Using a signal generator the frequency response of the pre-amplifiers and oscilloscope was confirmed to be completely flat across the full

specified range at the output amplitude observed, the intensity of the beams in the two arms of the interferometer were measured independently and found not to be changing over this period, and consequently the cause was isolated to the HgCdTe detectors. Attempts were made to reduce the intensity of radiation upon the detector, however this could only be accomplished over a very restricted range as the signal amplitude attainable without an additional stage of amplification was at the limit of sensitivity of the digital oscilloscope, and no significant change could be observed. Once a suitable low noise, broad band amplifier has been procured it is intended that this experiment should be repeated. The effect of this phenomenon has been that, in order to process the results obtained, the rising and falling signals have had to be normalised independently before conversion to phase shifts and may be observed as a slight increase in the (negative) signal from about 1,000 ns in Figure 4.3. From the fact that the fringe shift generated by the rising electron density must be equal to that produced by the same density falling the two half traces could be matched up, however at the cost of assuming that no change in electron density occurred during the period over which the gain, and therefore the measured signal, were assumed to have changed from one regime to the other. This is a reasonable assumption as, over the period that the electron density is at its maximum, the electron temperature in the plasma is too high to allow any significant recombination to occur (This statement will be discussed further and justified in Chapter 8).

4.3.2 (V) Measurement of the pre-pulse electron density

To measure the absolute value of the initial (pre-pulse) electron density, it was necessary to measure the fringe shift as the electron density fell to zero. As described above, a remote, hand held, momentary action switch was connected to both the CVL trigger source pulse inhibit socket and the oscilloscope. With a 470 nF capacitor connected across the switch to inhibit switch bounce, a brief press brought the 5 V inhibit line to ground in 1 μs (followed by about 5 μs - 10 μs of small amplitude ringing), where it stayed for typically 150 ms - 200 ms, thus gating off the trigger pulses to the CVL for this period. This allowed ample time for the electron density to fall to the (negligible) Saha value (the population being reduced sensibly to zero after typically 5 ms), but giving

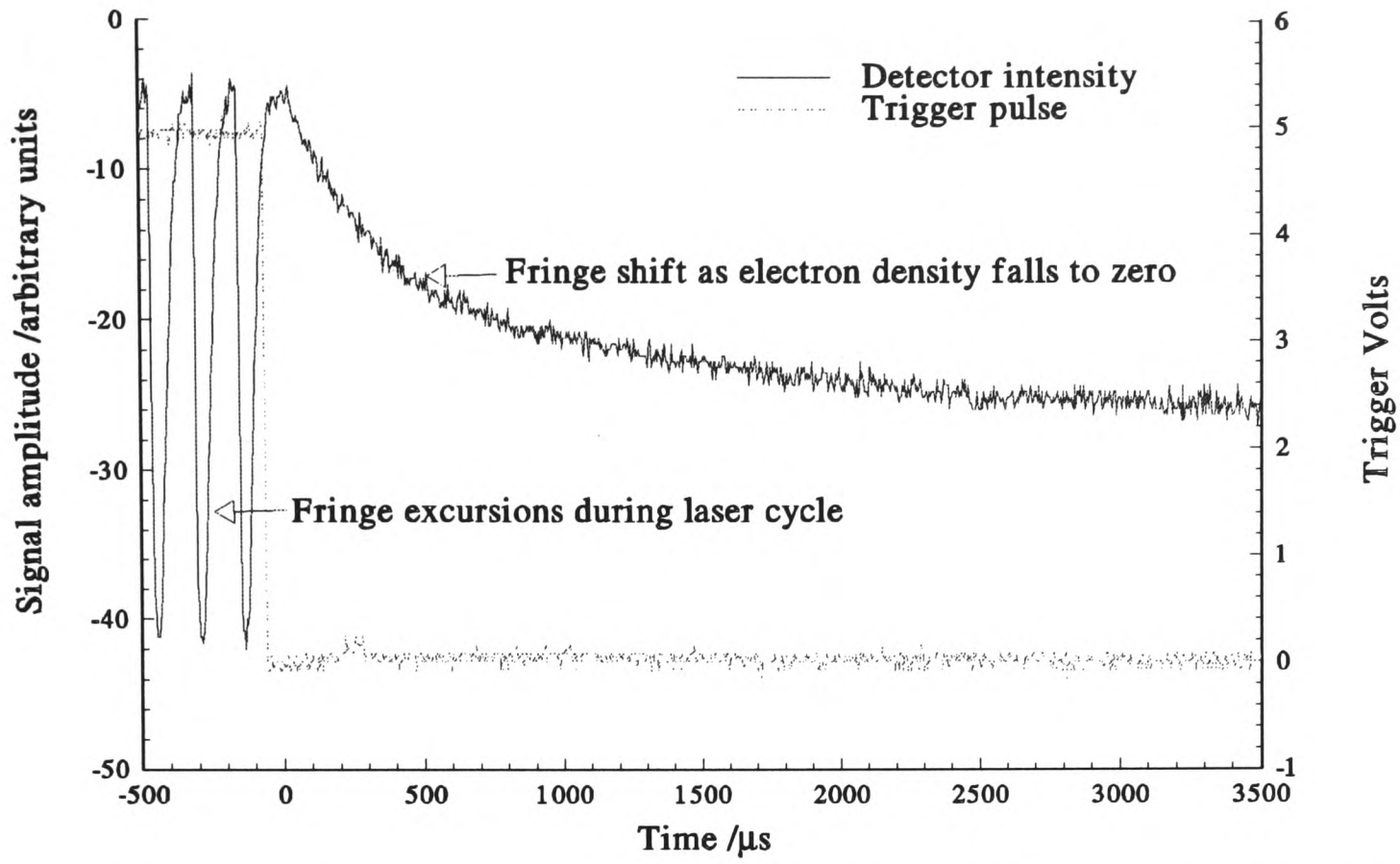

Figure 4.4 A typical (corrected) trace showing the fringe shift as a result of the fall in the electron density to the Saha value, during a brief cessation of CVL discharge pulses, to measure the pre-pulse electron density

little time for the temperature of the plasma tube to fall[1] and thus causing minimal perturbation to the system. Pairs of traces at each probe wavelength could thus be obtained as before, transferred to computer, the background subtracted, converted to a phase shift and finally to a change in electron density as before. A typical trace of this experiment is illustrated in Figure 4.4, in which the inhibit pulse is also displayed. The three pronounced dips prior to the inhibit trigger pulse in Figure 4.4 are the fringe shifts as a result of the electron density changes over the course of previous CVL discharge cycles. As these shifts are $\Delta m \approx 0.7$, and the initial point may be seen to be at minimum fringe intensity, the full fringe amplitude may be calibrated from these, against which to compare the fringe shift from the decaying residual electron density.

---

[1]The measured cooling curve of the CVL plasma tube showed an initial cooling rate of roughly 0.6 Ks^{-1}.

4.3.2 (VI) Final data handling

The analysis was performed using a commercial graph plotting and spreadsheet package in which data handling programmes could be written for the routine analysis of similar data sets. A final datasheet was produced in which the raw data was contained, before and after subtraction of the background trace, together with the results of the calculations. This allowed the reinspection of any stage of the calculation should it be required.

4.4 FINAL COMMENTS

Using the technique described above electron density measurements could be made in real time, using equipment all well within its specifications, and with the minimum of assumptions and no complex calculations relying critically upon assumptions. Pulse to pulse stability of the 10.6 μm interference traces was extremely good, however the stability of those from the laser diode was rather poorer as a result of slight air movements in the reference arm of the interferometer despite a cover over it. This would not prejudice the accuracy of such measurements as such effects would not be significant over the timescale of a single CVL pulse-delay cycle, it would merely necessitate slightly more careful analysis by hand to measure both initial and final phase if it could not be accurately locked to a convenient starting point. When measured, however, the fringe shift observed at the visible red wavelength was always sufficiently small to represent a negligible contribution to that at 10.6 μm, being 15.8 times smaller, as discussed above.

5 DISCHARGE PARAMETERS

5.1 INTRODUCTION

In order to interpret any results obtained it is clearly necessary to be able to relate them to the timing of the discharge pulse through the CVL, and that of the laser light output pulse. In this chapter the results of measurements of the excitation discharge parameters are presented and their interpretation discussed.

5.2 MEASUREMENT CONSIDERATIONS

The equipment to make the necessary measurements of discharge current and head voltage has been described in Section 1.5, and the traces obtained, together with the laser light output on axis, may be seen in Figure 5.1. It must be stressed that the cables to all three detectors were matched to ensure equal propagation times, and the detectors themselves all had manufacturers' specified rise times of 5 ns or better (<1 ns for the photodiode, 2 ns for the Pearson current probe). In addition the timing of the current trace was checked using three different current probes, as also described in Section 1.5. The timing of these traces may therefore be related together with confidence and, owing to the calibration of the population density measurements employed, as described in Chapter 3, likewise related to any of these. The Pearson current probe was set up to register a positive signal for the direction of current flow produced by a negative voltage on the CVL HT electrode. Owing to its position, measuring the current flow through one of eight identical bolts holding the earth end flange onto the coaxial water jacket (the earth return path), the current measured corresponds to (one eighth of) the current flowing through the laser tube.

5.3 INDUCTANCE EFFECTS

The reason that the current is out of phase with the voltage is purely a result of the geometrical, coaxial structure of the laser head. The self inductance of the laser head may be calculated by considering the energy W_m stored in the magnetic flux density B in volume element $d\tau$ according to:

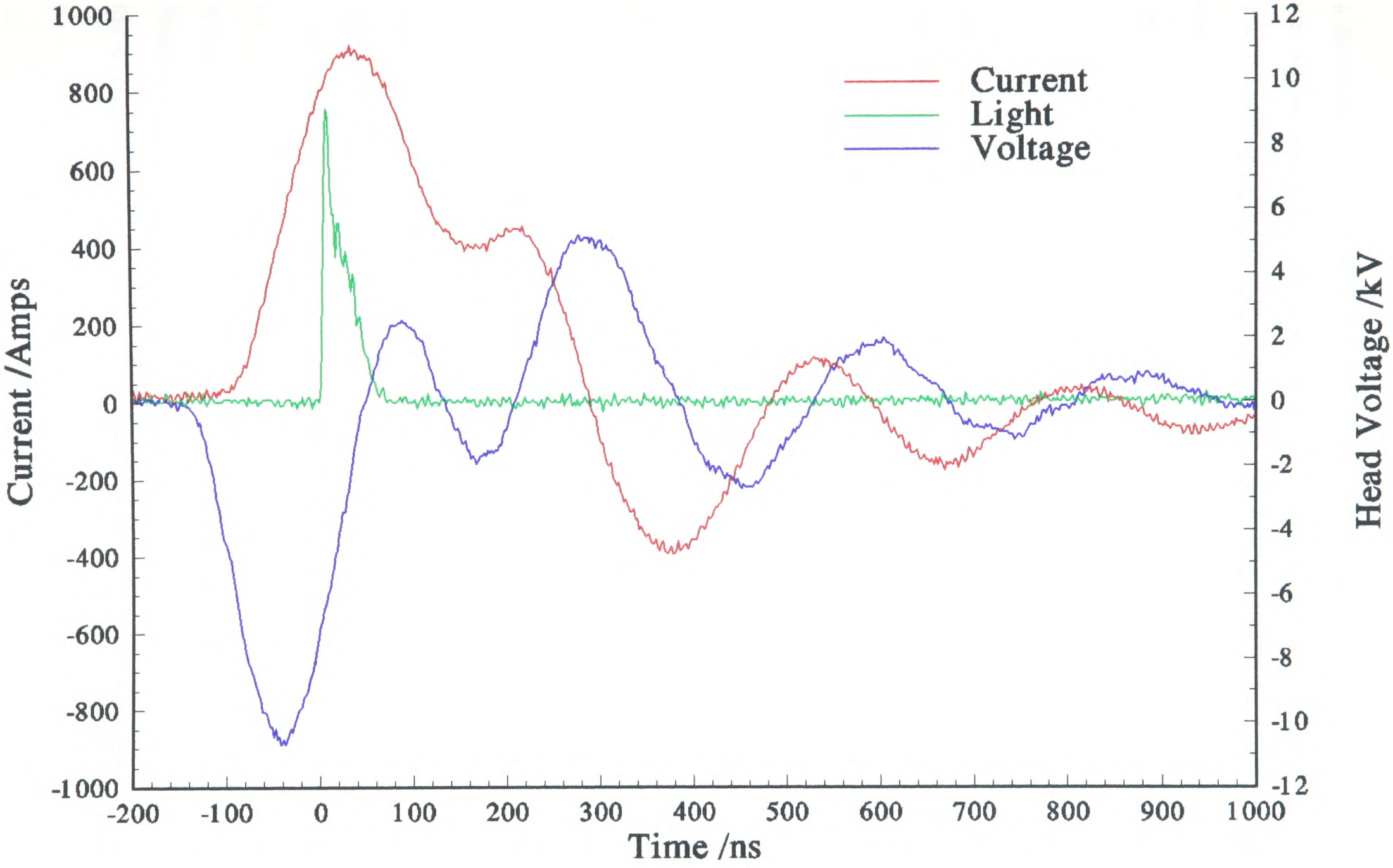

Figure 5.1 Voltage, current and laser light pulses under standard running conditions

$$L = \frac{1}{\mu_0 I^2} \int_{\infty} B^2 d\tau \qquad \textbf{(5.1)}$$

In a structure of the dimensions of the laser head the inductance of the water jacket earth return path in isolation is negligible, especially at high frequency owing to the skin effect, and so the self inductance of a laser head with a plasma of radius a and a coaxial earth return of radius b is composed of the central conductor (the plasma) and the volume between the two conductors, and may be written:

$$L = \frac{\mu_0}{2\pi}\left(\frac{1}{4} + \ln\frac{b}{a}\right) \qquad \textbf{(5.2)}$$

Based on a resistive plasma core of 42 mm diameter, with a large skin depth (see Kushner & Warner, 1983), surrounded by a stainless steel earth return path of 200 mm diameter (and skin depth of 0.3 mm) a total inductance for the head of 750 nH (500 nHm^{-1}) may be calculated which agrees well with measurements of similar laser heads in which the plasma column has been replaced by a copper rod (Abbott, 1990). Of this inductance 90% arises as a result of magnetic energy stored in the volume between the two conductors (the second term in Equation 5.2), while the remaining 10% represents energy stored within the plasma column itself.

In the regime where the electron momentum transfer collision frequency ν_m is low in comparison to the frequency of a sinusoidal electric field ω the electron acceleration is in phase with the electric field, and the velocity, the integral of acceleration, is $\pi/2$ radians out of phase with the field (a cosine function). The current, therefore, is $\pi/2$ out of phase with the applied voltage and plasma is inductive. When, however, the frequency of the field is lower, or the momentum transfer collision frequency higher, the rate of gain of momentum is no longer purely proportional to the electric field, but is equal to this minus the rate of loss of momentum by collision. This latter rate is proportional to both the electron drift velocity and the momentum transfer frequency and consequently the velocity is no longer $\pi/2$ out of phase with the field, but lags it by a phase ϕ given (Francis, 1960) by:

$$\tan\phi = \frac{\omega}{\nu_m} \qquad (5.3)$$

The plasma is therefore both inductive and resistive. When $\omega \ll \nu_m$ then ϕ is very small and the plasma is essentially purely resistive. When the electron energies are low, less than a few eV as in the case of the CVL, $\nu_m = \nu$, the total electron collision frequency as scattering is equally probable in all directions. For the plasma of the CVL a momentum transfer collision frequency of 160 MHz can be calculated from the electron-neon elastic collision cross section alone, which is considerably greater than the frequency equivalent to the fastest part of the discharge pulse (about 3 MHz) and it therefore represents a purely resistive load. A total electron-heavy particle momentum transfer collision frequency of 3.77 GHz is used under similar plasma conditions by Kushner (Kushner & Warner, 1983) in his calculation of electrical conductivity to obtain his expression for skin depth electric field penetration time.

This discussion, however, refers to the behaviour of the positive column of the discharge which, although it corresponds to the vast majority of the length of the plasma, does not necessarily represent the majority in terms of voltage fall. The behaviour of the cathode sheath potential on the timescale of interest is not well understood and consequently the nature of the load presented to the external power supply by the laser discharge as a whole is not readily determined.

5.4 THE FORM OF THE CURRENT PULSE

Close inspection of the traces obtained however yields the interesting observation that the nature of the discharge through the CVL plasma is not exactly as might be expected. The current appears to start to rise only about 40 ns after the commencement of the voltage pulse, some 80 ns before its peak, the point normally regarded as "breakdown". The laser output pulse, on the other hand, appears to start rather late with respect to both the current and voltage pulses, commencing some 40 ns after the peak of the voltage pulse, and 120 ns after the start of the current pulse. Part of the delay might arise because the laser output pulse represents light generated from the plasma tube axis, and there is known to be a delay in this pulse relative to pulses at the tube wall as a

result of the skin effect (see Section 2.9; Kushner & Warner, 1983). This can account for a delay of only about 10 ns for a 42 mm diameter plasma tube however.

To explore this phenomenon further the relative timing between the current and voltage pulses was also observed whilst bringing the CVL up to its operating temperature, before there was any copper vapour in the discharge. Without appreciable copper density it was possible to collect light from spontaneous emission from the neon with a fast vacuum photodiode. Spontaneous emission was observed to commence not with the onset of the current pulse, but approximately at the peak of the voltage pulse. The spontaneous emission profile then rose to a peak, coinciding with that of the current pulse, before falling with the current. There therefore seemed to be a "dark" component to the leading edge of the current, not associated with excitation of gas in the tube. That part of the current pulse that appears to flow during this period, without excitation, has been termed by us "phantom current".

5.5 INVESTIGATION OF THE "PHANTOM CURRENT"

5.5.1 AN HYPOTHESIS

One possible explanation of these observations is that during the early part of the voltage pulse the current detected by the current probe consists of just that carried by the residual electrons present prior to the discharge pulse, of which an insignificant number have acquired the 2.1 eV minimum energy necessary to commence stepwise ionisation. If a sufficient number of electrons already existed in the plasma prior to the discharge pulse then the current demanded by the external discharge circuit could be obtained simply by accelerating these. Only when the discharge current demanded gave these electrons sufficient energy to initiate inelastic collisions could stepwise ionisation commence and a phenomenon analogous to breakdown occur. That the processes leading to the generation of new electrons should not occur for 80 ns after the beginning of the current pulse seemed rather unlikely, however it was decided to test the hypothesis by looking at the form of the current pulse both with and without an existing electron density. It is of interest to calculate that only at a current of about 1250 A would the electron drift velocity exceed the thermal mean velocity at an average electron temperature of 2000 K, based on the measured electron density profile across the plasma tube.

5.5.2 EXPERIMENTAL

The trigger pulses for the CVL were generated by an external digital delay generator which incorporated an external trigger inhibit socket. By taking the 5 V line to this socket to ground via an external switch the trigger pulses to the CVL PSU, and thus the CVL discharge pulses, could be suspended for any desired time. By thus blanking the CVL discharge for about 150 ms the electron density could be allowed to fall to the negligible Saha value (of about 7×10^7 cm^{-3}), and the profiles, and timing, of the following few voltage, current and light output pulses observed. This is similar to the technique employed to measure the pre-pulse electron density, as discussed in Chapter 4. By triggering the oscilloscope from the pulse generator, and normalising the timing to that of the laser pulse (on axis) timing compatib le with the limit imposed by the total jitter of the system ($\pm$3 ns, Section 3.3.4 (V)) could be ensured.

5.5.3 RESULTS

The first voltage and current pulses following the period of blanking may be seen in Figure 5.2. The device did not lase at all during this first discharge following the period of blanking and consequently no light pulse is shown. The spontaneous emission was not observable as a result of the attenuation required to prevent damage to the detector from lasing during subsequent discharges. To obtain such a trace of the spontaneous emission would have required a shutter with high precision synchronisation which, though desirable, was not vital as the necessary information could be gained from this and subsequent traces. The traces of Figure 5.2 can immediately be seen to be very different from the steady-state discharge profiles of Figure 5.1. The current is far lower at all times, the overall timescale is slower and the ringing oscillations have been replaced by a series of humps. In particular, the current now appears to start at about the time that the voltage peaks, the "breakdown" behaviour that would be expected in the absence of any pre-pulse electron density. The electron density generated during the first lobe of the discharge pulse is low however, hence the low current and the long time taken for the voltage to fall. The second, positive, lobe of the voltage pulse is likely to be a result of ringing into the "bypass" inductor of the CVL power supply which, as a result of the electrons generated during the first phase of the discharge pulse, is able to drive a more substantial current, though in the opposite direction.

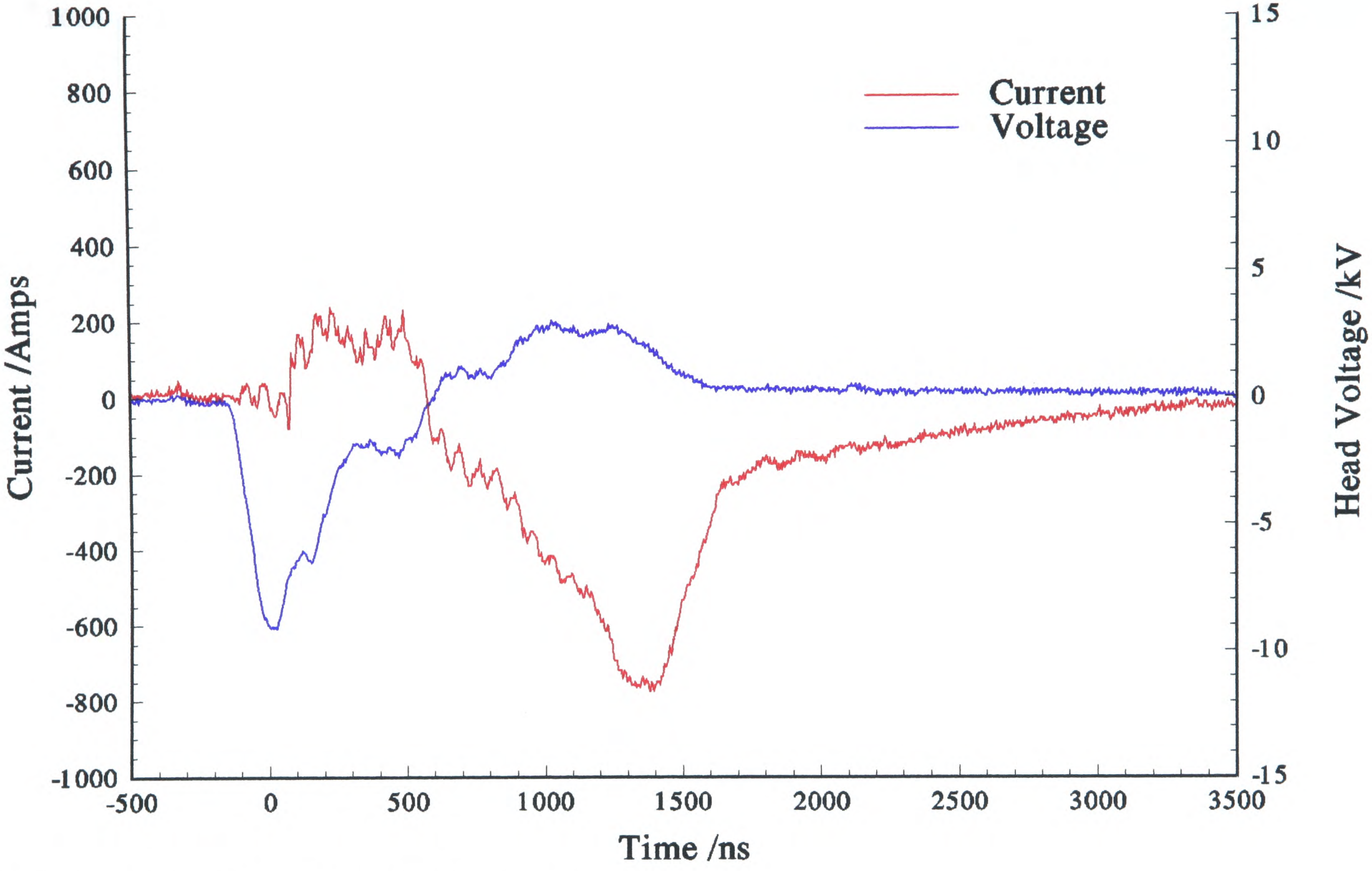

Figure 5.2 First discharge after period of blanking: Voltage and current

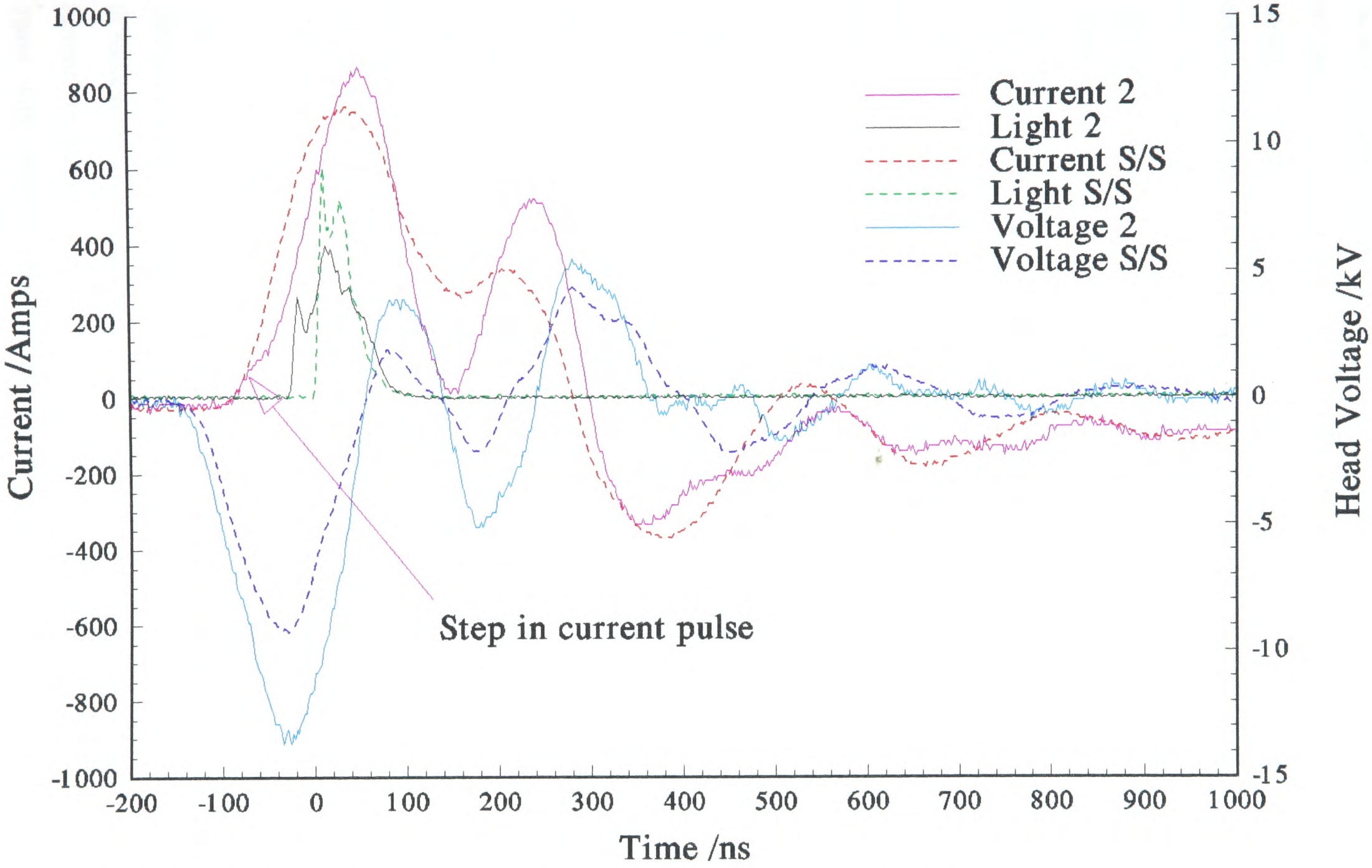

Figure 5.3 Second discharge after period of blanking and steady state: Voltage, current and laser light

Possibly the most interesting set of traces is that of Figure 5.3, in which the measurements made during the second discharge following the period of blanking of the CVL are displayed together with the steady-state profiles for ease of comparison. In this case there is a low pre-pulse electron density, high enough to allow a good quality discharge, but too low to sustain the discharge for very long without demanding additional ionisation. It can be seen that, although starting at the same time, the voltage pulse rises faster, and to a 50% higher peak value, though at about the same time, than in the steady-state case. The reason that the peak voltage in the first discharge pulse is no greater than that in the steady-state case is because, as a result of the anti-trip inductor across the thyratron in the PSU, the voltage on the thyratron decreases approximately linearly from its peak value of 17 kV for 50 ms, to a value of 9 kV, at which it stabilises (Figure 5.4). Following this first pulse, however, the voltage on the thyratron can be seen to "overshoot" to a value slightly higher than before for a number of pulses before stabilising.

When comparing the two current pulses it can be seen that they too start to rise at the same time, in contrast to the hold-off observed in the very first discharge after blanking. In the case of the second discharge, however, the "phantom current" flow merely corresponds to a small shoulder on the leading edge of the profile which is arrowed in Figure 5.3. The rest of the leading edge can be seen to rise approximately parallel to, though about 25 - 30 ns later than, the steady-state current pulse. The second current pulse following the period of blanking may also be seen to peak about 15% higher, and about 10 ns later than in the steady-state case. From the first to second discharge, therefore, the form of the current pulse may be seen to progress from a poor quality pulse, of low amplitude, commencing at the peak of the voltage pulse, to a high amplitude pulse with a small step on the leading edge preceding the voltage peak. With successive current pulses the amplitude of the step prior to the peak of the voltage pulse can be seen to rise until it reaches the full height of the pulse and no longer has the appearance of a step, as in the case of the steady-state case. This progression is also consistent with a small pre-pulse electron density, which increases with successive discharges, and is accelerated by the increasing electric field. This gives a current, restricted by limited numbers and elastic collisional energy losses (which increase with velocity), though with insufficient energy for inelastic processes and

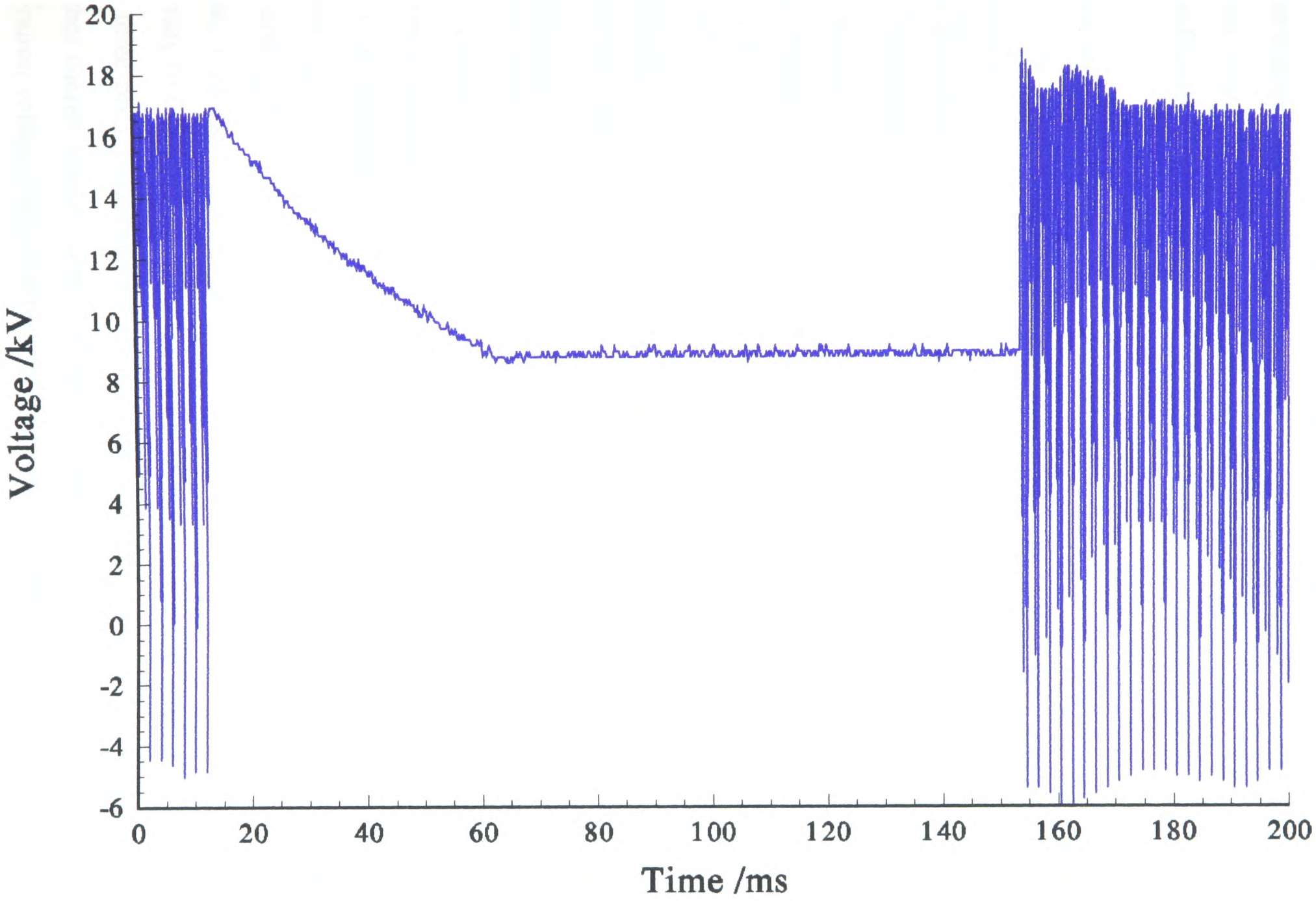

Figure 5.4 Voltage on anode of thyratron during blanking

stepwise ionisation. The electrons finally acquire sufficient energy at the point of "breakdown" when the current rises sharply, the voltage peaks and direct inelastic collisional excitation to low lying and intermediate energy copper levels, including the $4p\ ^2P_{3/2,1/2}$ upper laser levels, occurs and gain, and lasing, commence almost immediately, as can be seen from Figure 5.3. The excitation under these conditions gives rise to a laser output pulse which, while of slightly lower peak amplitude than the steady-state value, starts about 30 ns earlier, is 20 - 30% longer, fwhm, and thus contains significantly higher energy.

5.5.4 DISCUSSION

It has been suggested (eg Bokhan, 1984) that a limitation to high repetition rate operation of the standard CVL is a result of the residual pre-pulse electron density giving rise to reduced plasma impedance, reduced breakdown voltage and thus decreased peak electron temperature. The results obtained here graphically illustrate the two effects of the pre-pulse electron density. When the pre-pulse electron density is negligible there is not the seeding allowing the formation of a good quality discharge filling the plasma tube and the result is a constricted, snaking discharge. When the pre-pulse electron density is too high, however, the plasma behaves as a simple, ohmic conductor and there is no reason for the electron temperature to rise and excitation and stepwise ionisation to occur. It can be seen that the optimum pre-pulse electron density would be about that present at the start of the second discharge pulse after the blanking period. The low residual value yields a good quality discharge, but permits very little power to be deposited into the plasma prior to breakdown which occurs at a higher voltage, giving a higher peak electron temperature and thus more selective pumping of the upper laser levels. As a result of the more decisive breakdown the laser pulse starts earlier though ends at the same time, this being a function of the falling electron temperature following the fall and reversal of the voltage pulse, the behaviour of which shows very similar timing in each case. If an electron scavenger could be incorporated into the CVL to reduce the electron density to this optimum value during the afterglow, at a rate higher than that permitted by three body recombination, then higher efficiency could be obtained as a result of higher energy output pulses, less power wasted during the "dark" current and a higher thyratron voltage could thus be employed without exceeding the optimum copper vapour

density. It may also be deduced that a faster voltage pulse applied to a conventional tube would tend to diminish the deleterious effects of this dark current.

6 DEPENDENCE OF LASER PULSE TIMING ON RADIAL POSITION

6.1 INTRODUCTION

As has been discussed in Chapter 2, it has long been known that, in all but very small diameter devices, laser action in a CVL commences near the wall of the plasma tube before it does so on axis. Also introduced in Chapter 2 were three mechanisms by which the delay observed on axis might arise. In order to determine whether the observed delay is entirely due to a discharge related phenomenon, such as the skin effect (Kushner & Warner, 1983) or pre-pulse electron density, or is a laser kinetics effect, it was decided to compare the timing of pulses of spontaneous emission from transitions unrelated to the laser action, with that of the laser pulses. In this way the radial timing of the discharge pulse could be observed in isolation from any kinetics effects.

6.2 SPONTANEOUS EMISSION MEASUREMENTS

As the relative timing difference between laser pulses from the wall and the axis in a laser of 42 mm diameter is only of the order of 10 ns, it was decided to perform the measurements on a 60 mm diameter device, with a 2.2 m plasma tube length, by kind permission, and at the premises, of Oxford Lasers Ltd.

6.2.1 CHOICE OF TRANSITIONS

The choice of transitions from which to collect spontaneous emission was important if erroneous conclusions were not to be drawn. The source of spontaneous emission should preferably be the same longitudinal region of plasma tube as that from which laser action was to be observed. For this reason copper lines rather than lines from the neon buffer gas or hydrogen impurity (always present in CVL tubes) were selected. Secondly the plasma should be optically thin for the transitions of interest. If significant absorption, or even gain, were to be present on the line at any point in the laser cycle then this would distort what was intended to be a simple trace of the excitation by the discharge. Finally the lines should not be too weak as spatial resolution could

only be obtained if sufficient spontaneous emission could be accumulated from a restricted volume.

6.2.2 SELECTION OF EMISSION FROM WITHIN DEFINED CYLINDRICAL VOLUMES

In order to collect the spontaneous emission from a cylindrical volume at a precise radial position within the CVL plasma the method of Webb (Webb, 1968) was employed. Figure 6.1 shows a diagram of the equipment used.

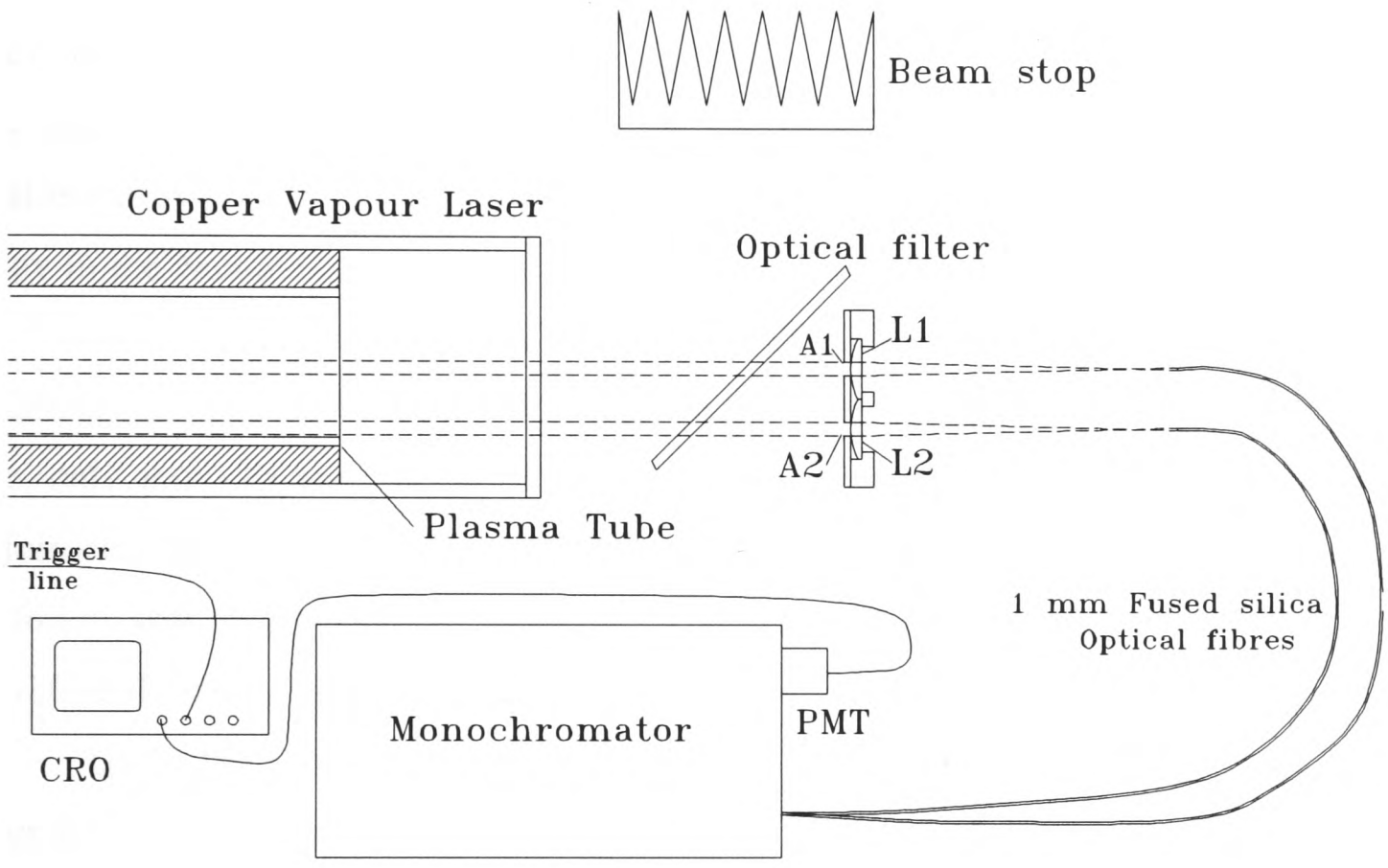

Figure 6.1 Apparatus employed to acquire spontaneous emission pulses from two defined, cylindrical volumes within CVL plasma

The spontaneous emission from cylindrical volumes within the plasma, of diameter determined by the two 6 mm diameter apertures A1 and A2, was imaged by the lenses L1 and L2 onto the apertures formed by the cleaved ends of the two 1 mm fused silica optical fibres. The fibres conveyed the light signals to a pair of fibre optic terminators mounted one above the other at the entrance slit of an 80 cm monochromator, by which the required transition could be selected. By the use of beam stops either light from the tube axis, or close to the tube wall, or both, could be selected for detection by a photomultiplier, and the appropriate trace displayed on a digital oscilloscope and

transferred to a computer for storage. Oscilloscope triggering was accomplished by means of the laser trigger pulse. In order to reduce the level of unwanted green and yellow laser radiation the rear mirror of the laser was blocked during the experiment, and the residual ASE was further reduced by means of interference filters.

6.2.3 RESULTS OBTAINED

In Figures 6.2, 6.3 and 6.4 the spontaneous emission traces from three copper lines are displayed and Figure 6.5 shows where the transitions employed lie in the copper term diagram. Despite the poor signal to noise owing to the weak spontaneous emission lines and the small, 6 mm diameter collection volumes, the relative timing of the discharge pulse at the wall and on axis may be seen. Since emission on these lines is unaffected by population in the $4s^2\,^2D$ levels it may be concluded that there is indeed a delay in the excitation pulse reaching the centre of the tube.

On closer inspection it may be seen that, although the spontaneous emission at the wall rises relatively cleanly, in each case, the emission on axis appears to display a small rise, only about 10 ns or so after that at the wall, lasting about 20 ns, followed by a fall, before commencing the final rise. The main rise of spontaneous emission on axis seems to follow that at the wall by almost 40 ns, although it would appear to rise faster and therefore the delay near the peak is somewhat less than this.

Using the same optical arrangement, temporal profiles of the green and yellow laser pulses were obtained (Figures 6.6 and 6.7). In Figure 6.7 the step before the main pulse may be clearly seen, while a vestigial step may also be seen in the green pulse of Figure 6.6. The measured timing between the two yellow laser pulses in Figure 6.7 is about 32 ns, however that between the two green pulses in Figure 6.6 is considerably greater at about 48 ns. That such a large discrepancy in radial delay between the two lines should exist, and in particular between the spontaneous emission and green pulses, suggests that there may be a contribution from copper laser kinetics in addition to the observed delay in excitation reaching the tube axis.

6.3 THERMAL POPULATIONS IN THE LOWER LASER LEVELS

If there were a contribution to the timing of the onset of laser action as a result of the additional time taken for the population in each upper laser level to achieve

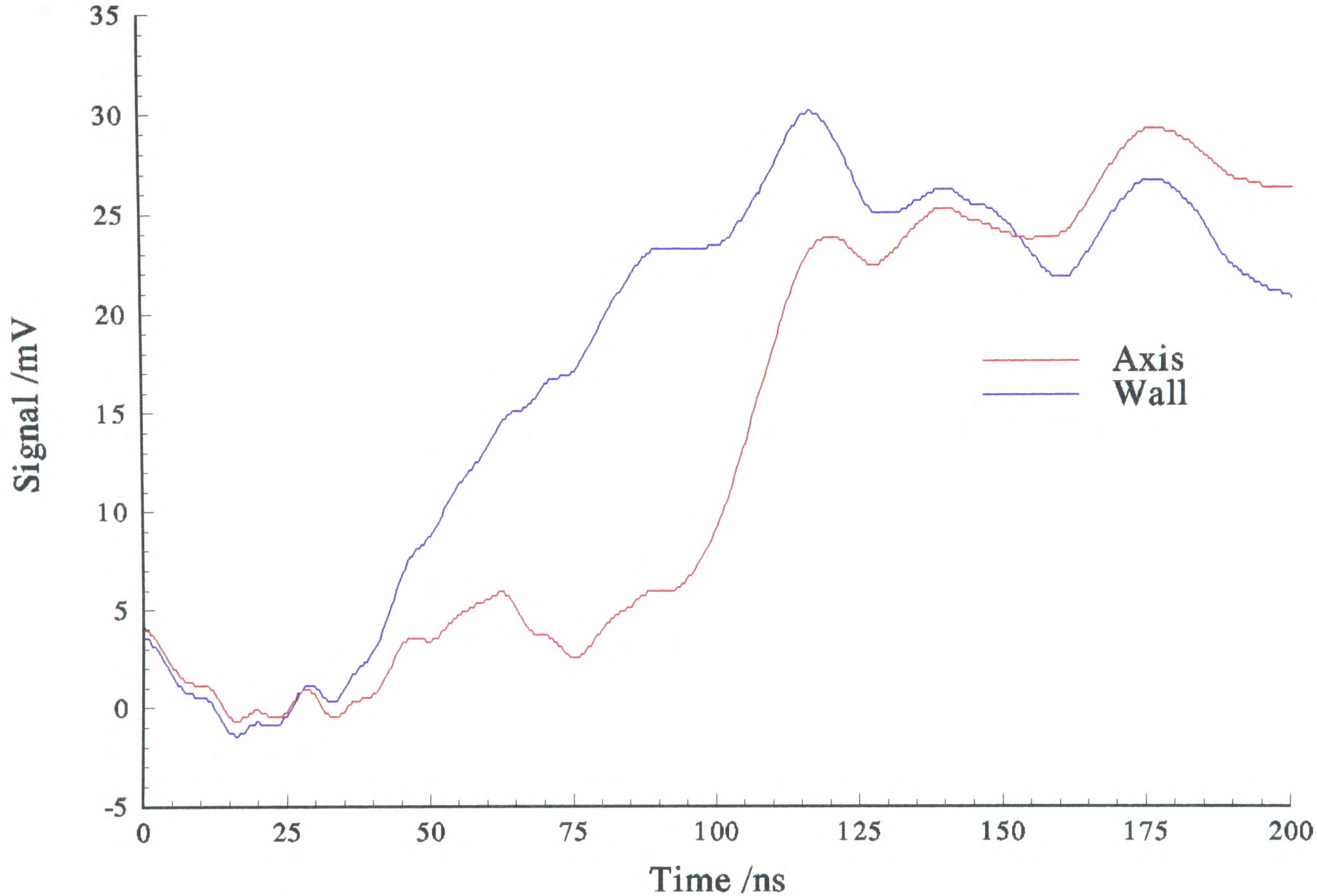

Figure 6.2 Spontaneous emission pulses on copper 402.3 nm transition

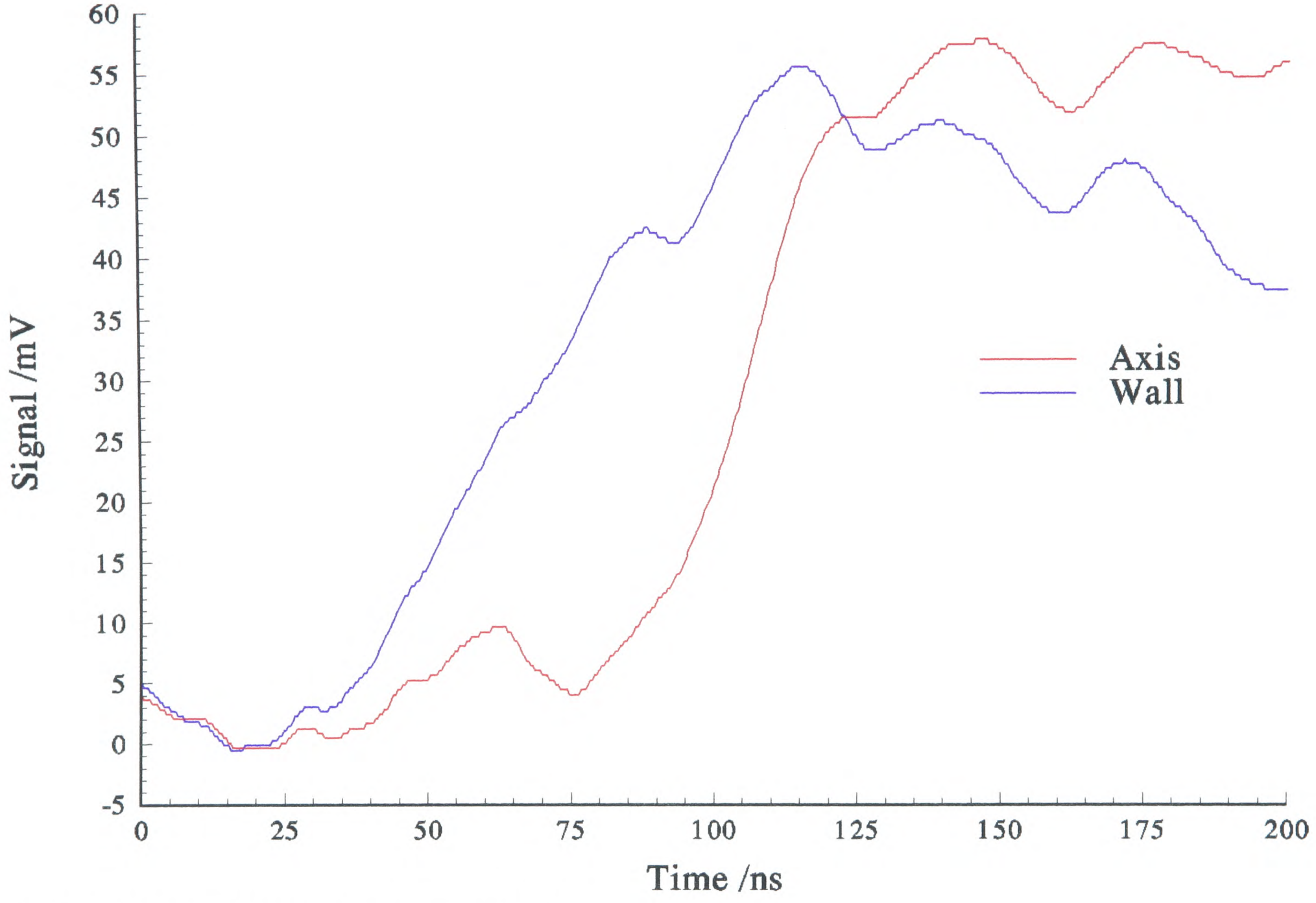

Figure 6.3 Spontaneous emission pulses on copper 406.3 nm transition

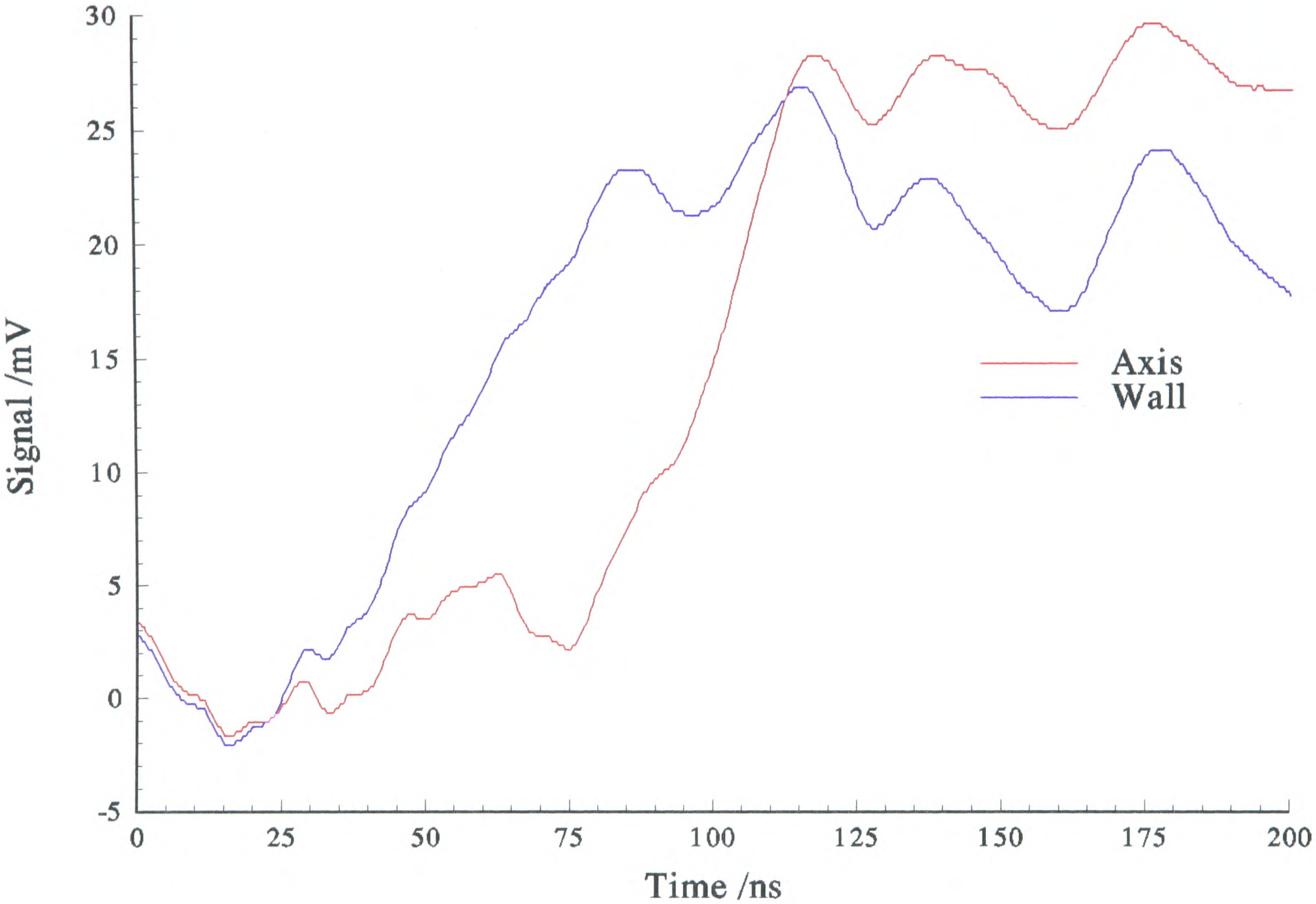

Figure 6.4 Spontaneous emission pulses on copper 453.1 nm transition

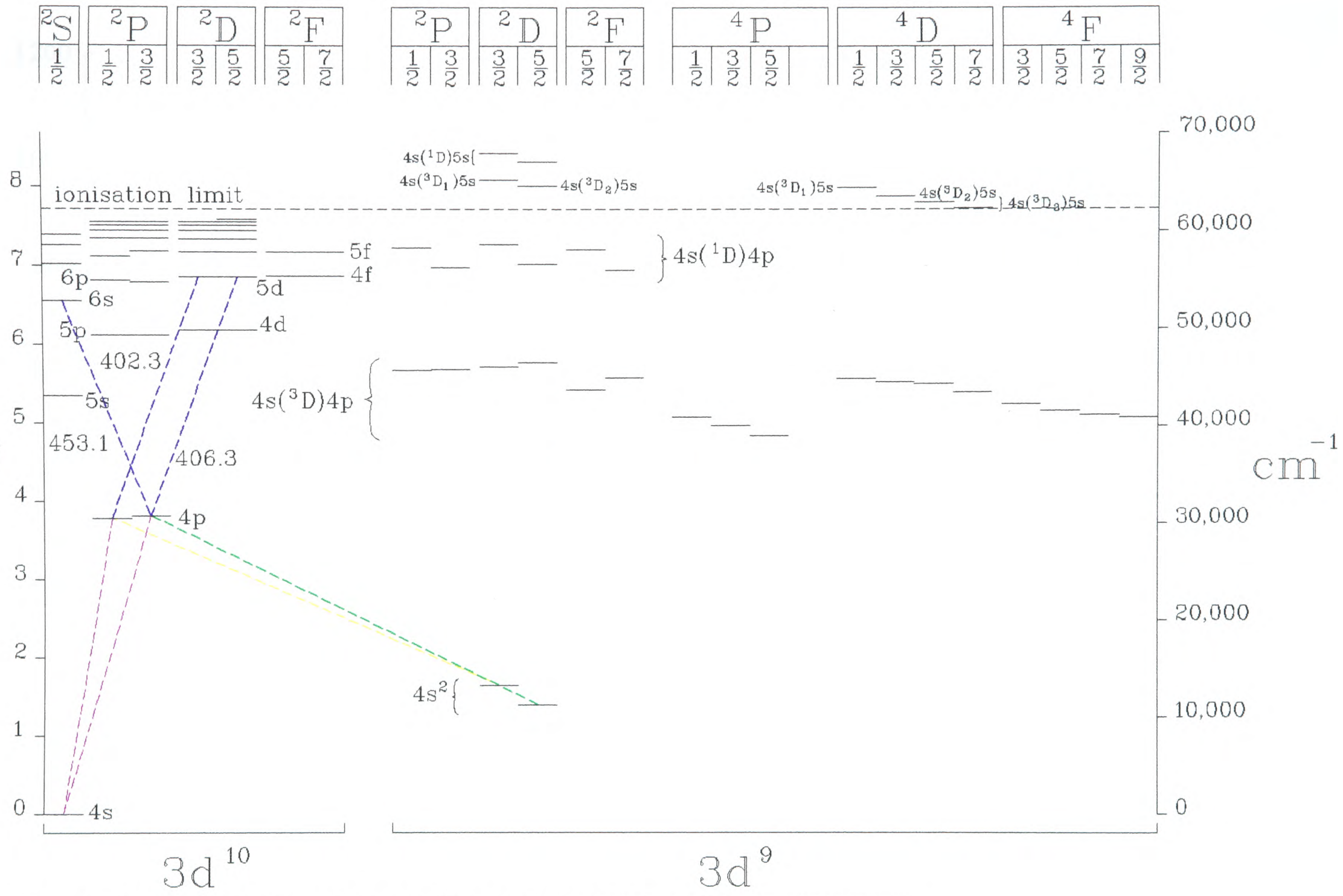

Figure 6.5 Copper term diagram showing transitions used in spontaneous emission experiments

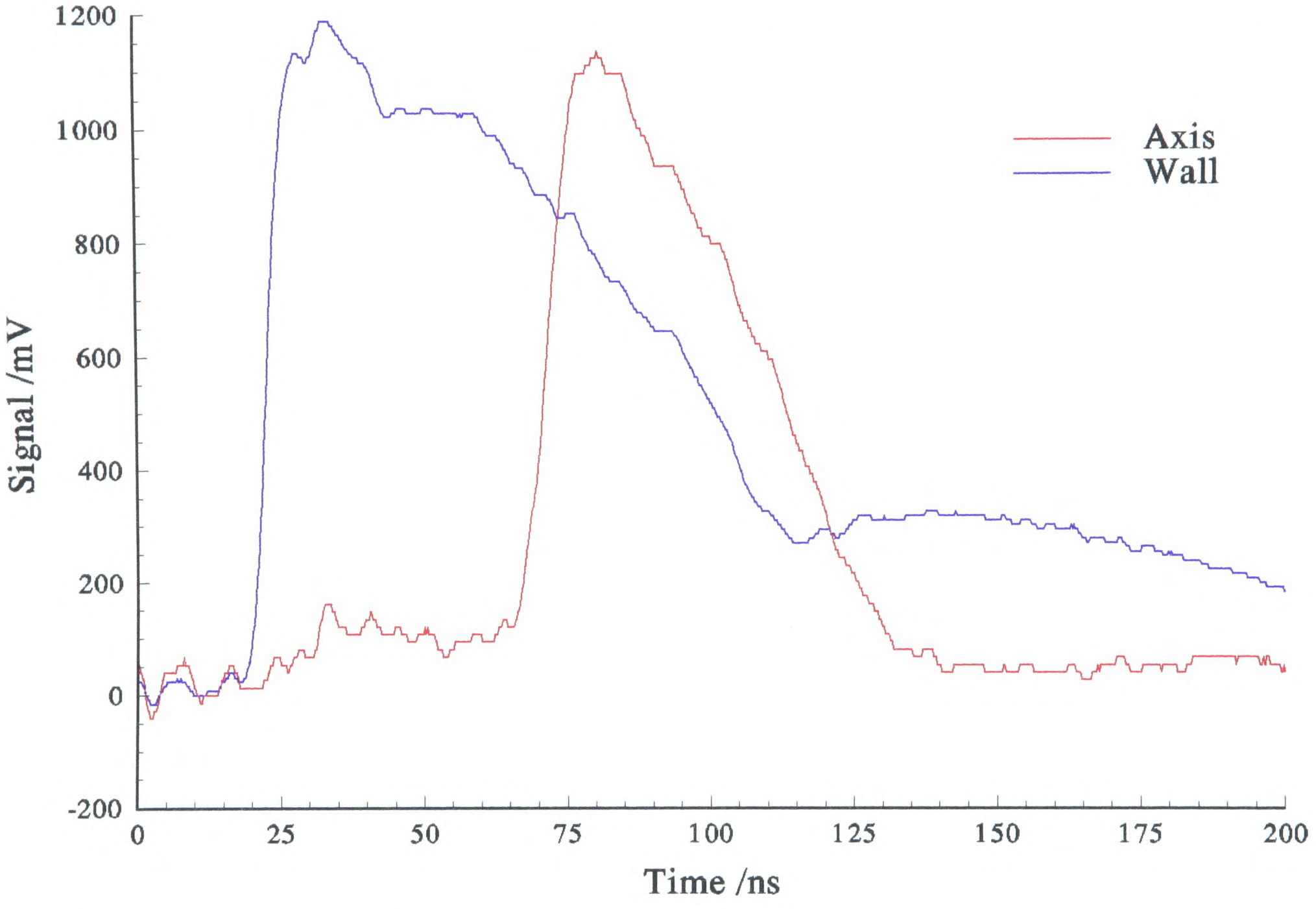

Figure 6.6 Relative timing of green laser pulses

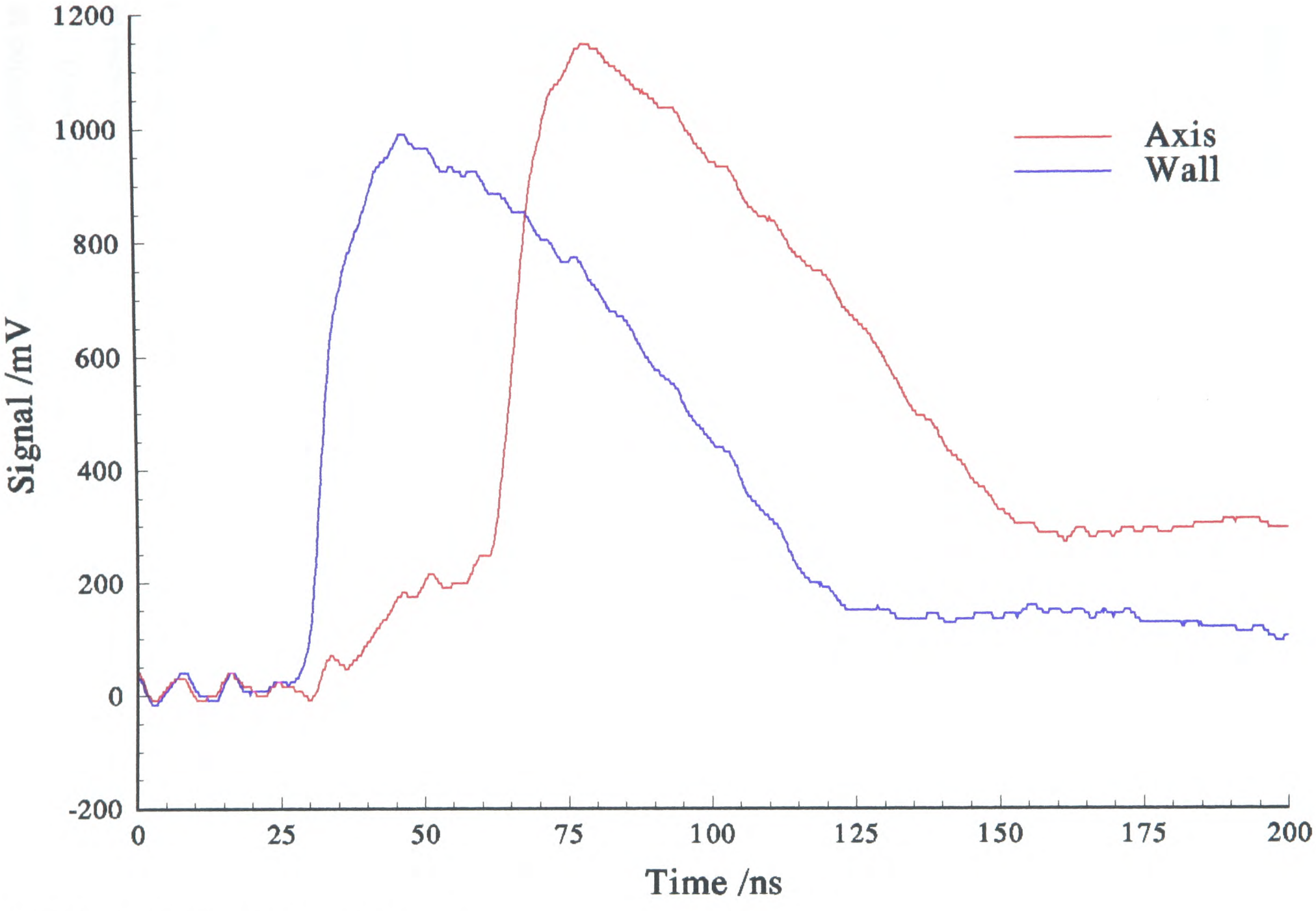

Figure 6.7 Relative timing of yellow laser pulses

inversion over a thermal, pre-pulse population in the lower laser levels then it is to be expected that this effect would be far greater on the green transition than on the yellow. This is because the green lower laser level ($4s^2\ ^2D_{5/2}$) is 15% lower in energy than the yellow lower level ($4s^2\ ^2D_{3/2}$) and consequently, its thermal population per state will always be greater. This may be calculated from the expression for a Boltzmann distribution at electron temperature T_e in which the population densities N_i and N_j in two energy levels separated in energy by E_j - E_i with degeneracies g_i and g_j respectively are related by:

$$\frac{N_j}{N_i} = \frac{g_j}{g_i}\exp -\left(\frac{E_j - E_i}{kT_e}\right) \qquad \textbf{(6.1)}$$

The issue of the pre-pulse electron temperature radial profile is discussed a number of times in this thesis, and here its significance is observed as it is upon the relative value of electron temperature on axis compared with that at the wall that any lower level radial timing effect would depend. If the pre-pulse electron temperature radial profile is essentially flat, as predicted by Kushner (Kushner & Warner, 1983) and Carman (Carman et al, 1993), or even only very slightly greater on axis, then, provided that they acquire thermal equilibrium with the ground state at the local electron temperature, the radial profile of the pre-pulse lower laser levels will show a minimum on axis, reflecting the radial profile of the copper ground state, which is in turn determined by the radial gas temperature profile. If, however, the radial profile of the pre-pulse electron temperature is similar to that of the gas temperature then the equilibrium thermal population density in the lower laser levels will display a marked maximum on axis, especially the green lower level. Based on the pre-pulse copper ground state radial profile and the gas temperature profile calculated from it, the pre-pulse thermal lower laser level populations at the plasma tube wall and on axis of the (42 mm diameter) study laser have been calculated, and the results are displayed in Table 6.1. For comparison the measured peak population densities in the two upper laser level have been included.

Displayed in this way it is easy to see that if these were the pre-pulse lower laser level population densities then it would not be surprising if a significant time was

	Axial Populations /cm^{-3}	Wall Populations /cm^{-3}
Temperature /K	2680	1700
Ground State $^2S_{1/2}$	405×10^{12}	640×10^{12}
Lower Green $^2D_{5/2}$ (Thermal)	3.0×10^{12}	14.6×10^{10}
Lower Yellow $^2D_{3/2}$ (Thermal)	0.7×10^{12}	1.7×10^{10}
Upper Green $^2P_{3/2}$ (Peak)	7.8×10^{12}	5.1×10^{12}
Upper Yellow $^2P_{1/2}$ (Peak)	5.2×10^{12}	3.7×10^{12}

Table 6.1

required to overcome them before the laser pulses could commence, and that such an effect would be considerably greater on the green transition. The pre-pulse population density in the green lower level, in this case, would represent 38% of the maximum ultimate population in the green upper laser level, while that in the yellow lower level would represent 13% of its peak upper laser level population.

In Section 2.10 a theoretical expression for the radial dependence of gas temperature was presented (Equation 2.15). The dependence of the axial gas temperature upon plasma tube radius is relatively complex owing to the effect of the wall temperature, however, taking a binomial expansion yields, predominantly, an R^2 dependence. Based on this therefore the pre-pulse lower laser level populations on axis could be expected to increase extremely rapidly with plasma tube diameter and while the results of Table 6.1 suggest the potential for a significant effect in a 42 mm diameter plasma tube, in a 60 mm device any effect is likely to be considerably more so.

Based on these calculations, and the significant difference observed between the radial timing difference for the green and yellow laser pulses, coupled with a number of studies that have measured a radial population density profile for the lower laser levels that displays a maximum on axis (Lewis, 1985; Izawa et al, 1989), it seems reasonable to conclude that such a convex radial profile does indeed exist and has a significant effect on the timing of the laser pulses originating along the axis, especially in the case of the green transition.

6.4 RADIAL DEPENDENCE OF LASER PULSE SHAPE AND TIMING

At a late stage in the present work it was decided to repeat the measurements of the laser pulse temporal profiles from the two transitions as a function of radial position in the 60 mm diameter, 100 W CVL, but in this case using fast (< 1 ns rise time) silicon photodiodes instead of the photomultipliers used in the spontaneous emission measurements.

6.4.1 APPARATUS

An intensity monitor (Figure 6.8) allowed one of a pair of 1 mm diameter fused silica optical fibres to be mounted on a translation stage, attached to the back face of a large anodised aluminium heat sink, such that it could be moved backwards and forwards behind a narrow slit, while the other fibre was mounted directly onto the heatsink. The other end of each fibre was then taken to a separate unit. On this the light collected by the static fibre was allowed to fall directly upon one photodetector, which could then be used to supply a trigger pulse to a digital oscilloscope that was almost jitter free with respect to light collected from the CVL. The light from the movable fibre was separated into the two spectral components by a dichroic filter, with additional filters to remove any remaining contamination from the colour not required. The green and yellow laser pulses could thus be monitored separately and simultaneously by a second and third photodiode, and the signals displayed on the oscilloscope, triggered by the first detector. Owing to the requirement of fitting in experimental time with the availability of a 100 W laser at the premises of Oxford Lasers Ltd these measurements were made on a 60 mm diameter laser similar, but not identical to the one on which the spontaneous emission measurements were made. Minor alterations had been made to the power supply and head designs in the interim.

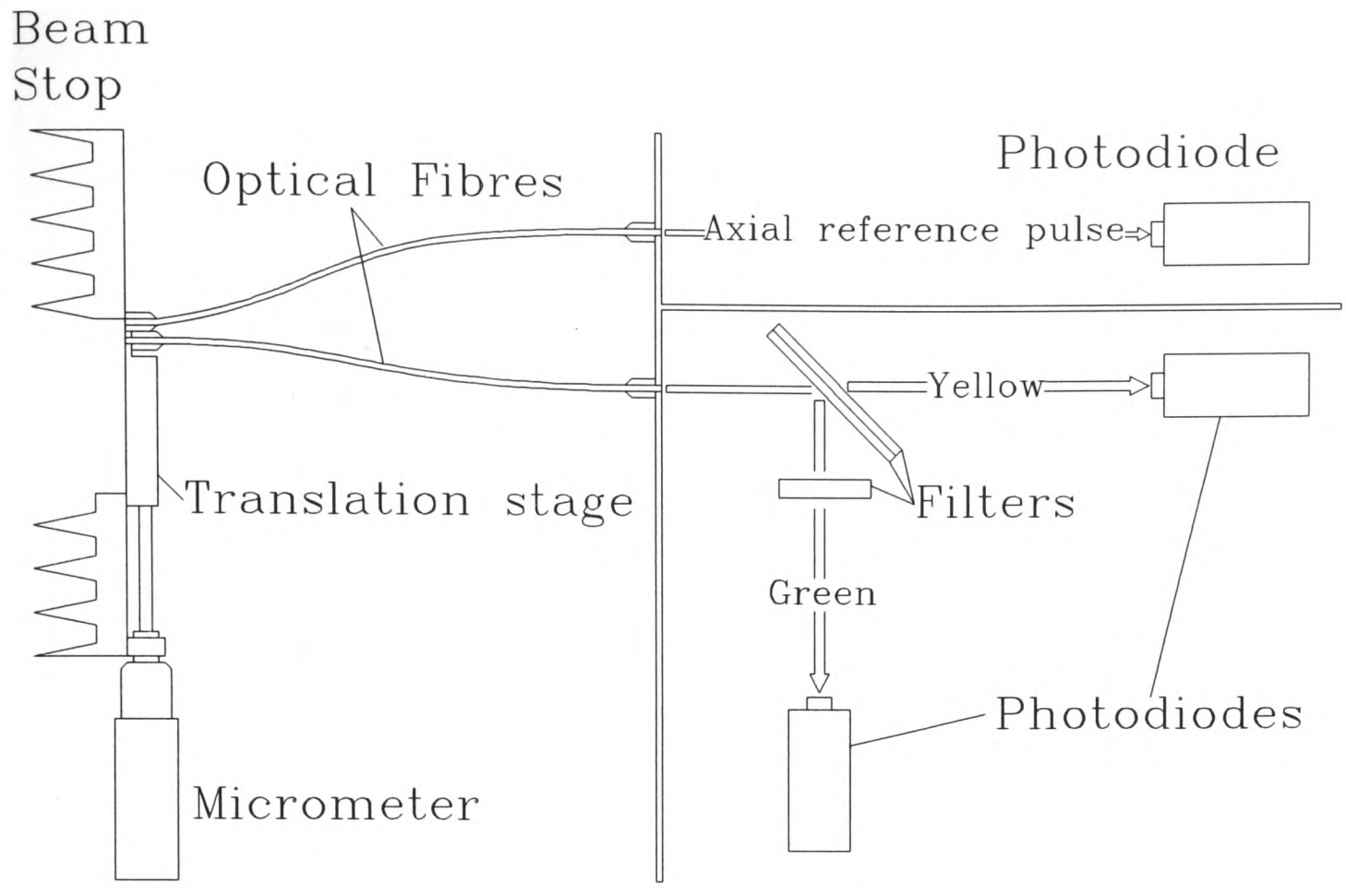

Figure 6.8 Schematic of apparatus to acquire time correlated laser pulses from many positions along radius of plasma tube

In this way a full set of time correlated profiles of the laser pulse shapes at each wavelength was obtained, at various positions across a horizontal radius of the tube.

6.4.2 RESULTS

In Figure 6.9 the green and yellow laser pulses obtained from the axis and from 4 mm from the wall are plotted. Several observations may be made. Looking first at the traces obtained in close proximity to the wall it can be seen that the green pulse appears to start about 2 ns earlier than the yellow, but that this lead increases with time as the yellow pulse rises more slowly. In the case of laser light from the axis of the plasma tube, however, the yellow pulse can be seen to start to rise about 2 ns before the green. Following this, although the yellow rises relatively slowly for the first few nanoseconds, it soon starts to rise faster. The green pulse, however, rises only a very little initially and remains at a fairly constant intensity for about 8 ns before abruptly starting to rise at the same rate as the yellow, though 5 ns behind it. The overall delay between the green laser pulse at the wall and on axis is about 24 ns (excluding the initial

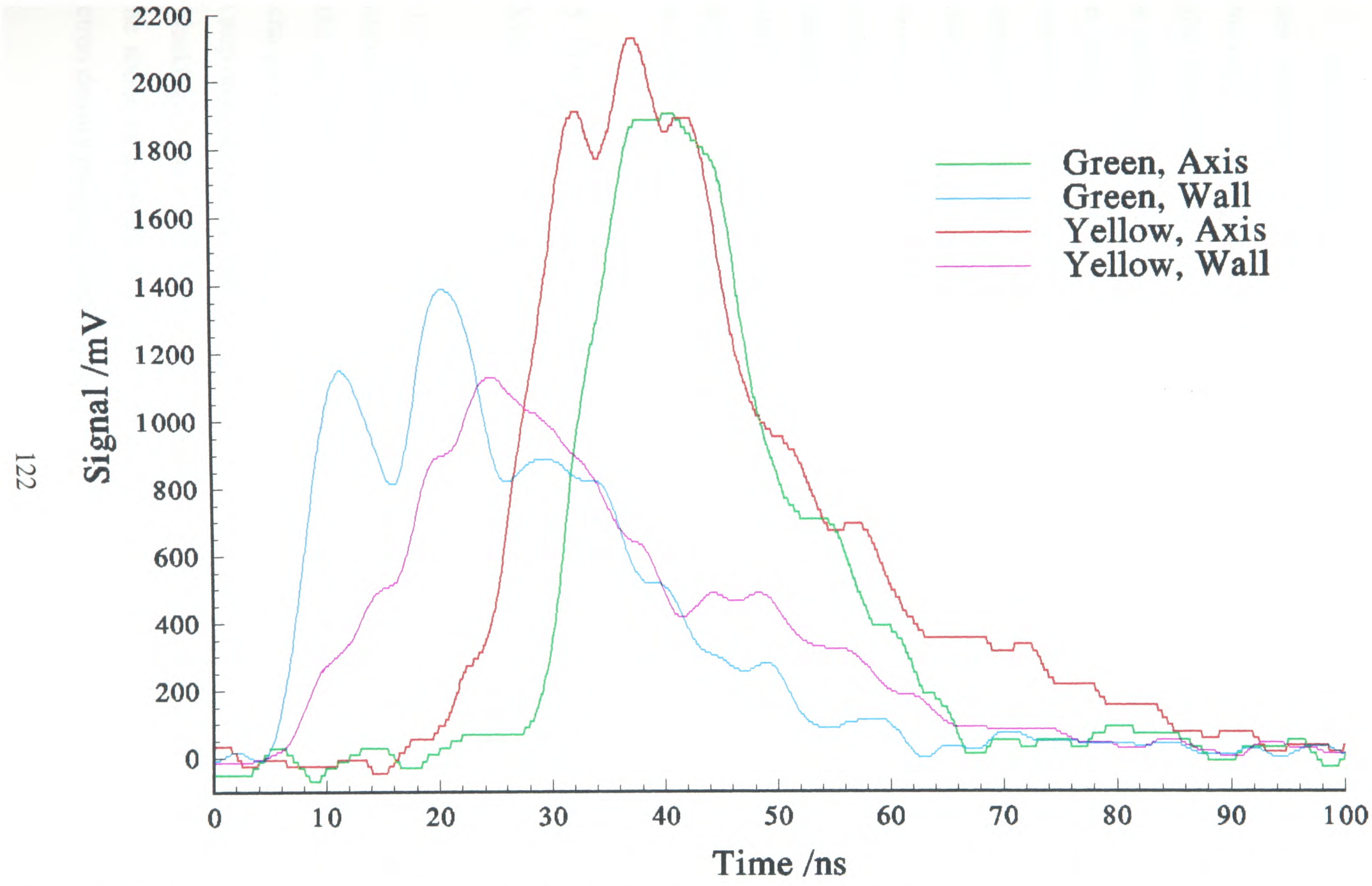

Figure 6.9 Relative timing of green and yellow laser pulses obtained using photodiodes

step), while for the yellow the pulse on axis starts to rise 11 ns after that at the wall, with a delay, once the pulses have started to rise properly, of about 14 ns. Further evidence for the differential nature of the wall-axis delay between the two laser pulse wavelengths is therefore observed, once again supporting the hypothesis that, for green laser emission at least, the pre-pulse lower level population density radial profile has a significant effect.

It is of interest to note the difference in the delays for the green and yellow laser pulses measured on this occasion in comparison with those measured during the spontaneous emission experiment. The delay observed on the spontaneous emission lines is also greater than that observed on this occasion between the yellow pulses. It would thus appear that on the previous occasion both the discharge propagation delay and the laser kinetic effect were significantly greater. It would seem therefore that both the plasma conductivity (predominantly the electron density) and the pre-pulse axial electron temperature were higher on the occasion of the first set of measurements (the spontaneous emission study) than on that of the second. It was not possible to set all the operating parameters the same on the two occasions owing to the fact that, although on both occasions the device used had a 60 mm diameter plasma tube, many modifications had been made to both the power supply and laser head, and consequently the CVL was simply set up to give maximum output on each occasion. It was not expected that such large differences would be observed between two devices with the same diameter plasma tube, and this result suggests the potential for manipulation of these delays.

6.5 THE STEP ON THE LEADING EDGE OF EMISSION PULSES ON AXIS

In every case, emission acquired from the axis of the plasma tube displays a more or less pronounced step on the leading edge, a phenomenon entirely absent from all emission detected from close to the plasma tube wall. As this step is observed equally in the spontaneous emission as in the laser pulses it would seem to be associated with the discharge pulse rather than a lower level effect. Although in some ways reminiscent of the step observed on the leading edge of the second discharge current pulse after a period of blanking (Section 5.5.3, Figure 5.3) it must be remembered that in that case the step came about as a result of a low level of ohmic conduction current in the pre-pulse electron density prior to "proper breakdown". Under normal operating conditions no step

is observed in the current trace as the conduction current rises smoothly to the full amplitude of the current pulse. The presence of a step is interpreted as the result of a lower than normal pre-pulse electron density. In the case of the step in the spontaneous (and stimulated) emission pulses, it is only observed in traces taken close to the axis where the pre-pulse electron density is highest.

It has been hypothesised (Chapter 5) that the ohmic conduction current in the existing pre-pulse electron population, although it has the effect of causing current to flow earlier in the discharge pulse, also has the effect of delaying the onset of lasing by reducing the rate of rise of the voltage pulse, and consequently electron temperature. It would be surprising if the radial profile of the pre-pulse electron density did not have such an effect on the radial profile of the time of lasing (and similarly spontaneous emission), contributing to the skin effect by retarding the onset of excitation on axis. To separate the magnitude of the two effects would be extremely difficult, requiring the radially resolved measurement of the timing of either the electric field in the plasma or the current density. What has so far been achieved is the radially resolved measurement of the timing of the rise in excitation, probably reflecting a corresponding step rise in electron temperature. It was demonstrated in Chapter 5, that this does not necessarily directly follow the timing of the rise in current.

The skin effect occurs because of the electric fields generated by the changing magnetic flux density caused by a rapid rate of rise of current in a conductor (Section 2.9). In the case of the laser discharge pulse the initial rate of rise of electric field, and hence current in the CVL plasma, is relatively slow, mainly as a result of the thyratron switch-on characteristics. Initially, therefore, the skin depth δ, given by:

$$\delta = \left(\frac{2}{\omega \mu_0 \sigma} \right)^{1/2} \qquad \textbf{(6.2)}$$

is large (corresponding to a low effective value of ω in Equation 6.2), and a small current can flow across the whole diameter of the plasma. Fairly soon however the rate of rise of electric field, and hence current, increases, the skin depth decreases, and the majority of the rapidly increasing current is constrained to flow in the regions of the plasma closer to the wall. Once the electron density starts to increase too, observed to occur at about the time that the total (sum of yellow and green) laser pulse on axis commences, the

conductivity is likely to increase significantly (although the increase in electron temperature causes increased collision frequency), thus reducing the skin depth still further. Where a high pre-pulse electron density exists on axis, as it generally does, the initial small current allowed to flow on axis immediately is unlikely to cause excitation of copper levels until the electric field rises sufficiently to raise the electron mean energy to values high enough to initiate inelastic collisions.

Exactly what the observed result of the effects described above would be on the spontaneous emission temporal profile on axis is difficult to predict with any degree of certainty without a full three dimensional computer model of the discharge, including the precise shape of the voltage pulse applied to the electrodes, a function of many factors including the complex impedance of the power supply and transmission line, the switching characteristics of the thyratron, and the time and radially resolved electron density. It is reasonable to suggest, however, that the acceleration afforded to the electrons by the low level electric field on axis that arises while the rate of change of current is low at the beginning of the current pulse gives some of them sufficient energy to initiate excitation, and consequently spontaneous emission, before the penetration of the main electric field, retarded by the skin effect, and the main pulse of emission.

6.6 CONCLUSIONS

It has been shown that in a 60 mm diameter CVL a combination of discharge excitation propagation and lower laser level effects retard the onset of lasing on axis, and that the latter effect is of considerably greater importance in the timing of the green laser pulse. It has not been possible to separate the contributions of the electromagnetic skin effect and the pre-pulse electron density, in the timing of the excitation of the copper, although it reasonable to expect that there is a contribution from both.

7 RESULTS OF POPULATION DENSITY MEASUREMENTS ON AXIS

7.1 COPPER GROUND STATE DENSITY

7.1.1 GENERAL BEHAVIOUR OF COPPER GROUND STATE POPULATION OVER FULL INTERPULSE PERIOD

The first result to be considered is the behaviour of the copper ground state population density on the axis of the plasma tube as a function of time in the CVL pulse cycle. Figure 7.1 is a plot of the full set of results obtained from these measurements. From this plot may be seen the basic form of the behaviour with time of the ground state population density. There is an initial, very fast, depletion in population, presumably during the discharge pulse, during which the population falls from its pre-pulse value of 420×10^{12} cm^{-3} to 190×10^{12} cm^{-3}, a depletion of 55%. This is followed by what appears to be a two, or more, stage recovery, initially relatively fast, with time constant of 4 μs, then much slower with a time constant of 71 μs from 10 μs to the end of the interpulse period. The population can be seen to be still rising significantly as it reaches its initial, pre-pulse value immediately prior to the subsequent discharge pulse. In this plot each individual measurement result has been plotted separately, allowing assessment of the reproducibility of the measurements in the comparison of the duplicate pairs.

7.1.2 POPULATION DEPLETION OF COPPER GROUND STATE DURING DISCHARGE

Having looked at the entire interpulse period it is appropriate to look in more detail at the behaviour of the population density over the course of the discharge pulse. Figure 7.2 therefore is a plot the first 1,000 ns of data points from the copper ground state population density measurements in conjunction with the discharge current pulse and the laser light output pulse. The benefit of the structure of the acquisition program, in which the time increment between successive measurements may be selected to provide optimal coverage for each part of the laser cycle, may readily be appreciated when considering Figures 7.1 and 7.2. From this plot may be seen further confirmation of the results discussed in Chapter 5. The depletion of the ground state population density can

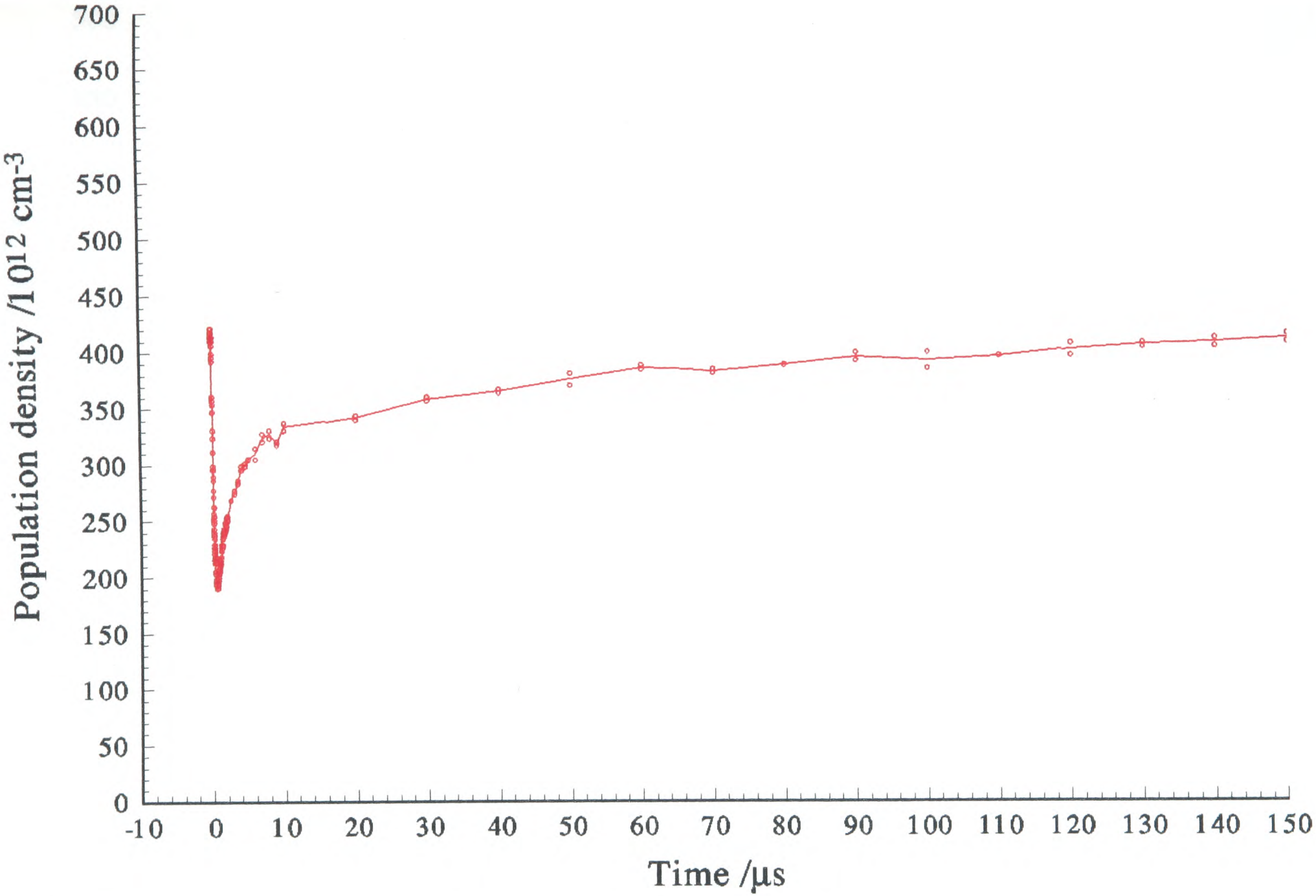

Figure 7.1 Population density on axis in copper ground state; full interpulse period

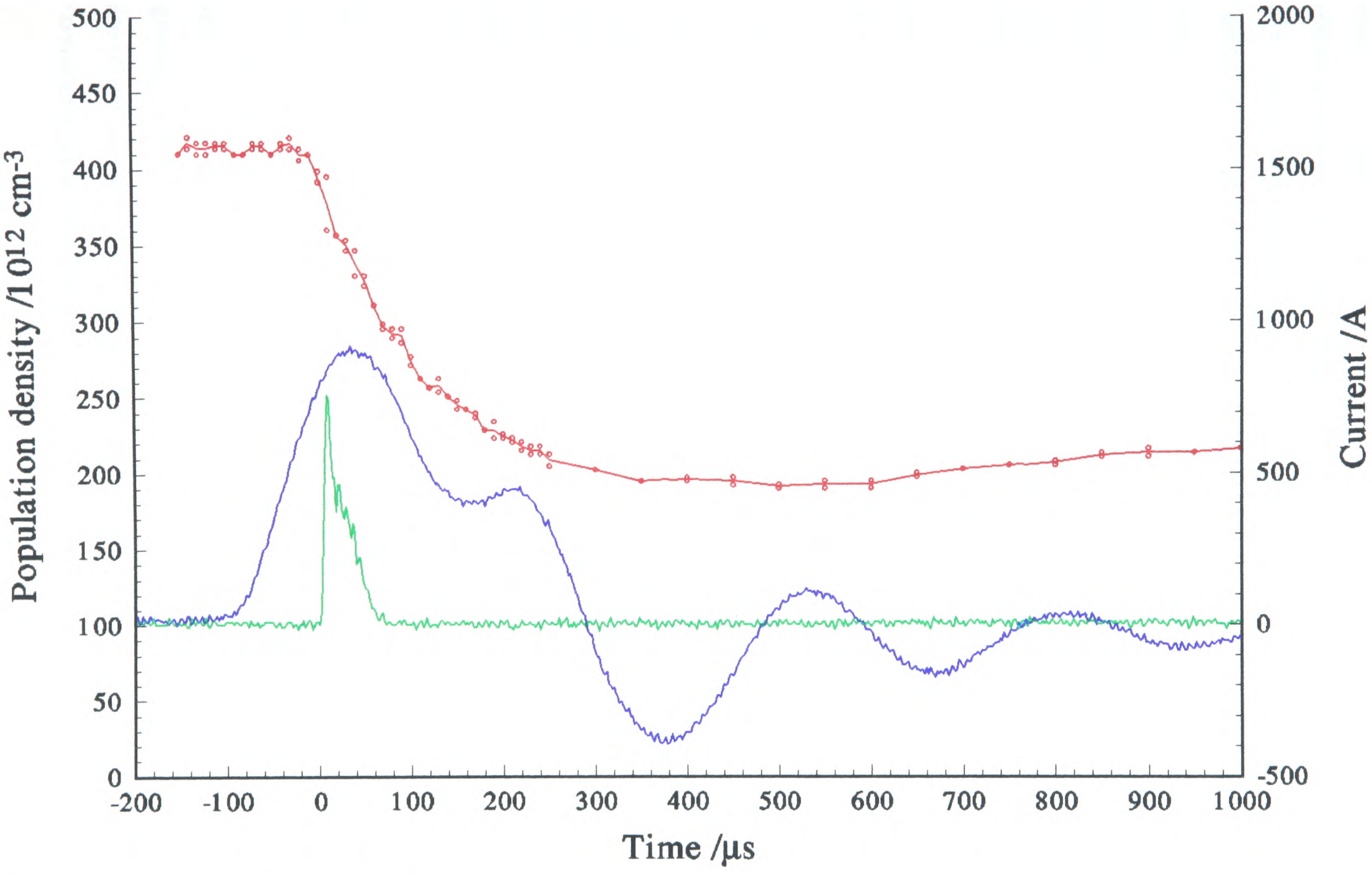

Figure 7.2 Population density on axis in copper ground state with current and laser light pulses; first 1 μs

be seen to commence nearly 100 ns after the start of the current pulse, preceding that of the laser pulse by only about 20 ns. As mentioned above, a delay of around 10 ns between discharge related events at the plasma tube wall and those on axis may be expected as a result of the skin effect, but a delay of 100 ns may not be dismissed so easily. The second observation to be made is that, apart from the leading edge, the rate of depletion of the ground state seems approximately to follow the magnitude of the current pulse. The laser pulse, however, occupies a brief period around the peak of the current pulse, coinciding with the period of maximum rate of depletion. It can be seen that population continues to be removed from the ground state for about 300 ns after the (80 ns full width) laser pulse is extinguished. The population removed during this time corresponds to approximately half of all the population lost from the ground state. As the extinguishing of the laser pulse occurs shortly after the inversion of the voltage pulse, it can be seen that this population is essentially "wasted" (as it makes no contribution to laser action) and is pumped from the ground state both by the energetic electrons accelerated during the second half of the first current lobe, and also by the ringing oscillations following this, as a result of imperfect impedance matching between the discharge circuitry and the dynamic CVL plasma. In addition to representing wasted power deposited in the plasma, a significant proportion of this population pumped from the ground state, and from other copper levels simultaneously, is likely to end up as ionised copper. These extra ions therefore contribute to the excessive pre-pulse electron density observed in Chapter 5 to have a deleterious effect on the excitation quality of the subsequent discharge. The duration of increase in electron density may be observed in the results of Chapter 8.

7.2 COPPER 4p $^2P_{3/2,1/2}$ UPPER LASER LEVEL POPULATIONS

7.2.1 OVERALL TIME DEPENDENCE OF THE UPPER LASER LEVELS

In Figures 7.3 and 7.4 the measured population density in the two upper laser levels (4p $^2P_{3/2}$ and 4p $^2P_{1/2}$) on axis are plotted as a function of time for 1 μs after the beginning of the laser pulse, together with the profile (in arbitrary units) of the laser pulse of the appropriate transition. It is reasonable at this point for these two levels to be considered as a pair owing to their analogous positions in the copper term diagram

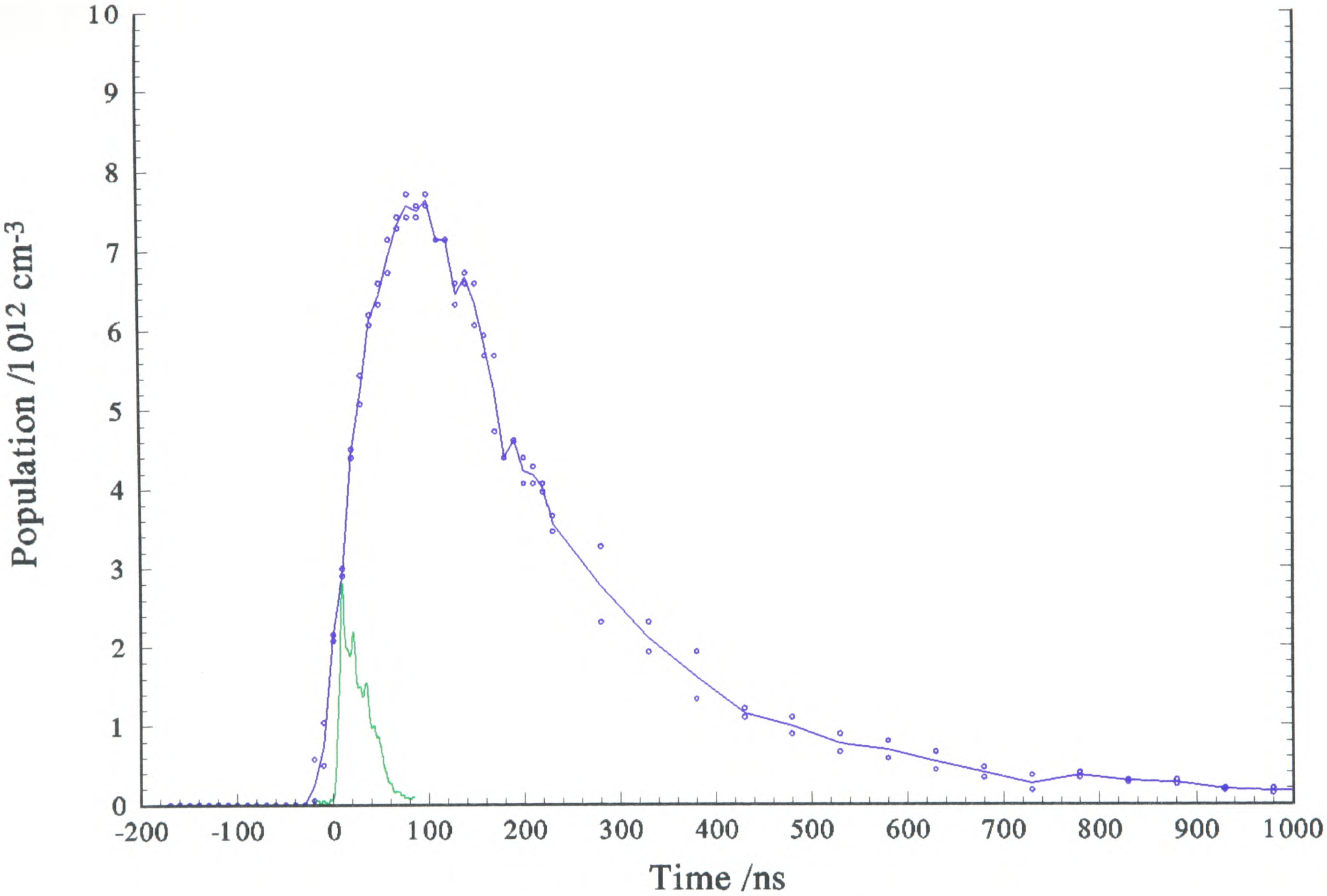

Figure 7.3 Population density on axis in copper 4p $^2P_{3/2}$ level; measured using 809.3 nm transition

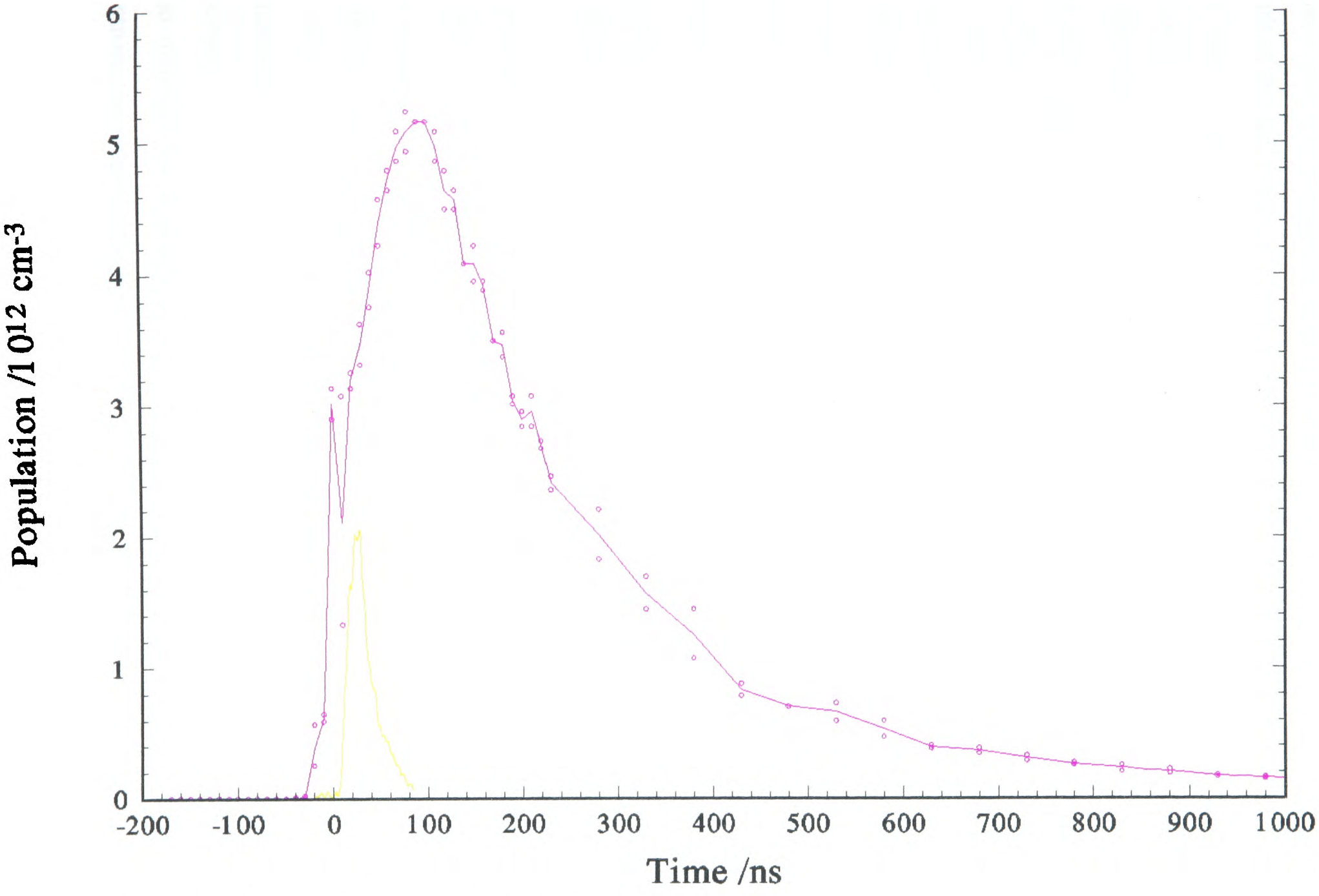

Figure 7.4 Population density on axis in copper 4p $^2P_{1/2}$ level

(see Figure 3.6). In the same way the two lower laser levels will also be considered as a pair in due course.

In attempting to interpret the overall time dependencies for these population densities it is appropriate to consider the approximate form expected. As the electric field in the CVL rises (the resultant field, out of phase with the applied voltage as a result of the inductance of the structure) the residual electrons present from the previous discharge are accelerated and the current density rises. As this happens the number of electrons with kinetic energy greater than the threshold for collisional excitation of the ground state copper atoms to the upper laser levels (3.8 eV) increases. While these electrons merely comprise the extreme high energy tail of a low energy Maxwellian distribution, the population rate of the upper laser levels is insignificant. As the electron temperature, and thus the energy of the bulk of the electron population, rises then the population density in these levels begins to rise rapidly at rates determined by the relative collisional cross-sections of the two transitions. There are two predominant loss mechanisms from these levels: further collisional excitation to higher lying levels, and radiative decay to the lower laser levels. The copper ground state density is too high to allow resonance radiation to escape from the plasma without being reabsorbed, thus eliminating this loss mechanism (radiation trapping), and super-elastic collisional de-excitation to the lower laser levels is insignificant in comparison with these other two processes at this stage.

Owing to the relatively low pre-pulse population density in the lower laser levels (see Section 6.3 for qualification and further discussion of this) population inversion is relatively quickly established and emission on the two laser lines commences immediately the cavity round trip losses have been exceeded. As the intracavity radiation density increases the rate of stimulated radiative depopulation on these transitions also increases. During this period however stepwise excitation of the copper causes significant additional ionisation and "breakdown" of the plasma may be said to have occurred. As a result the electrode voltage ceases to rise as the impedance of the external circuit no longer allows it to maintain the electrode voltage necessary to give the rapidly growing number of electrons the kinetic energy necessary to maintain the electron temperature. The rate of rise of current, dI/dt, decreases giving a smaller reactive voltage and the longitudinal electric field in the plasma tube, the electron temperature, and the current all peak.

Throughout the whole duration of the discharge current pulse, and for several microseconds afterwards, the electron temperature is too high to allow significant recombination (Section 8.1.6). As the electric field within the plasma falls, owing to the large number of inelastic collisional processes by which the electrons can lose energy, the electron temperature starts to fall. The rate of excitation from the copper ground state to the upper laser levels starts to decrease, mainly as a result of the falling electron temperature, but also partly due to the depleting ground state population density (Figure 7.2). Direct excitation from the copper ground state to the lower laser levels, however, does continue (in fact the rate coefficient for this process does not decrease as the electron temperature falls from 5 eV to 1.5 eV, at which point this process dominates over excitation to the upper laser levels (Figure 7.5)). Excitation of copper population from the upper laser levels to higher lying levels also occurs with significant cross-sections, with rate coefficients for the transitions from the $4^2P_{3/2}$ level to the $5^2S_{1/2}$ and $4s^2\ ^2D_{5/2}$ levels being around three times greater than that of the transition from the ground state to the upper laser level (Figure 7.5). Below about 1.5 eV excitation to the ^4P, ^4D, and ^4F levels also dominates.

The result of these processes is that about the same time that the current pulse peaks, and hence too the electron temperature, gain on the laser transitions also peaks. This is the point where rate of rise of population density in the upper laser levels is at its greatest. In order to determine exactly at what time the various loss processes dominate and the population density reaches a peak would require a full computer simulation of the kinetics, however once the rate of population of the upper laser levels starts to decrease this rapidly leads to self-termination of the laser pulse. Following this the population density in the upper laser levels will decay by the combined effect of the loss mechanisms described above.

From Figures 7.3 and 7.4 it may be seen that the forgoing discussion appears to describe the observed behaviour fairly well.

7.2.2 THE RATIO OF POPULATIONS IN THE 4p $^2P_{3/2}$ AND 4p $^2P_{1/2}$ LEVELS

There are, however, three additional observations to be made. The first concerns the relative magnitudes of the two populations. Although both curves appear to have similar profiles, both starting and peaking at the same time, the peak population densities

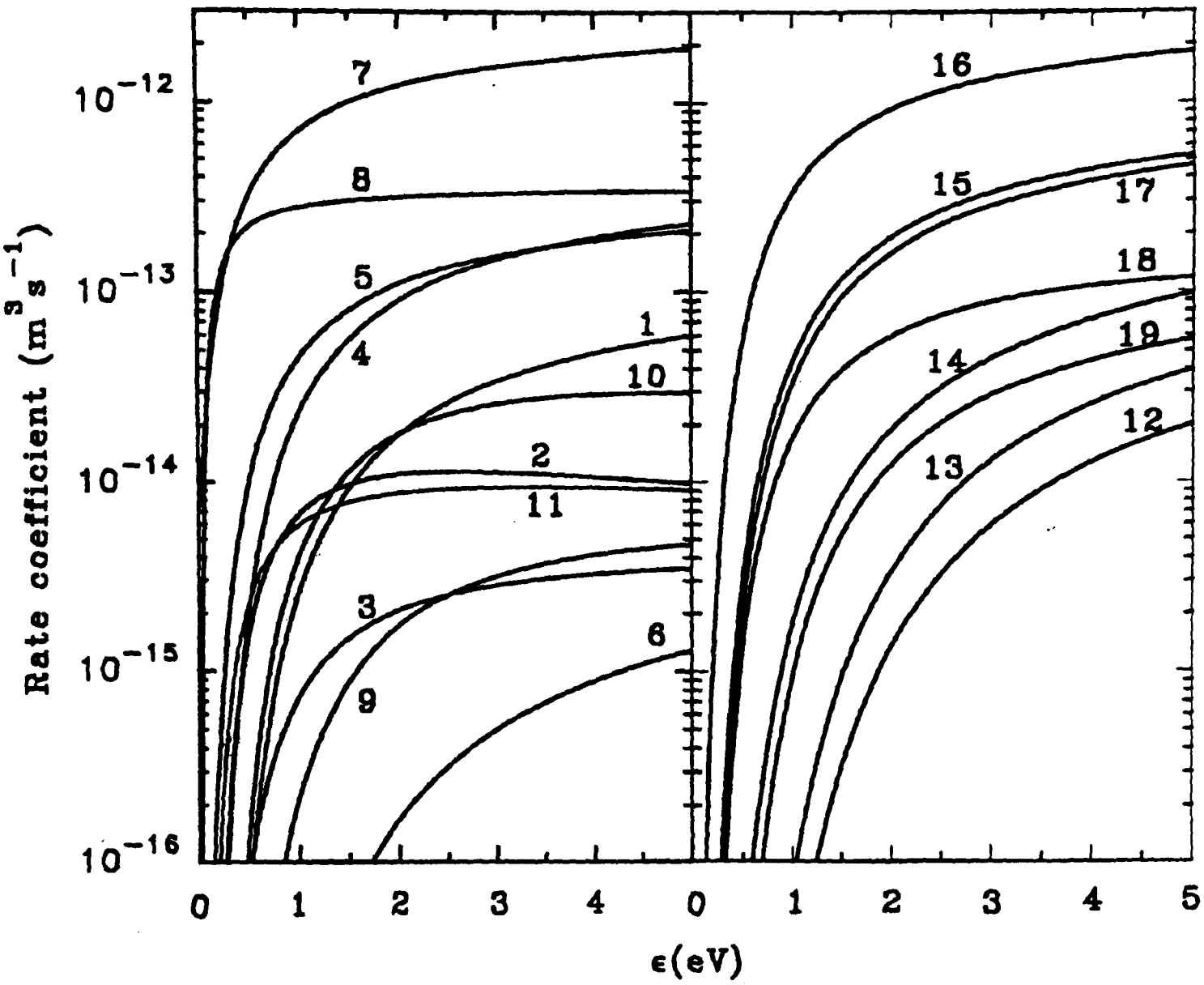

Figure 7.5 Electron collisional rate coefficients for copper. For designations of curves see following page.

(Reproduced by kind permission of Dr R J Carman)

in the $4^2P_{3/2}$ and $4^2P_{1/2}$ levels are in the ratio of 1.5:1. On the whole this remains the case throughout the majority of the time course to within the accuracy of the data, except for a few brief periods of structure in the population profile, especially one of population depletion observed on the rising edge of the $4^2P_{1/2}$ level (and of which there will be further discussion below). This can most easily be seen by plotting both curves on one graph against axes scaled in the ratio 1:1.5 as in Figure 7.6. The proximity and equivalence of the two levels is such that the excitation cross-section per state from the ground state should be the same, thus giving rate coefficients for the two levels in the ratio of their degeneracies ie 2:1, which is indeed the case. The actual relative population densities in the two levels, at a given time, therefore, is determined by the

Curve Number	Initial level	Final level
1	$3d^{10}\ 4s\ ^2S_{1/2}$	$3d^{10}\ 4p\ ^2P_{3/2}$
2	$3d^{10}\ 4s\ ^2S_{1/2}$	$3d^9\ 4s^2\ ^2D_{5/2}$
3	$3d^9\ 4s^2\ ^2D_{5/2}$	$3d^{10}\ 4p\ ^2P_{3/2}$
4	$3d^{10}\ 4p\ ^2P_{3/2}$	$3d^{10}\ 4d\ ^2D_{5/2}$
5	$3d^{10}\ 4p\ ^2P_{3/2}$	$3d^{10}\ 5s\ ^2S_{1/2}$
6	$3d^9\ 4s^2\ ^2D_{5/2}$	$3d^{10}\ 5p\ ^2P_{3/2}$
7	$3d^{10}\ 5p\ ^2P_{3/2}$	$3d^{10}\ 5p\ ^2P_{3/2}$
8	$3d^9\ 4s^2\ ^2D_{5/2}$	$3d^9\ 4s^2\ ^2D_{3/2}$
9	$3d^{10}\ 4s\ ^2S_{1/2}$	$3d^9\ 4s(^3D)\ 4p\ ^4P,\ ^4D,\ ^4F$
10	$3d^9\ 4s^2\ ^2D_{5/2}$	$3d^9\ 4s(^3D)\ 4p\ ^4P,\ ^4D,\ ^4F$
11	$3d^{10}\ 4p\ ^2P_{3/2}$	$3d^9\ 4s(^3D)\ 4p\ ^4P,\ ^4D,\ ^4F$
12	$3d^{10}\ 4s\ ^2S_{1/2}$	$3d^{10}\ ^1S_0\ +\ e^-$
13	$3d^9\ 4s^2\ ^2D_{5/2}$	$3d^{10}\ ^1S_0\ +\ e^-$
14	$3d^{10}\ 4p\ ^2P_{3/2}$	$3d^{10}\ ^1S_0\ +\ e^-$
15	$3d^{10}\ 5p\ ^2P_{3/2}$	$3d^{10}\ ^1S_0\ +\ e^-$
16	Excited copper pseudo-state	$3d^{10}\ ^1S_0\ +\ e^-$
17	$3d^9\ 4s(^3D)\ 4p\ ^4P,\ ^4D,\ ^4F$	$3d^{10}\ ^1S_0\ +\ e^-$
18	$3d^{10}\ ^1S_0\ +\ e^-$	Excited ion pseudo-state
19	Excited ion pseudo-state	Doubly excited ion pseudo-state

Table 7.1 Designations of rate coefficient curves in Figure 7.5

relative strengths of the loss processes from the two levels, both downwards to the lower laser levels, and upwards to higher lying levels.

To the extent that electron collision cross-sections tend to reflect optical transition probabilities it is of interest to consider the factors that affect relative optical transition probabilities within a multiplet (Woodgate, 1980). For transitions for which $\Delta L = \pm 1$ the strongest are those for which ΔJ has the same sign as ΔL. For the $4^2P_{1/2}$ level this, together with the requirements that $\Delta J = \pm 1,0$ and $\Delta S = 0$, corresponds to transitions

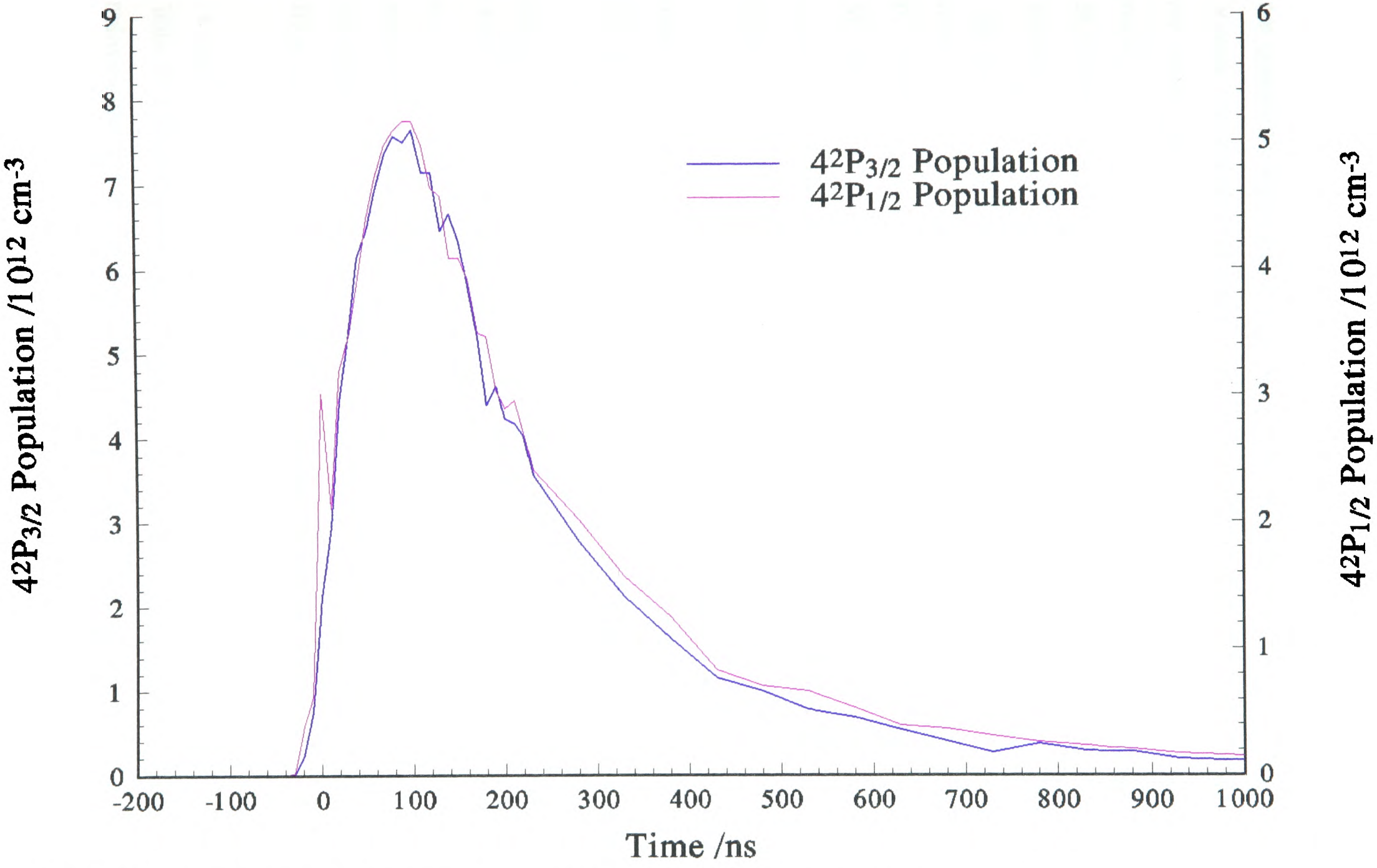

Figure 7.6 Population density on axis in copper 4p $^2P_{3/2}$ and 4p $^2P_{1/2}$ levels; scaled to compare profiles

to the $^2D_{3/2}$ series of levels only for strong transitions. For the $4^2P_{3/2}$ level this also allows transitions to the $^2S_{1/2}$ series of levels. In addition, while the "cross-over" transitions: $4^2P_{3/2}$ to $^2D_{3/2}$ levels, both upwards and downwards, are allowed, though not strong, the converse transitions $4^2P_{1/2}$ to $^2D_{5/2}$ are entirely optically forbidden. From qualitative arguments like these it could be expected that a larger number of loss processes are available to deplete population in the $4^2P_{3/2}$ level compared to the $4^2P_{1/2}$ level so that the total loss rate would be higher, with the result that the population densities in the two levels do not observe a strict 2:1 ratio. These arguments could only hold because it has been shown (Hollins, 1980; Lewis, 1985) that there is insignificant collisional mixing of the two upper laser levels on the timescale of the lifetime of an atom in the levels, and therefore deviation from the 2:1 statistical weight ratio for the two levels is possible. It has been remarked above that the rate coefficient for the transition $4^2P_{3/2}$ to $5^2S_{1/2}$ is three times that of excitation from the ground state to the level (Figure 7.5). The optical transition probability of the equivalent transition from the $4^2P_{1/2}$ level is half of that from the $4^2P_{3/2}$ level. This argument is not intended to be in any way rigorous, especially as true reflection of optical transition probabilities by collisional ones can only be expected at electron energies far greater than those encountered in the CVL plasma, but merely to suggest that it would not be surprising if the loss rate, per state, from the $4^2P_{3/2}$ level were greater than from the $2^2P_{1/2}$ level.

The flaw in the argument above is the fact that the observed shapes of the time dependencies of the two populations are very similar, a fact confirmed in Figure 7.6. If additional loss processes were responsible, differences in profile would be expected as the relative significance of these processes changed with the electron temperature, for instance giving rise to population density decay curves of slightly different shapes. No such differences are observed in this case. In addition to this, any such rate coefficient differences are likely to be fairly minor.

It remains to be confirmed for certain whether the observed 1.5:1 ratio is genuine or a result of inaccuracy in the oscillator strength values employed in the calculations (Table 3.1) however the measurement had also been performed using the hook method employing the 521.8 nm transition $4^2P_{3/2}$ to $4^2D_{5/2}$ (see copper term diagram Figure 3.6). There is unfortunately a second, weaker transition from the same lower level to the $4^2D_{3/2}$ level that lies only 0.2 nm away from the one of interest, at 522.0 nm. This causes the

problems of significant overlapping perturbations to the real refractive index discussed in Appendix A2. Attempts were made to interpret the hook patterns thus obtained by using the "outside" hook of the strong line alone (also as discussed in Appendix A2) and the results of Figure 7.7 were obtained. In this case the ratio of measured population density to that in the $4^2P_{1/2}$ level is very close to the expected 2:1. A slight inaccuracy in the placing of the centre of the absorption line of ± 2 pixels, however, would give rise to an error of about $\pm 10\%$ at the peak, reducing this to 1.9:1. In order to ensure that the decreased population density ratio was not a result of a genuine, long term drift in operating conditions in the CVL, since the $4^2P_{1/2}$ population density measurement had been made at the same time as the first $4^2P_{3/2}$ measurement employing the 521.8 nm line, the $4^2P_{1/2}$ measurement was repeated and the result showed a difference in the peak value of less than $+4\%$ over a time period of 7 months.

It is of interest to note that in Brown's study of a 18 mm bore CVL (Brown, 1988) he observed a ratio between the peak values of the population density in the two levels of 1.7:1, though overall he reports an average ratio of $1.9(\pm 0.2):1$.

In view of the discussion above it seems possible that the true ratio is not an exact 2:1, as predicted by the statistical weights of the levels, but slightly less than this, however to be able to offer an accurate value would require a better knowledge of oscillator strengths than we have at present.

7.2.3 STRUCTURE IN THE 4p $^2P_{3/2,1/2}$ LEVELS TIME PROFILE

The second point of interest in the upper laser level population density curves relates to the observed structure. The most obvious instance occurs on the leading edge of the $4^2P_{1/2}$ level plot (Figure 7.4), coinciding with the rising edge of the yellow laser pulse, where there is a marked dip in the measured population density. Following this dip the population density appears to rise as before, though the curve is then parallel to the original rise, rather than above it. This suggests that the kink observed is a real effect, rather than the result of jitter in the probe pulse timing or noise in the data. Looking at the $4^2P_{3/2}$ population density measurements curve, a pronounced dip of this kind is not observed, however a slight kink in the curve, at about the time of the rising edge of the green laser pulse, may be observed.

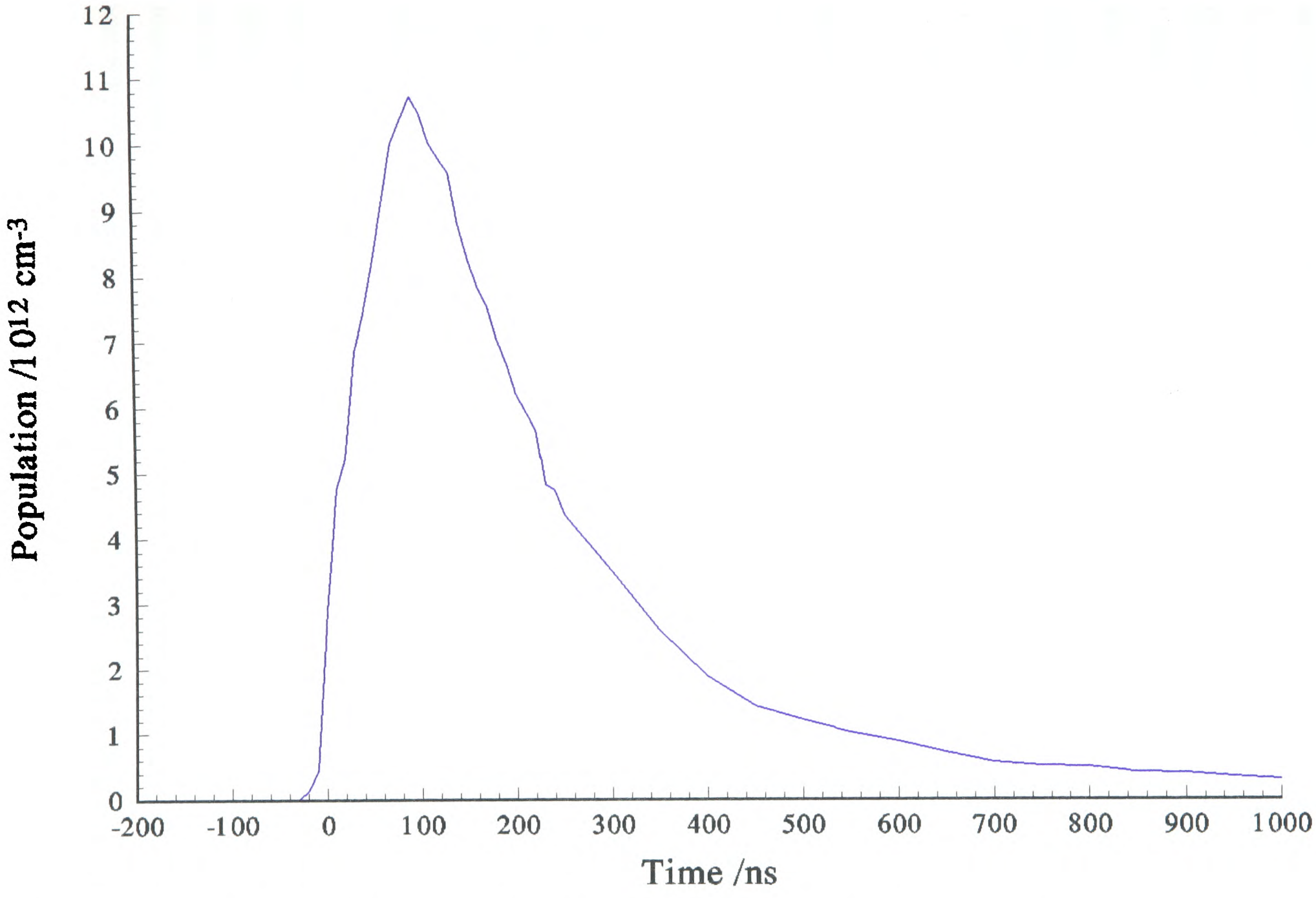

Figure 7.7 Population density on axis in copper 4p $^2P_{3/2}$ level; measured using 522.0 nm transition

It seems likely that the dip observed in the $4^2P_{1/2}$ level population density is the result of the pulse of stimulated emission on the yellow laser line causing visible, transient depletion of the upper laser level population, as was briefly mentioned in Section 2.2.1. Owing to the timing jitter of the probe pulse with respect to the CVL pulse (a total of ± 3 ns, Section 3.3.4 (V)) the scatter in the data points when measuring such sharp structure is fairly significant, however both duplicate data points display a marked halt in the rise in population density. That this is a real effect is further confirmed by the repetition of the observation, at the equivalent temporal position, to a greater or lesser extent, on all measurements of the $4^2P_{1/2}$ population density made, at all radial positions, and on two independent occasions, 7 months apart. It is noticeable that this effect is somewhat less marked in the $4^2P_{3/2}$ level than in the $4^2P_{1/2}$ level. This too may be observed at 7 radial positions, and on both occasions that this measurement has been made.

An explanation of this anomaly may lie in the shapes of the laser pulses from each transition. In Section 9.1 below the radial dependence of the timing of the 510.6 nm and 578.2 nm laser pulses will be discussed, and the measurements of laser pulse shapes presented (Figures 9.1 and 9.2). It is evident that in all cases there is a marked fundamental difference between the two sets of pulse shapes. In all measurements the yellow pulse consists of a single prominent peak, of about 15 ns length, followed by a slower decay, whilst the green pulse is always seen to consist of a series of peaks of decreasing intensity, separated by about 15.5 ns, the optical cavity round trip time. In a number of cases small subsidiary peaks may be seen half way between the main peaks. Owing to the method used to obtain these traces the amplitudes may not be compared directly. The timing, however, is absolute.

It is generally accepted that the structure observed on the temporal profile of the green laser pulse is the result of a wave of amplified spontaneous emission (ASE), building up as gain is initially established, and, as it progresses along the length of the gain region, causing temporary depletion of the upper laser level population. This gives reduced gain for further ASE, and thus reduced optical flux density. That proportion (about 8%) of the original pulse that is fed back into the optical cavity by the output coupler then makes two more transits of the cavity (and gain length) before 92% of it re-emerges at the output coupler as the next peak of high quality laser light. This process

then repeats for as long as population inversion, and thus gain, continues. In between successive main peaks in intensity in which the population inversion is depleted in the path of the surge of laser action, the upper level population density continues to be increased at a rate determined by the electron temperature via its effect on the relative rates of collisional transfer to and from the upper laser level. Secondary peaks in laser output, between the main ones, may occur as a result of a secondary local maximum in gain length product for spontaneous emission starting at the furthest end of the gain length from the output coupler at the time of emission of the main pulse. Both before and after this time the total gain will be lower, following the more recent passage of the main pulse in one direction or the other.

That the structure described above is not observed on the time dependence of the yellow laser pulse would initially seem surprising. If the relative timing of the yellow and green laser pulses is considered, however, it may be observed that, on axis, the green precedes the yellow by about 5 ns. Collisional excitation from the copper ground state to both upper laser levels commences simultaneously, and the pre-pulse (thermal) population in the yellow lower level may be expected to be smaller than that in the green lower level. The reason for this time difference, therefore, must represent the additional time taken for gain to exceed cavity round trip losses on the yellow laser transition, following the rise in electron temperature during the discharge pulse, and the shift from preferential population of the lower threshold lower laser levels, to the upper levels, owing to its cross-section of one half that to the $4^2P_{3/2}$ level. The population (and de-population) rates of both upper laser levels, however, are determined by the same electron temperature and consequently these population densities peak, and, more importantly, display decreased rate of increase, at the same time; amply illustrated by Figure 7.6. By the time net gain is observed on the yellow transition the rate of increase in the upper laser level population density has reached its peak and therefore the time taken to deplete this population sufficiently to terminate the first peak of this pulse is greater than for the green line. The combination of this extended first peak with a later commencement means that soon after the end of this the fastest rate of rise of the upper level population density is soon over, and begins to decrease (for both upper levels). By the time the initial, broad laser pulse has completed its first round trip of the optical cavity gain is already very much decreased and no obvious second peak is observed. If

the time that a second peak would be expected is compared with the green laser pulse it will be observed that no peaks are to be observed by this time in the green pulse either.

Returning to the structure observed in the time dependence of the upper level population densities, it may be seen from the argument above that the first depletion in the $4^2P_{1/2}$ (yellow upper) level population density should be expected to occur slightly higher up the leading edge of the population increase, around the steepest part, than that in the $4^2P_{3/2}$ (green upper) level, which should occur just before it. The depletion of the yellow upper level. moreover, should be expected to last for around 15 ns, and have a more lasting effect than that of the green upper level, though if a secondary dip be observed it would be near the peak, during the roll-off of population, broad, and relatively shallow. Depletion of the green upper level would be expected to consist of a series of narrow (about 5 ns), shallow dips at 15.5 ns intervals up the leading edge of the population density profile. Owing to the sampling rate of these population density measurements (10 ns over the period in question) although it is expected that the depletion in the yellow upper level should be observed directly, that of the green upper level may be expected to appear just as slight kinks. The population densities measured do indeed seem to fit this hypothesis reasonably well.

Structure may also be observed on the trailing edges of the measured population density curves. As these are of approximately the same order of size as the scatter in the data at this level, and do not significantly alter the shape of the curve, they may at first glance be taken merely to represent noise in the data. If, however, measurements are compared at a number of radial positions, then in both the $4^2P_{1/2}$ and $4^2P_{3/2}$ level measurements it is be noted that the two most prominent blips always seem to occur at times of about 150 and 200 ns (after the arbitrary time origin). Comparison with the discharge current curves of Figure 5.1 reveal that these time points correspond to a dip and subsequent peak in the first lobe of the current pulse, corresponding, in turn, to the first and second reversal peaks of the voltage pulse. It is likely that these turning points coincide with changes in electron temperature and thus changes in the relative rates of population and de-population of these levels, although the exact nature of this balance, and the effect of a given change, varies with electron temperature and would require a computer plasma model for full interpretation.

7.2.4 DECAY RATES OF THE 4p $^2P_{3/2,1/2}$ LEVELS

The final observation from these two curves is that of the two stage nature of the decay. Figures 7.8 and 7.9 show the profiles with two part exponential fits to the decay curves. Despite the difference in the absolute amplitudes of the population densities high quality fits may be obtained with, for the $4^2P_{1/2}$ level, a time constant of 188 $\pm$3ns from 100 ns to 480 ns, and 336 $\pm$14 ns from 480 ns to 1 μs (the errors quoted represent calculated standard errors from the least squares fit algorithm), and for the $4^2P_{3/2}$ level 178 $\pm$3 ns from 100 ns to 500 ns, and 321 $\pm$29 ns from 500 ns to 1 μs. A likely explanation for this observation is that, as the electron temperature falls, the dominant loss process from the 4^2P levels ceases to be excitation upwards, predominantly to the ^4P, ^4D, ^4F group of levels, the $5^2S_{1/2}$ level and the 4^2D levels (Figure 7.5) and becomes predominantly downwards, via super-elastic electron collisions and radiative transition, to the $4s^2\,^2D$ levels and the ground state to restore Boltzmann equilibrium with the copper ground state. It may be noticed that at 480 ns the last major lobe of the current pulse finally ends and with it any significant power input to support the falling electron temperature.

Again it is of interest to note that in his study of kinetics in an 18 mm diameter CVL Brown (Brown, 1988) observed both a two phase decay process in these population densities, and a slight kink coinciding with the secondary hump of the discharge current pulse. His transition occurred earlier on (about 200 ns on my time scale), with time constants of 60 $\pm$10 ns and 320 $\pm$60 ns. Observable in his data, although small and not commented upon, is another kink, slightly earlier, coinciding with the dip in his current pulse.

7.3 COPPER $4s^2\,^2D_{5/2,3/2}$ LOWER LASER LEVEL POPULATIONS

7.3.1 INTRODUCTION

Problems were experienced in the measurement of population in the $4s^2\,^2D_{3/2}$ (yellow lower) level using the hook method owing to the combination of the very low oscillator strength of the transition to be employed (two orders of magnitude below those employed in the hook measurements of other groups of levels), the magnitude of the population density itself, and the dispersion of the spectrograph at the appropriate wavelength and order. The hook spacings generated by these measurements therefore

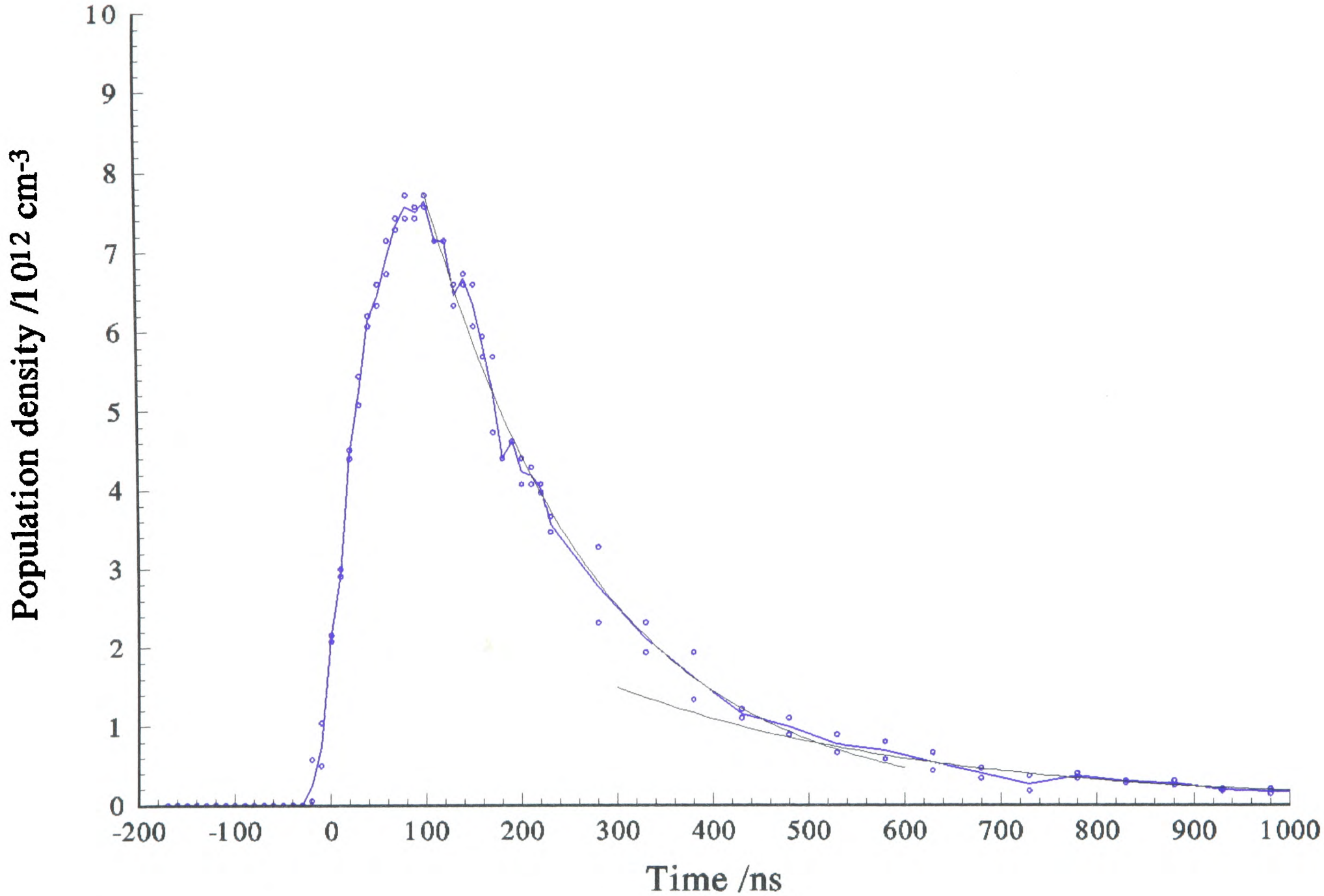

Figure 7.8 Population density on axis in copper 4p $^2P_{3/2}$ level; two stage exponential fit

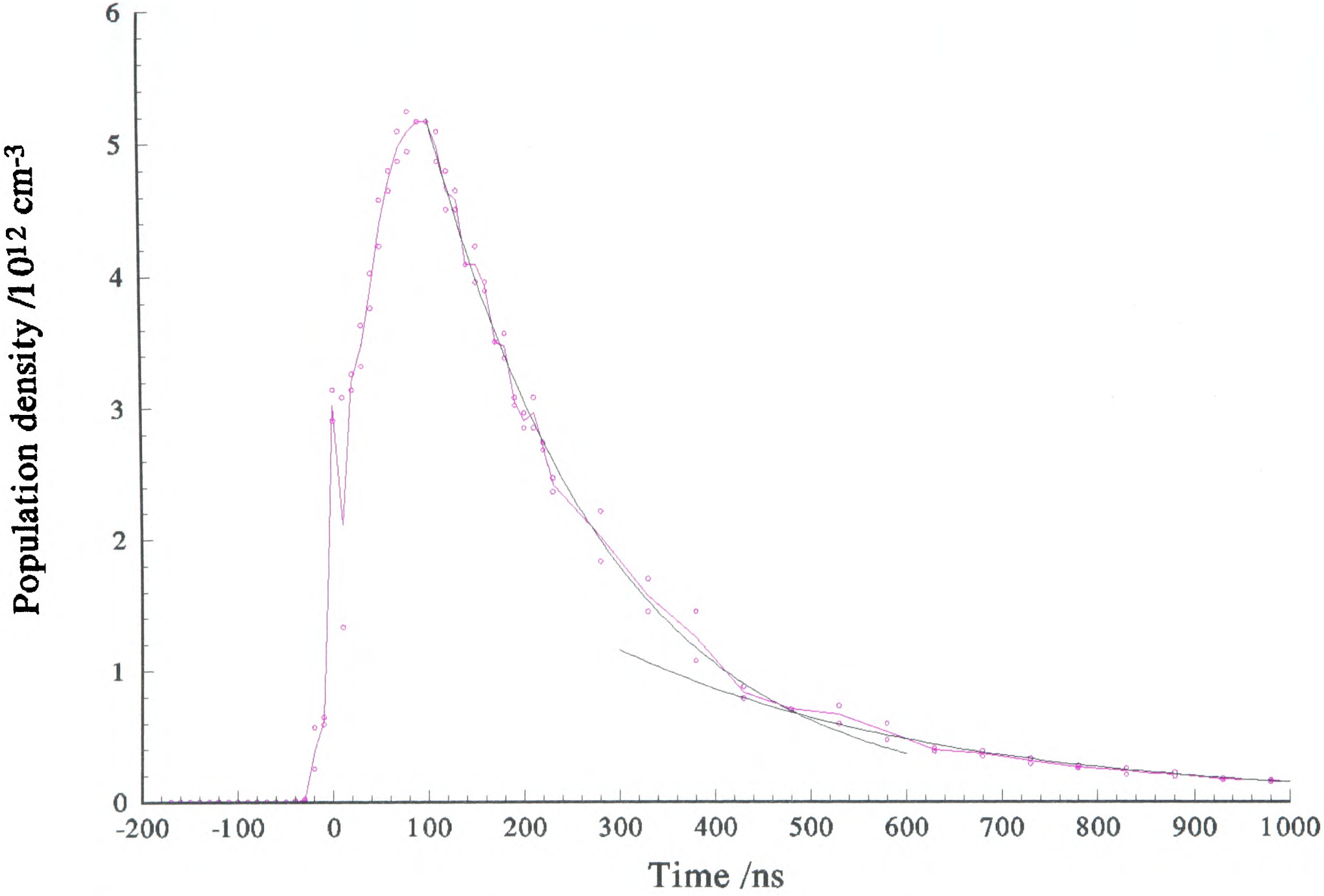

Figure 7.9 Population density on axis in copper 4p $^2P_{1/2}$ level; two stage exponential fit

consisted of only a few pixels, and consequently scatter in the data points is correspondingly great.

In addition to this (expected) problem it would have been desirable to have followed the population densities in the metastable lower laser levels throughout the laser cycle, a task well beyond the sensitivity limits of the hook method. For the majority of the interpulse period it is expected that the population densities remain in thermodynamic equilibrium with the copper ground state population density at the prevailing local, electron temperature. If the radial and temporal profiles of the electron temperature could be obtained in this way it would bring a number of benefits. If the radial profile of the electron temperature could be obtained then the extent of ambipolar diffusion could be assessed, and a more reliable gas temperature profile calculated. In Chapter 6 experiments to determine the relative importance of the skin effect and pre-pulse metastable population density in determining the relative timing of the green and yellow laser pulses as a function of radial position were discussed. From the results presented there (including the pulse timing measurements made on the study laser presented below (Section 9.1)) the radial electron temperature profile emerges as a parameter of significance, in particular whether it is flat, as proposed by Kushner (Kushner & Warner, 1983) and Carman (Carman et al, 1993) or significantly convex, as suspected by the present author, and supported by the measurements of Lewis (Lewis, 1985) and Izawa (Izawa et al, 1989) as discussed in Section 6.3.

In order to extend the high level of absolute accuracy of the hook method into the *Nf* region where its sensitivity does not otherwise extend it was intended to make the necessary measurements using an absorption technique, employing probe beams of bandwidth considerably less than those of the transitions of interest to measure the absorption far in the wings of the absorption lines. The precise wavelength to be used would be selected empirically as that giving 95% absorption at the peak population density. This value of population density could then be calibrated using that obtained from the hook method. In this way it was intended that the dynamic range of the absorption technique should be combined with the accuracy and freedom from assumptions of the hook method to give an extended time course of metastable population density measurements, the profile of which could then be compared with that obtained from the hook method over the range covered by the latter as an additional safeguard.

The software to run the experiment, controlling the probe pulse timing and acquiring the pulse amplitudes and areas from two detectors have been written and tested, and provisional runs have been made. Unfortunately, a recent failure of the Nd:YAG laser rendered it impossible to perform these experiments within the time constraints of the project. It is intended that these be completed by the author at a later date.

7.3.2 CORRECTIONS TO THE MEASURED $4s^2\ ^2D_{5/2,3/2}$ POPULATIONS

The results of the hook method measurement of the population density temporal profiles of the $4s^2\ ^2D_{5/2}$ and $4s^2\ ^2D_{3/2}$ (lower laser) levels on axis are plotted in Figures 7.10 and 7.11. From the end of the laser pulse (t = 100 ns) these results have been corrected for the population density in the upper levels of the transitions employed (the upper laser levels). For the 10 data points over the gain period however it would have been necessary to realign the hook method apparatus to allow the measurement of the population inversion by the inverse hook technique (Smilanski et al, 1980). This was not, unfortunately, performed at the time owing to the desire to complete the standard hook method measurements on the full set of atomic levels before realigning the hook method apparatus. It was therefore intended that these final measurements be performed after the absorption measurements, time permitting, thus being ruled out by the damage to the Nd:YAG laser.

7.3.3 RATE OF INCREASE OF $4s^2\ ^2D_{5/2,3/2}$ POPULATIONS

In Figure 7.12 the first 1 μs of data points of the $4s^2\ ^2D_{5/2}$ level measurements have been plotted against an expanded axis to allow the form of the rising edge to be seen in detail. In addition a straight line fit to the data points from 100 - 300 ns has been added, both to illustrate the almost linear nature of the rise in population over this period, and to give a very approximate idea of the behaviour of the population density over the first 100 ns. From this it may be seen that the rise in population in this level appears to exhibit two stages, consisting of a very fast rate of rise over the first 300 ns, followed by a slower one until the peak in population of 80 $\times 10^{12}$ cm^{-3} at about 550 ns.

It can be conjectured that these stages correspond approximately to the first lobe of the discharge current pulse, and the period to the end of the last significant positive current lobe (Figure 5.1). Referring to Figure 7.5, an electron temperature of

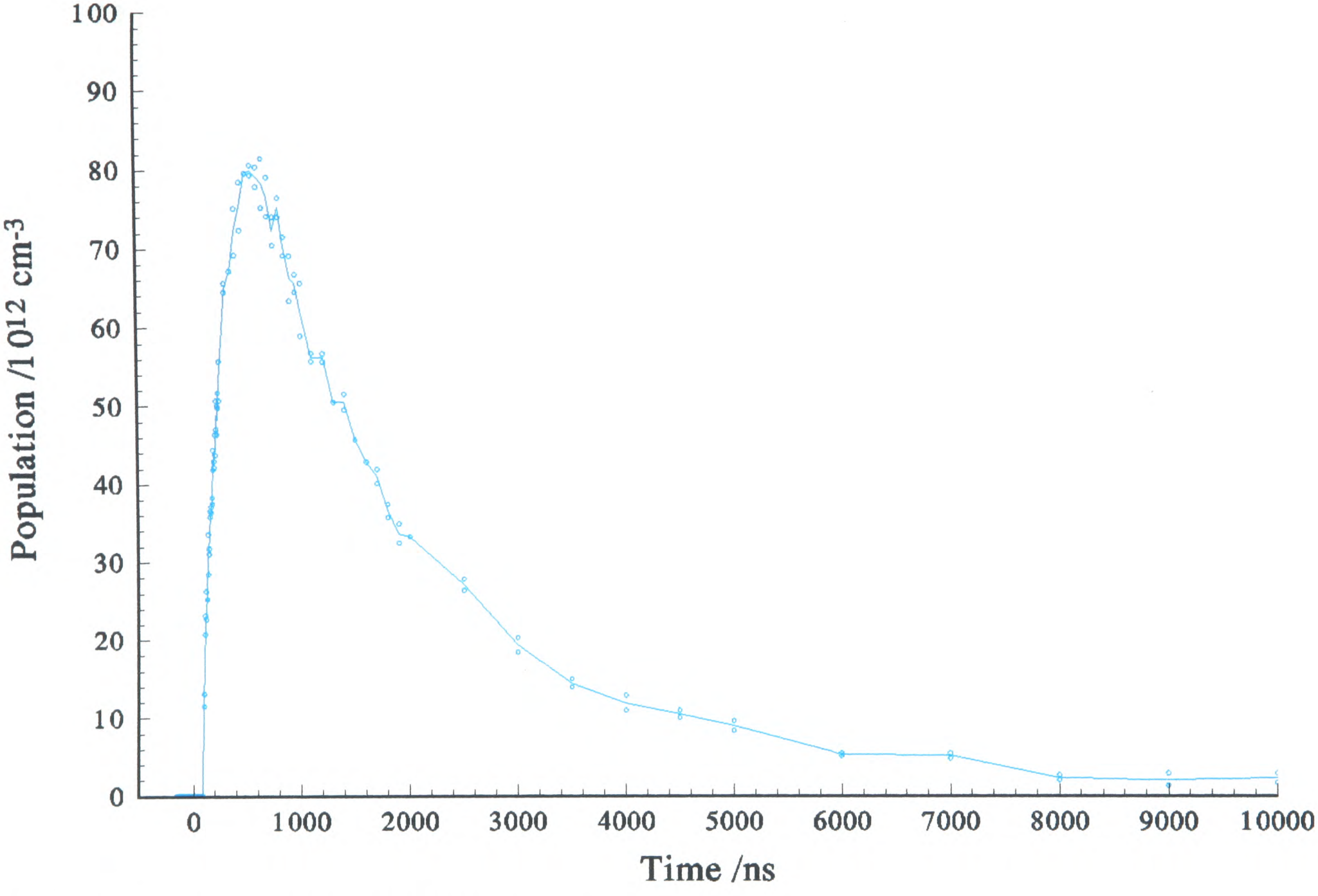

Figure 7.10 Population density on axis in copper $4s^2\ ^2D_{5/2}$ level

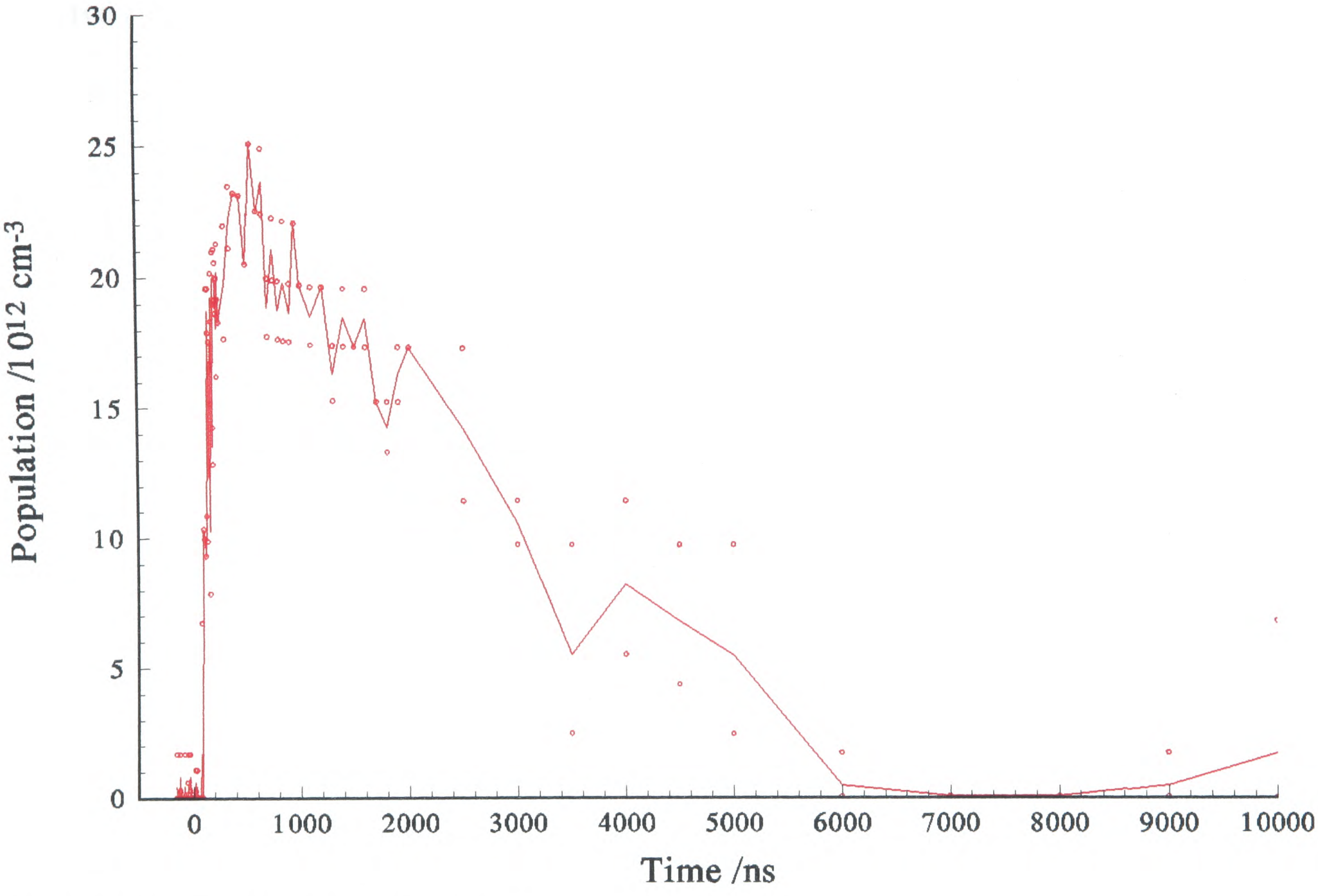

Figure 7.11 Population density on axis in copper $4s^2\,{}^2D_{3/2}$ level

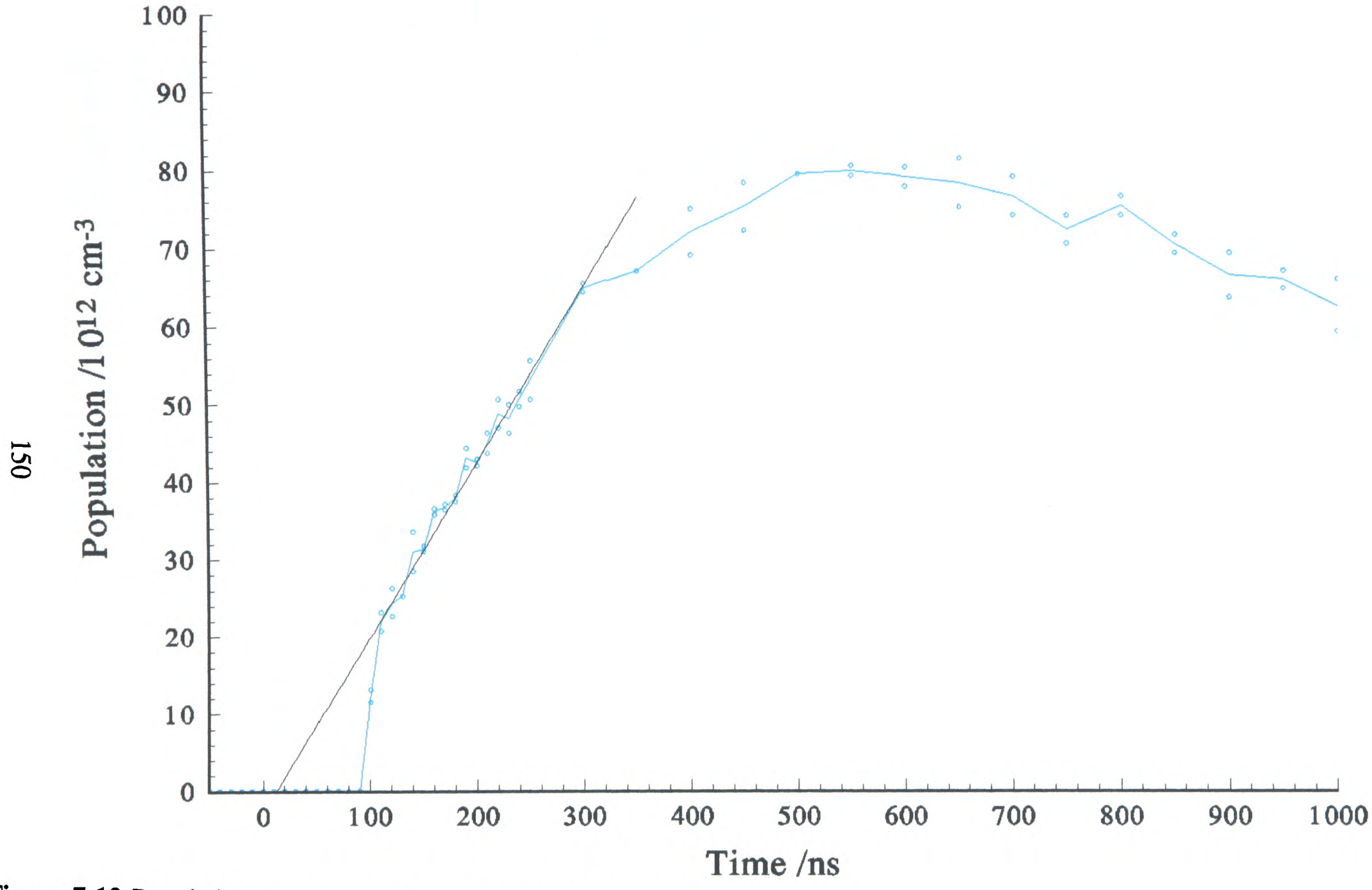

Figure 7.12 Population density on axis in copper $4s^2\,{}^2D_{5/2}$ level; first 1 μs

approximately 1 eV may be assumed at the end of the initial, almost linear rate of rise of $4s^2\,^2D_{5/2}$ population density at 300 ns, as this value corresponds to a "knee" in the rate coefficient curve (second derivative reaches a maximum) for direct excitation from the ground state. At the point at which the $4s^2\,^2D_{5/2}$ population density peaks, at 550 ns, the electron temperature must have fallen to around 0.4 eV, at which point the rate coefficient for direct excitation from the ground state is beginning to fall rapidly.

7.3.4 DECAY RATES OF THE $4s^2\,^2D_{5/2,3/2}$ LEVELS

Figure 7.13 shows the first 10 μs of measurements on this level, with the addition of the fitting of two exponential curves to the population density decay. From this it seems reasonable to characterise the decay in population density over this period as a bi-exponential process, with time constants of 1.68 $\pm$0.03 μs up to 3.6 μs, and 3.1 $\pm$0.3 μs from then until the end of measurable population at 10 μs. It should be remembered that, owing to the small hook separations corresponding to the later time points, the actual errors may be larger than those reflected by the standard errors in the exponential curve fits. Once again it would be extremely desirable to have the absorption measurements of the lower laser level population densities to complete the picture, and, in particular, to obtain a final population decay rate value over the majority of the interpulse period. In his study Lewis (Lewis, 1985) observed a two stage decay with a time constant of about 200 μs from about 10 μs onwards, corresponding to the period where the electron temperature had fallen to a value near that of the gas and thus was constrained to cool at the same rate. It is however likely that the two stage population density decay observed in the present study, following the cessation of the discharge pulse, represents behaviour before equality of electron and gas temperatures had been established.

Three possible explanations for the two stage decay observed over this time scale may be proposed:

(I) The first possible explanation is that 3.6 μs is the time at which, in the absence of significant recombination, Boltzmann equilibrium is first established between the copper excited levels and the ground state once the non-equilibrium population distributions produced during the discharge pulse have relaxed back to equilibrium values and so significant feeding of the $4s^2\,^2D_{5/2}$ level from higher lying levels becomes negligible.

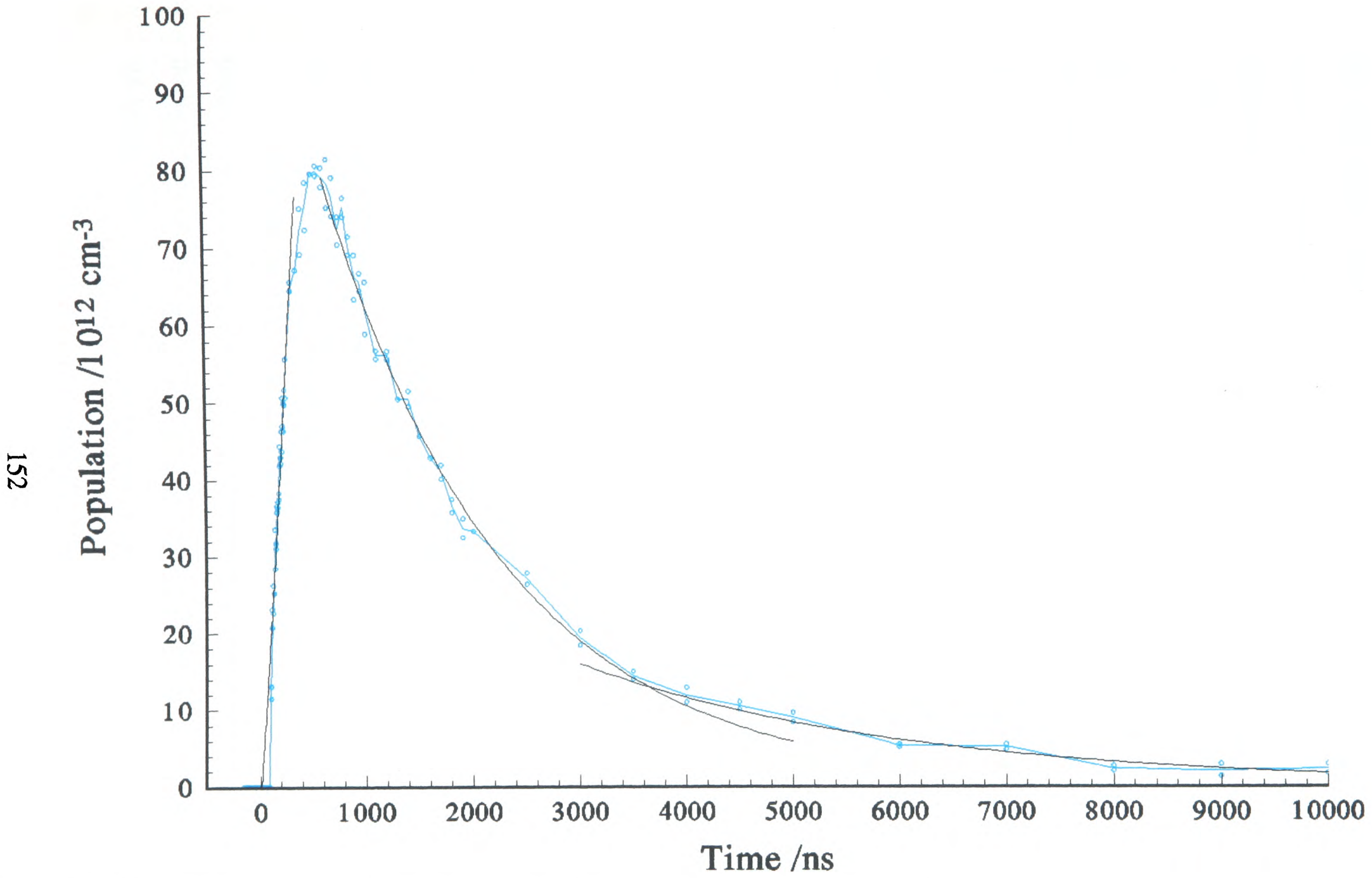

Figure 7.13 Population density on axis in copper $4s^2\,{}^2D_{5/2}$ level; two stage exponential fit

(II) The second explanation is that, owing to the lower heavy particle density (ground state copper and neon atoms) on axis with respect to the wall, it is reasonable that during the discharge pulse a radial electron temperature profile is established across the plasma tube, with a maximum on axis. Immediately after the end of the discharge pulse the high thermal conductivity of the electrons causes this radial profile to collapse to a relatively flat profile, and the copper metastable lower laser level radial profile will tend to follow this to reflect the copper ground state density profile. During this period the electron temperature at all radial positions has been decreasing, though fastest on axis, however once this flat temperature profile has been established electron cooling can occur at an approximately constant rate across the whole plasma tube until the gas temperature is reached, when a third, far slower, rate of cooling begins, this, however, not being observed in the hook method results. This reasoning suggests that the $4s^2\ ^2D_{5/2}$ level is at equilibrium with the ground state at the local electron temperature throughout the decay period as, if it were not, a third decay rate would be observed.

(III) The third possible explanation for the two stage metastable population density decay curve is that, owing to the T_e^{-5} dependence of recombination rate (Section 8.1.6) negligible recombination occurs for a number of microseconds after the discharge pulse, while the electron temperature falls. Although the peak of recombination is likely to occur when the electron temperature reaches the gas temperature (Lewis, 1985) when the rate of further fall is considerably reduced but the electron density is still relatively high, for a short while before this significant recombination starts to appear. This is likely to have two effects on copper lower laser level decay rates. Following the generation of a growing number of copper atoms in highly excited levels, following recombination, a process of "recombination heating" of the plasma occurs as electrons undergo super-elastic collisions, thus reducing the rate of decrease of the electron temperature. Secondly, as this body of recently recombined atoms cascade through the copper energy levels they will increase the rate of feeding to the $4s^2\ ^2D$ levels, thus reducing the overall rate of population loss from these levels.

This explanation too suggests equilibrium with the ground state throughout the decay period.

In order to establish which of these mechanisms is primarily responsible for the observed phenomenon, consideration of the behaviour of the same populations measured close to the plasma tube wall (Chapter 9) may yield some clues. If the change in decay rates reflects the time taken to recover equilibrium following the discharge pulse then it may be expected that a higher electron temperature on axis (though not significantly higher total population in excited states owing to the gas temperature dependent ground state radial profile) would hasten the attainment of equilibrium and this decay rate change would therefore be observed later at radial positions near to the wall. If it is the collapse of the electron temperature radial profile that is responsible then the population densities nearer the wall would be expected not to show a steep decay followed by a more gentle one as on axis. Instead they would be expected to show a uniform rate of decay (equal to the final rate on axis) over the whole decay time period, or even an initial rate of decay marginally lower than that on axis, followed by reversion to the same rate, occurring at about the same transition time. Following the change of decay rate, at about 3.6 μs for all radial positions, the metastable population density radial profile should be concave, mirroring that of the ground state. If, however, it is the effect of recombination, and "recombination heating" that is responsible for the slow rate of population decrease later in the time course, then this should commence at approximately the same electron temperature, regardless of radial position and, as the peak electron temperature is likely to have been lower nearer the plasma tube wall, and the rate of cooling higher, owing to the larger gas number density, then the change in depopulation rate should occur earlier nearer the wall, with a higher decay rate both before and after it.

Another approach to determining which of the mechanisms discussed above is responsible for the observed change in decay rate is to consider the electron temperature implications. If the $4s^2\,{}^2D_{5/2,3/2}$ level populations are in equilibrium with the ground state throughout the decay period then, whatever the reason for the change in cooling rate, it would be expected that the $4^2P_{3/2,1/2}$ levels should be either at or above the equilibrium population determined by the value of electron temperature obtained from the distribution over states temperature of the metastable population. As the time constant for population

decay in the two upper laser levels over the 500 ns to 1 μs time period is about 330 ns, whereas that of the first stage of the $4s^2\,{}^2D_{5/2}$ decay is 1.68 μs over this period, it may be deduced that the populations in the former levels are above equilibrium. In fact the population calculated for the $4^2P_{3/2}$ level at the electron temperature obtained by assuming the $4s^2\,{}^2D_{5/2}$ level is in equilibrium at 600 ns (0.7 eV) is 2.5 times larger than that measured. It is also not in agreement with the hypothesis that the cause of the peak in $4s^2\,{}^2D_{5/2}$ level at 550 ns is because of the rapidly falling rate coefficient for direct excitation from the ground state for electron temperatures below 0.4 eV, a value which gives an equilibrium value for the $4^2P_{3/2}$ below that measured. We can therefore deduce that the lower laser levels are not at equilibrium before this time and it therefore seems likely that equilibrium is attained only at 3.6 μs. The value of electron temperature of 0.4 eV at 550 ns agrees well with an extrapolation of the second stage of the $4s^2\,{}^2D_{5/2}$ decay curve back to this time, again supporting this argument. A fuller discussion of electron temperature deductions from the results obtained, together with a predicted curve of electron temperature against time that agrees with all the observed facts, may be found in Section 7.6.

Owing to the considerable scatter in the $4s^2\,{}^2D_{3/2}$ measurements it is difficult to gain very much reliable information from them in addition to that obtained from the $4s^2\,{}^2D_{5/2}$ measurements. The most obvious point noted in their comparison is the difference in peak population density, 23 $\times 10^{12}$ cm^{-3} compared with 80 $\times 10^{12}$ cm^{-3} for the $4s^2\,{}^2D_{5/2}$ level, although it occurs at the same time. If these two levels were at Boltzmann equilibrium with each other at the electron temperature at the time of their peak population density, estimated to be about 0.4 eV above, then a ratio of population density of 2.8:1 would be expected owing to the difference in energy between them of 0.25 eV and their respective degeneracies. The ratio observed is 3.5:1, however this discrepancy is not surprising as the two levels are unlikely to be in thermal equilibrium with each other at this early stage of the CVL cycle as the rate coefficient for collisional exchange between them is unlikely to be high enough to maintain equilibrium on this time scale. In addition, the value of electron temperature estimated, from rate coefficient curves, as the point at which the $4s^2\,{}^2D_{5/2}$ population will peak, is unlikely to be of great accuracy. The electron temperature of 0.3 eV required to give the observed population ratio under

equilibrium conditions, however, is unlikely. The peak population ratio observed by Brown is 2.6:1.

7.4 POPULATIONS IN QUARTET LEVELS OF COPPER

7.4.1 INTRODUCTION

The only additional copper level to have been studied is the $4s(^3D)4p\ ^4F_{9/2}$ level. This had been chosen as being representative of the quartet levels, and typical of the relatively high lying excited levels not belonging to the main series in the copper term diagram to which both upper and lower laser levels are connected by reasonably strong transitions. Again the transition used to measure this population density is fairly weak ($f_{ij} = 0.109$), and the population density is low, and there is consequently a relatively high level of scatter in the data points.

7.4.2 PERIOD OF INCREASING POPULATION DENSITY IN $^4F_{9/2}$ LEVEL

Again it would be unwise to draw any major conclusions from the two kinks observed in the rising edge of the population density curve of Figure 7.14 without comparing them with similar measurements made at other radial positions. This having been done it would appear that the two kinks are merely artefacts as a result of noise in the data as they are not observed at other radial positions (Chapter 9). An observation of which there seems little doubt, however, is that whereas measurable population could be observed in both upper laser levels from around time -25 ns or so, there appears to be no observable population density in the $^4F_{9/2}$ level until after time 0 ns. This delay between the initiation of population increase between the upper laser levels and the $^4F_{9/2}$ level is observed at all radial positions. The other observation to be made about the rising edge of the $^4F_{9/2}$ population density is that it peaks at about 280 ns whereas the upper laser level populations peak at 100 ns. Taken together with the fact that the $^4F_{9/2}$ level lies at 5.07 eV above the ground state and that the electron temperature falls from a peak of very approximately 5 eV at 30 ns (the peak of the laser pulse) to 3.5 eV at 100 ns (when the laser pulse is finally extinguished when the net population rate of the upper laser levels equals that of the lower laser levels), and it becomes reasonable to assume that the majority of population flux into the $^4F_{9/2}$ level consists of stepwise excitation, probably via the upper and lower laser levels, rather than direct excitation

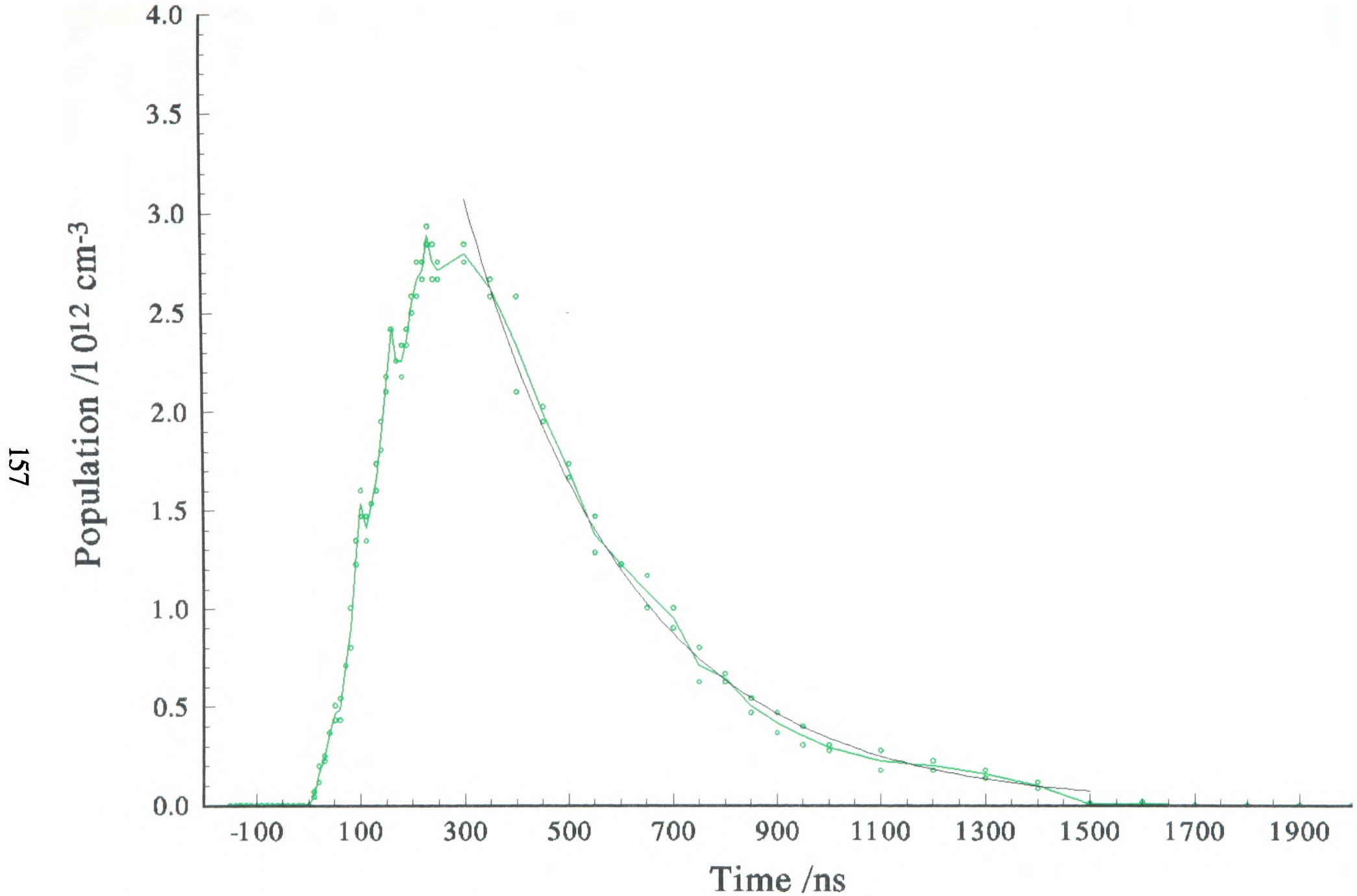

Figure 7.14 Population density on axis in copper $^4F_{9/2}$ level

from the ground state. As the population in the upper laser levels is around an order of magnitude smaller than that in the lower laser levels at 280 ns the observed behaviour is consistent with the explanation that this peak occurs when the electron temperature falls to about 1.5 eV as this is when the rate coefficient for the excitation process $4s^2\,{}^2D_{5/2}$ to the quartet levels ^4P, ^4D, ^4F reaches a knee as the second derivative reaches a maximum (Figure 7.5).

7.4.3 DECAY RATE OF THE $^4F_{9/2}$ LEVEL

Following its peak the population density decays as a single exponential with a time constant of 318 $\pm$7 ns. The fact that this figure is very similar to the time constants for the final decay rate of the $4^2P_{3/2,1/2}$ levels (measured as 336 and 321 ns respectively) suggests that in some way the decay of the ^4F level population might be linked to that of the 4^2P levels. Unfortunately the actual figures make a connection of this kind unlikely as the populations in the $^4F_{9/2}$ and $4^2P_{3/2}$ levels are almost equal despite a difference in energy between the levels of 1.26 eV. At an electron temperature of 0.4 to 0.5 eV this would correspond to an equilibrium population in the $^4F_{9/2}$ level of 10% - 20% of that in the $4^2P_{3/2}$ level.

Once again it is of interest to look at the comparison between Carman's calculated data and Brown's hook method measurements (Carman et al, 1993). Carman discovers that the calculated data, though displaying the same time behaviour as the measured values, are "consistently a factor of 2-3 lower" than the measured populations. As the calculations assume that the quartet levels are populated according to their degeneracies (in the absence of reliable collisional coupling data) one possible explanation is that this does not accurately represent the real situation and that the population in the $^4F_{9/2}$ level (the level measured by Brown) may represent a greater proportion of the total population in the quartet group than its degeneracy might suggest. This is supported by measurements by Smilanski (Smilanski, 1979).

7.5 POPULATIONS IN THE $2p^5$ 3s LEVELS OF NEON

7.5.1 INTRODUCTION

Hook method measurements were made of the population density in the neon $2p^5$ 3s $^3P_0$ level. There exists a very high degree of coupling between the four levels of

the neon ^1P, ^3P configuration by both heavy body collisional excitation transfer (Parks & Javan, 1965) and electron excitation transfer (Phelps, 1959) and consequently the population density per state in each level may be calculated by measurement of just one. As the level chosen has a degeneracy of 1, and the total number of states is 12, multiplication of the population densities obtained by 12 gives the total in the $2p^5$ 3s group of levels. This was confirmed in the CVL by Brown (Brown, 1988). In the absence of this collisional coupling both the 3^3P_0 and 3^3P_2 levels are metastable as direct transition to the 2^1S_0 ground state involves $J=0 \rightarrow J'=0$ or $\Delta J=2$, respectively.

The choice of length l used to convert the measured hook spacings to population densities is particularly difficult in the case of neon because, whereas the copper vapour is predominantly present only in the "hot" region of the plasma tube, neon is present for the full distance between the two electrodes. Excitation to neon levels above the ground state however is likely to be minimal within those regions where a significant density of copper vapour is present. This is the phenomenon considered in Carman's paper (Carman, 1993) and which he has modelled using Vriens' two electron group model (Vriens, 1973) to mimic the effect of the depletion of the high energy tail of the electron energy distribution function (above 16.7 eV, corresponding to the energy of the first inelastic loss process in neon, to the $2d^5$ 3s group) by the inelastic collisions with copper within the "hot" region of the plasma tube. The result he calculates is that the population density of neon excited states in the "cool" end regions of the plasma tube is typically about two orders of magnitude higher than in the "hot" region. In the laser at present under investigation the "cool" regions consist of two lengths of nominally 0.1 m length each (discussed in Section 3.3.6) while the "hot" region is of 1.3 m nominal length. The use of a value of l of 0.21 m was therefore chosen based on these assumptions to give a realistic value of neon excited state population density in the "cool" end regions of the laser.

7.5.2 OVERALL BEHAVIOUR

The results thus obtained for the neon $^3P_0$ population density on axis is plotted as a function of time in Figure 7.15.

The most obvious observation to be made is that the time profile consists of a primary peak, after which the population density falls back below a measurable level,

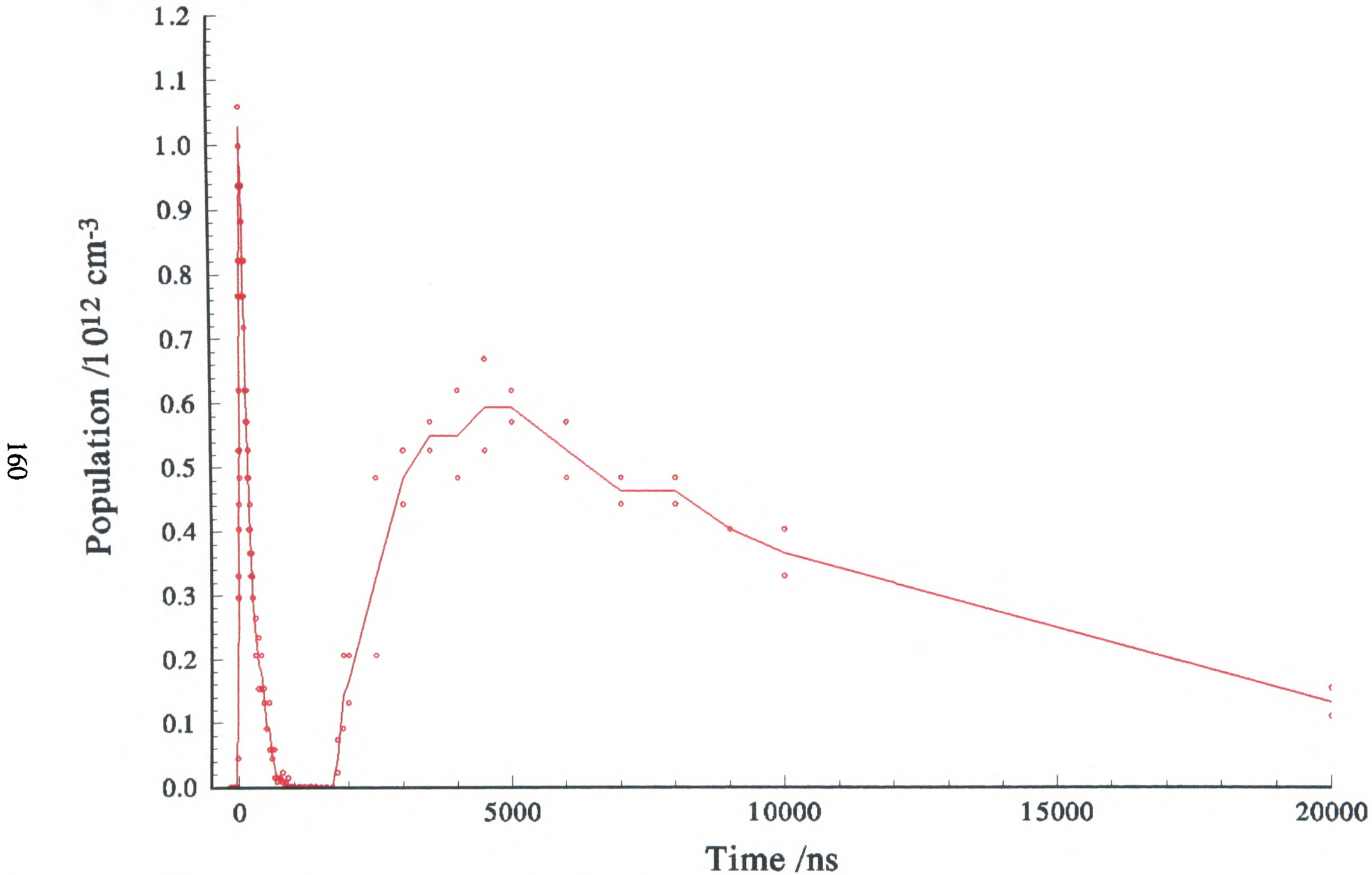

Figure 7.15 Population density on axis in neon $2p^5\ 3s\ {}^3P_0$ level

which is then followed by a second peak, about 5 μs later, of about half the amplitude of the first. This second peak comes about as a result of the onset of recombination as the electron temperature falls. Recombination leaves the neon atom in a highly excited state, from which it relaxes by super-elastic electron collisional, and radiative transitions back to the ground state. Owing to radiation trapping of the resonance radiation, and the consequent metastable nature of the neon $2p^5$ 3s group of levels, their position 16.7 eV above the ground state and the proximity of other, higher levels up to the first ionisation limit only 4.9 eV above, further excitation upwards to ionisation is highly favourable. Once ionised, recombination is minimal until the electron temperature has fallen considerably. As discussed above, the peak in the recombination population is expected to occur at about the time that the local electron temperature fall is arrested by the value of the gas temperature as, from this time, additional fall in temperature is very much slower, but electron/neon ion density fall will be subsequently fast.

7.5.3 THE FIRST PEAK OF NEON ^3P POPULATION DENSITY

What is seen from Figure 7.15 is a rapidly increasing population in the neon $2d^5$ 3s levels, starting at the same time as the directly excited copper levels, but reaching a peak of 1.03×10^{12} cm^{-3} at 80 ns, about 20 ns before the upper laser levels. As mentioned above the remoteness of the neon $2d^5$ 3s levels from the ground state (16.7 eV) and the proximity of higher lying levels and the ionisation limit (4.9 eV above) mean that, while the rate of direct excitation from the ground state is highly electron temperature dependent, further excitation is considerably less so. The falling electron temperature from its peak at around 30 ns (the peak of the laser pulse) thus rapidly reaches the point at which the rate of loss from the $2d^5$ 3s levels via continued upwards excitation becomes greater than that of feeding the population, and it reaches a peak.

If an attempt is made to fit an exponential to the decay of the first peak of the $^3P_0$ population density (Figure 7.16) it is found that what is observed is a decay from 80 ns to 250 ns with a time constant of 133 ns, followed by a period of very much reduced decay rate for 200 ns, before continued decay with a time constant of 132 ns from 450 ns until 800 ns. If the discharge current trace is considered in conjunction with this plot then it is noticed that the large negative current lobe is observed to coincide with the 200 ns interruption to the otherwise monotonic decrease in population from the $^3P_0$ level.

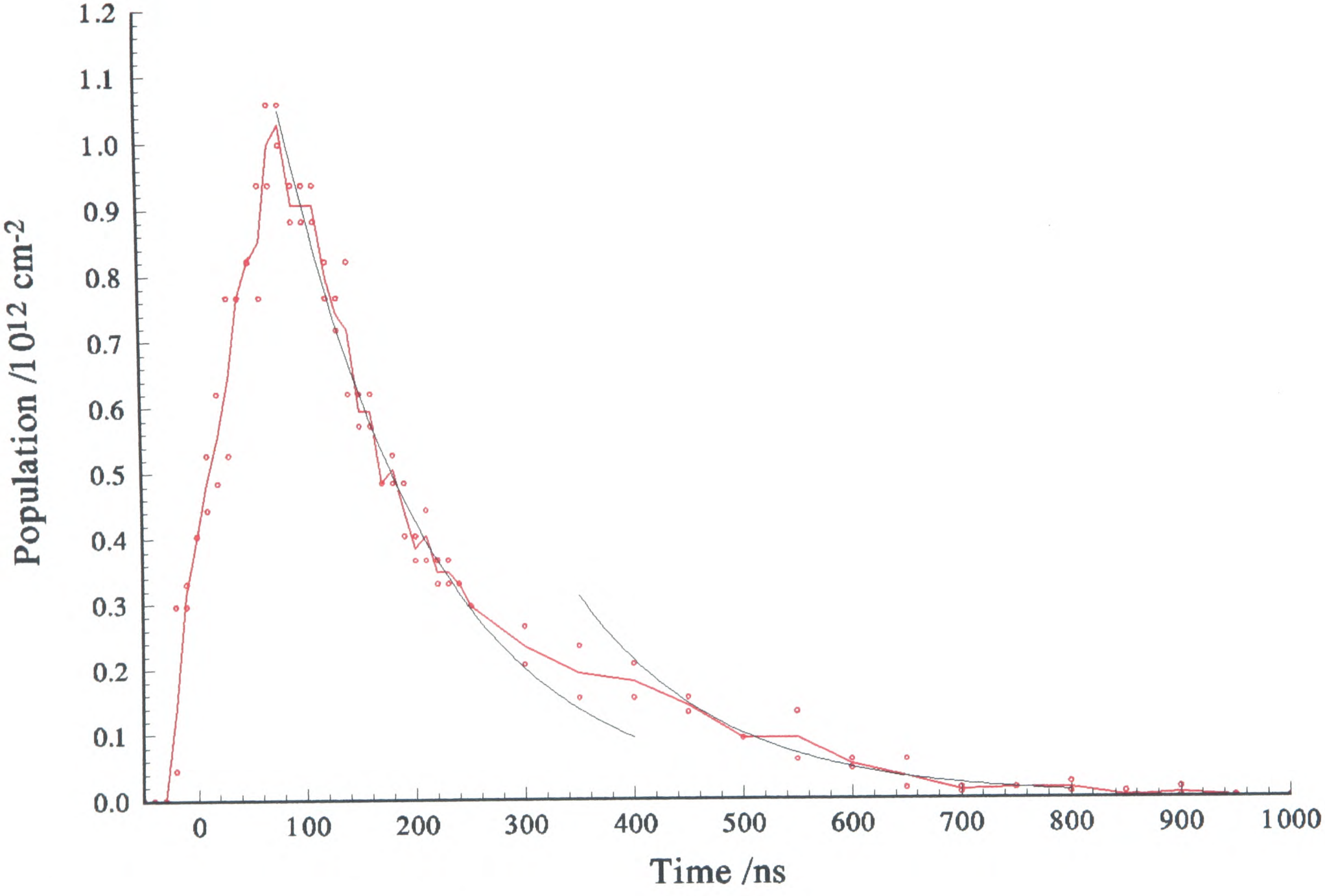

Figure 7.16 Population density on axis in neon $2p^5\ 3s\ ^3P_0$ level; first peak with two stage exponential fit

This negative current lobe came about as a result of a substantial voltage reversal on the CVL electrodes during the ringing, though delayed because of the reactance of the coaxial laser head structure. With the voltage reversed the electron drift velocity, and thus current, is also reversed, however acceleration in the E field still occurs and a consequential increase, or temporary retardation of decrease, in electron temperature results. It would appear therefore that this temporary support of falling electron temperature shows itself as a temporary halt in the decline of population in the neon $^3P_0$ level.

7.5.4 THE RECOMBINATION PEAK

Following this decline the population in the $^3P_0$ level remains below measurable levels for nearly a microsecond before rising again from 1.7 μs to a second peak of 0.6 $\times 10^{12}$ cm^{-3} at 4.6 μs as recombined neon ion/electron pairs fall rapidly from highly excited levels back to the $2d^5$ 3s levels as discussed above. In Figure 7.17 decay of population density from this peak can be seen to follow a curve that may be approximately fitted by a single exponential with a time constant of 11 ± 1 μs from 5 μs until at least 10 μs. There are insufficient data points to attempt to extend this until population is last measurable at 30 μs. The expected form of this curve is not a pure exponential as it will represent the difference between the rate of increase in population as a result of recombination (for which the rate is given by Carman (Carman et al, 1993)

as $$\frac{dn_e}{dt} = -4.0\times10^{-19} n_e^2 N_i T_e^{-5}$$ where n_e is the electron density, N_i is

the ion density and T_e is the electron temperature and from which an expression for electron density (assumed equal to ion density) as a function of time is obtained in Chapter 8 as Equation 8.2) and the rate of decrease of population which is likely to have the form of an exponential decay. The choice of an exponential curve to fit it was thus made purely on the basis that it allowed a reasonable empirical description of the curve and yielded a decay time constant by which it could be compared to other curves, however its use will be further justified in Section 9.6.3.

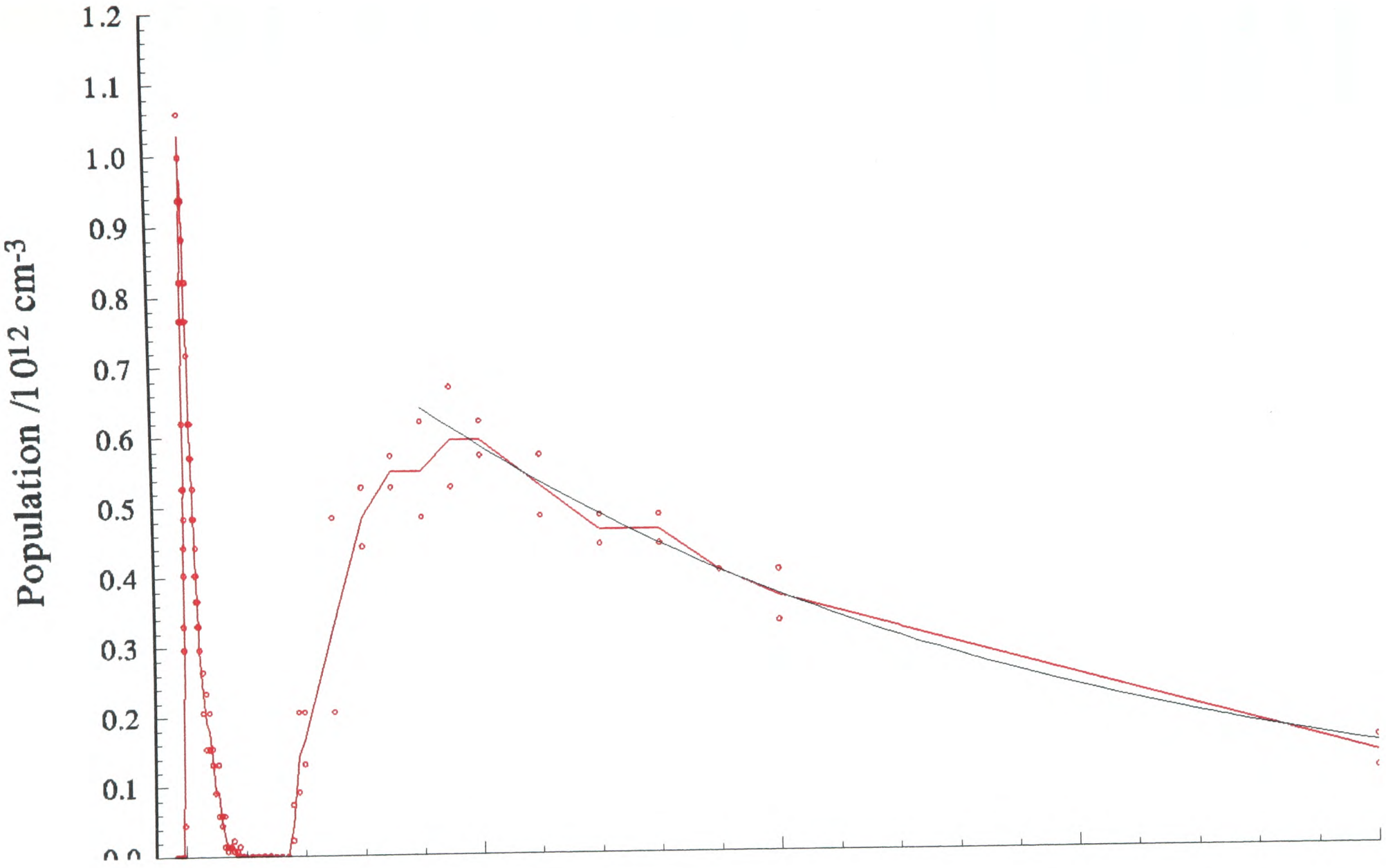

Figure 7.17 Population density on axis in neon $2p^5\ 3s\ {}^3P_0$ level; exponential fit to decay of recombination peak

7.5.5 THE LOCATION OF THE OBSERVED NEON

As the neon observed in these measurements is predominantly that in the "cool" end regions of the plasma tube the timing of the peak of recombination population cannot be used to infer the time that the electron temperature in the "hot", copper bearing, region of the plasma tube falls to that of the gas. In order that both the degree and rate of ionisation in the "cool" end zones match that in the "hot" central region to preserve continuity of current the electron temperature in the end regions must be considerably higher than that in the central region owing to the much higher ionisation energy of neon than copper. As the gas temperature in this region is lower than that in the main body of the plasma tube, and the particle density therefore higher, the electric field within the end regions may be expected to be relatively higher still. This lower gas temperature, and higher particle density, however, are likely to lead to more rapid falling of the electron temperature.

7.5.6 DE-EXCITATION OF NEON METASTABLE POPULATION

Owing to the high energy of the neon $2d^5$ 3s levels in those regions of the plasma tube where significant population densities of both neon $2d^5$ 3s and copper vapour exists Penning ionisation of the latter by collision with the former represents a significant de-excitation mechanism for these levels. Carman (Carman et al, 1993) uses an expression for the Ne^*-Cu Penning ionisation rate based on Riseberg's measurements on zinc and cadmium (Riseberg et al, 1973) of $1.49 \times 10^{-17} T_g^{1/2}$ $m^3 s^{-1}$. In order to give the observed rate of loss of neon $2d^5$ 3s population a copper population density of about 10^{14} cm^{-3} would be required. This corresponds to about one quarter of the copper population density on axis in the "hot" region of the plasma tube. In addition to this, however, the radiative transition probability of the 3^1P_1 level to the neon ground state is $A_{ji} = 6.64 \times 10^8$ s^{-1} (Weise et al, 1966), and from the 3^3P_1 level of 0.476×10^8 s^{-1}, although these transitions are highly optically trapped and so the probability for the 3^1P_1 transition is reduced to about 10^3 s^{-1} (Phelps, 1959) under the conditions found in the CVL.

7.6 ELECTRON TEMPERATURE DEDUCTIONS

Although it has not been possible to measure electron temperature directly as part of this study, a number of clues as to its value at a number of time points have emerged from the behaviour of some of the population densities. As electron temperature is probably the most important parameter in determining the kinetics of the plasma at any given time it is instructive to attempt to piece together the deductions made to give as good a picture as possible, and to ensure that they are all self-consistent. Accordingly Figure 7.18 has been drawn up showing the estimated temporal profile of the electron temperature on axis over the first 10 μs.

The first data point is at -120 ns, before the current pulse starts to rise, when the electron temperature is close to the pre-pulse axial gas temperature at 2500 K, or 0.215 eV. At 0 ns laser emission starts indicating that the electron temperature has risen to 3.5 eV, peaking, with the current, at 30 ns at a value that can be estimated as very approximately 5 eV. Laser emission ceases at 100 ns suggesting that the electron temperature has fallen back to 3.5 eV.

Using information from the rate coefficient curves of Figure 7.5 the following deductions can be made. At 280 ns the $^4F_{9/2}$ population peaks, corresponding to an electron temperature of 1.5 eV at which there is a knee in the excitation rate from the $4s^2$ $^2D_{5/2}$ level. At 300 ns the rate of increase in population in the $4s^2$ $^2D_{5/2}$ level decreases, suggesting that the electron temperature is about 1 eV, corresponding to the rate coefficient for direct excitation from the ground state falling off rapidly. At 550 ns the population in the $4s^2$ $^2D_{5/2}$ levels peaks suggesting that the electron temperature has now fallen to about 0.4 eV at which point direct excitation from the ground state enters its fastest rate of fall.

From this point two curves are plotted, the solid one representing a fit to the final rate of decrease in the $4s^2$ $^2D_{5/2}$ level (time constant 3.1 μs), extrapolated back to 550 ns at which point it will be seen to meet the previous data point. The broken line represents the values obtained assuming that this level is in equilibrium with the ground state during the first decay period too, a possibility discussed, but rejected, in Section 7.3.4 above.

From about 10 μs it is to be expected that the electron temperature has fallen to the value of the gas temperature, at which point further fall is arrested. The final point of this curve gives a value of 0.214 eV, or 2,484 K, which agrees well with this. If it

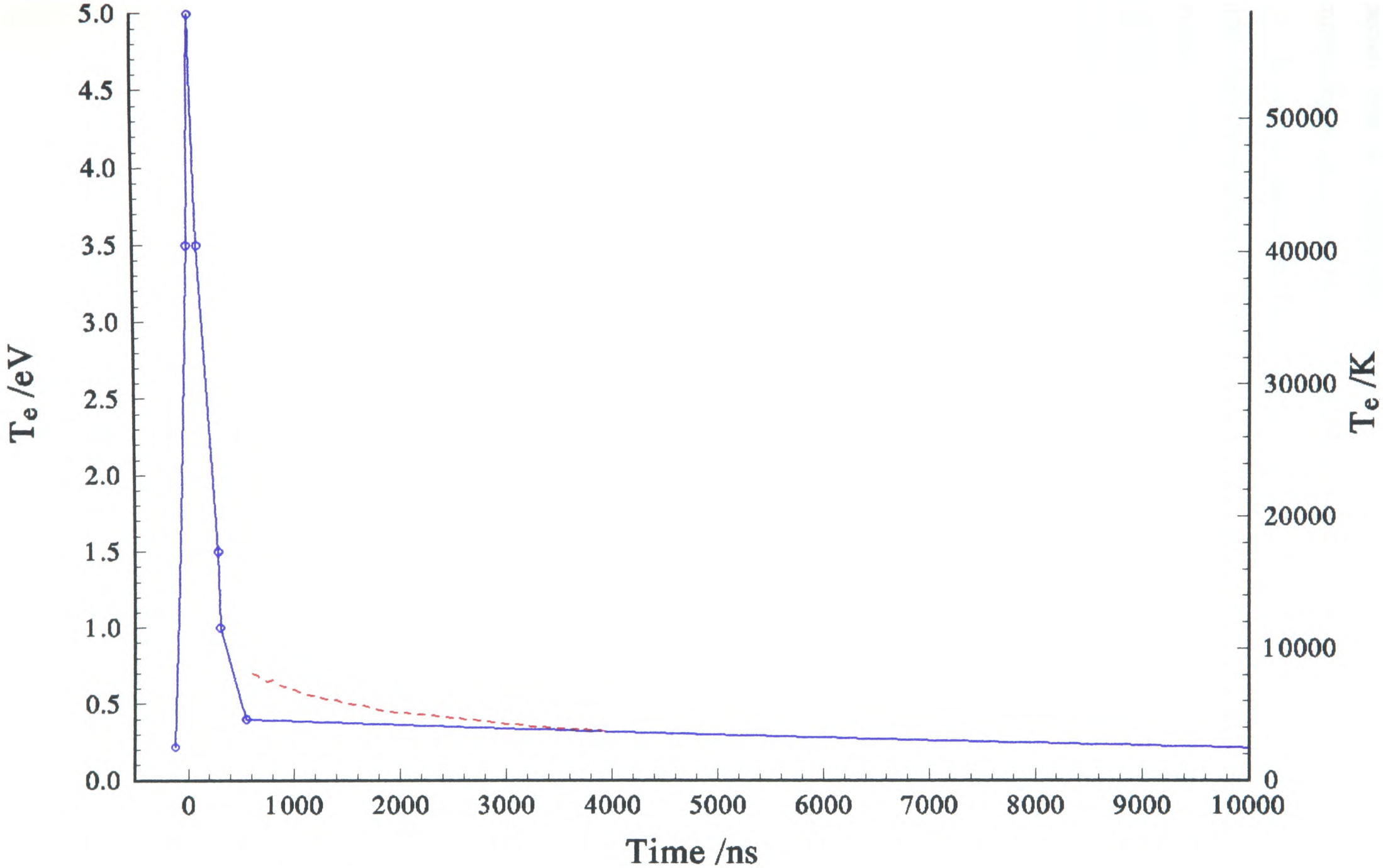

Figure 7.18 Speculative plot of electron temperature on axis; first 10 μs

had been possible to follow the decrease in population in the lower laser levels over the full course of the interpulse period, by means of absorption measurements, it is to be expected that a considerably slower rate of decay would have been observed, commencing at about this time, corresponding to the small fall in gas temperature.

It can be seen that this proposed time course for the electron temperature is entirely self-consistent and, although conjectural and fairly approximate in a few details, provides a framework with which to compare not only the observed behaviour of the measured population densities, but also the results of a computer model that fits the observed results.

8 ELECTRON DENSITY MEASUREMENTS

8.1 ELECTRON DENSITY ON AXIS

8.1.1 INTRODUCTION

Plots of measured electron density as a function of time over both the early excitation phase of the laser cycle and the full time-course of the cycle may be seen in Figures 8.1 and 8.2. It may be observed that the peak electron density measured in these two plots differ by a small amount (4%). The reason for this is that the plots consist of different measurements made consecutively with a different time base selected on the digital oscilloscope to exploit optimal digitising rate, and thus temporal resolution, for each. As described in Chapter 4 these measurements were made with the interferometer set up to give a starting point at a fringe minimum. This means that the starting point may be set up relatively reproducibly, independent of any overall change in absolute intensity of the source laser, however, owing to the nature of the cosine function employed in the data reduction, it is possible for a very slight fringe shift to be introduced between measurements as a result of slight air movement in the interferometer compensation arm and to pass unnoticed, while causing a disproportionate change in total measured electron density. Notwithstanding this minor difference in absolute amplitude, however, comparison of the rising edge of the two curves shows them to be of identical form within the resolution of the oscilloscope sampling rates.

8.1.2 THE PRE-PULSE ELECTRON DENSITY

From Figure 8.2 the first point to note is the high pre-pulse electron density of 39×10^{12} cm^{-3}. This represents 9% of the total copper population density and means that at the onset of the discharge pulse the plasma is already highly conducting. If this value is compared with the maximum electron density attained of 131×10^{12} cm^{-3} it will be seen that the electron density only increases by a factor of about three during the discharge. These observations are entirely consistent with the interpretation given to the relative timing and forms of the voltage, current and laser pulses discussed in Chapter 5. Further in support of the deductions made in that discussion is the fact that there is no observed rise in electron density before time 0 ns.

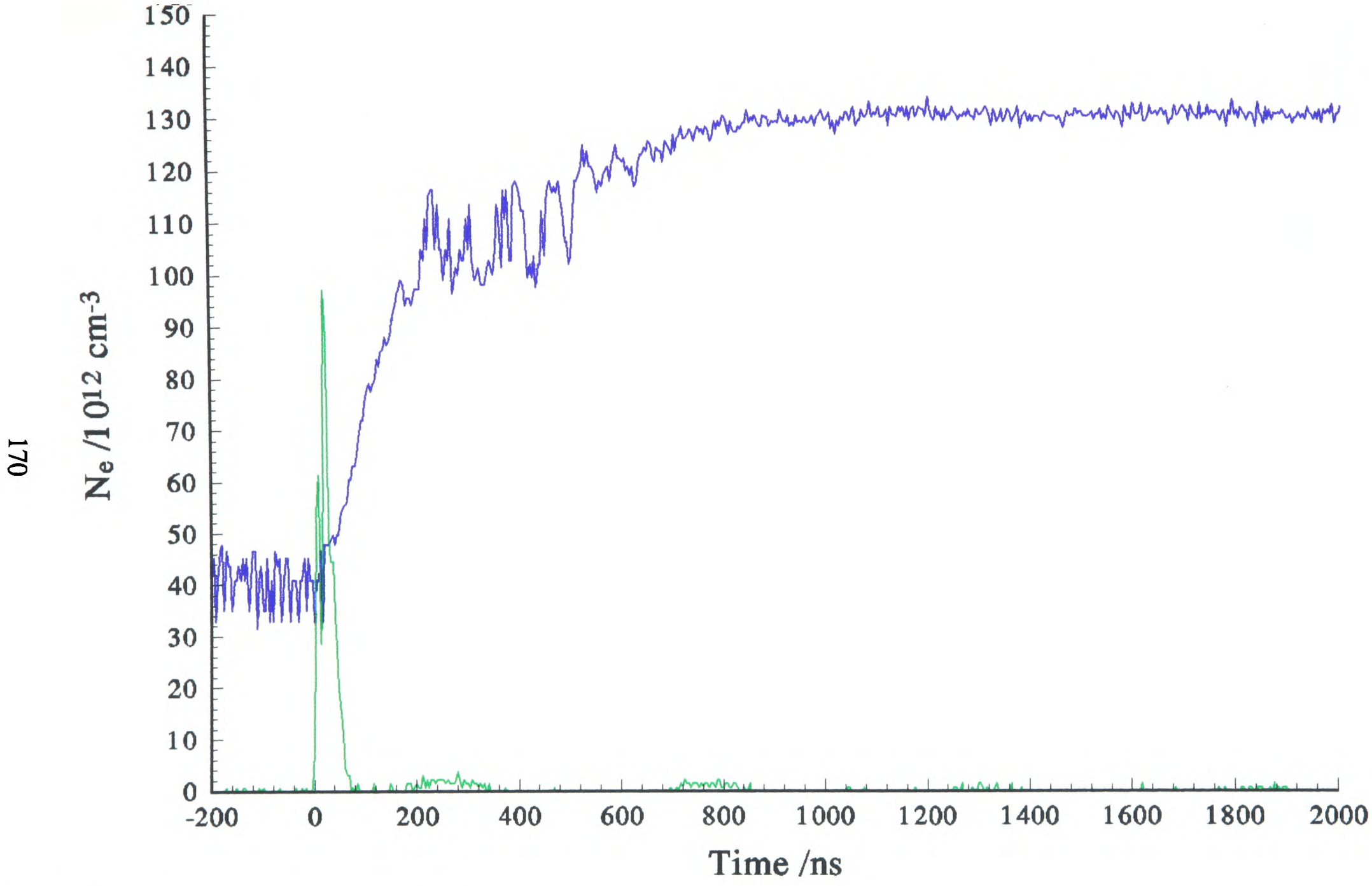

Figure 8.1 Electron density on axis; first 2 μs

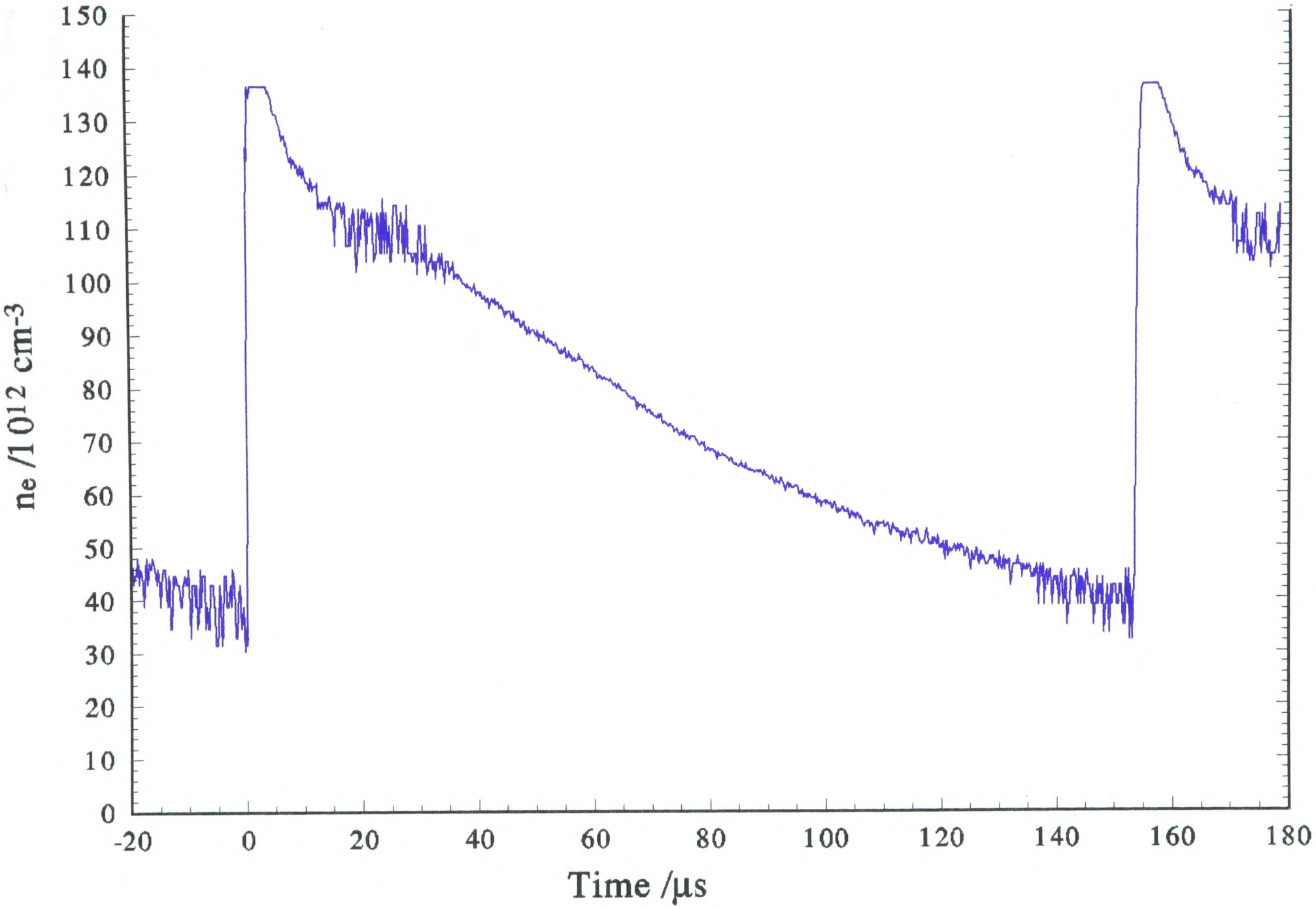

Figure 8.2 Electron density on axis; full interpulse period

8.1.3 THE SOURCES OF ELECTRONS

The length over which the electron density has been calculated is the full 1.5 m between the electrodes. Because of the effect of depletion of the high energy tail of the electron energy distribution function (EEDF) by the inelastic collisions with copper atoms below 16.7 eV (the first excitation energy of neon) excitation of neon within the "hot" region of the plasma tube, in which there is a significant partial pressure of copper vapour, is very much lower than would be predicted by the temperature of the bulk of the electrons (the value referred to throughout this thesis simply as "electron temperature"). It was in order to model this that Vriens (Vriens, 1974) and then Carman (Carman et al, 1993) employed a two electron group model in which there was an energy distribution for those electrons below the first significant inelastic loss process in the neon (16.7 eV) approximately described by a Maxwellian with a temperature T_b, the "bulk temperature", with those with energies above this described by a second Maxwellian characterised by a temperature T_t the "tail temperature", lower than T_b. As a result Carman found that the neon excited state densities within the "hot" region of the plasma tube were around two orders of magnitude lower than those of the copper, and thus the electron density in this region was equal to the copper ion density.

In the "cool" end regions of the plasma tube, however, the copper density is negligible and all electrons must be obtained from the ionisation of neon.

8.1.4 THE PERIOD OF INCREASING ELECTRON DENSITY: 0 μs to 1 μs

Before time 0 ns there is no observable increase in electron density, within the limitations of the noise level. There then follows a period of slow increase for 30 ns, up to a value of 45 $\times 10^{12}$ cm^{-3}, after which point there follows a period of much faster rise from 30 ns to 140 ns during which the electron density nearly doubles to a value of 85 $\times 10^{12}$ cm^{-3}. After this it continues to rise slowly to 125 $\times 10^{12}$ cm^{-3} at 800 ns before the entering a final stage of very slow increase to a peak of 131 $\times 10^{12}$ cm^{-3} at about 1000 ns. The behaviour of the measured electron density suggests that until the electron temperature reaches a value of about 3.5 eV at 0 ns (calculated as the value at which the rate of population of the lower laser levels is exceeded by that of the upper levels, and thus gain begins) there would appear to be very little direct excitation from the copper ground state to the ion. Ionisation of the copper commences as the energy of the existing

electrons increases in the increasing electric field up to a peak value that may be estimated as about 5 eV at 30 ns (the peak of the laser and current pulses). The importance of stepwise ionisation may be seen from the fact that, although from this time onwards the electron temperature is falling, the electron density now enters its fastest rate of rise as the population densities in the various excited levels rise rapidly, continuing until just after the peak of the upper laser level populations. It seems likely that it is this rapid increase in electron density from 30 ns that brings about the simultaneous rapid fall in electron temperature. The third stage of population increase then starts, at a slower rate, while the populations in the two lower laser levels continue to increase, continuing until shortly after they peak. The rate of increase then falls again, with very little additional increase in electron density, up to its peak at about 1000 ns.

8.1.5 THE PERIOD OF STABLE ELECTRON DENSITY: 1 μs to 4 μs

Before discussing the behaviour of the electron density following its peak as plotted in Figure 8.2 it is necessary to consider the effects of a phenomenon observed in making these measurements. In Chapter 4 the problem of the slight frequency dependence of the gain of the HgCdTe detectors for the 10.6 μ probe beam was discussed and the technique required to circumvent this in the data reduction. The result of this is that the flat region at the peak of the electron density consists not of measured data, but of a line to join two regions of "good" data. The apparently abrupt commencement of decrease in electron density at 4 μs therefore occurs as a result of this artefact. While the T_e^{-5} dependence of three body recombination precludes any significant recombination of Cu^+ until the electron temperature has fallen to a few tenths of an eV, it is possible that there is a small population of Cu^{++} for which recombination may occur at higher temperatures, an effect that cannot be explored until either the frequency response of the HgCdTe detectors has been determined, or further experiments performed under different operating conditions. Such conditions might consist of considerably lower beam intensity if the problem is detector slew rate related, once a suitable amplifier can be obtained, or by multiple repetitions of the fringe measurements starting from different values of initial phase.

8.1.6 THE INITIAL RATE OF DECAY OF ELECTRON DENSITY: 4 μs to 25 μs

In addition to Cu^{++} recombination however it has been seen that measurable recombination population is observed on axis in the neon population density measurements from as early as 1.7 μs, peaking at 5 μs, although this is predominantly confined to the "cool" end regions of the plasma tube that are relatively short. It might be expected therefore that the impact of neon recombination on the measured electron density would be small, as, averaged over the total plasma tube length, the 3^3P_0 level population density peaks at only 0.08 $\times 10^{12}$ cm^{-3}. This however corresponds to a total population density in the whole $2p^5$ 3s group of levels peaking at 1 $\times 10^{12}$ cm^{-3} if they are all in equilibrium with each other and populated according to their degeneracies (discussed in Section 7.5.1). At the pressure of neon encountered in the CVL (25 mbar) the neon resonance transitions experience a very high level of radiation trapping, reducing the transition rate for the transition from the 3^1P_1 level from A_{ji} = 6.64 $\times 10^8$ s^{-1} to about 10^3 s^{-1} (Phelps, 1959). In comparison to this the collisional coupling between the four levels allows them to be treated as a block and consequently a peak radiative flux of about 10^9 μs^{-1} may be calculated. The proportional decrease in electron density over the period 4 μs to 20 μs is 19% and is not inconsistent with the recombination of the majority of the electrons in the end regions of the plasma tube (14% of the total length) if it were substantially accomplished over this time period (together with a small proportion of those in the central region).

In Figure 8.3 an attempt has been made to fit the two stages of the electron density decay curves. Carman's expression for three particle recombination rate coefficient for T_e below 3100 K is:

$$\frac{dn_e}{dt} = -4.0\times10^{-19} n_e^2 N_i T_e^{-5} \qquad \textbf{(8.1)}$$

If it is assumed that $n_e = N_i$ and that the electron temperature cools from an initial value of T_0 K in a linear fashion at a rate a Ks^{-1} (ie $T_e = T_0 - at$), then it possible to integrate Equation 8.1 to obtain an expression for n_e as a function of time:

$$n_e = n_0 - \sqrt{5}\, a^{3/2} 10^9 (2T_0 t - a t^2) \qquad \textbf{(8.2)}$$

in which n_0 is the initial electron density.

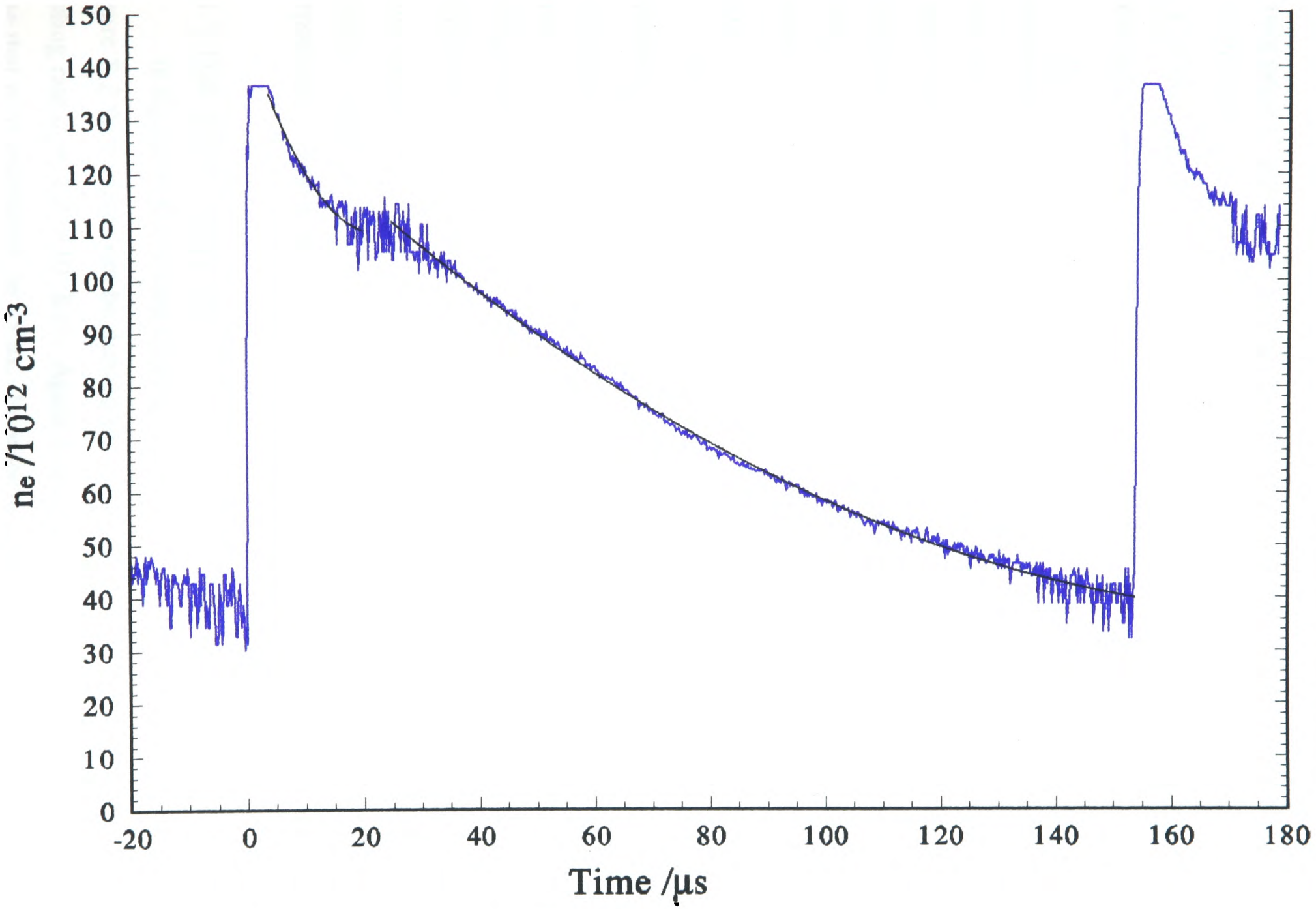

Figure 8.3 Electron density on axis; two stage fit

If the initial fast rate of decrease in measured electron density is taken in isolation from the rest of the curve, subtracting that corresponding to the copper ions in the central region of the tube, by assuming negligible electron density in the "cool" end regions at 25 μs (when negligible neon 3^3P_0 population remains), and appropriate correction being made for the proportion of the length in which it is assumed that high neon excited state density occurs, then values for the parameters may be obtained of: $n_0 = 181 \times 10^{12}$ cm^{-3}, $T_0 = 2679$ K, and the rate of cooling: $a = 14.8 \times 10^7$ Ks^{-1} (or 148 K per μs). The value of T_0 is that relating to n_0, ie 4 μs, as before this it is likely that T_e is much higher and more rapidly falling.

It must be remembered that these calculations are performed subject to a number of assumptions and may only be taken to illustrate the behaviour of this first part of the decay curve. It has been implicitly assumed that there is negligible recombination of the copper ions during the first 25 μs, an assumption that may or may not be true. The partitioning of the plasma tube into two, rigidly delineated regions, each behaving homogeneously, is also an inaccurate model, although it helps in the interpretation of the observed phenomena. The calculated value of a appears to be about a factor of 10 higher than is realistic.

If alternatively an exponential decay function is fitted to the curve relative to the population at 25 μs, a fit can be obtained with a time constant of 9 μs. While the value of this calculated time constant is very dependent upon the figure estimated as the final value of this stage of decay, it may readily be seen that it is similar to the decay time constant of the neon 3^3P_0 population density (11 μs) over the period 5 μs to 20 μs. Whilst there is no reason for this decay to display an exponential behaviour, its form being expected to be that described in Equation 8.2 above, this has been performed simply in order to obtain a value for a time constant to characterise the decay for purposes of comparison with that of the neon 3^3P_0 recombination peak (Section 7.5.4).

8.1.7 THE FINAL RATE OF DECAY OF ELECTRON DENSITY: 25 μs to 154 μs

If Equation 8.2 is used to obtain a fit to the second section of the decay curve of Figure 8.2 then values can be derived of: $n_0 = 128 \times 10^{12}$ cm^{-3}, $T_0 = 2998$ K, and the cooling rate $a = 1.8 \times 10^7$ Ks^{-1}. Again T_0 is the value of the electron temperature at the time that n_0 is calculated, ie 25 μs. In order to get these values it was assumed that the

observed electron population was no longer distributed over a length of 1.5 m (the full length between the electrodes, but only over the "hot" central region of the plasma tube of 1.3 m. Again the computed value of a is a factor of 10 larger than is realistic.

There is no reason why the electron density on axis in the "cool" end regions, originating from the neon, should be the same as that in the "hot" middle section of the plasma tube. Although the total electron population across the whole cross sectional area of the plasma tube must be equal at all longitudinal positions during the discharge pulse to allow continuity of current flow, the radial profiles need not be the same. In Chapter 9 it will be proposed, and evidence provided in support of the hypothesis, that the electron density during the discharge and in the early stages of the afterglow is more strongly peaked on axis in the end regions than in the central region of the plasma tube. This is observed too from the calculations above in which the peak value of electron density of 136 $\times 10^{12}$ cm^{-3} is composed of a central region of 1.3 m length in which there is a predominantly copper ion density of 128 $\times 10^{12}$ cm^{-3} on axis, and two end regions of 0.1 m length each containing a density of neon ions of 181 $\times 10^{12}$ cm^{-3}, on the axis. These numbers, however, are given subject to the cautions above.

It is reasonable to deduce from the behaviour observed above that despite the higher peak value of electron temperature in the "cool" end regions of the plasma tube it falls rapidly to a lower gas temperature and recombination of neon ions is substantially completed within about 25 μs. Even once the electron temperature in the "hot" central region of the plasma tube has fallen to the gas temperature the high value of the latter and the T_e^{-5} recombination rate dependence still limits recombination of the copper ions and decrease in electron density from 25 μs onwards is very much slower.

8.2 ELECTRON DENSITY AS A FUNCTION OF RADIAL POSITION

8.2.1 RADIAL PROFILE OF PRE-PULSE ELECTRON DENSITY

In Figure 8.4 can be seen the radial profile of the measured pre-pulse electron density. As this principally reflects the value in the "hot" central region of the plasma tube where the electrons are predominantly derived from the ionisation of copper it is not surprising to observe that for about 14 mm on either side of the axis the electron density radial profile is relatively flat, falling by only about 30% over this distance. Beyond this, however, the value of n_e falls rapidly towards the walls. As the pre-pulse copper atom

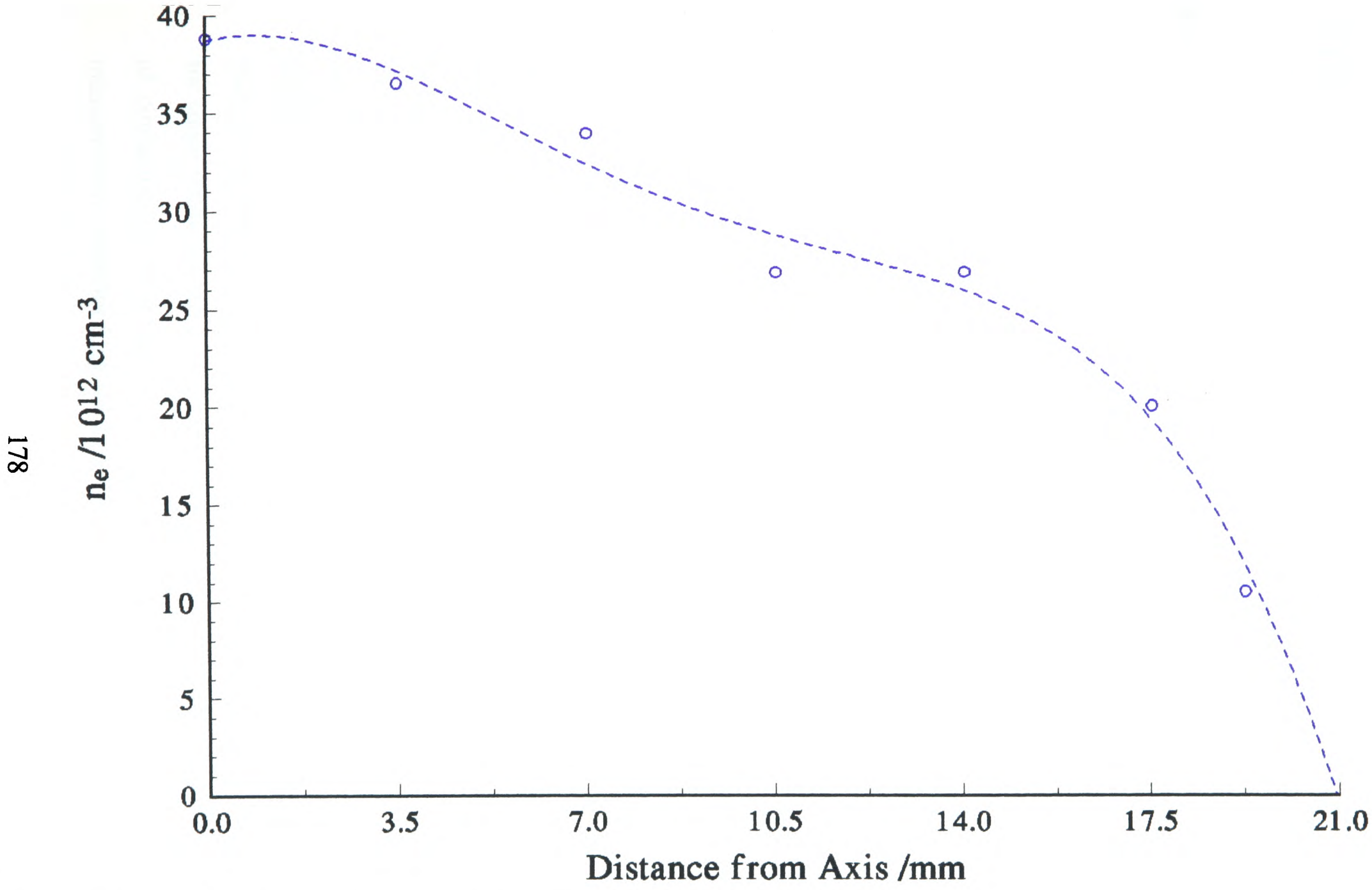

Figure 8.4 Pre-pulse electron density; radial profile

ground state density radial profile displays a minimum on axis as a result of the gas temperature radial profile (Figure 9.10) this means that the percentage of the copper that remains ionised falls rapidly with increasing radial distance from the peak value of 9% on axis.

8.2.2 THE PERIOD OF INCREASING ELECTRON DENSITY: 0 μs to 1 μs:

In Figure 8.5 the measured rising electron density during the discharge pulse has been plotted for all seven radial positions at which it was measured and a number of observations may be made:

Firstly, the beginning of the rise in electron density appears to occur either marginally earlier on axis or at approximately the same time (within the accuracy imposed by the level of noise) at all radial positions.

Secondly, the significance of the period of extremely fast increase in electron density (approximately 30 - 140 ns) appears to decrease away from the axis. Out to about 7 mm it can clearly be discerned, however beyond this the rise seems to be more gentle.

Thirdly, the period of increase in electron density appears to continue longer close to the axis than at radial positions nearer to the plasma tube wall.

Fourthly, the radial profile of n_e at the time corresponding to the peak n_e value is very much more curved than that of the pre-pulse values. It must however be remembered that a small proportion of the measured electron density is due to the ionised neon in the "cool" end regions of the plasma tube and it has been proposed in the previous section that the radial profile in these regions is more highly peaked on axis. What is observed in both the radial profile of the pre-pulse electron density, and in these time course measurements is that the electron density at 10.5 mm is lower than might be expected relative to the neighbouring measurements. Without repeating the measurements it would be difficult to be sure whether this is an artefact or a genuine effect. It is possible that, as the measurements at this radial position are less than a half fringe shift, for some reason an inaccurate calibration value was obtained, perhaps as a result of contamination of a laser tube end window between making the calibration measurement and performing the experiment.

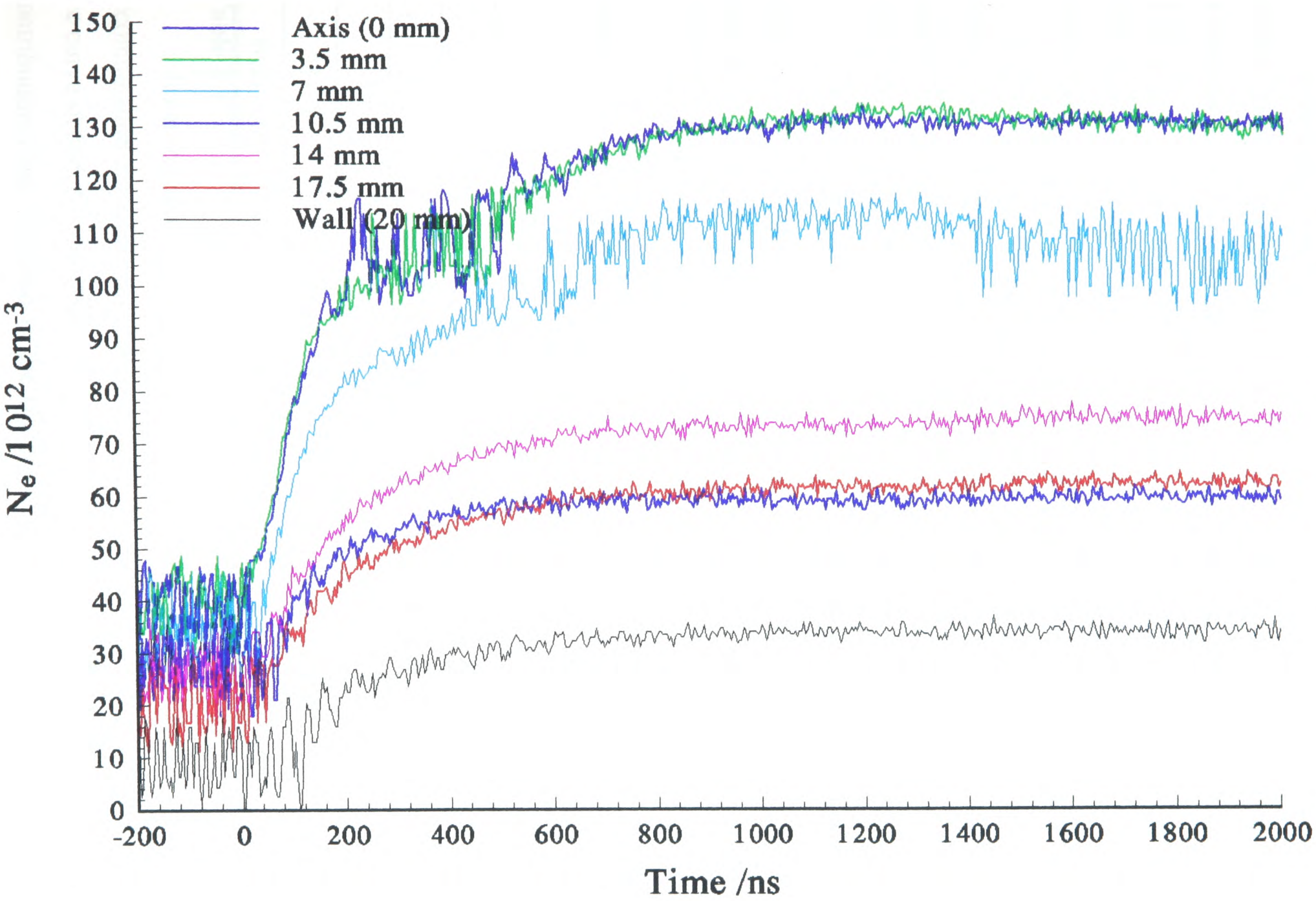

Figure 8.5 Electron density at seven radial positions; first 2 μs

The significance of these observations will be discussed in connection with the measurements of the radial profiles of population densities presented in Chapter 9.

8.2.3 THE DECAY OF ELECTRON DENSITY: 4 μs to 154 μs

In looking at the electron density decay curves (Figure 8.6) it can be seen that the period of rapid decay during the early part of the process is only observed in the two sets of measurements closest to the plasma tube axis. This agrees entirely with the hypothesis of Section 8.1.6 that this period represents the much more rapid recombination of the neon ions in the end regions of the plasma tube where it is thought that the gas temperature, although rising to a higher peak value on axis, falls more rapidly too. It is thought that the decreasing relative importance of this component away from the plasma tube axis reflects the more highly peaked electron density in the neon-only end regions. It can be seen that if this neon ion component of measured electron density is subtracted the radial profile of the electron density is still relatively strongly curved.

If the decay curves of Figure 8.6 are all fitted in the same way as was described above then approximate values of initial temperature at the onset of recombination, and average cooling rate may be derived (Table 8.1).

Radial Position /mm	Recombination start time /μs	n_0 /10^{12} cm^{-3}	T_0 /K	a /10^6 Ks^{-1}
Axis (0)	25	128	2998	18.3
3.5	25	125	2956	18.4
7.0	25	109	2780	17.2
10.5	20	61	2003	11.9
14	10	74	2468	11.4
17.5	5	61	2495	10.1
Wall (20)	2	32	1835	14.5

Table 8.1

It can be seen from Figure 8.6 and Table 8.1 that the time at which significant recombination commences varies with radial position, being a maximum on axis. From the curve obtained 7 mm from the axis, the first in which there appears to be negligible contribution from the neon in the end regions, it can be seen that the assumption of

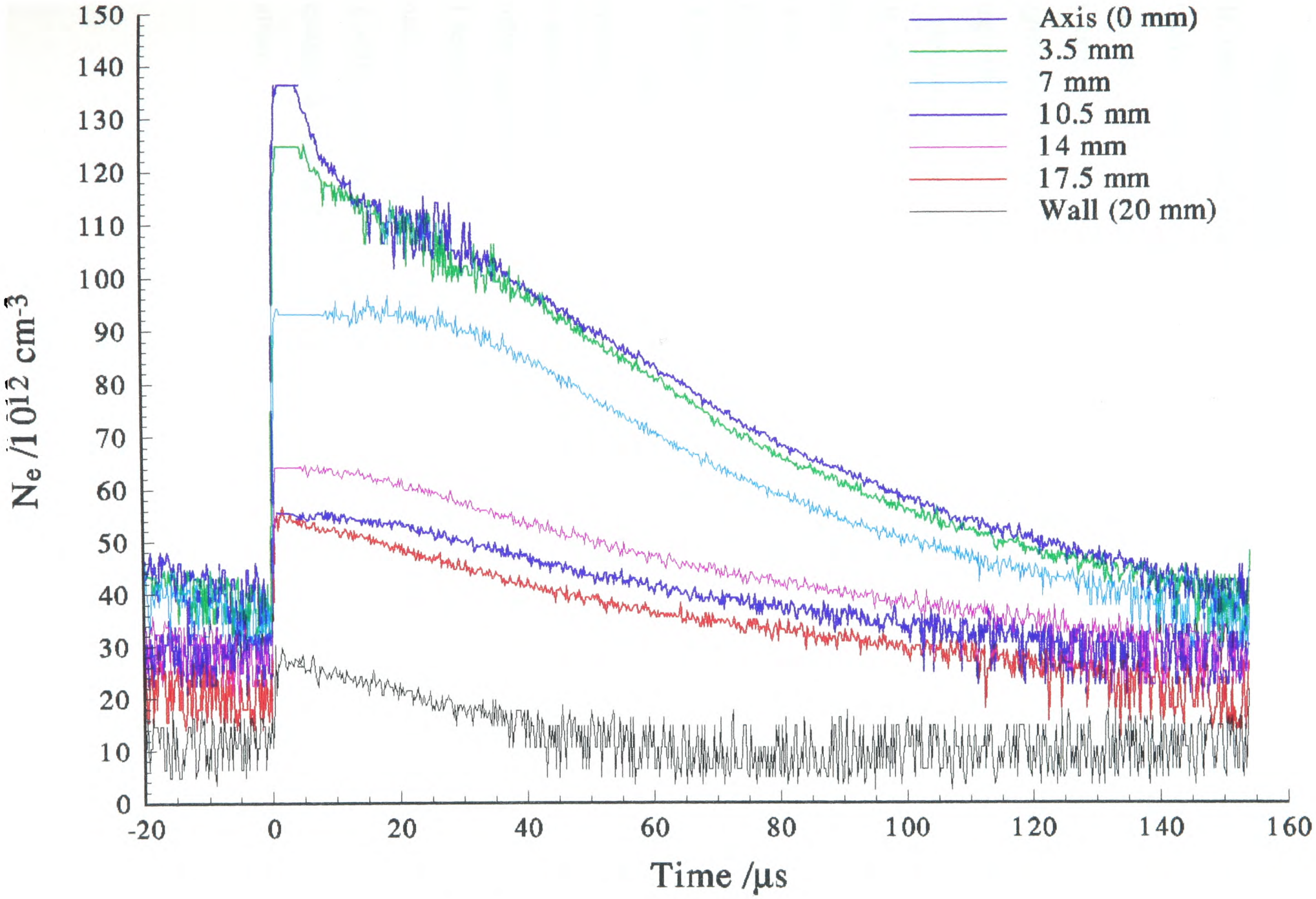

Figure 8.6 Electron density at seven radial positions; full interpulse period

Section 8.1.6 that negligible recombination of the copper occurs before about 25 μs appears to be well founded. It is of interest to note that, despite the fact that the initial measured value of electron density at the 10.5 mm radial position is almost the same as that at 17.5 mm, recombination can be seen to commence considerably later, suggesting a higher initial electron temperature.

With the exception of the measurement made in close proximity to the plasma tube wall, the calculated electron temperature cooling rate falls with increasing distance from the axis. Also the value of T_0, the value of the electron temperature at the time that significant recombination commences, on the whole falls with increasing distance from the axis, with the exceptions of the measurement at 10.5 mm (sufficiently small to suggest that its low value is in fact an artefact) although the value at 14 mm is also marginally lower than that at 17.5 mm. These observations support the hypothesis that the electron temperature, initially very high immediately following the discharge pulse, falls very rapidly until it reaches the local value of the gas temperature, and at which point it is constrained to fall at the same rate. At this time recombination can commence. The fact that recombination is observed to start earlier near the plasma tube wall than on axis suggests that the peak electron temperature on axis is higher than nearer the wall, and falls more slowly.

The radial profile of the calculated T_0 values might be expected to reflect the gas temperature profile, however it must also be remembered that the values do not refer to the same absolute time. Despite this it is interesting to notice that the temperature radial profile suggested by these values is strongly peaked towards the axis, and therefore does not seem to support the theory of a relatively flat radial profile of electron temperature. Finally, however, it must be remembered that an attempt is being made to fit to a decay rate with a dependence upon electron temperature of T^{-5} and upon electron density of n_e^3 (Equation 8.1) and therefore the results of this fitting must be viewed with a degree of caution.

9 RESULTS OF POPULATION DENSITY MEASUREMENTS AS A FUNCTION OF RADIAL POSITION

9.1 LASER LIGHT OUTPUT

9.1.1 INTRODUCTION

In order to interpret the results of population density measurements as a function of radial position across the plasma tube it would be useful to gain some understanding of some of the radially dependent phenomena responsible for generating radial inhomogeneity in the parameters to be measured. As is frequently the case it was not always appropriate to attempt to divide such phenomena into primary and secondary effects, the operating environment of the CVL being the equilibrium resultant of many complex, interactive processes. A number of such radially inhomogeneous processes and parameters have been discussed earlier, either as fact or conjecture, and the justification, or otherwise, of some conclusions already reached should emerge in this chapter.

One parameter that is likely to give rise to radially dependent effects, that has been referred to a number of times already in this thesis is the radially dependent nature of the discharge. The basis and result of the skin effect have been discussed in Chapter 2, and the results of a series of experiments on a 60 mm diameter CVL to study the radial dependence of the onset of gain in the CVL have been presented in Chapter 6. In order to assess the magnitude of such effects in the 42 mm diameter laser under investigation the acquisition of a series of laser pulse profiles, with accurate timing, for each of the two wavelengths, and at 1.75 mm radial resolution was undertaken.

9.1.2 EXPERIMENTAL

As the study laser was mounted on a translation stage it was possible to obtain spectrally and radially resolved traces of laser pulse output using a prism to disperse the two laser lines, a pair of photodiodes and an iris aperture. Oscilloscope triggering was accomplished using a third photodiode mounted to detect the leakage radiation through the rear laser mirror, which was obscured apart from an aperture on the axis of the plasma tube. The CVL could thus be translated to allow the acquisition of laser pulses from all necessary radial positions.

9.1.3 THE TIMING OF THE LASER PULSES AS A FUNCTION OF RADIAL POSITION

The results are presented in Figures 9.1 and 9.2 for the green (510.6 nm) and yellow (578.2 nm) laser pulses respectively.

It may readily be seen that the magnitude of the delay in lasing between the plasma tube wall and the axis is considerably smaller in the study laser than in the 60 mm diameter laser on which the initial radial laser pulse timing study was performed. In addition, the difference between the wall-axis delay displayed by the green pulse and that by the yellow pulse in the case of the 42 mm diameter laser is also extremely small.

The delay between the onset of lasing at the wall and on axis is 8.5 ns for the green transition, and 7 ns for the yellow, with the green line commencing 7 ns before the yellow at the wall.

In Section 2.9 the skin effect was discussed and a very approximate theoretical expression for the time constant for the propagation of the electric field from the surface of the plasma to the axis was presented. The dependence of this value on plasma tube radius was predicted to be R^2.

As discussed in Section 6.3, the dependence of axial gas temperature upon plasma tube radius is also likely to show a predominantly R^2 dependence, with the thermal pre-pulse lower laser level populations increasing extremely fast, owing to the exponential nature of the function.

Taking these two functions together with the results of Chapter 6 it could be expected that the timing difference between the wall and the axis purely as a result of the skin effect should be smaller than that observed in the 60 mm diameter laser by a factor of about 2 (for the same average conductivity). As the radial distributions of both pre-pulse electron density and pre-pulse lower laser level are such a strong function of electron temperature, such a simple dependence is very unlikely in practice, even for the skin effect, and the differential delay experienced by the green pulse on axis is likely to be considerably more complex.

As the plasma tube wall temperature is very similar in the two cases (as this determines the copper vapour pressure), and the pre-pulse populations in the lower laser levels negligible near the tube wall, the relative timing between the green and yellow laser pulses represents the time taken for round trip gain on the transition to overcome

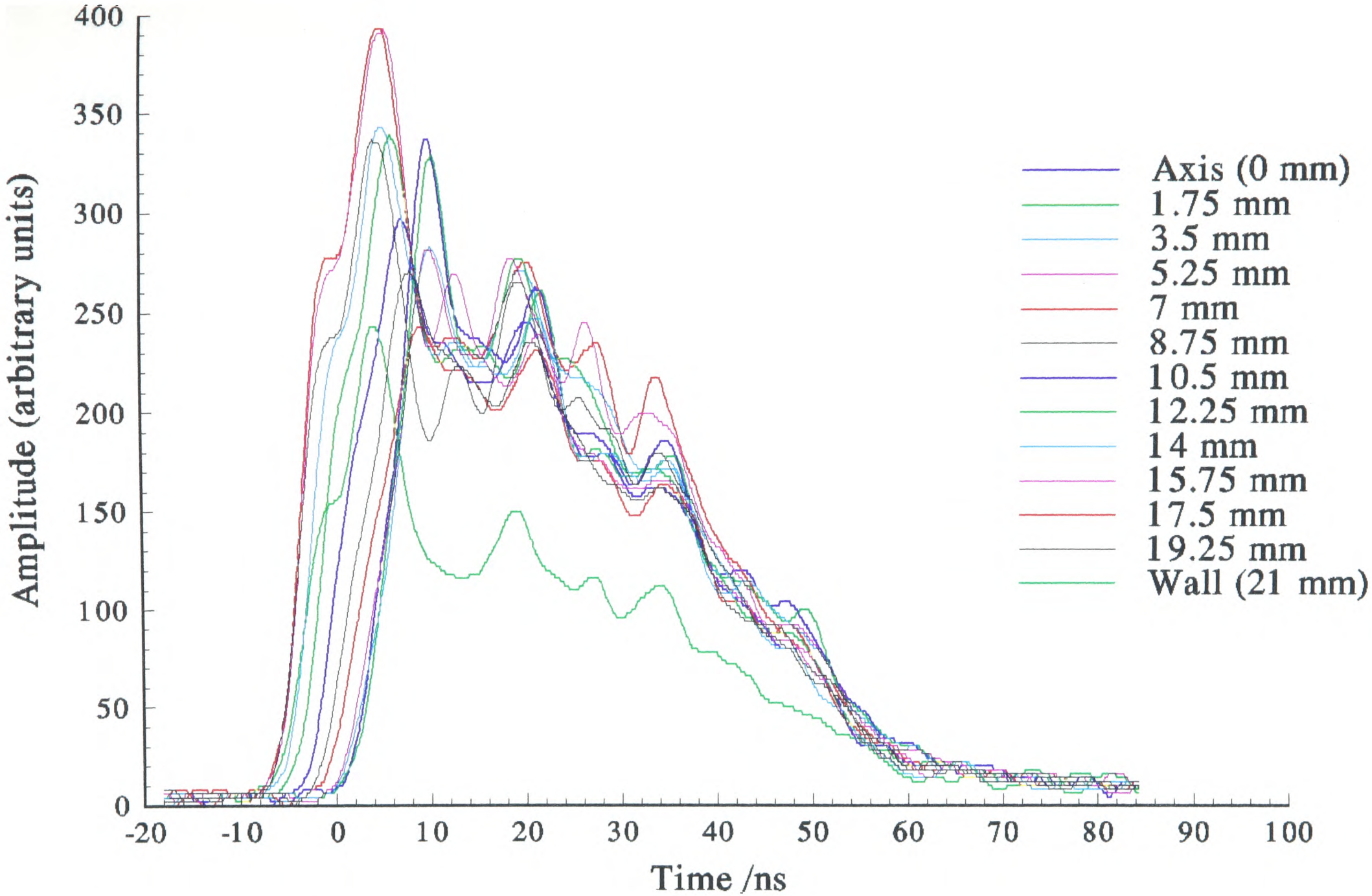

Figure 9.1 Green laser light pulse at 13 radial positions

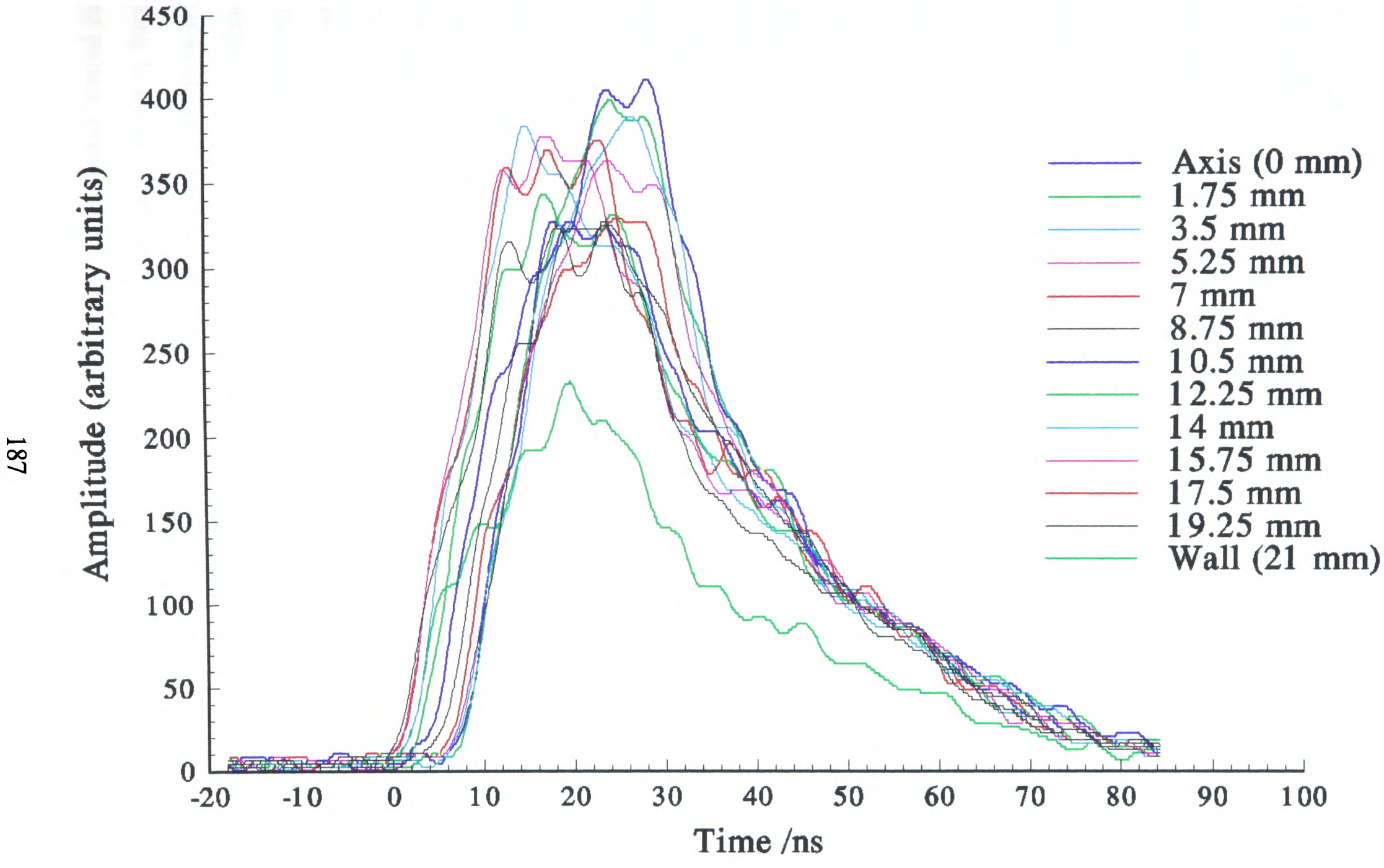

Figure 9.2 Yellow laser light pulse at 13 radial positions

the round trip losses. Owing to the longer gain length in the 60 mm device (2.2 m instead of 1.5 m) it may be expected that for essentially fixed round trip losses (about 92% at the output coupler in each case) both transitions should reach threshold more quickly in the case of the longer plasma tube, and thus the relative delay between them should be smaller. This is observed to be the case with a delay between the two lines at the wall of 2 ns in the big laser, and 7 ns in the small.

9.1.4 THE FALLING EDGE OF THE LASER PULSES

It can be seen that the trailing edges of the laser pulses at each radial position decay together. By this stage both the skin effect and the pre-pulse lower level populations are no longer relevant, and the termination of the laser pulses is determined by the relative rates at which population feeds and depletes the populations in the upper and lower laser levels. For the reasons discussed in Chapter 8 it seems likely that the peak electron temperature is highest on axis. The effect of this, combined with the higher pre-pulse electron density, will tend to lead to higher excitation rates on axis (neglecting the discharge effects), counteracted by the lower ground state density. The time at which the upper laser level populations peak, and the laser pulses cease, will be determined by the timing of the rapid fall in electron temperature, in turn determined by the onset of ionisation (Section 8.1.4). Without a full computer model of the laser and discharge kinetics it would be difficult to estimate the expected radial dependence of this timing, however the evidence of these results is that it is almost radially independent.

One final observation from the time dependence of the radially resolved laser pulses is the increasing degree of coherence between the successive amplitude peaks in the green pulses. Although there is spread of about 6 ns in the timing of the first peak, subsequent peaks appear to become more and more in phase, with a spread of only about 3 ns in the second peak, and still less in the third. This is interesting as it shows the effect of stimulated emission following paths that are not precisely aligned with the axis of the cavity and occurs as a result of the relatively short effective cavity length. As the divergence of the laser output beam decreases with successive round trips of the cavity (as it would with the employment of a longer cavity) the tendency for this radial emission mixing to occur decreases with it. No such structure can be seen on any of the yellow laser pulses, presumably reflecting the lower gain on this transition (Section 7.2.3).

9.1.5 THE RADIAL DEPENDENCE OF PEAK AMPLITUDE

In addition to the timing of the pulses it is of interest to study their relative peak amplitudes as a function of radial position (Figures 9.3 and 9.4). To facilitate this the amplitude of laser radiation on each line has been plotted as a function of both time and radial position in the form of a contour plot. In order to assist visualisation of the data, the measured values have been duplicated to display the population densities across a diameter, rather than across a radius as they were measured. The strict symmetry of the plots is therefore artificial. This applies to all the contour plots displayed in this thesis

In each case there is a local maximum on axis, with intensity falling off slightly to a minimum at about 8.75 mm away, from where it starts to increase again up to an overall maximum at 17.5 mm (3.5 mm from the wall), before finally decreasing again to the wall. This differential, however, appears to collapse relatively quickly giving rise to an approximately uniform radial intensity profile by about 30 ns in the case of the green pulse and 40 ns in that of the yellow. This radial dependence of peak amplitude represents not only the relative rates of excitation to both the upper and lower laser levels as a result of radial ground state, electron density and electron temperature profiles, but also the radial profile of the pre-pulse thermal lower level populations.

9.2 COPPER GROUND STATE AS A FUNCTION OF RADIAL POSITION

9.2.1 COPPER GROUND STATE RADIAL DENSITY PROFILE

Figures 9.5 and 9.6 display the results equivalent to those of Figures 7.1 and 7.2 for the measured population density in the copper ground state, across the whole diameter of the plasma tube, in contour format. In Figure 9.7 the individual curves showing the depletion of the ground state population density at seven radial positions have been plotted. The most obvious observation is that at all times the population density on the axis of the plasma tube is around 200×10^{12} cm^{-3} lower than that at the wall. This is a result of the temperature profile across the plasma tube discussed in Section 2.10. Within the accuracy of the measurements the recovery of the ground state population density would appear to be parallel, and thus possessing approximately equal time constants for at least 14 mm from the axis, and probably right out to the plasma tube wall.

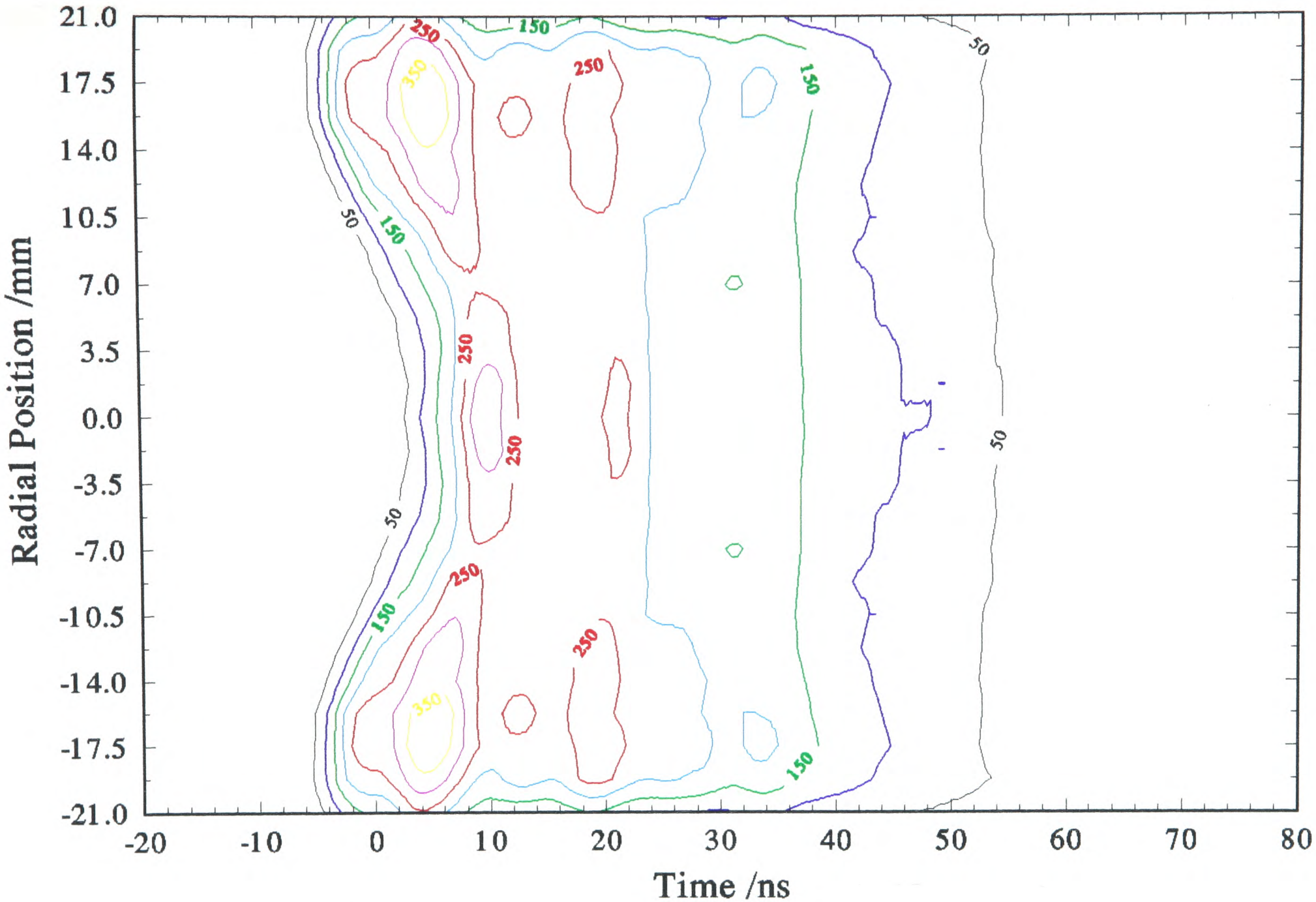

Figure 9.3 Contour plot of green laser light pulse as a function of time and radial position

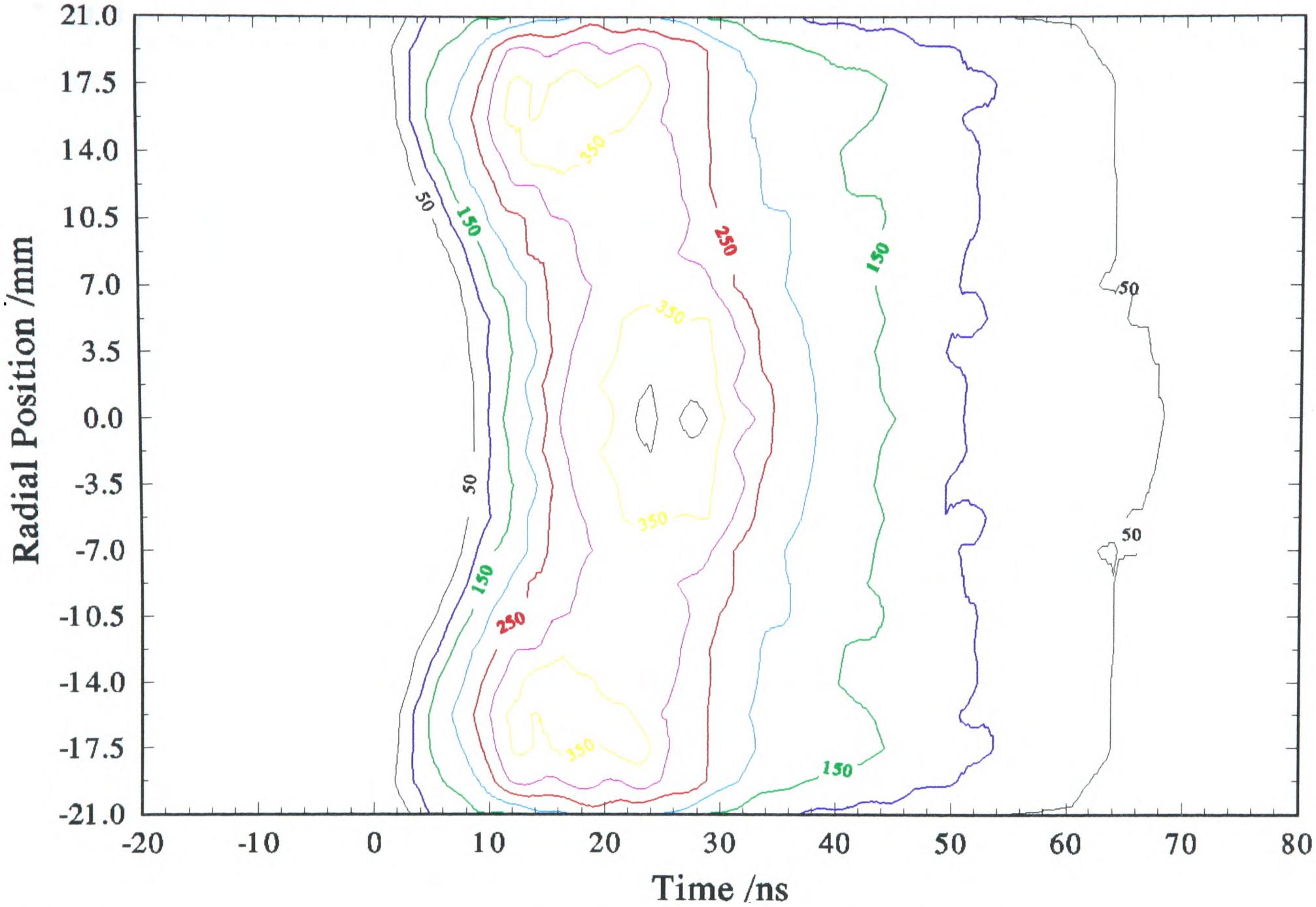

Figure 9.4 Contour plot of yellow laser light pulse as a function of time and radial position

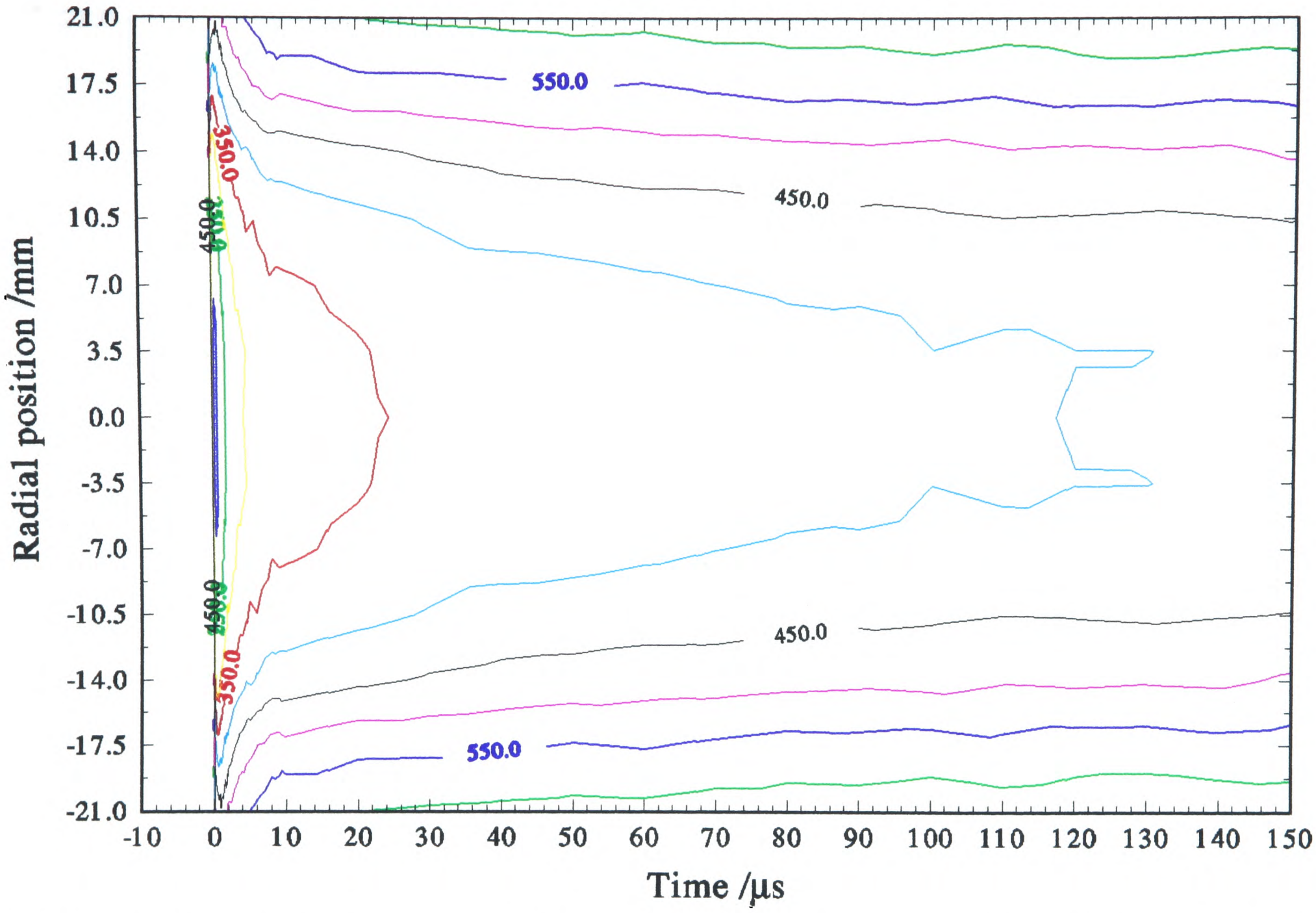

Figure 9.5 Contour plot of copper ground state population density as a function of time and radial position; full interpulse period

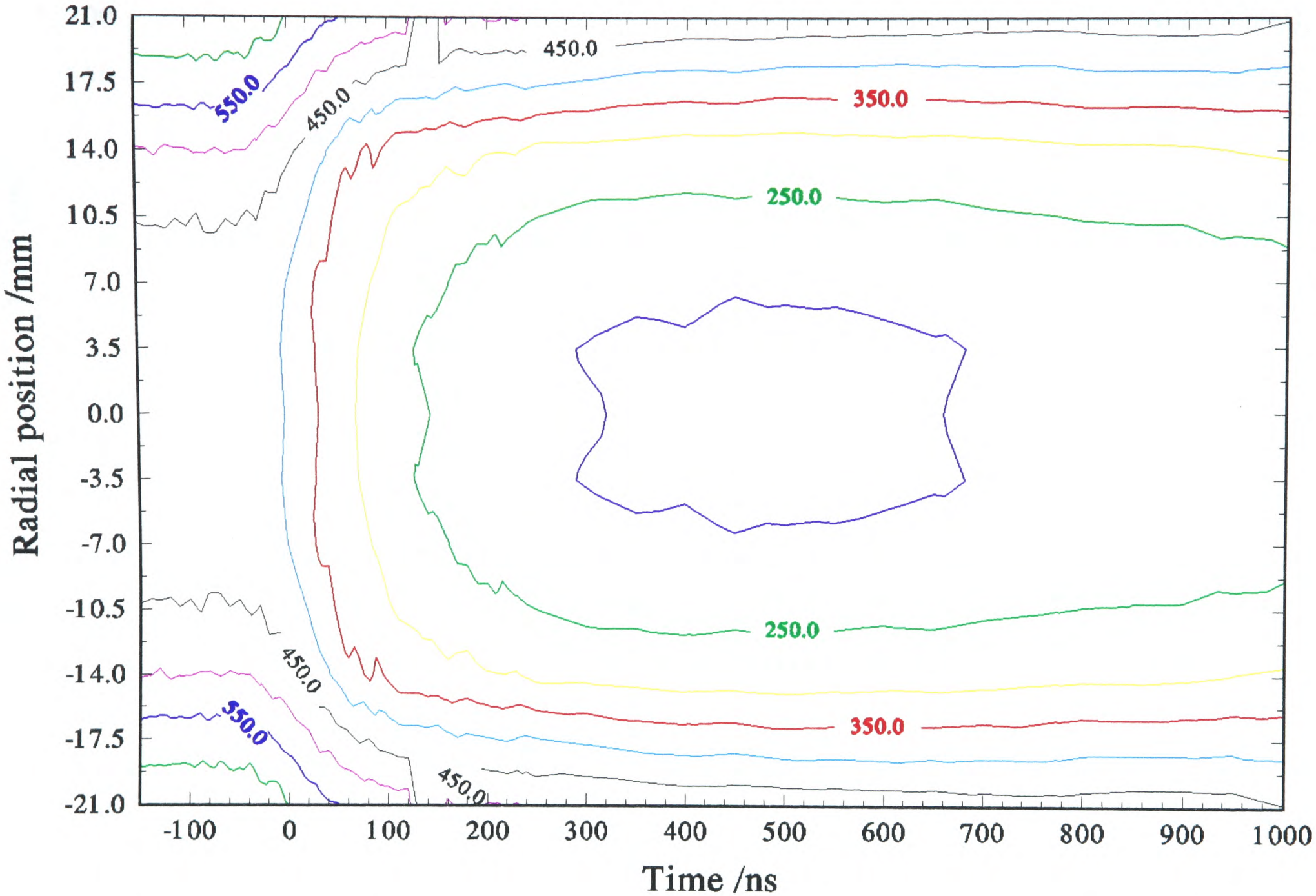

Figure 9.6 Contour plot of copper ground state population density as a function of time and radial position; first 1 μs

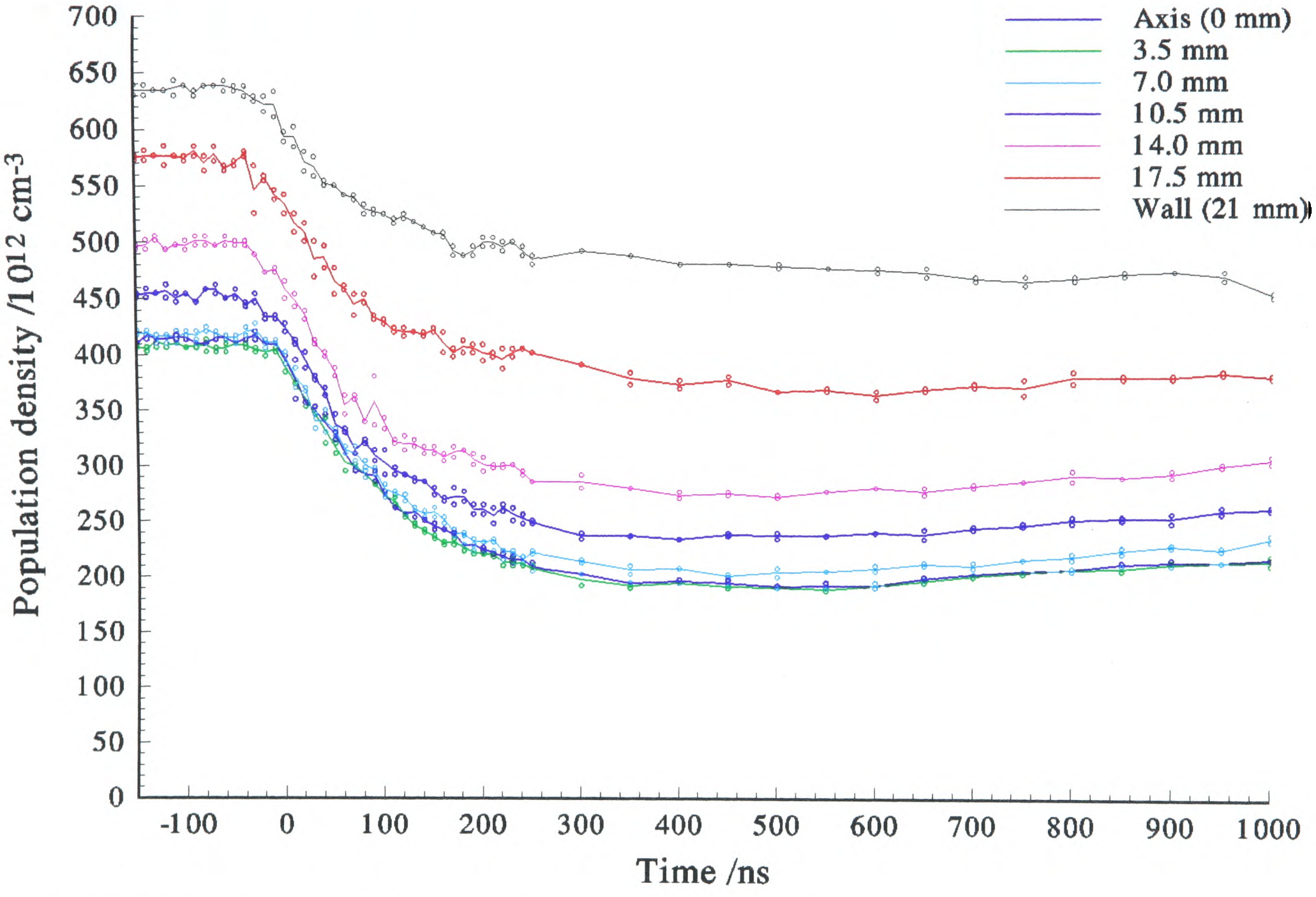

Figure 9.7 Copper ground state population density at seven radial positions; first 1 μs

9.2.2 THE PERIOD OF DEPLETION OF THE GROUND STATE POPULATION DENSITY

The depletion of the copper ground state during the early stage of the laser cycle also appears to show an approximately equal absolute loss of population density up to 14 mm from the axis, and only marginally less nearer the wall. Close inspection of the period of population depletion suggests that, close to the axis of the plasma tube it begins more abruptly, and later, than near the walls where it starts more gradually. Three factors are likely to contribute to this effect. The skin effect means that there is a delay between the onset of current flow at the edge of what is a cylindrical conductor, and at the core. Using the calculation of Kushner and Warner (Kushner & Warner, 1983) a skin depth of 2.6 cm can be calculated, and a time constant for the electric field penetration to the core of a 42 mm diameter plasma tube to reach 1/e of the wall value of 12 ns. In addition to the skin effect the lower particle density, of both copper and neon, as a result of the radial temperature profile, and therefore greater mean free path for the electrons, means that the peak electron temperature on axis is likely to be greater than nearer the wall. Finally, the dominant recombination mechanism (Lewis, 1985), electron stabilised three body recombination, occurs at a rate (Carman et al, 1993):

$$\frac{dn_e}{dt} = 4.0\times10^{-19} n_e^2 N_i T_e^{-5} \qquad \textbf{(9.1)}$$

in which n_e is the electron density and N_i the ion density. A higher electron temperature on axis, therefore, would have a very profound retarding effect on recombination, owing to the T_e^{-5} term. For this reason it is likely that the pre-pulse electron density on axis is also greater than closer to the wall. The consequence of this combination of effects is that, although excitation should start earlier near the wall because of the skin effect the rate per atom is likely to be slower because of the lower electron temperature and initial electron density. The greater copper ground state population density near the wall means that the total observed rate of excitation, as a function of radial position and time, is not readily predicted in isolation from a full computer model. Higher electron temperature and density on axis would explain the observed, almost constant depletion across the plasma tube, despite the greater available population near the wall.

9.2.3 COPPER VAPOUR PRESSURE NEAR THE PLASMA TUBE WALL

In Sections 2.4.1 and 2.4.2 the information to be gained from the ground state density measurements concerning temperature were discussed. It was pointed out that the total copper population density at the wall of the plasma tube should be equal to that obtained from the copper vapour pressure curve at the temperature of the copper blobs, assumed to be in equilibrium with the plasma tube wall.

9.2.3 (I) Measurement of plasma tube wall temperature

As described in Section 3.2.3, by mounting a calibrated optical pyrometer on a carefully aligned, hinged mount such that it could be brought down into position immediately the CVL had been switched off, a series of measurements of temperature could be made without touching the device, at intervals of a few seconds. In this way an accurate cooling curve for the plasma tube has been obtained (Figure 9.8). In order to obtain accurate readings from the pyrometer it was necessary previously to have obtained values for the emissivity of the alumina plasma tube wall (0.9) and the effect on the reading of a single, clean quartz window, 6 mm thick (-10 K). Although the plasma tube cooling curve in the case of a water cooled CVL represents the combined effect of a number of cooling mechanisms, and it is thus impossible to attempt to fit it to any theoretically obtained expression for cooling with any great confidence, a reasonably good fit may be obtained over the 5 minutes of the temperature measurements to a curve of the form:

$$T_w(t) = T_l + T_0 \exp -\left(\frac{t}{\tau_c}\right)$$

in which T_l is the temperature of the cooling water (really increasing with distance along the water cooling jacket), averaged at approximately 300 K, T_0 is the initial, operating temperature of the plasma tube wall above T_l, t is time after switching off the laser, and τ_c is the cooling time constant. From this an initial operating temperature of 1693 K, and cooling time constant of 48 minutes may be obtained.

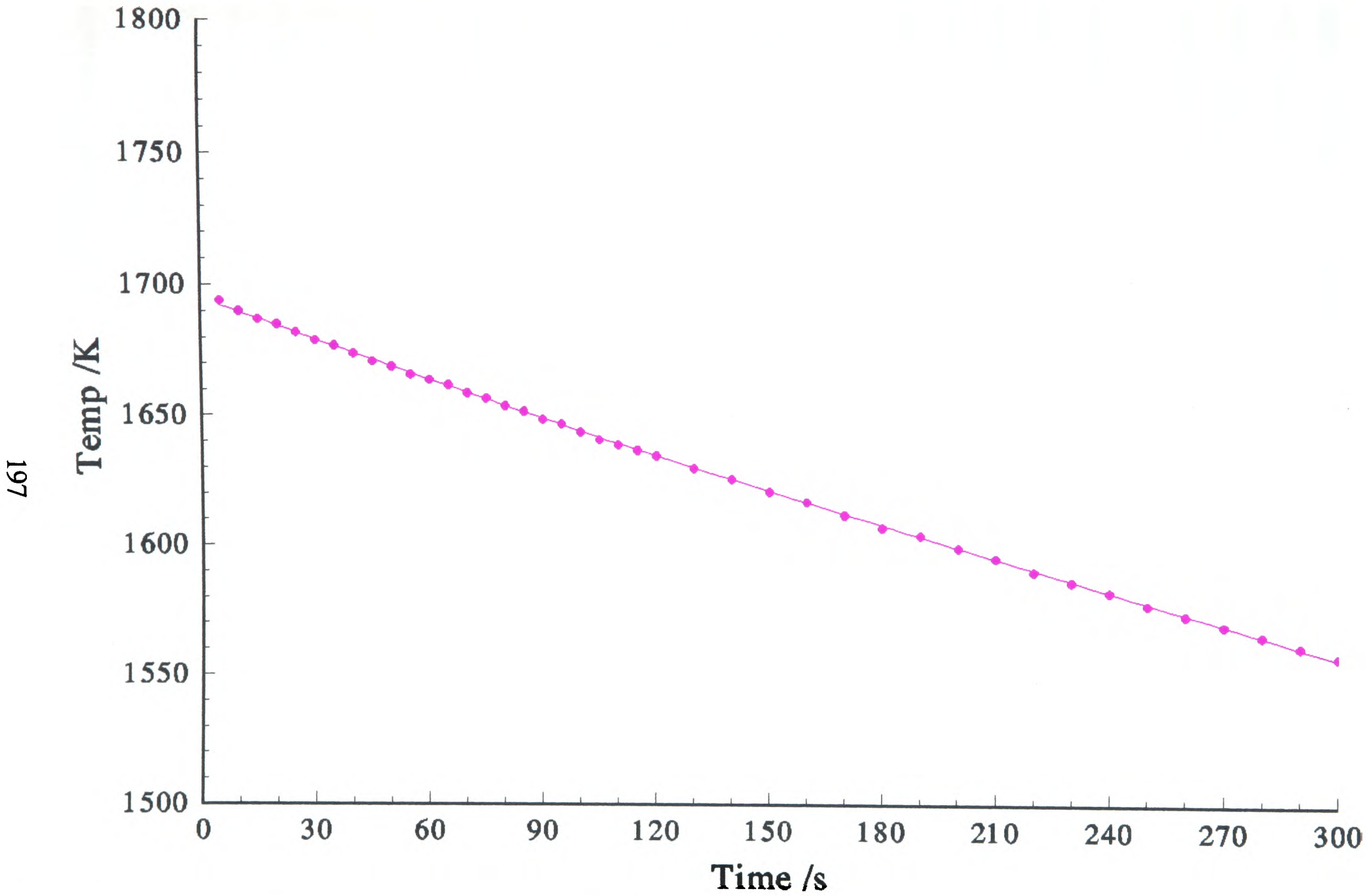

Figure 9.8 Plasma tube wall temperature cooling curve

9.2.3 (II) COMPARISON OF MEASURED COPPER VAPOUR PRESSURE WITH PUBLISHED VALUES

From the results displayed in Figure 9.7 the pre-pulse copper ground state population density in proximity to the plasma tube wall may be seen to be 640×10^{12} cm^{-3}. A number of authoritative sources offer vapour pressure data for copper. In Figure 9.9 copper vapour pressure curves from three such sources (Dushman, 1949; American Institute of Physics Handbook, 1972; Kaye & Laby, 1989) have been plotted with lines corresponding to this population density and the two values of temperature derived.

The average value of wall temperature thus obtained is 1705 K which is in reasonable, though not perfect, agreement with that obtained from the optical pyrometer. There are a number of potential causes for this observed discrepancy. The oscillator strength is assigned an accuracy of $\pm 5\%$ for the resonance lines employed in the measurement of the copper ground state density. This on its own however is not sufficient to explain the discrepancy.

In order to obtain a value for population density it is necessary to assume a length of plasma over which there is a uniform copper density, the ends of which are well defined and abrupt. Discussion has been made in Section 3.3.6 of the choice of length to be used in this calculation, and mention has been made of the difficulties involved. It was concluded that for the value chosen the accuracy may be estimated to be no better than $\pm 2\%$.

The correction value of -10 K for a single quartz window for the optical pyrometer requires that it be clean. Although the windows had been cleaned prior to the measurements being made for the first time several hours of operation is required for the CVL to display fully stable, equilibrated operation. During this time it is possible that a very small amount of copper condensation might have occurred upon the window within the field of view of the pyrometer, giving rise to an artificially low reading. Sets of cooling curve data were obtained on a number of occasions to ascertain reproducibility, sometimes with slight realignment of the pyrometer, with maximum total variation of 5 K.

Another explanation is that the copper blobs were genuinely at a slightly higher temperature than the plasma tube wall where it was measured. The copper reservoir

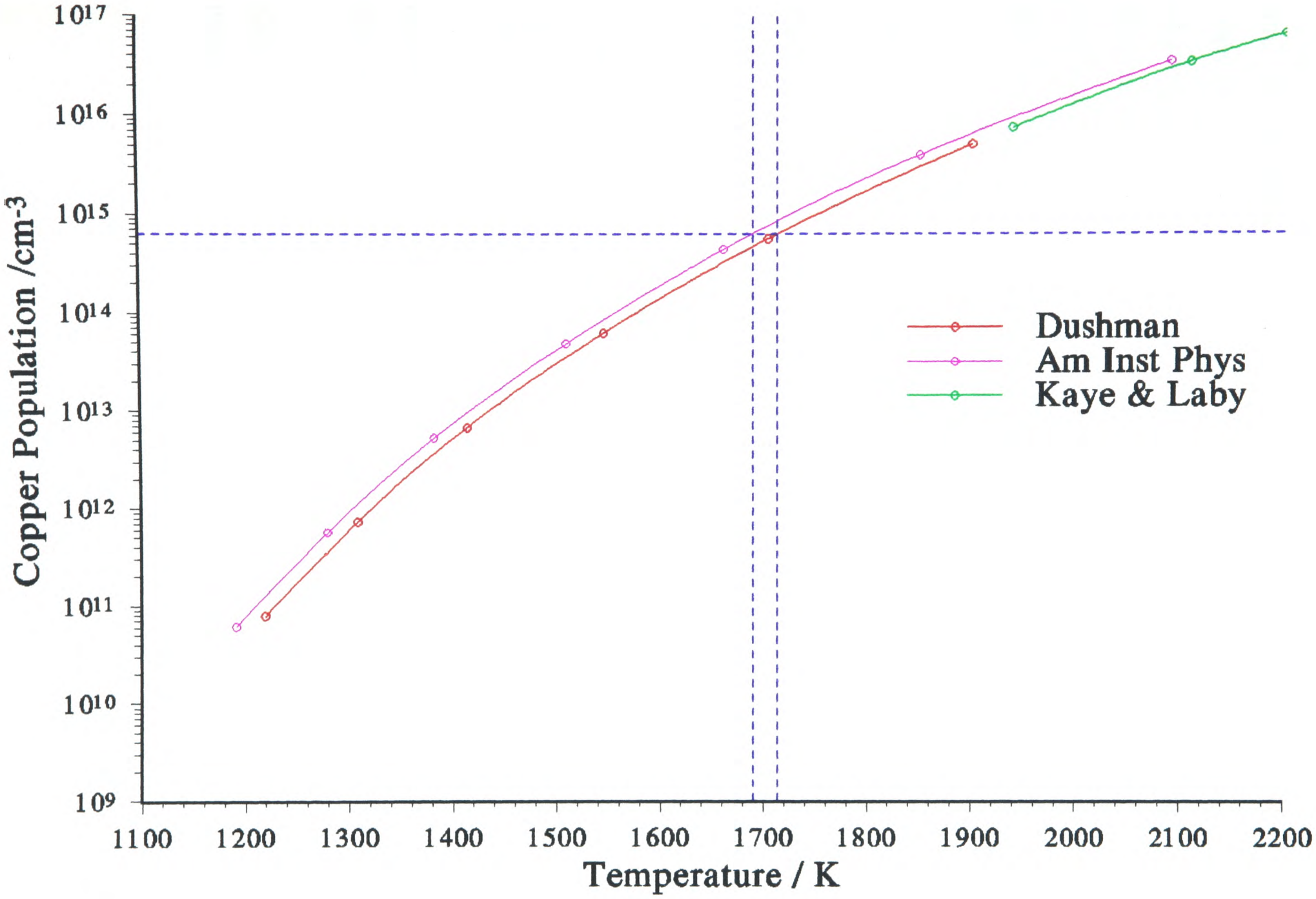

Figure 9.9 Copper vapour pressure curves from three sources

consists of a line of copper blobs along the floor of the plasma tube. The population density measurements were taken along a horizontal radius to allow measurements close to the plasma tube wall without local effects caused by the copper blobs. The temperature measurements were also made of a piece of plasma tube wall on one side of the tube, half way along its length. The copper blobs had an average diameter of about 8 mm. In the absence of the copper this distance from the wall corresponds to an increase in gas temperature of about 600 K (see below) however the high thermal conductivity of copper would ensure a very small thermal gradient across the blobs. It is thus reasonable to suggest that the temperature of the copper blobs together with the adjoining region of alumina tube wall are at a temperature slightly elevated with respect to the majority of the plasma tube, giving rise to a slightly higher copper vapour pressure than predicted by the wall temperature remote from the copper blobs.

9.2.4 CALCULATION OF GAS TEMPERATURE RADIAL PROFILE

If the gas adjacent to the plasma tube wall is assigned the measured wall temperature then the next step is to calculate the radial gas temperature profile by assuming a radially independent partial pressure of copper vapour so that the ground state copper number density is inversely proportional to temperature. Prior to the discharge pulse the only significant copper populations are in either the ground state or the ion. The ambipolar diffusion current of ions to the wall will contribute to the rate of return of neutral copper and thus tend to reduce the equilibrium vapour pressure from its value in the absence of ions. For this reason the value of p_{Cu} employed in the expression $p_{Cu} = N_{Cu}kT_g$ might be slightly below the value calculated directly from the wall temperature and vapour pressure curves. This has been discussed in Section 2.4.2 and it has been shown that the reduction may be expected to be of no more than about 1%.

In Figure 9.10 the pre-pulse ground state copper population density has been plotted as a function of radial position. From this, and the measured plasma tube wall temperature a calculated radial gas temperature profile has also been plotted.

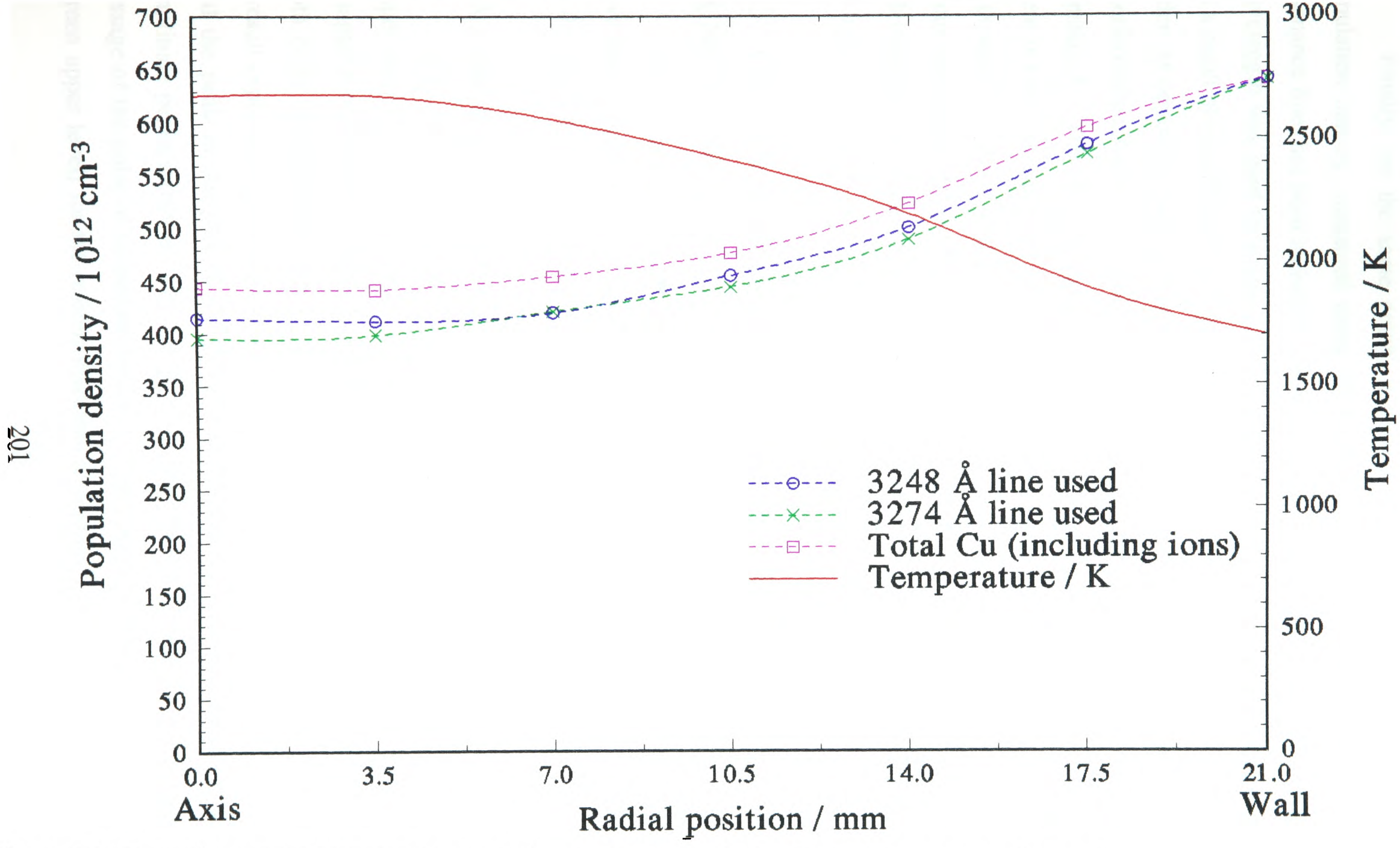

Figure 9.10 Pre-pulse copper ground state population density and calculated gas temperature; radial profile

9.2.5 COMPARISON OF DATA OBTAINED USING TWO DIFFERENT TRANSITIONS

Finally, on the same graph, a second plot of pre-pulse copper ground state population density, measured using the hook method but employing the other copper resonance line, has been included. To obtain these measurements a different probe beam wavelength was used to access a different transition with a different oscillator strength. As a result of the difference in oscillator strengths the spectrograph could be used in third order, as opposed to second order for the previous measurements, and consequently the interferometer had to be readjusted for optimal hooks, giving rise to a different hook constant K. The absolute agreement between the two sets of data points suggests that there is little random error in the oscillator strengths of the two lines, and the accuracy with which the hook separations, and the hook constant, may be measured. However, about systematic error in these values, the accuracy of the figure for l used in the calculations, the length over which the populations extend, or timing jitter, nothing may be inferred.

9.3 COPPER UPPER LASER LEVEL POPULATIONS AS A FUNCTION OF RADIAL POSITION

In Figures 9.11 and 9.12 the population densities in the two upper laser levels have been plotted as a function of time and radial position in the form of contour plots. In this form a number of observations may be made.

9.3.1 THE RISE IN COPPER 4p $^2P_{3/2,1/2}$ POPULATION

The concave front edge of both plots shows how the onset of excitation to the upper laser levels occurs later on axis than at the wall, supporting the conclusions of Chapter 6 that there is a delay in excitation reaching the axis. Despite this however, in both cases the population peak at all radial positions occurs at the same time (100 ns), a result expected by the measurements of Section 9.1.4. Between the onset of excitation and the peak in the plot of the $4^2P_{1/2}$ level (Figure 9.12), it is possible to see local amplitude peaks (arrowed) as a result of the depletion of population occasioned by the passage of the pulse of stimulated emission. Such peaks cannot be seen in Figure 9.11 (green upper level) for the reasons discussed in Section 7.2.3.

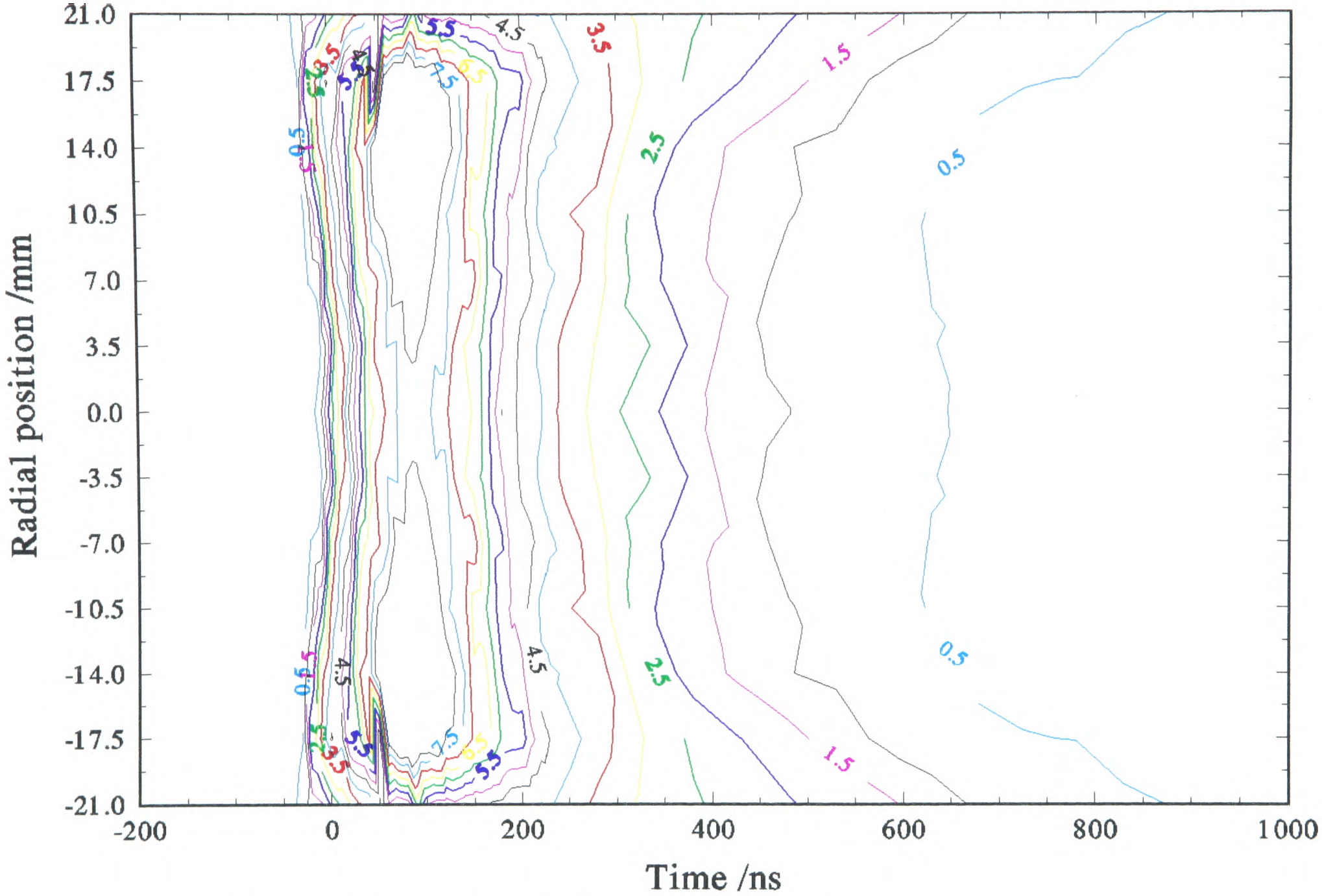

Figure 9.11 Contour plot of copper 4p $^2P_{3/2}$ level population density as a function of time and radial position

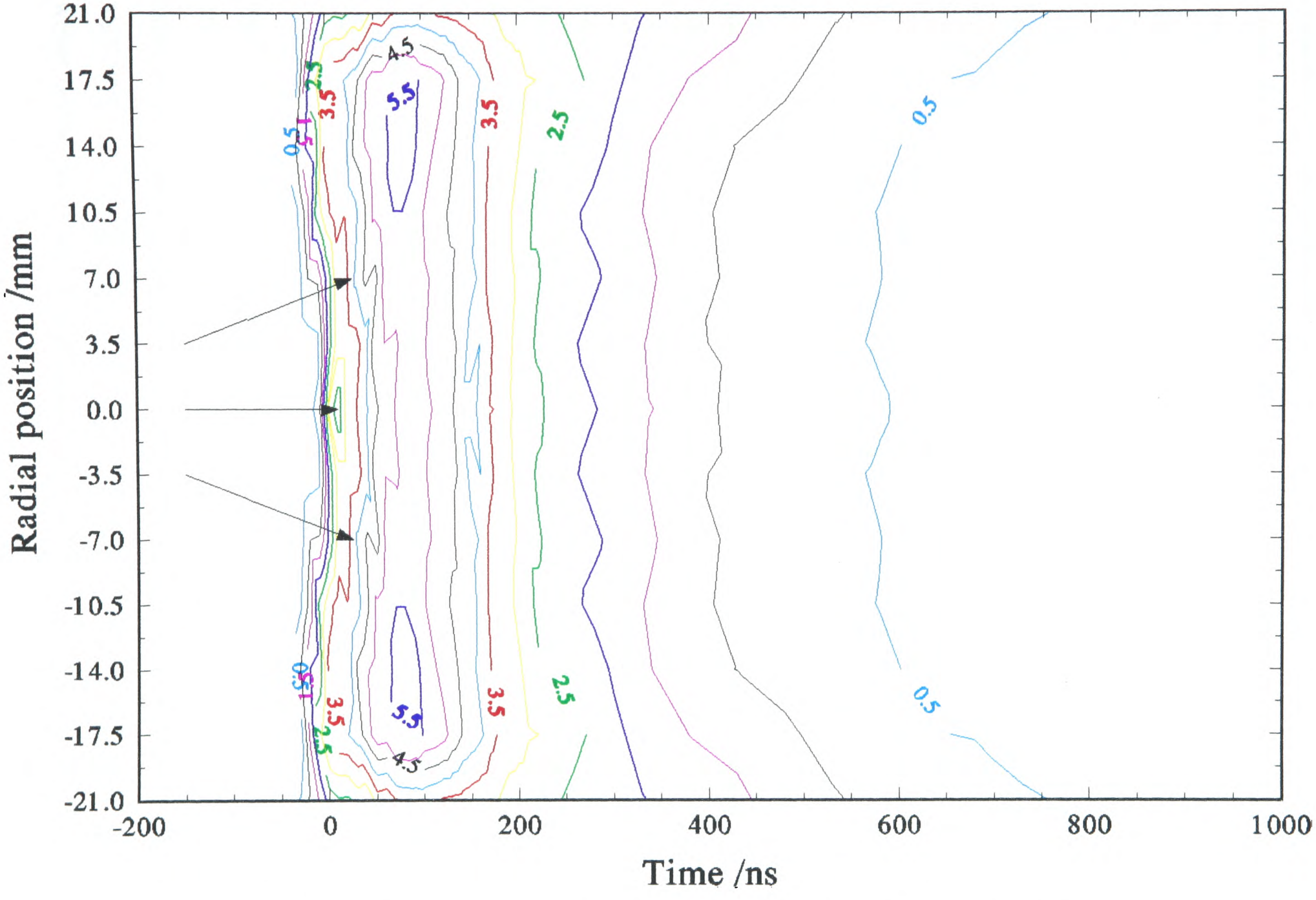

Figure 9.12 Contour plot of copper 4p $^2P_{1/2}$ level population density as a function of time and radial position

What may also clearly be seen is the fact that at the time that the population in these two levels peaks the maximum population densities occur not on the axis, but at a radial position 14 mm from the axis. In Section 9.1.5 the radial profile of the peak amplitude of the two laser pulses was presented and discussed in terms of the radial dependence of excitation rates as a result of radial profiles of ground state density, electron density and electron temperature and the pre-pulse lower level population density. Looking at Figures 9.11 and 9.12 it appears that the maxima in the radial profile of the peak upper level populations occur not as a result of any significant difference in excitation rate, but simply because excitation starts earlier. Closer to the wall than these maxima, however, the rate of excitation does appear to be considerably reduced, despite the enhanced ground state population density, because of the lower electron temperature and electron density.

9.3.2 THE DECAY OF COPPER 4p $^2P_{3/2,1/2}$ POPULATION

Following the peak in population, the slight minimum on axis observed at the population peak soon appears to be smeared out (by about 170 ns), after which the radial dependence of the decay rates appears to be relatively flat across the middle two thirds of the $4^2P_{3/2}$ level plot (out to about 14 mm from the axis), and the middle half (out to about 10.5 mm) of the $4^2P_{1/2}$ level plot. Outside this relatively flat region however the rate of decay appears to be somewhat slower giving rise to a change from the population minimum initially observed near the wall, through a radial profile almost completely flat across the whole tube at about 300 ns, to one in which the largest population density is close to the wall.

Referring again to Figure 9.10 it can be seen that from the axis, for about 10.5 mm on either side, the ground state density and the gas temperature radial profiles are relatively flat. This seems to suggest that both the electron temperature and electron density over this central region are also relatively flat, both falling off significantly only relatively near the wall. This would have the observed effect of giving a roughly constant rate of decay of population over the majority of the diameter of the plasma tube, though with a markedly lower rate of decay in proximity to the wall. This is not however borne out by the measured electron density profile (Section 8.2.3).

9.4 COPPER LOWER LASER LEVEL POPULATIONS AS A FUNCTION OF RADIAL POSITION

Owing to the scatter in the measurements of the $4s^2\,^2D_{3/2}$ level population density, as discussed in Section 7.3.1, a contour plot of the $4s^2\,^2D_{5/2}$ level population density only is presented here (Figure 9.13). Correction for the population density in the upper level of the transition employed was made as described in Section 7.3.2.

9.4.1 THE RISE IN COPPER $4s^2\,^2D_{5/2}$ POPULATION

In Figure 9.14 only the rising edge of the $4s^2\,^2D_{5/2}$ has been plotted and, in contrast to the behaviour of the upper laser levels, there is a noticeably lower rate of rise of population on axis compared with that seen at about 14 mm. Right at the plasma tube wall, however, the rise is very slow. It must be remembered that the majority of this observed rise in population occurs during the decaying tail of the discharge current pulse (Figure 5.1), while the electron temperature is falling. It may be conjectured that this observed lower rate of rise on axis, in contrast to that observed in the upper laser level populations, reflects the relatively slow dependence of the rate coefficient for direct excitation from the ground state on electron temperature above about 1 eV (Figure 7.5). Consequently the ground state density radial profile, together with population from higher lying levels, including, and via, the upper laser levels, assume a relatively greater significance. As the slower rate of rise on axis appears to continue right up to the peak in population it could be conjectured that by the time the electron temperature has fallen below about 1 eV (at about 300 ns on axis - Sections 7.3.3 and 7.6) its radial profile is approximately flat, and thus the ground state radial population density profile still continues to dominate.

Very close to the plasma tube wall it would seem that the significantly lower electron density still proves to be the dominant parameter leading to decreased excitation rate, and reduced peak population, despite the higher ground state density.

Again it can be seen that the timing of the peak of the population density appears to be independent of radial position, suggesting again that, even if the electron temperature rises to a higher peak value on axis, by 550 ns, if not before, this radial profile has collapsed.

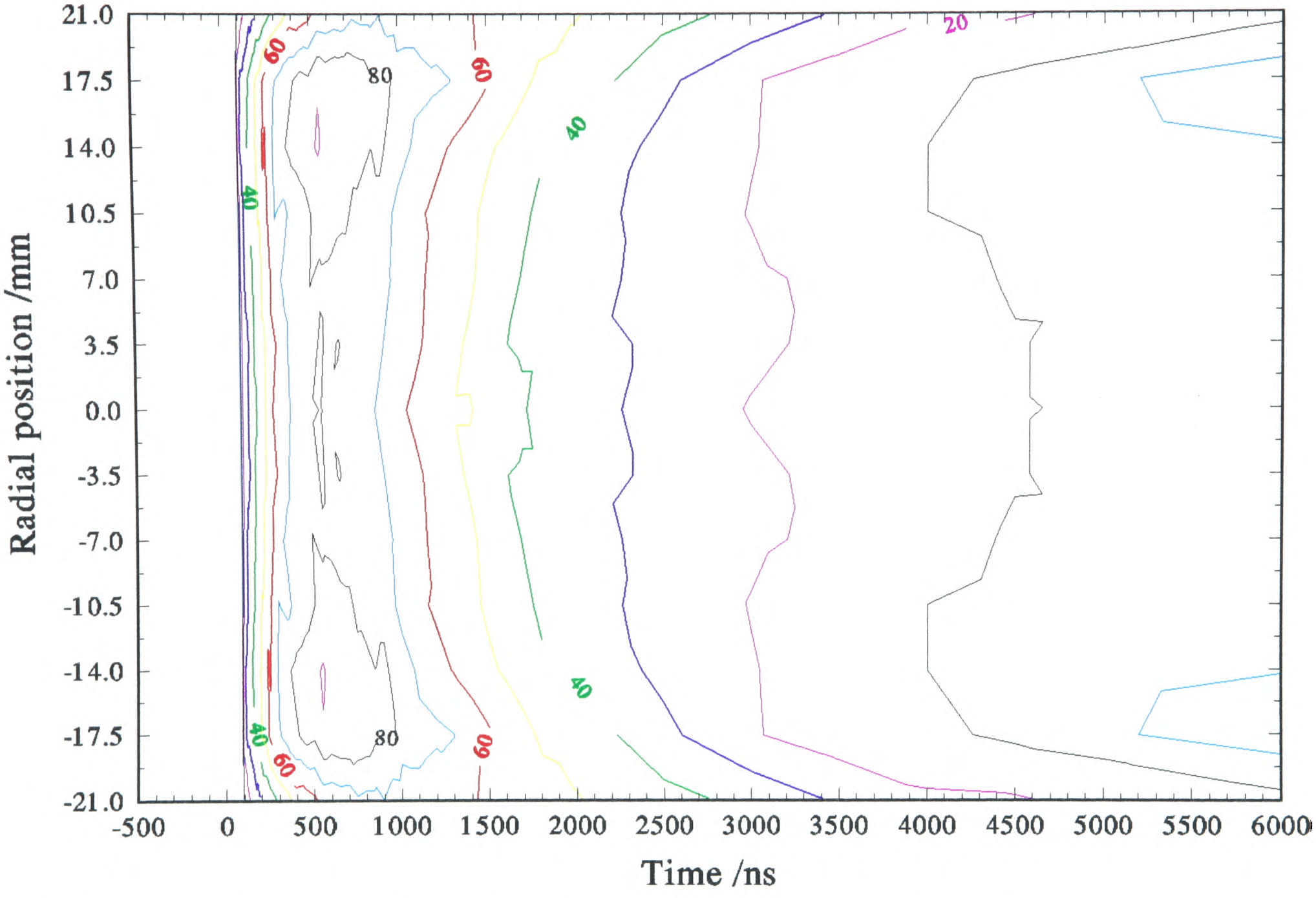

Figure 9.13 Contour plot of copper $4s^2\ ^2D_{5/2}$ level population density as a function of time and radial position

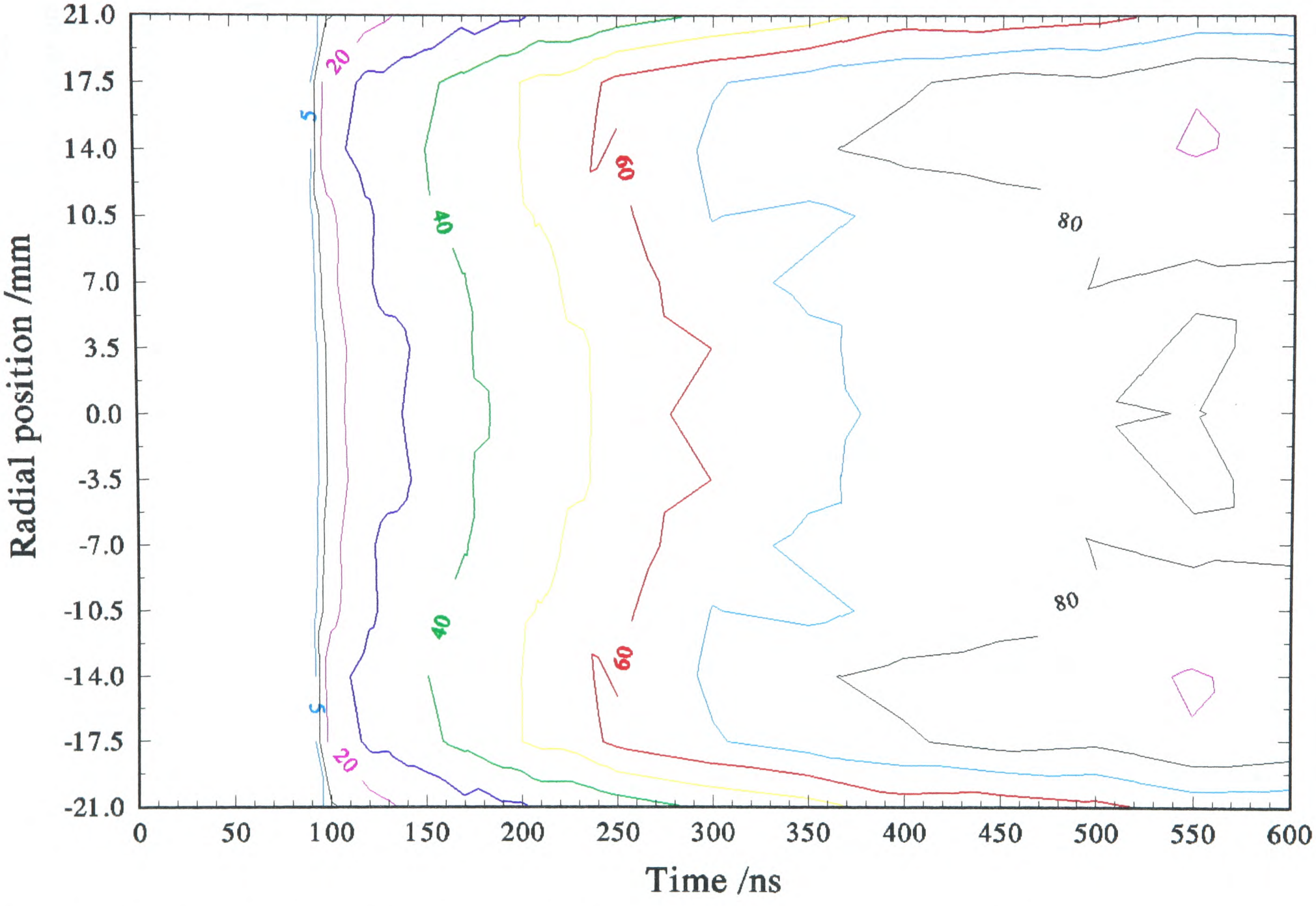

Figure 9.14 Contour plot of copper $4s^2\ ^2D_{5/2}$ level population density as a function of time and radial position; first 600 ns

9.4.2 DECAY OF COPPER $4s^2\,^2D_{5/2}$ POPULATION

Returning to Figure 9.13 it can be seen that, although initially the rate of decay of population density appears to be approximately uniform across the central majority of the diameter of the plasma tube, from about 1400 ns the rate of decay on axis seems to slow down. This gives rise to a population density radial profile which is highest at the plasma tube walls, falls slightly to minima at about $\pm$14 mm, before rising again to give a convex distribution across the central two thirds of the diameter.

The most likely explanation for the observed behaviour is that initially decay rate is determined predominantly by electron density distribution, falling off towards the walls, until thermal equilibrium with the ground state at the local (though by this time approximately radially invariant) electron temperature is established. By this time the electron temperature has fallen to less than 0.4 eV (Section 7.6, Figure 7.18) allowing a very low level of recombination to commence, in proportion to the local electron density. This has the effect of generating "recombination heating" of the plasma as the electrons undergo super-elastic collisions with highly excited, recently recombined atoms. With the highest electron density on axis, and therefore the greatest level of "recombination heating", the rate of fall of the electron temperature close to the axis is lower than further away from it, once more giving rise to a radial electron temperature profile that is greatest on axis. Over the period covered by the plot of Figure 9.13 therefore Boltzmann equilibrium with the ground state is re-acquired at different radial positions at a time determined by local electron density, electron temperature and extent of existing disequilibrium. Following the attainment of equilibrium the rate of decay is determined by the rate of change of electron temperature and of the ground state population.

9.5 POPULATION IN COPPER QUARTET LEVELS AS A FUNCTION OF RADIAL POSITION

In Figure 9.15 the population density in the copper $4s(^3D)\ 4p\ ^4F_{9/2}$ level is plotted in the form of a contour plot.

The first observable population appears to occur neither right at the wall, as a result of discharge propagation delay, nor at the centre of the tube, as might be predicted by considerations of electron density and electron temperature, but at about

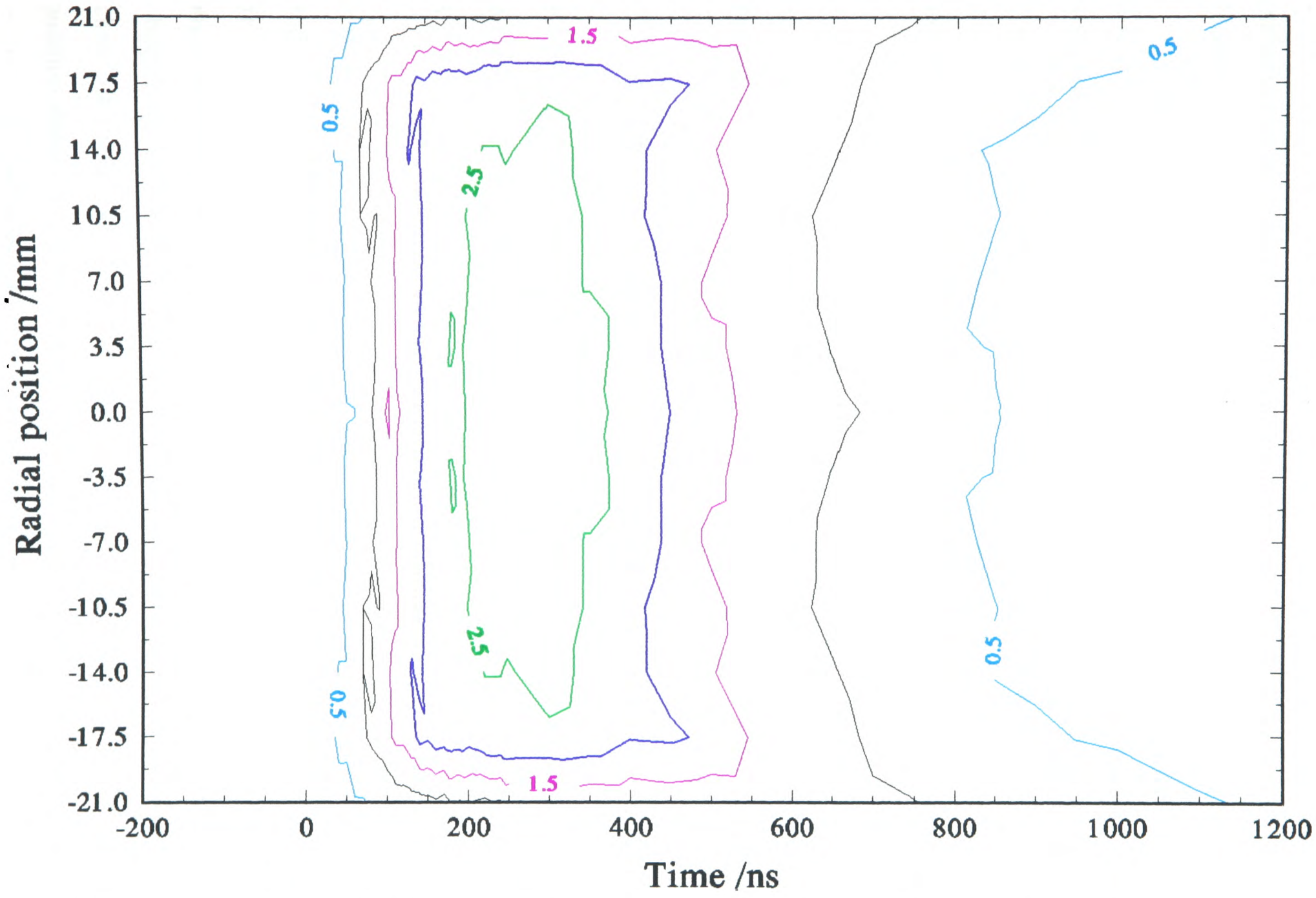

Figure 9.15 Contour plot of copper $^4F_{9/2}$ level population density as a function of time and radial position

14 mm - 17.5 mm from the axis. This could be a result of the combined effect of the excitation rate coefficient, electron density, ground state density product, but a more likely explanation is that it arises as a result of the maxima in the radial profiles of the population density in the 4^2P levels (which do start to rise first at the plasma tube walls) and the $4s^2\,^2D$ levels, which occur at this radial position. This is in agreement with the hypothesis that the majority of population of these levels occurs by stepwise excitation via lower lying levels such as the upper and lower laser levels.

These maxima in the radial profile soon flatten out however, yielding a profile that is flat over the majority of the plasma tube diameter, falling off steeply close to the walls by about 150 ns. By referring back to Figures 9.11 and 9.12 it can be seen that this coincides with the flattening out of the radial profiles of the two 4^2P (upper laser) levels, further supporting the hypothesis of their role in populating the quartet levels. Once again the timing of the population peak appears to be radially invariant.

The decay in population appears to follow the same general form as that of the 4^2P levels, going from an approximately flat radial profile, falling off at the edges to a concave profile which is relatively flat across the majority of the diameter of the plasma tube, rising near the edges. As in the case of the 4^2P levels it is likely that this occurs as a result of the higher electron density across the middle portion of the tube available to depopulate the excited levels by collisions of the second kind.

9.6 POPULATION IN NEON ^3P LEVELS AS A FUNCTION OF RADIAL POSITION

9.6.1 THE RISE IN NEON ^3P POPULATION

In Figure 9.16 a contour plot shows the early part of the first peak of the neon $2p^5\ 3s\ ^3P_0$ level population density. It can be seen that the population starts to rise first at the centre of the plasma tube, with a strong radial dependence of the timing of this start. The rate of increase in population decreases after a few nanoseconds however, though the population continues to increase until 80 ns. Away from the axis, although the beginning of population increase starts later, the rate of increase does not appear to slacken off in the same way until later, consequently giving rise to a higher peak population density when it reaches its maximum value at about the same time as on the axis. It is of interest to note that these maximum values occur somewhat closer to the

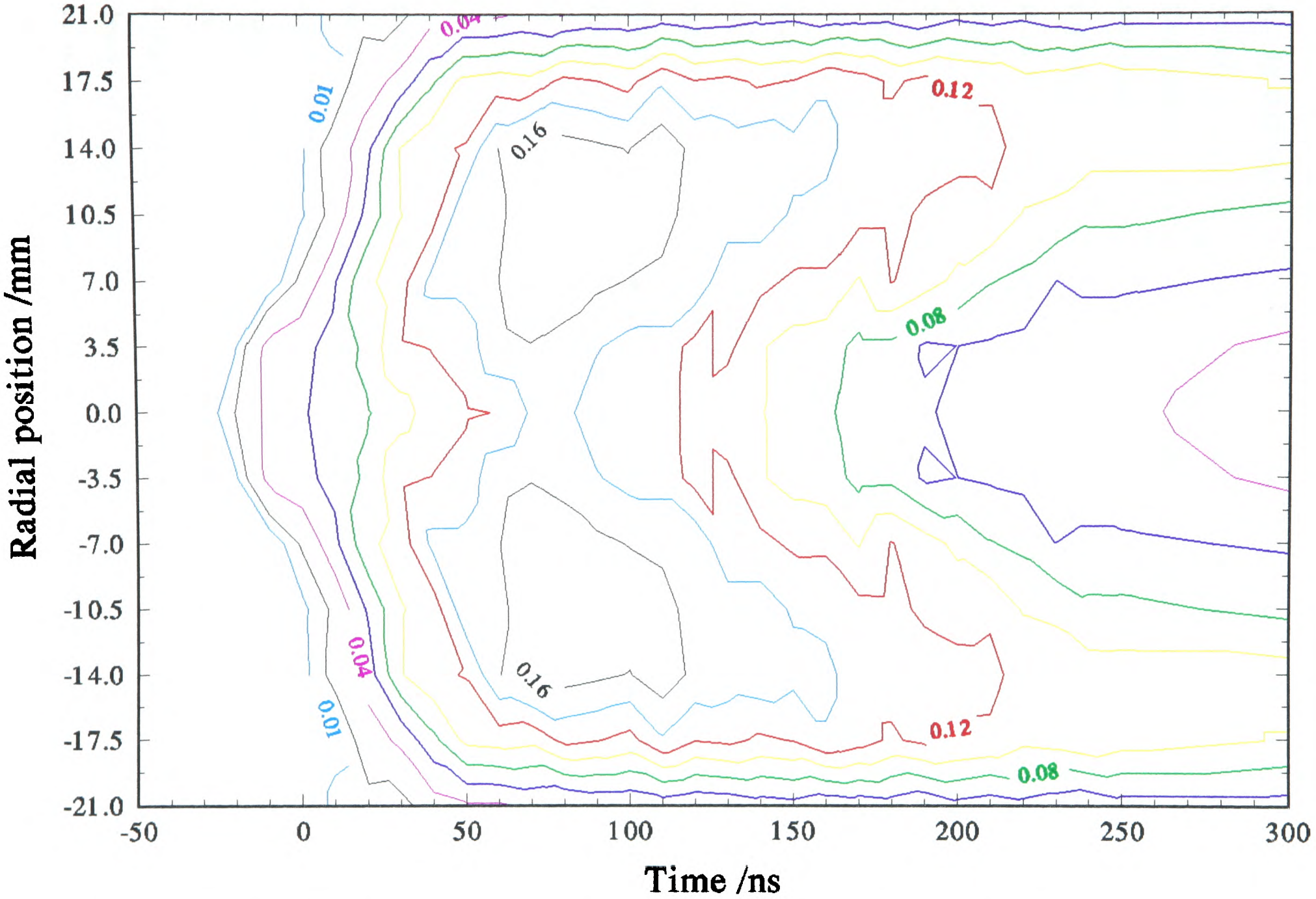

Figure 9.16 Contour plot of neon $2p^5\ 3s\ {}^3P_0$ level population density as a function of time and radial position; first 300 ns

axis than has been the case with the copper laser levels. Close to the plasma tube wall, again, the rate of rise of population is slower.

When considering the behaviour of the neon population it is necessary to remember that the excited population density being measured here is predominantly in the "cool" end regions of the plasma tube where the partial pressure of copper vapour is low. In this region the wall temperature is lower than in the central "hot" region, however, in order to maintain continuity of electron density despite the considerably higher ionisation potential of neon the peak electron temperature must be higher, and the power deposited per unit volume of this region must also be greater. Consequently the gas temperature on axis *during and immediately after* the discharge pulse will be higher than in the copper bearing region and so the radial profile of the gas temperature, and therefore that of the neon ground state number density, are likely to be far more pronounced (in their opposite directions) than that in the high copper density region. As a result of this, those parameters whose radial density profiles are determined by those of the gas temperature and ground state population density, such as peak electron density and peak electron temperature, are likely also to show more steeply peaked radial profiles. Following the end of the discharge pulse however the lower plasma tube wall temperature, and the relative proximity of the water cooled end flanges and end windows mean that the decrease in gas temperature, and possibly therefore electron temperature, is likely to be faster and to a lower final value giving a lower pre-pulse electron density. This hypothesis is supported by the observed decay of the measured electron density close to the axis, as discussed in Sections 8.1.6 and 8.2.3.

On the basis of the above discussion the observed behaviour of the neon $^3P_0$ population density may be explained. The earlier start to the increase in the population density, and the strong radial dependence of this timing, occurs as a result of the very much more rapid rise of electron temperature and electron density on axis. This leads to rapid population of the neon ^3P levels, however, as discussed in Section 7.5.2, the proximity of higher lying excited levels in the neon, and the ionisation limit, mean that this high excitation rate on axis leads to a high level of continued excitation out of the ^3P levels into higher levels, and finally ionisation to generate the electrons required to carry the current. It would seem likely therefore that the observed lower value of peak population on axis arises not as a result of lower absolute excitation rate, but because of

a higher rate of further excitation and ionisation. It may also be conjectured that the fact that the maxima in the radial profile of the peak population density are closer to the axis also occurs as a result of the more steeply peaked radial profile of electron density and temperature.

9.6.2 THE DECAY OF THE FIRST NEON ^3P POPULATION PEAK

In Figure 9.17 the measured population density in the neon $^3P_0$ level may be seen over a longer time scale. The loss of population during the first phase may be seen to be considerably faster on axis than further out, although it can be seen that the peaks in the radial population density profile have now moved out slightly from being centred at about ± 10.5 mm to about ± 14 mm. It is likely that this happens not just because of the greater values of electron temperature and density on axis, but also because the high rate of ionisation on axis tends to pull down the electron temperature much faster here. This theory is supported by the fact that the initial appearance of recombination population on axis occurs almost before the initial population nearer the wall has completely disappeared.

9.6.3 THE NEON ^3P POPULATION RECOMBINATION PEAK

The steepness of the radial electron density profile in the end regions of the plasma tube may be observed in the shape of the neon recombination peak, which can be seen to be very narrow. Over the limited range over which measurable population occurs the timing of the peak of the recombination occurs at the same time regardless of radial position suggesting that the falling electron temperature reaches the value of the gas temperature at the same time at all the radial positions over which recombination may be observed. There is insufficient evidence to attempt to predict whether this extends over the whole diameter of the plasma tube.

In Figure 9.18 the whole of the recombination peak may be seen and it can be seen that its radial profile goes from being highly peaked on axis to being far flatter, displaying a faster decay rate on axis than nearer the wall. As discussed when considering the decay of the recombination peak in Section 7.5.4 this decay rate consists of the resultant of the processes feeding the population from recombination, via high lying levels, and the loss of population to the ground state. As it is unlikely that the

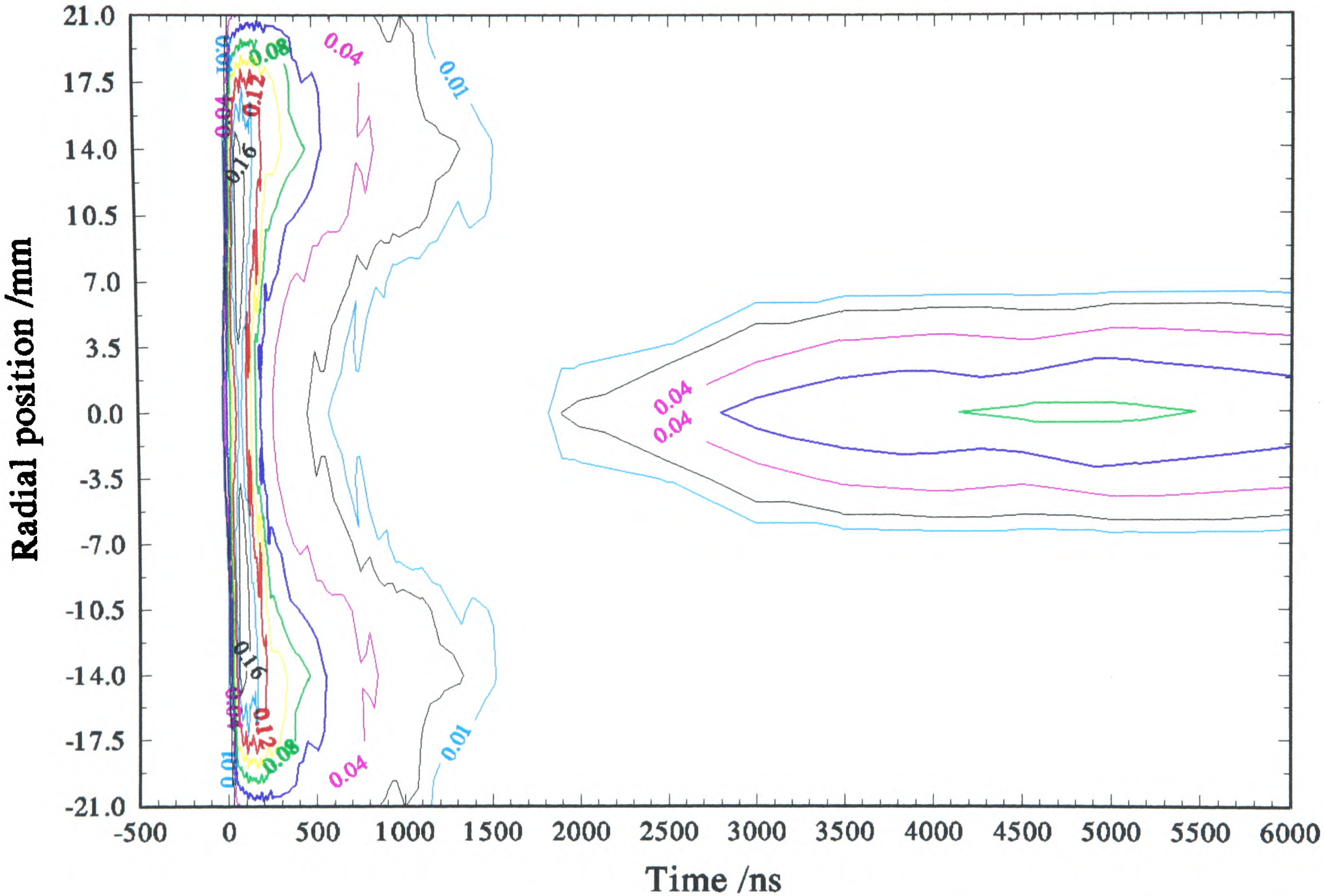

Figure 9.17 Contour plot of neon $2p^5\ 3s\ {}^3P_0$ level population density as a function of time and radial position; first 6 μs

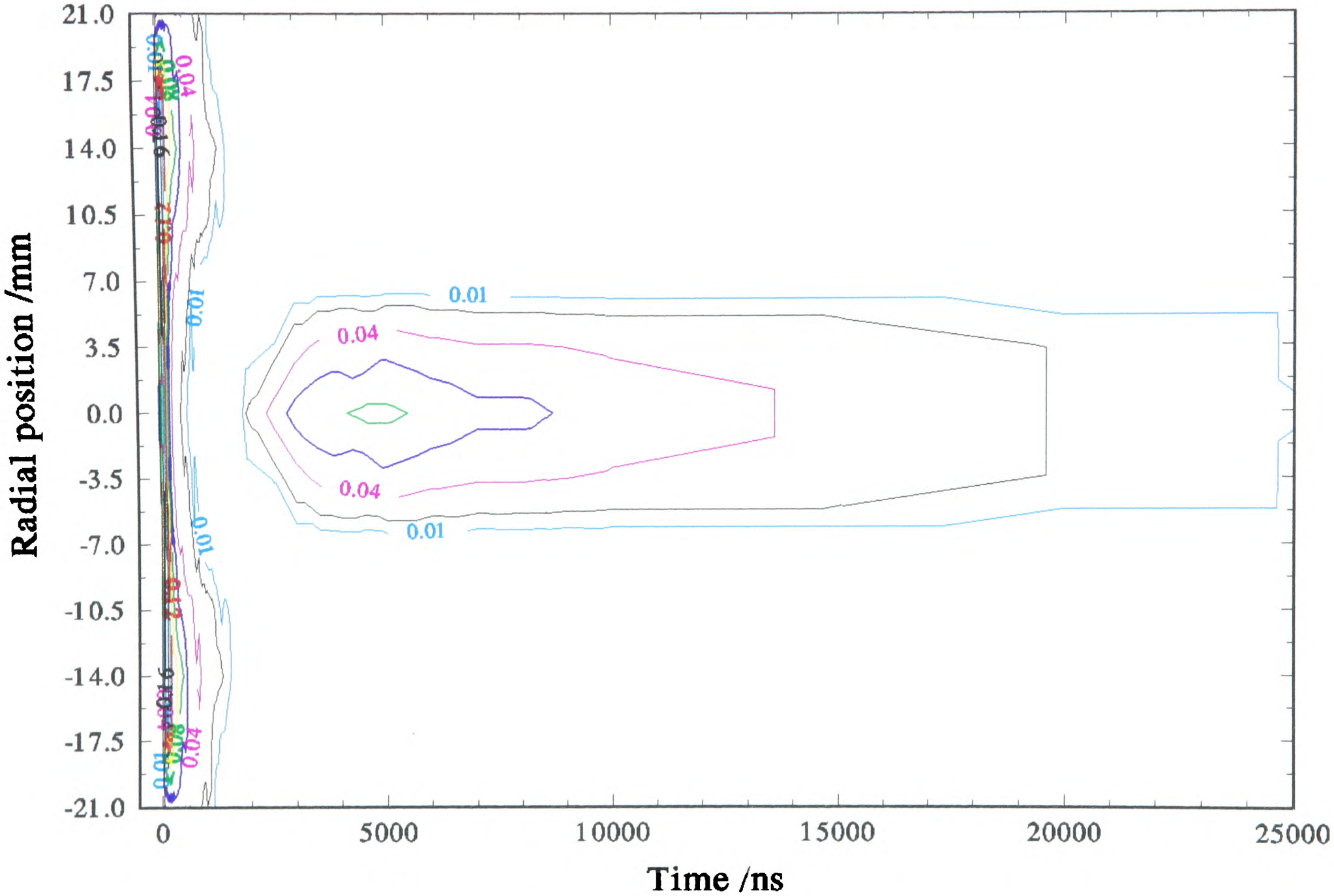

Figure 9.18 Contour plot of neon $2p^5\ 3s\ {}^3P_0$ level population density as a function of time and radial position; first 25 μs

electron temperature is lower on axis than further away, and thus the rate of recombination must be slower on axis, the dominant effect must be that of population loss downwards, which is likely to be faster on axis. This would explain why the decay curve observed on axis (Section 7.5.4) had an approximately exponential form.

10 CONCLUSIONS

10.1 THE WORK UNDERTAKEN

The brief of the project has been successfully met and a diagnostic facility for the direct measurement of many key parameters in an actively operating copper vapour laser has been set up that is, to the best of the knowledge of the author, peerless in the world in terms of the range of measurements offered, spatial and temporal resolution, measurement rate, and absolute accuracy. A set of measurements has been made to characterise a single, standard CVL operating under standard running conditions, that represents the fullest such data set known to be in existence, and initial observations based on those results have been made, and a number of deductions drawn. It is however as experimental data with which theoretical computer modelling of the CVL kinetics may be compared that it is believed that the greatest value of these results lies. The measurements reported here may be repeated on the same device under modified operating conditions, and on slightly or significantly different devices, and the results compared with those obtained in this study. In this way the level of understanding of the basic processes involved, as well as that of the direct and indirect effects of the modifications made, can be increased with each set of conditions. Such an iterative process however must be considerably slower than the computer simulation of different devices, different operating conditions and different excitation regimes that can be undertaken once a computer model has been developed that is known to reproduce the observed behaviour accurately and reliably.

10.2 FUTURE WORK

The continuation of the work so far undertaken may be divided into three sections: additional measurements to be made on the present device under the present operating conditions, data sets to be obtained from the same laser under modified operating conditions, and data sets to be obtained from other, analogous devices.

10.2.1 ADDITIONAL MEASUREMENTS TO BE MADE ON THE STUDY LASER UNDER ITS PRESENT OPERATING CONDITIONS

In respect of the first of these sections the most obvious lacuna is the continuation of the measurements of the lower laser levels through the full duration of the interpulse period using the absorption method as described in Section 7.3.1. Such a set of measurements would yield the radial and temporal variation of electron temperature, assuming these levels to be in local thermal quasi-equilibrium with the ground state at this temperature, as well as directly giving the pre-pulse population density in each of these levels and the radial profile of each. From these latter values the deduced importance of pre-pulse lower laser level population density (Section 6.3) in the onset of gain on axis could be directly confirmed.

10.2.2 MEASUREMENTS TO BE MADE ON THE STUDY LASER UNDER MODIFIED OPERATING CONDITIONS

As implied in Section 10.1, above, the potential for repetition of the full series of measurements on the same device under different operating conditions is nearly endless, however there are a number of studies that could be particularly advantageous.

Many claims for the beneficial effects of the addition of a small concentration of hydrogen gas into the buffer gas of both copper halide and elemental copper vapour lasers have been made (Section 1.1.2 (II)). The repetition of the full set of measurements on the study laser with low concentrations of hydrogen added to the buffer gas and the comparison of both the discharge characteristics and the copper kinetics with the device under standard conditions could give a far better understanding of what its real influence is.

The incorporation of magnetic pulse compression (MPC) as described by Nehmadi (Nehmadi et al, 1989), into the discharge circuitry, with its faster rising discharge pulse, higher voltage breakdown and reduced power dissipation in the thyratron offers the potential for a greater proportion of the power to be coupled into the plasma during the vital early stage of the discharge pulse. Measurements to assess the effect of the implementation of MPC in terms of excitation efficiency could aid a more thorough evaluation of its benefits.

The effect of operating the CVL at higher than normal buffer gas pressure is to channel a greater proportion of the input power into exciting the neon at the expense of the copper. It does however have ancillary benefits, especially in large bore lasers. A higher neon density has the effect both of increasing thermal conductivity and decreasing electrical conductivity. This would tend to give rise to a relatively lower axial gas temperature and consequently pre-pulse lower laser level population densities, as well as reducing the skin effect and decreasing the time taken for the discharge to propagate in to the axis of the laser. Where the time taken to penetrate to the axis is a significant proportion of the time of the rising edge of the current pulse significantly poorer excitation on axis can result. With a large number of CVL units now being used in the role of an amplifier in which maximum energy must be extracted in a single pass, the benefits of more radially uniform excitation and population inversion might outweigh the reduced efficiency the device would show as an oscillator. Investigation of the laser under conditions of higher than normal buffer gas pressure might suggest whether this could be a profitable operating regime in some specific applications.

10.2.3 MEASUREMENTS TO BE MADE ON OTHER LASERS

Reference has been made on a number of occasions in this thesis, to the HyBrID (Hydrogen Bromide In Discharge) laser developed at St Andrews University as offering both high efficiency and high specific power combined with reduced operating temperature. The opportunity to repeat the measurements made on the study laser on a device of the HyBrID type could yield a great deal of information about the true source of the high specific power and efficiency. In particular if this was combined with measurements made on a standard CVL with hydrogen added to the buffer gas, to evaluate the effect of the hydrogen alone, the facility would be there to answer a large number of questions.

PUBLISHED PAPERS NOT FILMED FOR COPYRIGHT REASONS

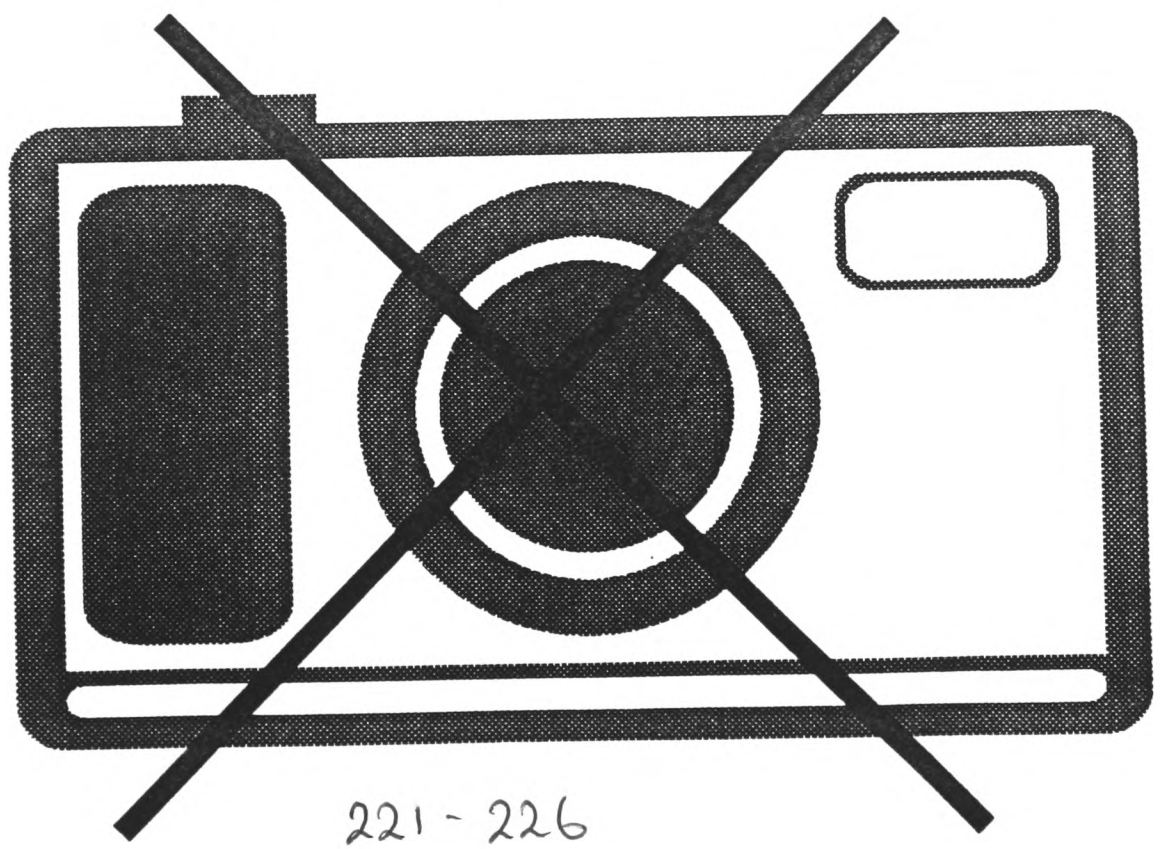

221 - 226

Meas. Sci. Technol. 4 (1993) 263–269. Printed in the UK

APPENDIX A1

The automation of the hook technique

G P Hogan, M Svoboda† and C E Webb

Department of Atomic and Laser Physics, University of Oxford, Clarendon Laboratory, Parks Road, Oxford OX1 3PU, UK

Received 28 August 1992, accepted for publication 28 October 1992

Abstract. We describe a hardware and software automation of the hook technique which allows rapid acquisition of large sets of atomic level population density data. The method for reducing the initial images to allow efficient storage of data for subsequent analysis is also presented. These techniques have been applied to the study of the plasma of a copper vapour laser.

1. Introduction

The 'hook method' first proposed in 1912 by Rozhdestvenskii for the accurate measurement of oscillator strengths was applied by Ladenburg and colleagues in the late 1920s (Ladenburg 1928, 1933) to the measurement of populations of excited states in a steady DC discharge positive column in neon. In those early studies the light source employed was an arc lamp which, in combination with photographic film detectors, required comparatively long exposures to acquire the fringe patterns. As a result stringent demands were placed upon the stability of the system.

Since the advent of high-intensity pulsed dye lasers in the 1970s the hook technique has undergone a renaissance in its 'fast' implementation. In this form of the technique a pulsed laser is the light source and data may be acquired from a single laser pulse which provides time resolution typically of the order of nanoseconds. As such it is a very powerful diagnostic technique for carrying out spatially and temporally resolved measurements of atomic level population densities in atomic gases, vapours and plasmas. Recently a number of studies have been performed using the 'fast' hook technique to monitor population kinetics in the copper vapour laser (CVL) plasma (Molander 1989, Brown *et al* 1989).

Although lack of sensitivity limits its use to relatively large population densities accessible by transitions of high oscillator strength, the hook technique possesses one very considerable advantage. This arises because the region of the spectrum of interest is at the extreme wings of the absorption line, well beyond the effect of any broadening mechanism and consequently no knowledge of line shape or broadening mechanisms is required. The interpretation of data is thus free of assumptions except those concerning plasma length and oscillator strength.

In order to make a measurement by the 'fast' hook technique a pulse from a broad band laser is passed through a Mach–Zender interferometer. One arm of the interferometer contains the test cell while the other contains plane glass or quartz compensation plates. The recombined beam is then dispersed by a spectrograph onto a two-dimensional (2D) detector such that the horizontal dimension represents wavelength, with the absorption line close to the centre of the range, and the vertical corresponds to the position on the entrance slit of the spectrograph (figure 1). When the interferometer is correctly set up and the compensation plates adjusted, the wedge fringes generated by the interferometer appear as a set of sloping straight lines in the focal plane of the spectrograph. In the presence of an absorbing population in the test cell, the fringes display the effect of anomalous dispersion excursions in the refractive index in the neighbourhood of an absorption line (as described, for example, by Sellmeier's formula) in the form of distinctive 'hooks' (figure 2). The separation Δ of these hooks is related to the line integral of the product N^*, the 'effective population density' of the absorbing species over the path length l of the probe beam within the plasma, and the oscillator strength of

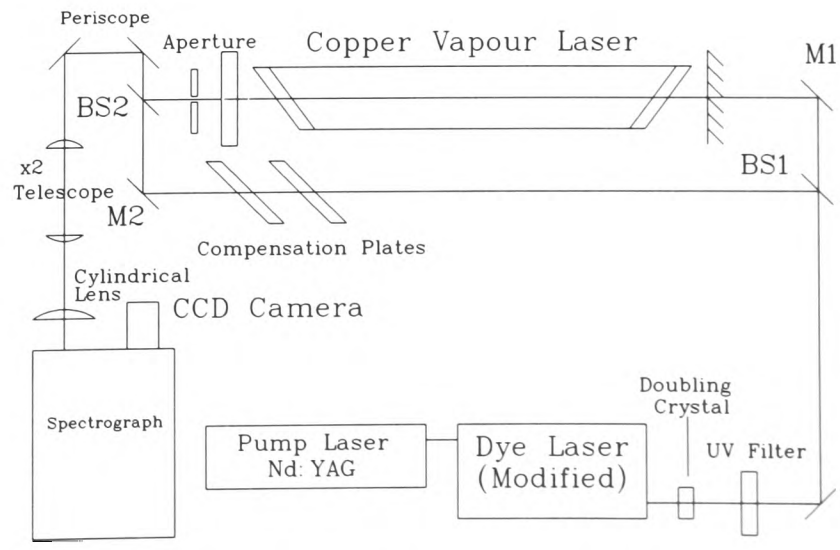

Figure 1. Optical arrangement for making hook measurements.

† On leave from Prague Technical University, Prague, Czechoslovakia.

0957-0233/93/030263+07 $07.50

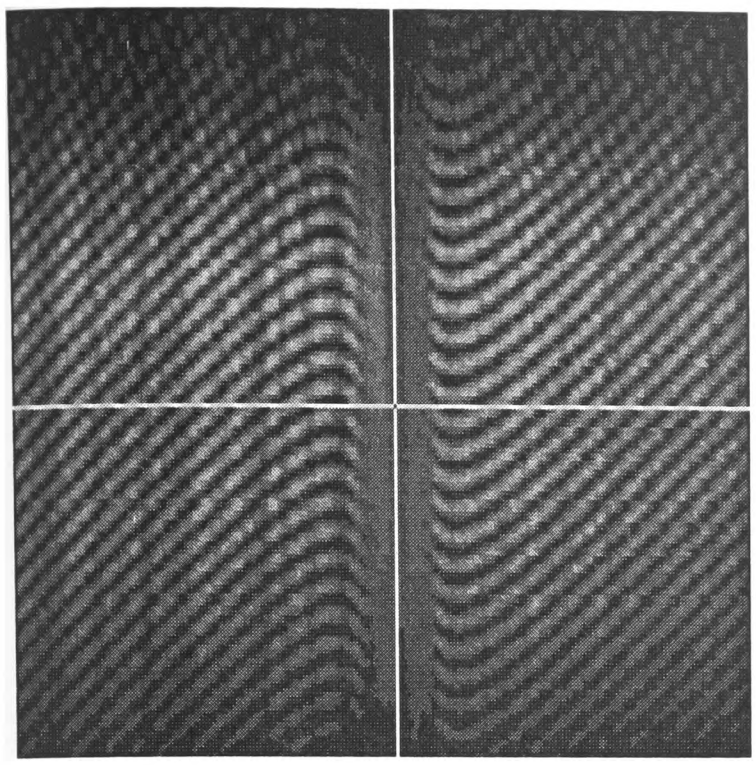

Figure 2. A typical hook pattern.

the transition f by the expression:

$$\int_0^l N^* f \mathrm{d}l = \frac{\pi K}{r_0 \lambda_0^3} \Delta^2 \tag{1}$$

in which λ_0 is the wavelength of the transition, $r_0 = e^2/4\pi\varepsilon_0 mc^2$ is the classical electron radius, and K is a dimensionless interferometer constant approximately equal to the fringe order (see e.g. Marlow 1967). N^* is defined as:

$$N^* = N_{\text{lower}}\left(1 - \frac{g_{\text{lower}} N_{\text{upper}}}{g_{\text{upper}} N_{\text{lower}}}\right) \tag{2}$$

where N_{lower}, N_{upper}, and g_{lower} and g_{upper} represent the population densities in the lower and upper levels, and the degeneracies of these levels respectively.

Provided there is no appreciable difference in population across a vertical diameter of the probe beam, the hook separation is constant at all points parallel to the vertical axis of the detector and is the only information to be derived from the image.

The short (5 ns) probe pulse ensures good temporal resolution, while the small width ensures good lateral spatial resolution. As one interferogram image must be obtained for each temporal or spatial measurement any extensive parameter mapping implies that a very large number of images must be recorded and analysed.

2. Experimental procedure

The present application required population density measurements for a number of atomic energy levels in the plasma of a copper vapour laser (CVL). In normal operation the CVL operates at a pulse repetition frequency (PRF) of 6500 Hz. Each laser pulse lasts about 50 ns, followed by around 150 μs of interpulse delay. In order to map accurately the behaviour of the populations over the whole of this period, 92 time points were required and, for safety, each measurement was repeated at each time point. This method was to be repeated for seven different radial positions across the laser plasma tube. Each atomic energy level studied therefore generated 1288 images. For these results to be usable they had all to be made on the system running under identical conditions. To eliminate drift in the CVL arising from minor variations in temperature with input voltage drift, particularly over a single time course, it was desirable that all of these data points should be obtained in a time period which was short with respect to that of the drift.

Two other factors become significant when dealing with data sets of this size. The first is the problem of storage of the large number of images obtained if they are not to be analysed in real time, and the second is that of the accurate measurement of the hook spacing in so many images.

The interference patterns generated may be stored in a number of ways. They may be recorded photographically onto film or as analogue information on a video tape or digitally as an array that may be analysed, manipulated and stored using a computer. For the present work we selected the last option, employing a CCD camera as our detector at the output of the spectrograph, from which the image could be downloaded to a PC. In this form, however, in which each image consisted of a 256×256 array, each one took up 64 kB of memory and consequently a full set of measurements for one level took up 80.5 MB of disk space. This presented problems as it was impractical to archive measurements in this form. Either the full data set of a day's run had to be analysed before the next could be obtained, or some kind of dramatic reduction of the information content to a more compact form had to be undertaken.

We therefore addressed the problems of obtaining data sets of this size in a reasonable time, archiving the information obtained, and analysing it in a fast and accurate way.

2.1. Hardware

The probe laser employed for the present measurements was a pulsed dye laser (Lumonics model HD-300) pumped by a flashlamp pumped Nd:YAG laser (Lumonics model HY-750). The Nd:YAG laser operates at typically 10 Hz and it is necessary to provide synchronization between it and the CVL. The timing electronics are represented schematically in figure 3, including those associated with the image grabbing and storage. The delay D_1 is incremented for the successive data points to cover the whole of the laser cycle. Delay D_2 is a fixed dummy delay by which the total delay is calibrated to allow D_1 to be set to 0 for our timing starting point. This calibration is accomplished using a single photodiode and appropriate filters so that both the CVL and the probe laser pulses may be observed simultaneously and delays adjusted empirically. D_3 is also a fixed delay, of

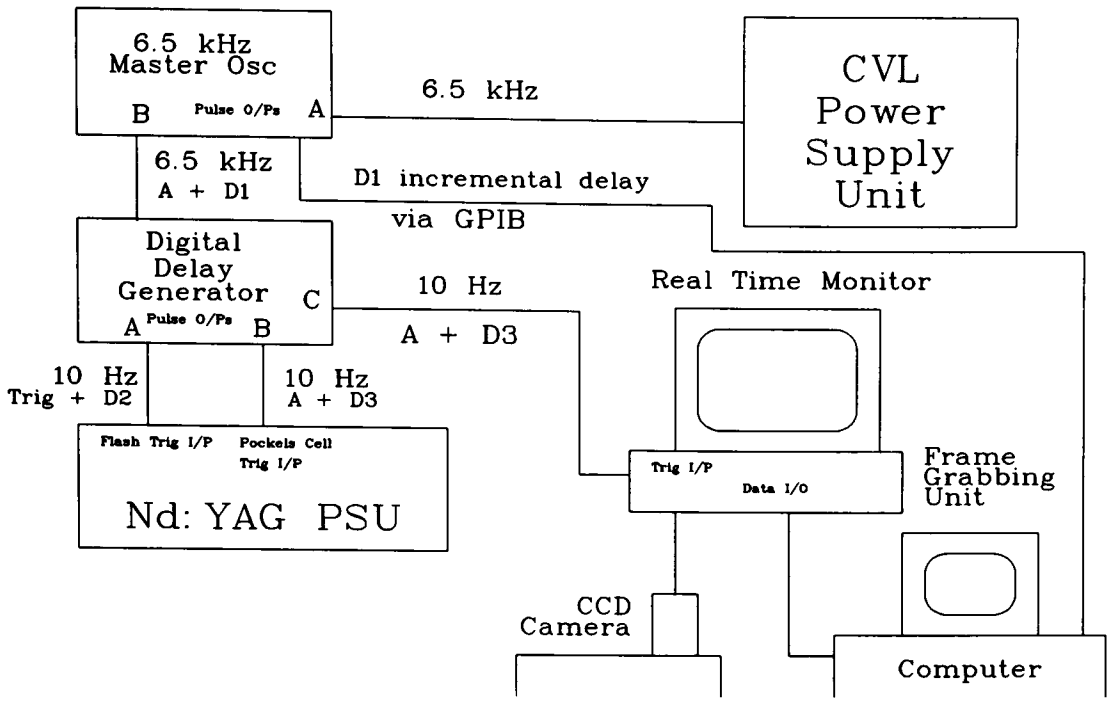

Figure 3. Schematic diagram of electronics for time-resolved hook measurements.

180 μs, the optimum delay between flashlamp and Pockels cell triggering of the flashlamp pumped Nd : YAG laser.

Figure 3 represents the situation prior to implementation of the automation. After the implementation the incremental delay D_1 (which was initially changed by hand) is under computer control. Likewise the image capture and storage functions were also initially made manually (from within an operating environment supplied by the manufacturers of the frame grabbing equipment). Both functions were included in the overall control program in the automated version.

As the frame grabbing system (an Exitech system Profile 256) was already interfaced to the computer, no hadware modification was needed. It was merely necessary to access the appropriate sections of program code to allow control to be assumed by our program. Consequently the only hardware modifications necessary were the connection of the master oscillator to the computer via a GPIB (general purpose interface bus, Protocol IEEE 488.2) card to allow delay D_1 to be accessed from the PC.

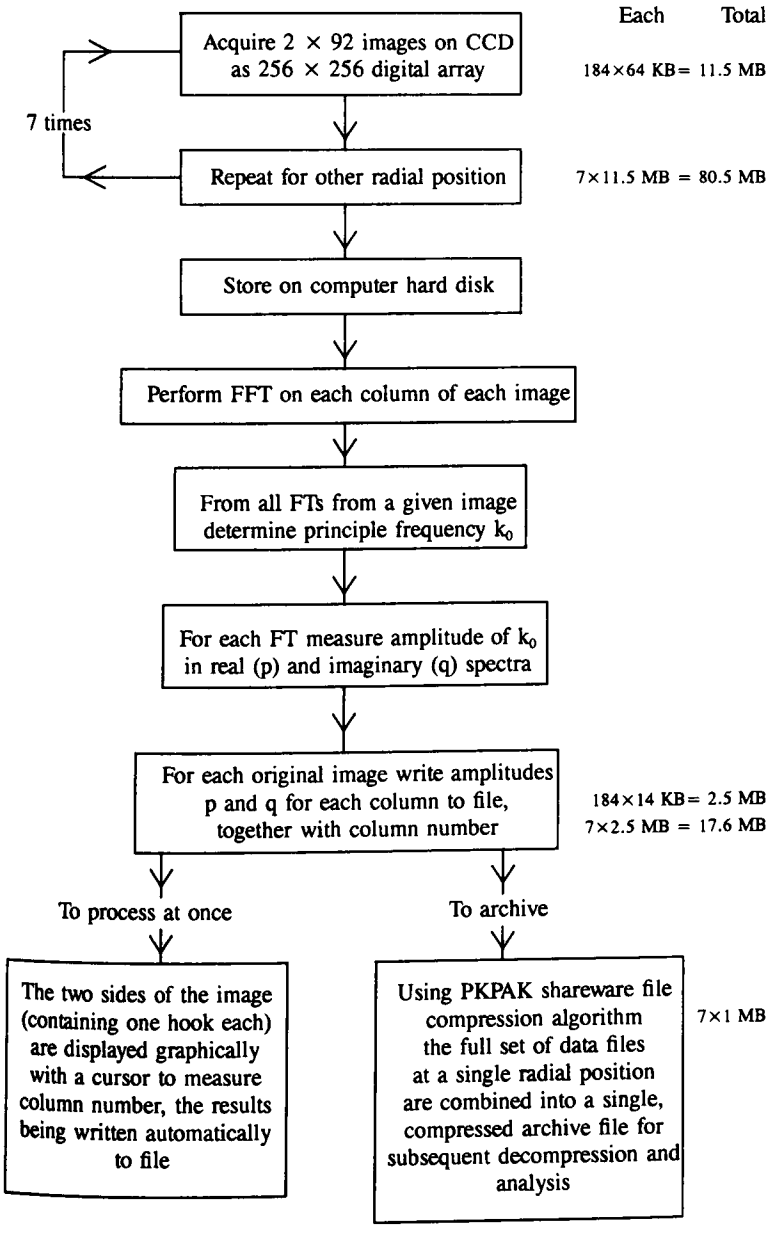

Figure 4. Flow diagram of the automated analysis of hook patterns.

2.2. Software

The programming language and environment chosen was Borland's TURBO PASCAL version 6.0. The software for the Exitech Profile 256 is written for compilation in TURBO PASCAL. A copy of the source code of the utilities we would require was supplied to us by Exitech Ltd. These were in the form of program units that could be called from, and compiled with, our own program. This allowed us to transfer the image from the equipment's own frame buffer into computer memory, and thence store it onto hard disk from within our program without having to write the code to perform these tasks ourselves. The TURBO PASCAL language interface for the GPIB was supplied by the manufacturers of the board.

Having obtained the software units for inclusion, their assembly into a functional program was relatively straightforward. Functions were built up and defined to send specific compound messages to the digital delay generator (DDG) such as 'increment digit at cursor by 5 units', and procedures to allow for the automatic gener-

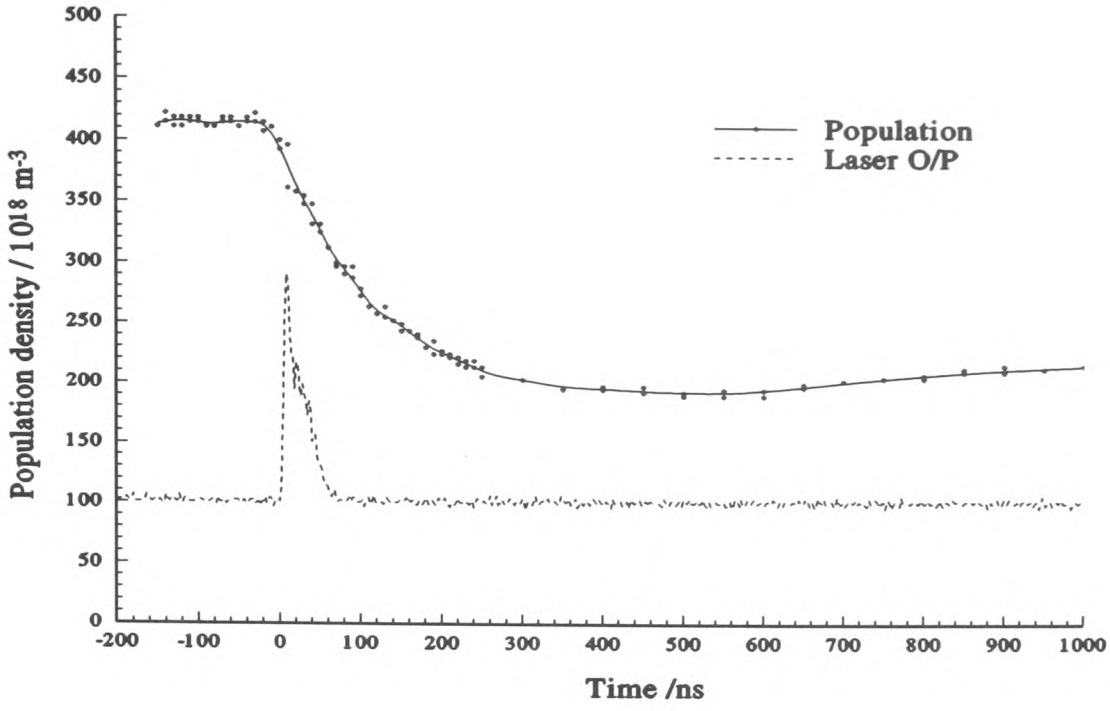

Figure 5. Population density in copper ground state on axis against time.

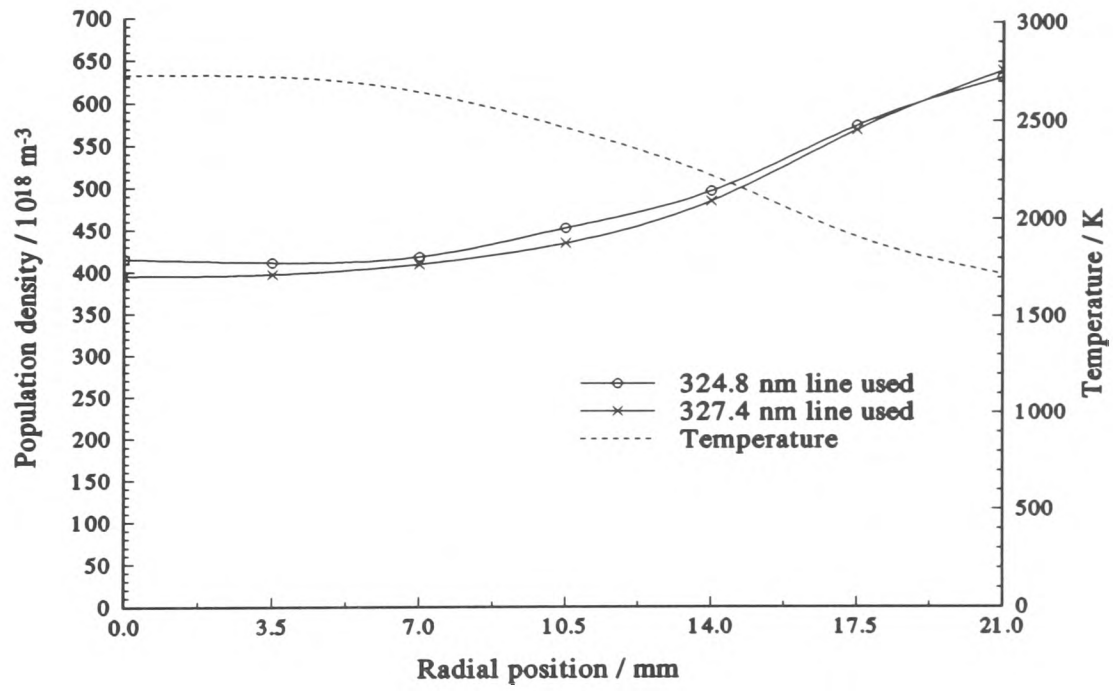

Figure 6. Radial profile of pre-pulse copper ground state population density.

ation of logical file names under which the images could be stored. Finally, to allow for the efficient coverage of the full time course with optimal resolution, the program was assembled in the form of a sequence of loops containing successively greater time increments as the expected rate of change of population decreased with time in the interpulse period.

A problem with the first draft of the program was that, although the overall timing was slow enough to prevent double acquisition of any of the (10 Hz) images, the acquisition of the next image after the delay incrementation (command) could occur before the incrementation had been implemented, with the result that the first of each pair of duplicate acquisitions had the previous delay. A dummy delay was included into each loop and cured the problem. The final program was able to obtain two duplicate hook patterns for each of 92 time points (including a final two with zero delay to assess any drift over the experiment) in about 5 min. Previously, to obtain a smaller data set would typically take around 50 min.

The final implementation of the experiment therefore allows both lasers to operate at their optimum frequencies, the CVL at an exact unperturbed PRF of 6.5 kHz and the Nd:YAG laser flashlamp-Pockels cell timing to remain constant. The Nd:YAG laser timing only deviates from 10 Hz when the delay is actually being changed, and the probe beam is synchronized exactly with any point in the CVL cycle reproducibly and indefinitely.

To obtain data at the required number (seven) of different radial positions 3.5 mm apart typically took 45 min. A further 10 min were required to obtain the necessary calibration fringe patterns in spectral regions remote from the hooks, from which the interferometer constant could be calculated. The operating parameters, particularly the input voltage, of the CVL could be closely monitored between each experiment and if any drift was observed appropriate action was taken and time allowed

for the system to recover its previous operating point, although this was seldom necessary.

2.3. Analysis of data

2.3.1. Data compression. As discussed above, the images acquired from a single series of experiments occupied 80.5 MB of disk space, and so a very limited number of these experimental runs could be made before analysis and deletion of the original data was necessary. Archiving onto floppy disk would have been possible but inordinately cumbersome. In addition, the analysis of such large numbers of images using standard image processing software, such as that supplied with the Exitech 256 unit, proved to be extremely arduous, especially as each file name had to be entered manually. It was therefore desirable to automate these processes also.

Assuming no change in the interferometer constant between acquisitions, of all the information stored in each image (64 KB) only one number need be extracted, namely $\bar{\Delta}$, the average hook separation. If there were significant variation in the refractive index, e.g. owing to a population difference across the vertical diameter of the probe beam, this would be observed as a variation of hook separation. However, in the case of our probe beam of less than 2 mm diameter, we could assume this to be negligible. All hook separations Δ on a given image are thus assumed to be equal and therefore should in principle be capable of adding to the accuracy of our final figure for $\bar{\Delta}$. This happens to a certain extent when cursors are fitted by eye, as the eye is run up the column of hooks to gain an overall impression of the fit, thereby minimizing the effect of noise on an individual hook.

In the absence of a dispersive medium in the measuring arm of the interferometer, the interference pattern would consist of a series of uniformly spaced bars sloping at a constant angle across the spectrograph focal plane. Along any slice in the y direction, the light intensity $I(y, x)$ is thus a sinusoidal function of y whose phase angle $\phi(x)$ varies linearly with distance x in the horizontal direction. In the presence of a dispersing medium the fringe pattern far away from line centre is unperturbed. However, as the dispersion hook is approached the gradient of $\phi(x)$, instead of being constant, begins to decrease with x, reaching zero at the value of x corresponding to the left-hand turning point of the hook pattern, before reversing. As x is increased beyond the line centre, a second extremum of $\phi(x)$ of opposite sign is encountered, corresponding to the right-hand turning value of the hook pattern.

The intensity $I(y, x')$ along a vertical column of $x = x'$ as a function of y can thus be expressed in terms of the fundamental spatial frequency k_0 as:

$$I(y, x') = I_0[1 + \cos(k_0 y + \phi(x')] + s(y, x') \qquad (3)$$

where $s(y, x')$ is the deviation from an ideal sine wave (i.e. any noise on the signal). To extract the required information content from each of the two-dimensional arrays of $I(y, x)$ values corresponding to a given hook pattern as captured on a single frame of the CCD camera therefore requires an algorithm that can determine $\phi(x)$ in a way as immune from noise as possible.

Performing a Fourier transform on the values of $I(y, x)$ helps to separate out the contribution of the sinusoidal component of $I(y, x)$ at the dominant spatial frequency k_0 from the noise and the zero-frequency component arising from the first term of equation (3). We therefore obtain $F(k, x) + S(k, x)$, where $S(k, x)$ is the Fourier transform of $s(y, x)$ and:

$$F(k, x') = \frac{I_0}{2\mathrm{i}}\left(\frac{2(\mathrm{e}^{\mathrm{i}kT} - 1)}{k} + \frac{\mathrm{e}^{\mathrm{i}(k+k_0)T} - 1}{k + k_0} \cdot \mathrm{e}^{\mathrm{i}\phi(x')} + \frac{\mathrm{e}^{\mathrm{i}(k-k_0)T} - 1}{k - k_0} \cdot \mathrm{e}^{-\mathrm{i}\phi(x')}\right) \qquad (4)$$

where T is the range of the y values (i.e. $y_{\min} = 0$, $y_{\max} = T$) at all values of x. Provided that the contribution in the vicinity of $k = k_0$ made by $F(k, x)$ dominates over $S(k, x)$ by a reasonably large factor, i.e. provided $S(k_0, x') \ll F(k_0, x')$, we can neglect the effect of noise around the main frequency. Furthermore, because the wavelength $2\pi/k_0$ of the dominant sine wave is very much less than T (i.e. there are many fringes in the vertical height of the frame):

$$Z(x) = \lim_{k \to k_0} F(k, x) = \frac{TI_0}{2} \mathrm{e}^{-\mathrm{i}\phi(x)}. \qquad (5)$$

Information on the phase $\phi(x)$ is thus contained in the real and imaginary parts of the complex number $Z(x)$ since:

$$p = \mathscr{R}\{Z(x)\} = \frac{TI_0}{2} \cos[\phi(x)]$$

$$q = \mathscr{T}\{Z(x)\} = \frac{-TI_0}{2} \sin[\phi(x)]. \qquad (6)$$

In principle, the variation of $\phi(x)$ with x could be obtained directly from these data since:

$$\phi(x) = \arctan\left(\frac{-q}{p}\right). \qquad (7)$$

However, such a procedure is not the best way to locate the turning points in $\phi(x)$ since it may happen that the turning point occurs near a value of x for which p or q may be near zero, so that the condition $S(k_0, x) \ll F(k_0, x)$ is not well satisfied, allowing noise to corrupt the result.

To provide some degree of noise immunity the procedure adopted was to store the values of

$$\cos[\phi(x)] = \frac{2p}{TI_0} \qquad \sin[\phi(x)] = \frac{2q}{TI_0} \qquad (8)$$

for each column of the frame. If $\sin[\phi(x)]$ and $\cos[\phi(x)]$ are plotted against x for regions of the frame well away from line centre, the linear variation of $\phi(x)$ with x gives rise to a pair of sine waves which are always $\pi/2$ out of phase with one another. For this reason they cannot both be at a low amplitude at the same time, thereby minimizing the effect of noise on a small signal. The hook can be determined as the only point where both

curves display a turning point at the same value of x. The analysis of the sine and cosine waves is discussed further in the next section.

In this way the CCD picture is reduced to two pairs of sine and cosine waves (pairs corresponding to the left-hand and right-hand sides of the picture). Because only one frequency is involved, these sine and cosine waves are in themselves much more compact than the original image. However, they can also be compressed further using standard data compression software and stored on a disk for later analysis. This means a substantial reduction of memory size required for storing the same physical information. Using this method has allowed us to compress the full set of the measurement of 80.5 MB into around 7 MB, allowing a complete run at one radial position to be stored, together with its calibration images in full, on a single high-density floppy disk for subsequent analysis or archiving.

The total process is represented in the flow diagram of figure 4.

2.3.2. Data analysis. Three techniques were considered for the analysis of the hook spacings.

The first was a simple graphical program that calls up each sine/cosine pair (for each side of the hook pattern) sequentially and displays them, with a superimposed cursor together with the cursor position, in column numbers. The one point at which both waves exhibit a turning point together represents the hook position.

The manually set position of the cursor is written to a file for each set of waves so that the left and right hook position numbers (and their separation) together with an index representing the quality of the data are stored in order that, for poor fringes, a 'best guess' could be input with the knowledge of this fact. Direct importation into a spreadsheet/graph plotting program allowed the column of raw hook separations (in units of columns) to be converted to population densities and then displayed.

The second technique considered was a fully automatic program based on the fact that $\phi(x)$ is nearly constant near the hook positions and that the only common local extremum of both $\sin[\phi(x)]$ and $\cos[\phi(x)]$ is the hook position as discussed above. In order to improve this technique's resistance to noise on the data we have used the fact that the two hooks will always be symmetrical about the absorption line, and this is always positioned at the centre of the detector array (column 128). For the ground state measurements this automatic method was comparatively efficient for the good-quality CCD pictures — in these cases it could use up to 95% of the original pictures from the measurement in fully automated data processing. Where the signal-to-noise ratio (SNR) of the original image was poor, however, or where there was the presence of artifacts (for instance owing to other absorption or emission lines, e.g. from the neon buffer gas, at the edge of the image), there was still the potential for incorrect assignment.

Thirdly we also experimented with the fitting of a polynomial to the peak of the hook function in order to find its turning point mathematically.

Although the last two automated techniques would work well for the ground state measurements where the change in hook separation is of the order of 20%, problems arose for all other levels that start at zero separation, rise to a maximum (optically arranged to make optimum use of the available detector area) and then back to zero. To eliminate false readings reliably from the central region about the absorption line where the periodic sine and cosine functions abruptly became random (for small hook spacings this is within a very few pixels of the hook position) proved extremely difficult. In our application it seemed to offer insufficient benefit over the simple graphical method to warrant extensive development.

In practice, the graphical analysis technique was the method adopted as it allowed for an element of operator discretion which could easily prevent a number of false results owing to residual noise in the data as the overall shape of the turning point could be considered and, with automatic file handling after the initial file name root had been given, proved to be very efficient.

3. Results

We have used the modifications of the hook technique discussed above in our routine analysis of atomic level populations in a CVL in order to compile a complete parameter map of a single CVL system under standard operating conditions. The full results will be published at a later date (Hogan 1993). However a typical plot of the copper ground state population density on the axis for 150 ns before, and the first 1 μs after, the onset of lasing, related to the laser light output from the same region is presented in figure 5. The scatter of the duplicate points, particularly on the rapidly changing part of the curve, gives us some confidence in the reproducibility and precision of our measurements. We have checked the absolute accuracy of the system by comparison of the equilibrium (pre-pulse) ground state population density at the wall of the plasma tube with that predicted from the value of the copper vapour pressure curve at the wall temperature measured by taking a series of readings at regular time intervals after switching off the laser, using an optical pyrometer, calibrated at the melting point of copper and corrected for the laser end windows, and extrapolating back to time zero. This gives a population in excellent agreement with the value obtained. In addition, measurement of the pre-pulse ground state population density, using the two copper resonance lines and therefore operating both the spectrograph and the interferometer in different orders, different oscillator strength transitions and other differences, give the agreement shown in figure 6 (together with the radial temperature profile obtained from these values).

4. Conclusions

The techniques discussed above have been employed in the Clarendon Laboratory for the measurement of popu-

lation densities in an operating, unperturbed copper vapour laser and have shown themselves to be reliable, accurate and user friendly.

Acknowledgments

The authors would like to express their gratitude to the following organizations for their support for the project: British Nuclear Fuels plc for finance for the equipment, the Science and Engineering Research Council for a research studentship for G P Hogan, and the British Council Tempus Scheme for support for M Svoboda as a Visiting Scholar.

References

Brown D J W, Künnemeyer R and McIntosh A I 1989 Radial excited-state density effects in a small-bore copper vapour laser *SPIE* **1041** 25–33

Hogan G P 1993 *DPhil. Thesis* Oxford University to be published

Ladenburg R 1928 Untersuchungen über die anomale Dispersion angeregter Gasse. I Teil. zur Prüfung der quantentheoretischen Dispersioformel *Zeit. Phys.* **48** 15–25

Ladenburg R 1933 Dispersion in electrically excited gases *Rev. Mod. Phys.* **5** 243–56

Marlow W C 1967 Hakenmethode *Appl. Opt.* **6** 1715–24

Molander W A 1989 Measurement of ground state copper density using hook spectroscopy *SPIE* **1041** 11–18

Rozhdestvenskii D S 1912 Anomale Dispersion im Natriumdampf *Ann. Phys., Lpz* **39** 307–45

APPENDIX A2 COMPLICATIONS IN THE ANALYSIS OF HOOK PATTERNS

There are three regimes under which measurements employing the hook method may not be entirely straightforward. The first is that in which the population density in the upper level of the transition under investigation is not negligible in comparison with that in the lower level and the full expression for F_s (Equation 3.5) must be employed. In this case it must also be possible to obtain a value for the population density in the upper level either by using the hook method on another transition, or by another method, such that it may be inserted explicitly. The ultimate extension of this condition is that found between two laser levels where inversion is experienced, and F_s becomes negative, the condition termed by Smilanski "inverse anomalous dispersion" and exploited in his paper (Smilanski et al, 1980) in the investigation of the kinetics of population inversion. In order to generate hooks in this case the sign of K, and consequently that of m, must be inverted.

The second regime under which problems may be encountered is that mentioned in Chapter 3 when two absorption lines lie close together. In this case more than one term in the summation in the Sellmeier dispersion formula (Equation 3.6) must be included. For a value of K appropriate to the production of hooks about a single absorption line there are two possible resultant fringe patterns depending upon the F_s values of the two lines, their spacing and the value of K. Hooks will be generated wherever the equation $-l.dn/d\lambda = K$ (Equation 3.9) has a solution, regardless of whether a single term in the summation is taken (as in Equation 3.10) or two (or more). In the case of a doublet this means that there will be a pair of proper hooks outside the doublet, however there may or may not be two more hooks in the region between the two line centres depending on whether the maximum value of $-l.dn/d\lambda$ falls below K. The solution for the four real roots, where they exist, has been calculated by Prokofiev (Prokofiev, 1924). Where the interaction is slight, for example where there is a weak line in proximity to the stronger one of interest, it is sometimes possible to use $2(\lambda-\lambda_0)$ (measuring only the distance of a single hook from the line centre on the side of the absorption line remote from the perturbing line) in place of the full hook separation Δ without undertaking the full calculation, while introducing an error of only a fraction

of 1%. The size of this error, and thus whether such simplification is justified, must be calculated for each specific case.

The third regime under which care must be exercised in the interpretation of the hook separation is that in which the assumption that the wavelengths at which the hooks are formed are far enough away from the line centre for there to be negligible absorption, ie $\left(\omega_s^2 - \frac{F_s e^2}{3m\varepsilon_0}\right) - \omega^2 \gg \gamma_s\omega$, does not hold. This can usually be expected to hold well for a high resolution system, for which $\varepsilon \approx 4$ pm, and a minimum resolvable hook separation of around 0.2 Å is a reasonable estimate for the standard hook method (Bachor & Kock, 1980), or 0.12 Å for the vernier method. When employing broad lines however care must be taken to ensure the validity of this assumption. The application of the hook method to broad lines has been considered by both Marlow (Marlow, 1967) and Huber (Huber, 1971) in their reviews of the hook method. Marlow illustrates his results with a three dimensional graph on which he plots the fractional change in the observed hook separation against Lorentz and Doppler broadening, as a fraction of the unperturbed hook separation, as two of the axes. Huber represents the same information in two dimensional graphs in which one kind of broadening only is the dependent variable, and a number of lines are plotted for various values of the other.

The result that emerges from both papers is that as soon as broadening becomes an appreciable proportion of the unperturbed hook separation the original, single set of hooks about an isolated absorption line are replaced by two hooks on each side until the broadening becomes so great that no hooks at all are generated. Of this pair it will be the outside one that will be most readily observed and measured, the inner set being, in general, very close to the absorption line. In the case of pure Lorentzian broadening this has the effect, as it increases, of decreasing the observed (outer) hook separation, by about 1.5% for $\Delta\lambda_L = 0.1\Delta_0$, (ie the line-with is 10% of the unperturbed hook separation), increasing to about 6.7% at $\Delta\lambda_L = 0.2\Delta_0$. Hooks cease to be formed at the point where the inner set meet the outer set ($0.5\Delta_0$) where the homogeneously broadened line-width is around 35% of the unperturbed hook separation. The effect of Doppler broadening, on the other hand, is to increase the resultant hook separation and consequently will tend to ameliorate the effect of homogeneous broadening. In the case

where $\Delta\lambda_L = 0.1\Delta_0$, which, in the absence of Doppler broadening gives rise to 1.5% reduction in hook separation, this is reduced by about a half for $\Delta\lambda_D = 0.1\Delta_0$, and where $\Delta\lambda_D = 0.2\Delta_0$ there is a 1.5% increase in the observed hook separation. As the Doppler line-width increases the observed hook separation does so too up to a maximum of about +25% for $\Delta\lambda_D = 0.65\Delta_0$, after which it starts to decrease until the hooks disappear at $\Delta\lambda_D = 0.75\Delta_0$.

The Doppler width of the lines employed in the present study is around 0.013 Å, 10% of the minimum resolvable hook spacing, ie $\Delta\lambda_D \leq 0.1\Delta_0$, and its effect will be no more than +0.8% at the very smallest values. The effect of homogeneous broadening will be felt most on the measurement of the $^2D_{3/2}$ level (the yellow lower laser level) which uses the laser transition which has a line-width of 0.099 Å owing to the hyperfine structure and the Doppler broadening. For this reason hooks will not form until $\Delta_0 \approx 2.9\Delta\lambda_L = 0.25$ Å, at which point the observed hook separation will be 50% of this (0.12 Å) for both the internal and external sets, the limit of resolution of the hook vernier method. For measurements such as those undertaken in the present study, where many of the population densities must be measured from effectively zero, this effect must be considered when the smallest hook separations are being measured.

REFERENCES

Abbott J (1990)

Multi wavelength metal vapour lasers

DPhil Thesis Oxford University

Akirtava OS, Dzhikiya VL & Oleinik YM (1975)

Laser utilizing Cu I transitions in copper halide vapors

Sov. J. Quantum Electron. **5** (8) 1001-1002

American Institute of Physics Handbook (1972)

McGraw-Hill 3rd edition

Anderson RS, Bricks BG, Springer LW & Karras TW (1975)

A discharge heated copper vapor master oscillator power amplifier

IEEE/OSA CLEA '75 Digest of technical papers 56-57

Andrews AJ, Webb CE, Tobin RC and Denning RG (1977)

A copper vapour laser operating at room temperature

Opt. Commun. **22** (3) 272-274

Asmus JF & Moncur NK (1968)

Pulse broadening in a MHD copper vapour laser

Appl. Phys. Lett. **13** (11) 384-385

Astadjov DN, Sabotinov NV & Vuchkov NK (1985)

Effect of hydrogen on CuBr laser power and efficiency

Opt.Commun. **56** (4) 279-282

Astadjov DN, Vuchkov NK & Sabotinov NV

Parametric studies of the CuBr laser with hydrogen additives

IEEE J. Quantum Electron. **24** (9) 1927-1935

Bachor HA & Kock M (1980)

Limitations in the evaluation of hook spectra

J. Phys. B **13** 2497-2504

Batenin VM, Burmakin VA, Vokhmin PA, Evtyunin AI, Klimovskii II, Lesnoi MA & Selezneva LA

Time dependence of the electron density in a copper vapor laser

Sov. J Quantum Electron. **7** (7) 891-895

Biberman LM, Vorob'ev VS & Yakubov IT (1973)
Kinetics of impact-radiation ionisation and recombination
Sov. Phys. Uspek. **15** (4) 375-394

Bielski A (1975)
A critical survey of atomic transition probabilities for Cu I
J. Quant. Spectrosc. Radiat. Transfer. **15** 463-472

Blau P, Smilanski I & Rosenwaks S (1992)
Simultaneous time-averaged measurements of gas temperature and electron density in a copper-vapor laser using hydrogen emission spectroscopy
J. Appl. Phys. **72** (3) 849-854

Blau P, Smilanski I, Gabay S & Rosenwaks S (1993)
Radially and temporally resolved measurements of electron density and gas temperature in a copper-vapor laser
CLEO '93 456-458

Bokhan PA, Nikolaev VN & Solomonov VI (1975)
Sealed copper vapor laser
Sov. J. Quant. Electron. **5** (1) 96-98

Brown DJW (1988)
Experimental study of excited state densities in a copper vapour laser
PhD Thesis University of New England, Armidale, NSW

Brown DJW, Künnemeyer R & McIntosh AI (1989)
Radial excited state densities in a small-bore copper vapour laser
SPIE **1041** 25-33

Brown DJW, Künnemeyer R & McIntosh AI (1990)
Time-resolved measurements of excited state densities in a copper vapor laser
IEEE J. Quantum Electron. **26** (9) 1609-1619

Carman RJ, Brown DJW & Piper JA (1993)
A self-consistent model for the discharge kinetics in a high-repetition rate copper vapour laser
submitted to: *IEEE J. Quantum Electron.* preprint

Carslaw HS & Jaeger JC (1959)

Conduction of heat in solids

Oxford University Press

Chen CL, Nerheim NM & Russell GR (1973)

Double-discharge copper vapor laser with copper chloride as a lasant

Appl. Phys. Lett. **23** (9) 514-515

Collins CB, Hicks HS, Wells WE & Burton R (1972)

Mesurement of the rate coefficient for the recombination of He^+ with electrons

Phys. Rev. **A6** 1545-1558

Corliss CH (1970)

A review of oscillator strengths for lines of Cu I

J. Res. Natn. Bur. Stand. **74A** (6) 781-790

Cuthbertson C & Cuthbertson M (1931)

The refraction and dispersion of neon and helium

Proc. Roy. Soc. A **135** 40-47

Dushman S (1949)

Scientific foundations of vacuum technique

John Wiley & Sons New York

Feldman DW, Liu CS and Liberman I (1982)

Bathymetry CuBr laser

Applied Optics **21** (13) 2326-2329

Fowles GR & Silfvast WT (1965)

High-gain laser transition in lead vapour

Appl. Phys. Lett. **6** (12) 236-237

Francis G (1960)

Ionisation phenomena in gases

Butterworths Scientific Publications

Frich SE, Rasumovskaja JP & Rynsanov NS (1977)

Measurements of anomalous dispersion by the interference fringe shift

Opt. Commun. **22** (1) 87-90

Gabay S & Smilanski I (1980)

Effect of preionization on a copper vapor laser

IEEE J. Quantum Electron. **QE-16** (6) 598-601

Gould G (1965)

Collision Lasers

Appl. Opt. Suppl. **2** 59-67

Handbook of Chemistry and Physics (1983-84)

CRC Press 64th edition

Hayashi K, Iseki Y, Suzuki S, Watanabe I, Noda E & Morimiya O (1992)

Improvement in the output characteristics of a large-bore copper vapor laser by hydrogen

Jpn. J. Appl. Phys. **31** (2) 1689-1691

Heald MA & Wharton CB (1965)

Plasma diagnostics with microwaves

Wiley

Hogan GP, Svoboda M and Webb CE (1993)

The Automation of the hook technique

Meas. Sci. Technol. **4** 263-269

Hollins RC (1980)

Dye laser studies of gas kinetic processes

DPhil Thesis Oxford University

Howatson AM (1965)

An introduction to gas discharges

Pergamon Press

Huang Z-G, Namba K & Shimizu (1986)

Influence of molecular gases on the output characteristics of a copper vapor laser

Jpn. J. Appl. Phys. **25** (11) 1677-1679

Huber MCE (1971)

Interferometric gas diagnostics by the hook method

Modern Optical Methods in Gas Dynamic Research (Ed DS Dosanjh) 85-112

Isaev AA, Kazaryan MA & Petrash GG (1972)

Effective pulsed copper-vapour laser with high average generation power

J.E.T.P. Letters **16** (1) 27-29

Isaev AA, Kazaryan MA & Petrash GG (1973)

Pulsed gas lasers based on vapors of nonvolatile substances

Instrum. and Exp. Tech. **16** (1) 228-229

Izawa Y, Shimotsu T, Yamanaka Ch, Nakashima N, Fujiwara E, Yamanaka T, Nakai S, Kuruma S, Takeda T, Ojima Y & Yamanaka C (1989)

Density measurements of the lower laser level of a copper vapor laser

SPIE **1041** 19-24

Jones DR, Akerboom F, Maitland A & Little CE (1993)

Copper hybrid laser producing 149 W at 2.4% efficiency and 112 W at 3.1% efficiency

CLEO '93 460-462

Jones DR, Sabotinov NV, Maitland A & Little CE (1992)

A high-power high efficiency Cu-Ne-HBr (λ=610.6, 578.2 nm) laser

Opt. Commun. **94** (4) 289-299

Karras TW (1973)

Flowing vapor high power laser

United States patent No. **343,417**

Karras TW (1974)

Cesium quenched copper laser

United States patent No. **3,831,107**

Kaye GWC & Laby TH (1989)

Tables of physical and chemical constants (Fifteenth Edition)

Longman Scientific & Technical

Kim JJ & Im K (1985)

Transverse-discharge copper-vapor laser

IEEE J. Quantum Electron. **QE-21** (11) 1747-1748

Kim JJ & Sung N (1990)

Transverse-discharge copper-vapor laser at 5 kHz

IEEE J. Quantum Electron. **26** (5) 818-819

Koechner W (1988)

Solid-state laser engineering (Second Edition)

Springer-Verlag

Korff SA & Breit G (1932)

Optical dispersion

Rev. Mod. Phys. **4** (3) 471-503

Kozlov Yu G & Plekhotin GA (1974)

Possibilities of using an unformed Rozdestvenskii hook to determine the Nfl value

Opt. Spectrosc. **36** (5) 600

Krause L & Bielski (1974)

Excitation transfer and quenching induced in Cu-Cs collisions

Bull. Am. Phys. Soc. **19** 1173

Kushner MJ (1981)

A self-consistent model for high repetition rate copper vapor lasers

IEEE J. Quantum Electron. **QE-17** (8) 1555-1565

Kushner MJ & Warner BE (1983)

Large-bore copper-vapor lasers: Kinetics and scaling issues

J. Appl. Phys. **54** (6) 2970-2982

Ladenburg R (1921)

Die quantentheoretische Deutung der Zahl der Dispersionselektronen

Zeits. f. Physik **4** 451-468

Ladenburg R (1933)

Dispersion in electrically excited gases

Rev. Mod. Phys. **5** (4) 243-256

Leonard DA (1967)

A theoretical description of the 5106-Å pulsed copper vapour laser

IEEE J. Quantum Electron. **QE-3** 380-381

Lewis RR (1985)

Mechanisms of copper vapour lasers

DPhil Thesis University of Oxford

Liu CS, Sucov EW & Weaver LA (1973)

Copper superradiant emission from pulsed discharges in copper iodide vapor

Appl. Phys. Lett. **23** (2) 92-93

Livingstone ES & Maitland A (1989)

A low temperature, segmented metal, copper vapour laser

J. Phys. E **22** 63

Livingstone ES, Jones DR, Maitland A & Little CE (1992)

Characteristics of a copper bromide laser with flowing Ne-HBr buffer gas

Opt. Quantum Electron. **24** 73-82

Marlow WC (1967)

Hakenmethode

Appl. Optics **6** (10) 1715-1724

Miyazaki K, Nakata R, Tomita Y, Suemitsu M, Watanabe S & Fukuda K (1975)

Application of dye laser to the hook method on the population measurement of excited He and Ne atoms in the pulsed discharge

Japan J. Appl. Phys. **14** (7) 1075-1076

Miyazaki K & Fukuda K (1977)

Time-resolved population measurement with N_2-laser-pumped dye lasers

J. Phys. D **10** 1905-1910

Molander WA (1989)

Measurement of ground state density using hook spectroscopy

SPIE **1041** 11-18

Naylor GA, Kearsley AJ & Shaw H (1986)

High-power low-divergence injection-locked copper vapor laser

CLEO '86 160-161

Nehmadi M, Kramer Z, Ifrah Y & Miron E (1989)

Magnetic pulse compression for a copper vapour laser

J. Phys. D **22** 29-34

Parks JH & Javan A (1965)

Collision induced transitions within excited levels of neon

Phys. Rev. **A 139** 1351-1358

Petr RA, Zumdieck JF, Dembski J, Smilanski I, Ewing JJ & Center RE (1983)
Magnetic pulse-compression for copper vapor lasers
4th IEEE Pulsed Power Conf. 236-241

Petrash GG (1990)
Basic physical processes in pulsed metal vapor lasers
SPIE **1225** 216-227

Phelps AV (1959)
Diffusion, de-excitation and three body collision coefficients for excited neon atoms
Phys. Rev. **114** 1011-1025

Piltch M, Walter WT, Solimene N, Gould G & Bennett WR Jr (1965)
Pulsed laser transitions in manganese vapor
Appl. Phys. Lett. **7** (11) 309-310

Piper JA (1975)
A copper iodide laser excited by transverse discharge
Opt. Commun. **14** (3) 296-299

Prokofiev VK (1924)
Anomalous dispersion. I. Relations between the dispersion constants in the principal series of potassium
Optical Transition Probabilities **1** 1-33

Prokofiev VK (1927)
The ratio of the numbers of resonating electrons for the potassium doublets
Phil. Mag. S7 **3** (18) 1010-1025

Prowse (1967)
Astigmatism in the Mach-Zehnder interferometer
Appl. Optics **6** (4) 773

Riseberg LA, Parks WF & Schearer LD (1973)
Penning ionisation of Zn and Cd by noble gas metastable atoms
Phys. Rev. A **8** (4) 1962-1968

Rozhdestvenskii DS (1912)
Anomale dispersion im Natriumdampf
Ann. Physik. **39** 307-345

Russel GR, Nerheim NM & Pivirotto TJ (1972)

Supersonic electrical-discharge copper vapour laser

Appl. Phys. Lett. **21** (12) 565-567

Saito H & Hotuki T (1992)

Shortening of the excited lifetime of the lower laser level in CVL by an addition of Cs

Rev. Laser Eng. (Japan) **20** (10) 777-785

Sandeman RJ (1979)

Hook vernier

Appl. Optics **18** (23) 3873-3874

Scheibner KF & Hazi AU (1993)

Unpublished data in Carman et al, 1993

Scheibner KF, Hazi AU & Henry RJW (1987)

Electron-impact excitation cross-sections for transitions in atomic copper

Phys. Rev. A **35** (11) 4869-4872

Shukhtin AM, Mishakov VG, Fedotov GA & Ganeev AA (1975 a)

Interference method for observing the dissociation of copper halide molecules in a pulsed discharge

Opt. Spectrosc. **39** (4) 444

Shukhtin AM, Fedotov GA & Mishakov VG (1975 b)

Lasing with Cu I lines using copper bromide vapor

Opt. Spectrosc. **39** (6) 681

Smilanski I (1979)

Copper hooks - investigation of the copper vapor laser kinetics

Proc. Int. Conf. Lasers '79 327-334

Smilanski I, Levin LA & Erez G (1980)

Kinetics of population inversion investigated by a modified hook method

Opt. Lett. **5** (3) 93-95

Smilanski I, Moody SE, Warner B & Flint J (1981)

Use of modernized interferometric techniques for laser diagnostics

Proc. Int. Conf. Lasers '81

Tenenbaum J, Smilanski I, Lavi S, Levin LA & Erez G (1981)

Kinetic investigation of the upper laser levels of the copper vapour laser

Opt. Commun. **36** (5) 391-394

Tonks L & Langmuir I (1929)

A general theory of the plasma of an arc

Phys. Rev. **34** 876-922

Trajmar S, Williams W & Srivastava (1977)

Electron-impact cross sections for Cu atoms

J. Phys. B **10** (16) 3323-3333

Vetter AA & Nerheim NM (1977)

Addition of HCl to the double pulse-copper chloride laser

Appl. Phys. Lett. **30** (8) 405-407

Von Engel A (1965)

Ionized gases

Clarendon Press Oxford

Vriens L (1973)

Energy balance in low-pressure gas discharges

J. Appl. Phys. **44** (9) 3980-3989

Vriens L (1974)

Two- and three-electron group models for low pressure gas discharges

J. Appl. Phys. **45** (3) 1191-1195

Walder BT (1990)

A new generation of copper vapour lasers for high speed photography

SPIE **1358** 811-820

Walter WT, Piltch M, Solimene N and Gould G (1966 a)

Pulsed-laser action in atomic copper vapour

Bull. Am. Phys. Soc. **11** 113

Walter WT, Solimene N, Piltch M and Gould G (1966 b)

Efficient pulsed gas discharge lasers

IEEE J. Quantum Electron. **QE-2** (9) 474-479

Walter WT (1967)

40-kW pulsed copper laser

Bull. Am. Phys. Soc. **12** 90

Warner BE (1986)

Injection locking of a copper laser oscillator

CLEO '86 160-161

Warner BE & Kushner MJ (1981)

Controlling kinetic parameters of 100 W large bore copper vapor lasers

Proc. Int. Conf. Lasers '81 845-851

Warner B & Seeley G (1983)

Hook measurements in large copper lasers

LLNL Report

Webb CE (1968)

A new technique for measurements of radial distributions of excited species in plasmas and its application to capillary discharges in argon

J. Appl. Phys. **39** (12) 5441-5470

Webb CE (1976)

The fundamental discharge Physics of atomic gas lasers

High-Power Gas Lasers Institute of Physics Conference series No. 29

Weise WL, Smith MW & Glennon BM (1966)

Atomic Transition Probabilities (Vol 1)

NBS National Standard Reference Data Series

Withford MJ, Brown DJW & Piper JA (1993)

Hydrogen induced radial effects in the output of a copper vapor laser

CLEO '93 284-286

Woodgate GK (1980)

Elementary atomic structure

Clarendon Press Oxford

Zemskov KI, Isaev AA, Kazaryan MA, Petrash GG & Rautian SG (1974)

Use of unstable resonators in achieving the diffraction divergence of the radiation emitted from high gain pulsed gas lasers

Sov. J. Quant. Electron. **4** (4) 474-477